Models of vascular injury and the potential therapeutic benefits of magnesium supplementation

A dissertation submitted for the degree of Ph.D by

Robert G. Wallace, B.Sc.

Under the supervision of Dr. Ronan P. Murphy

August, 2019

Faculty of Science and Health, School of Health & Human Performance,

Dublin City University, Dublin 9, Ireland

I hereby certify that this material, which I now submit for assessment on the programme of study leading to the award of Doctor of Philosophy is entirely my own work, and that I have exercised reasonable care to ensure that the work is original, and does not to the best of my knowledge breach any law of copyright, and has not been taken from the work of others save and to the extent that such work has been cited and acknowledged within the text of my work.

Signed :

Candidate ID No. 12212419

Date : 28th August, 2019

Acknowledgement

This thesis is dedicated to my family at home in Carnone, Co. Donegal.

I wish to thank Dr. Ronan Murphy for the opportunity to do this PhD in his lab. I also wish to thank all those in the School of Health & Human Performance, School of Biotechnology, and the Faculty of Science & Health for their help and support over the years. Particular thanks to my thesis supervisory panel for their much-appreciated input and advice. Thanks also to the technical staff for their support and friendship over the years.

I made many friends and colleagues during my time in DCU. Thank you to all the XB11/XB20 lab gang who were there when I began (Brian, Ciaran, Shan and Alisha), and to those who joined along the way (Hannah, Emma, Mary Rose and Róisín), we all became lab family, with a shared experience and bond that will never be forgotten. Laura and I had many adventures in XB20, and life was never dull! Special thanks to Keith (now Assistant Prof. Keith!), with whom I engaged in many endeavours, some academic, …..some less so! John and Aidan, Success Inc.'s constant clients, were always around, as were Richie and Anna while on the run from Yeal; not forgetting Red Bucket, the lab ice bucket with its own Twitter account!

Scone Thursday, my favourite day of the week, became a weekly group therapy session with its own cult following (and monthly magazine)!

These combined experiences have shaped me both as a researcher and as a person, and I am extremely grateful for them all.

Publications (in chronological order)

Wallace, R. G., Twomey, L. C., Custaud, M.-A., Moyna, N., Cummins, P. M., Mangone, M. and Murphy, R. P. (2016) Potential Diagnostic and Prognostic Biomarkers of Epigenetic Drift within the Cardiovascular Compartment, *Biomed Res. Int.*

McGinn, C. M., MacDonnell, B. F., Shan, C. X., **Wallace, R.**, Cummins, P. M. and Murphy, R. P. (2016) Microparticles: A pivotal nexus in vascular homeostasis and disease, *Curr. Clin. Pharmacol*., **11**(1).

Forde, H., Harper, E., Davenport, C., Rochfort, K. D., **Wallace, R**., Murphy, R. P., Smith, D. and Cummins, P. M. (2016) The beneficial pleiotropic effects of tumour necrosis factor-related apoptosis-inducing ligand (TRAIL) within the vasculature: A review of the evidence, *Atherosclerosis*, **247**.

Duffy, E., Guzman, K. De, **Wallace, R.**, Murphy, R. and Morrin, A. (2017) Non-Invasive Assessment of Skin Barrier Properties: Investigating Emerging Tools for In Vitro and In Vivo Applications, *Cosmetics*, **4**(4).

de Abreu, S., Amirova, L., Murphy, R**., Wallace, R.**, Twomey, L., Gauquelin-Koch, G., Raverot, V., Larcher, F., Custaud, M.-A. and Navasiolava, N. (2017) Multi-system deconditioning in 3-day dry immersion without daily raise, Front. Physiol., **8**(10).

Degryse, B., Britto, M., Shan, C X., **Wallace, R.G.**, Rochfort, K.D., Cummins, P. M., Meade, G. and Murphy, R.P. (2017) Data on the regulation of moesin and merlin by the urokinase receptor (uPAR): Model explaining distal activation of integrins by uPAR, *Data Brief*, **15**.

Degryse, B., Britto, M., Shan, C.X., **Wallace, R.G.**, Rochfort, K.D., Cummins, P. M., Meade, G. and Murphy, R.P. (2017) Moesin and merlin regulate urokinase receptor-dependent endothelial cell migration, adhesion and angiogenesis, *Int. J. Biochem. Cell Biol*., **88**.

Wallace, R.G., Twomey, L.C., Custaud, M.-A., Turner, J. D., Moyna, N., Cummins, P.M. and Murphy, R.P. (2018) The role of epigenetics in cardiovascular health and ageing: A focus on physical activity and nutrition, *Mech. Ageing Dev.*

Oral Presentations

Wallace R.G. & Murphy R.P. **Organotypic Modelling**. School of Health & Human Performance, Research Day, 5 February, 2018, Dublin City University, Dublin.

Poster presentations (in chronological order)

Wallace RG., Twomey LC., Deering A., Ghrefa Z., O'Neill E., Fitzpatrick B., Cummins PM. & Murphy RP. **Organotypic Modelling Techniques to Screen and Elucidate Molecular Mechanisms of Action and Cellular Effect.** Nutramara Conference (Harnessing Marine Bioresources for Innovations in the Food Industry), 29-30 June 2015, Royal Dublin Society (RDS), Dublin.

Wallace RG., Twomey LC., Fitzpatrick B., Cummins PM. & Murphy RP. **An Investigation into the Effects of Seawater-Derived Magnesium on Cellular Function using Organotypic Modelling Techniques.** International Society for the Development of Research (SDRM) Magnesium in Health & Disease (XIV International Magnesium Symposium), 23-24 June, 2016, Rome, Italy

Wallace RG., Twomey LC., Fitzpatrick B., Cummins PM. & Murphy RP. **An Investigation into the Health Benefits of Oriel Mineral Complex using Cellular and Molecular Analytical Techniques.** Industry Research and Development Group

(IRDG) Conference (Unleashing the power of Innovation), 27 October, 2016, The Helix, Dublin City University, Dublin

Wallace RG., Brady AJ., Hurley N., Fitzpatrick B., Cummins PM. & Murphy RP. **Investigation of Thermal Burn Injuries Using *In Vitro* Organotypic Modelling Techniques.** Opportunities for Wearables in Skin Diagnostics Conference, 26 September, 2017, Dublin City University, Dublin

* **Wallace RG.**, Kenealy MR., Egan B., Cummins PM., Murphy RP. **An Investigation into Epigenetic Regulation of the Vascular Endothelium through Organotypic Modelling.** Irish Postgraduate Research Conference, 9 November, 2018, Dublin City University, Dublin

* Winner of Best Research Poster

Wallace RG., Kenealy, MR., Murphy RP. **Development of a Novel *In Vitro* Burn Model.** Biological Research Society Research Day, 25 January, 2019, Dublin City University, Dublin

Table of contents

Abbreviations xiii

Units xv

List of figures xvi

List of tables xxi

Abstract xxiv

Chapter One: Introduction 1

1.1 Background 3

1.2 The cardiovascular system 3

1.2.1 Blood 6

1.2.2 Endothelial cells 6

1.2.3 Vascular Smooth Muscle Cells (VSMCs) 9

1.2.4 The effect of blood pressure and pulse on vasculature 10

1.3 Vascular inflammation 11

1.3.1 Cardiovascular disease – vasculature gone wrong 12

1.3.2 Atherosclerosis 13

1.3.3 Causative factors of atherosclerosis 16

1.4 Mechanisms of arterial re-modelling 17

1.4.1 Influence of blood flow pattern 18

1.5 Epigenetic regulation 22

1.5.1 The epigenetic clock and vascular ageing 26

1.5.2 Epigenetic heritability 29

1.5.3 Blood-based biomarkers of epigenetic change 30

1.6 MicroRNA as agents of epigenetic change 31

1.7 Obesity and the effect of exercise on vasculature 35

1.8 Nutrition as an agent of epigenetic change 37

1.9 Magnesium and cardiovascular health 39

1.10 Complex systems as models of inflammation 42

1.10.1 An overview of human dermal tissue and its response to injury 42

1.10.2 Burn modelling as an experimental approach 46
1.10.3 Burn recovery 48
1.10.4 Burn Dressings as Therapeutic Delivery Agents 49
1.11 Study hypotheses and objectives 51
1.11.1 Study 1: Profiling the epigenetic effects of oscillatory shear stress on vascular endothelium 51
1.11.2 Study 2: Exploring the use of magnesium as an anti-inflammatory agent 51
1.11.3 Study 3: Exploring the use of magnesium as an anti-inflammatory agent in a multicellular model of inflammation 52
1.11.4 Study 4: Investigating the systemic circulatory effects of Mg supplementation explored as a human trial 52
Chapter Two: Materials and methods 53
2.1 Materials 54
2.1.1 Reagents, chemicals and consumables 54
2.1.3 Preparation of stock solutions and buffers 61
2.1.3.1 Magnesium dilutions 61
2.2 Methods 62
2.2.1 Cells and culturing techniques 62
2.2.1.1 Culture of Human Aortic Endothelial Cells (HAECs) 62
2.2.1.2 Culture of Normal Human Dermal Fibroblast Cells (NHDFs) 62
2.2.1.3 Culture of Human Epidermal Keratinocyte Cells (HEKCs) 63
2.2.1.4 LabSkin™ 3D skin model 63
2.2.1.5 Trypsinisation of cells 64
2.2.1.6 Cryogenic preservation and recovery of cells 64
2.2.2 Cell counting 65
2.2.2.1 ADAM^{MC} cell counter (Digital Bio, Korea) 65
2.2.2.2 Haemocytometer 66
2.2.3 Ibidi® (Integrated BioDiagnostics®) cell perfusion system 67
2.2.4 Analysis of RNA expression 69
2.2.4.1 RNA isolation 69

2.2.4.2 TRIzol® RNA extraction (guanidinium thiocyanate-phenol-chloroform extraction) from 3D skin model biopsies and 2D monocultures 70
2.2.4.3 *mir*Vana™ miRNA isolation kit 71
2.2.4.4 Quantification of RNA by NanoDrop® 1000 spectrophotometer 73
2.2.5 Polymerase Chain Reaction (PCR) techniques 74
2.2.5.1 Reverse transcription of miRNA 75
2.2.5.2 Reverse transcription/cDNA synthesis for miRNA TLDA arrays 76
2.2.5.3 Taqman® miRNA arrays 77
2.2.5.4 Pre-amplification and cDNA synthesis of RNA for analysis using Qiagen RT^2 Profiler arrays 79
2.2.5.5 Genomic DNA elimination 79
2.2.5.6 Reverse transcription of RNA for analysis using Qiagen RT^2 Profiler arrays 80
2.2.5.7 Pre-Amplification of cDNA for analysis using Qiagen RT^2 Profiler arrays 81
2.2.5.8 qRT-PCR using RealTime Ready (RTR) assays (Roche) 83
2.2.6 qRT-PCR data and bioinformatical analysis 84
2.2.6.1 qRT-PCR gene analysis and QC for RT^2 arrays 84
2.2.6.2 Data Filtration for miRNA/mRNA Analysis 85
2.2.6.3 Joint miRNA/mRNA Analysis 85
2.2.7 Analysis of protein biomarkers in platelet-poor plasma 85
2.2.7.1 Isolation of platelet-poor plasma from whole blood 85
2.2.7.2 Human Protein Biomarker Assay - Proseek® Multiplex Immunoassay* (* as performed in collaboration with Olink, Sweden) 86
2.2.7.3 Proseek® (Olink, Sweden) Sample Preparation 87
2.2.8 Whole cell analysis techniques 88
2.2.8.1 Immunocytochemistry 88
2.2.8.2 Confocal Microscopy using the Zeiss 710 89
2.2.8.3 xCELLigence® Real Time Cell Analysis 89
2.2.8.4 xCELLigence® adhesion assays 91
2.2.8.5 xCELLigence® cell migration assay 92
2.2.8.6 Crystal violet adhesion assay 93
2.2.8.7 Wound healing cell migration assay 94
2.2.8.8 Angiogenic tube formation assay 94

2.2.8.9 Determination of Reactive Oxygen Species (ROS) by flow cytometry using dihydroethidium (DHE) staining 95
2.2.8.10 Determination of oxidative stress in plasma samples by ELISA using 8-hydroxydeoxyguanosine (8-OHdG) 98
2.2.8.11 Assessment of platelet adhesion and aggregation by Impact-R cone and plate analysis 99
2.2.8.12 Application of burn insult to *in vitro* 3D skin model 100
Figure 2.17 Custom-milled brass burn weights used to inflict reproducible burn insults to LabSkin™ (Innovenn) in vitro 3D skin models 101
2.2.9 Human Intervention 101

Chapter Three: Genetic and epigenetic response of HAECs to oscillatory shear stress 103

3.1 Introduction 104
3.1.1 Study aims 105
3.2 Results 107
3.2.1 Suitability of the Ibidi® perfusion system as a method of mimicking the *in vivo* shear condition in HAECs 107
3.2.2 Inflammatory response of HAECs to oscillatory shear stress. 107
3.2.3 Impact of 24 h oscillatory flow on epigenetic gene expression in HAECs 108
3.2.4 Impact of 48 h oscillatory flow on epigenetic gene expression in HAECs 108
3.2.5 Impact of 72 h oscillatory flow on epigenetic gene expression in HAECs 109
3.2.6 Impact of oscillatory flow on miRNA gene expression in HAECs 110
3.2.7 Bioinformatic analysis of mMR:miRNA expression patterns: 24 h 110
3.2.8 Bioinformatic analysis of n = 3 mRNA:miRNA expression patterns: 48 h 111
3.2.8 Bioinformatic analysis of mRNA:miRNA expression patterns: 72h 111
3.3 Discussion 127
3.3.1 The effect of oscillatory shear (OSS) on mRNA/miRNA expression at 24 h 129

3.3.2 The effect of OSS on mRNA/miRNA expression at 48 h 131
3.3.3 The effect of OSS on mRNA/miRNA expression at 72 h 133
3.4 Summary 134

Chapter Four: HAEC response to magnesium in the presence of pro-inflammatory oscillatory shear stress 135

4.1 Introduction 136
4.2 Results 140
4.2.1 Cytotoxicity of OMC to HAECs 140
4.2.2 Crystal violet viability study on HAECs exposed to varying concentrations of OMC Mg 141
4.2.3 HAEC adhesion response to 10mM magnesium 141
4.2.4 Down-regulation of inflammatory marker genes, ICAM-1 and VCAM-1, when exposed to 10mM Mg in a pro-inflammatory model 142
4.2.5 HAEC Magnesium receptor response to 10mM magnesium after 48 h exposure to oscillatory shear stress 142
4.2.6 HAEC epigenetic-associated gene response to 10mM magnesium after 48 h exposure to oscillatory shear stress 143
4.2.7 10mM Mg elicits no effect on ROS production in HAECs exposed to TNF-α for 12 h 144
4.3 Discussion 150
4.3.1 HAEC Adhesion response to Mg 150
4.3.2 HAEC response to 10mM Mg in a simulated inflammatory environment 154
4.3.3 Effect of 10mM Mg on HAEC magnesium receptors 155
4.3.4 HAEC Epigenetic gene response to 10mM Mg in a pro-inflammatory vascular endothelial model 157
4.3.4.1 Effect of 10mM Mg on epigenetic enzymes (SETD6, AURKB and DOT1L) in a pro-inflammatory vascular endothelial model 157
4.3.4.2 Effect of 10mM Mg on epigenetic modification factors (PAK1, NCOA3 & BRD7) in a pro-inflammatory vascular endothelial model 158
4.4 Summary 161

Chapter Five: The effect of 10mM magnesium treatment on an *in vitro* multicellular skin burn model 163

5.1 Introduction 164

5.2 Results 167

5.2.1 The Effect of Control (unburned) v Burn (untreated) on wound healing mRNA expression in 3D skin model, 24 h post-burn (n = 3) 167

5.2.2 The Effect of Control (untreated burn) v Burn (hydrogel /- OMC) on wound healing mRNA expression in 3D skin model, 24 h post-burn (n = 3) 168

5.2.3 The Effect of Control (untreated burn) v Burn (hydrogel /+ OMC) on wound healing mRNA expression in 3D skin model, 24 h post-burn (n = 3) 168

5.2.4 The Effect of Control (hydrogel /- OMC) v Burn (hydrogel /+ OMC) on wound healing mRNA expression in 3D skin model: 24 h post-burn (n = 3) 168

5.2.5 The Effect of Control (unburned) v Burn (untreated) on fibrotic mRNA expression in 3D skin model, 24 h post-burn (n = 3) 169

5.2.6 The Effect of Control (untreated burn) v Burn (hydrogel /- OMC) on wound healing mRNA expression in 3D skin model, 24 h post-burn (n = 3) 169

5.2.7 The Effect of Control (untreated burn) v Burn (hydrogel /+ OMC) on wound healing mRNA expression in 3D skin model, 24 h post-burn (n = 3) 169

5.2.8 The Effect of Control (hydrogel /- OMC) v Burn (hydrogel /+ OMC) on wound healing mRNA expression in 3D skin model: 24 h post-burn (n = 3) 169

5.2.9 The effect of 10mM Mg on HAEC migration 170

5.2.10 The effect of 10mM Mg on wound closure in HAECs 171

5.2.11 The effect of 10mM Mg on NHDFC migration 171

5.2.12 The effect of 10mM Mg on wound closure in NHDFCs 172

5.2.13 The effect of 10mM Mg on HAKC migration 172

5.2.14 The effect of 10mM Mg on wound closure in HAKCs 173

5.2.15 The effect of 10mM Mg on tube formation in HAECs 174

5.3 Discussion 192

5.3.1 The effect of hydrogel (/+ OMC) on wound healing gene expression 24 h post-burn 192

5.3.2 The effect of hydrogel (/+ OMC) on fibrosis gene expression 24 h post-burn 195

5.3.2 Examination of the functional response of dermal cells to 10mM Mg treatment 197

5.4 Summary 202

Chapter Six: An examination of the functional effects of OMC as part of a dietary supplement in a randomised controlled intervention in middle-aged women 224

6.1 Introduction 205

6.1.2 Study design 207

6.1.3 Study aims 209

6.2 Results 210

6.2.1 The effect of OMC + *Boswellia serrata* supplementation on platelet function in a randomised population of 16 healthy women (45-65 years) 210

6.2.1.2 Platelet aggregation 211

6.2.2 The effect of OMC + *Boswellia serrata* supplementation on protein biomarker concentrations in a randomised population of 16 healthy women (45-65 years) 211

6.2.3 The effect of OMC + *Boswellia serrata* supplementation on ROS levels in a randomised population of 16 healthy women (45-65 years) 212

6.3 Discussion 216

6.4 Summary 220

Chapter Seven: Overall summary 222

7.1 Final discussion 223

7.2 The efficacy of OMC as an anti-inflammatory agent 223

7.3 Summary 225

7.4 Limitations and future work 226

7.4.1 Chapter Three and Four limitations and future work 226

Bibliography 230

Appendices 264

Abbreviations

µ	Micro
ABP	Actin-binding Protein
ADAM	Advanced Detection and Accurate Measurement
APC	Antigen-presenting Cell
ApoE-/-	Apolipoprotein-E knockout
Argo2	Argonaute 2
ATP	Adenosine Triphosphate
BCA	Bicinchonic Acid Assay
BMI	Body Mass Index
BSA	Bovine Serum Albumin
CCD	Charged Couple Device
Ca^{-}	Calcium ion
CO_2	Carbon Dioxide
CV	Coefficient of variance
CVD	Cardiovascular Disease
dH_2O	Distilled Water
DMSO	Dimethlysulphoxide
DNA	Deoxyribonucleic Acid
ECGS	Endothelial Cell Growth Supplement
ECM	Extra-cellular Matrix
EDTA	Ethylenediaminetetraacetic Acid
ELISA	Enzyme-Linked Immunosorbent Assay
FBS	Fetal Bovine Serum
FITC	Fluorescein isothiocyanate
GPI	Glycosyl Phosphatidylinositol
H_2O_2	Hydrogen Peroxide
HAECs	Human Aortic Endothelial Cells
HDKCs	Human Dermal Keratinocyte Cells
HRP	Horseradish Peroxidase

ICAM	Intracellular Adhesion Molecule
IL	Interleukin
JAM	Junctional Adhesion molecule
K^+	Phosphate ion
LDL	Low-Density Lipoprotein
LFA	Leukocyte Function-associated Antigen
Mg	Magnesium
Mg^{2+}	Magnesium ion
$MgCl_2$	Magnesium chloride
miRNA	Micro Ribonucelic Acid
MMP	Matrix Metalloproteinase
MP	Microparticle
mRNA	Messenger Ribonucelic Acid
MV	Microvessicle
NADPH	Nicotinamide Adenine Dinucleotide Phosphate-oxidase
NF-κB	Nuclear Transcription Factor Kappa B
NGS	Next-Generation Sequencing
NHDFs	Normal Human Dermal Fibroblast cells
NKC	Natural Killer Cell
NKTC	Natural Killer T-Cell
NO	Nitric Oxide
OMC	Oriel Mineral Complex
Ox-LDL	Oxidised Low-Density Lipoprotein
PAF	Platelet-Activating Factor
PBS	Phosphate-Buffered Saline
PC	Personal Computer
PCR	Polymerase Chain Reaction
PCS	Photon Correlation Spectroscopy
PGI2	Prostacyclin
PI	Propidium Iodide

PMN	Polymorphonuclear
PET	Polyethylene Terephthalate
PPP	Platelet-Poor Plasma
PRP	Platelet-Rich Plasma
PS	Phosphatidylserine
qRT-PCR	Quantitative Real-Time Polymerase Chain Reaction
RA	Rheumatoid arthritis
RISC	RNA-Induced Silencing Complex
ROS	Reactive Oxygen Species
SMC	Smooth Muscle Cell
TIMP	Tissue Inhibitor of Matrix Metalloproteinase
TLDA	Taqman Low Density Array
TMB	Tetramethylbenzidine
TNF-α	Tumor Necrosis Factor Alpha
UTR	Untranslated Region
VCAM-1	Vascular Cell Adhesion Molecule 1
WBC	White Blood Cell

A comprehensive list of gene symbols used in the results chapters is provided in Appendix A.

Units

cm	Centimetre
cm^2	Centimetre squared
°C	Degree Celsius
$Dyne/cm^2$	Dyne per centimetre squared
η^2	Eta squared
g	Grams
h	Hour
Kb	Kilobase

Kg	Kilogram
L	Litre
m	Metre
m^2	Metre squared
Mg	Microgram
Mm	Micrometre
µL	Microlitre
µM	Micromolar
μm^2	Micrometers squared
mA	Milliamps
mL	Millilitre
mM	Millimolar
Min	Minute
M	Molar
Ng	Nanogram
Nm	Nanometre
nM	Nanomolar
Px	pixel
RPM	Revolution per minute
U	Enzyme Unit
v/v	Volume per volume
w/v	Weight per volume

List of Figures

Figure 1.1 Simplified diagram of the cardiovascular system showing blood flow and relative pressure

Figure 1.2 Structure of the human artery

Figure 1.3 Endothelial response to the vascular environment

Figure 1.4 European Union CVD statistics

Figure 1.5 Transition between healthy and atherosclerotic vessel status

Figure 1.6 Diagram illustrating differing types of shear stress and typical forces experienced at branching points in the arterial tree

Figure 1.7 Diagram illustrating the mechano-transductive stimuli of cyclical strain and shear stress on vasculature, both of which result in modification to the arterial wall

Figure 1.8 Illustration of epigenetic re-programming in vascular endothelial cells, where the extra-cellular stimulus results in modified genetic architecture, ultimately leading to altered gene transcription and lower disease threshold

Figure 1.9 Epigenetic drift over time can result in measurable differences between physiological and chronological age

Figure 1.10 DNA methylation (writing, reading and erasing) represents one of a number of means through which epigenetic modification of DNA can occur

Figure 1.11 Simple diagram illustrating miRNA biogenesis and action

Figure 1.12 Total Mg distribution

Figure 1.13 Diagram of healthy skin, indicating morphologically-distinct sub layers

Figure 1.14 Diagram illustrating skin burn damage progression from healthy skin through to third-degree burn

Figure 1.15 Burn wound healing and angiogenesis following inflammatory phase

Figure 2.1 Phase contrast microscopy images (100X magnification) of cells used throughout this thesis

Figure 2.2 ADAM^{MC} electronic cell counter and AccuChip™ system principle of operation

Figure 2.3 Ibidi® fluidic unit, perfusion tubing, and μ-slides used for simulation of various physiological vascular conditions (continuous unidirectional, oscillating, and pulsatile flow) *in vitro*

Figure 2.4 Illustration of phase separation during TRIzol® RNA extraction

Figure 2.5 Diagram illustrating the main steps of the *mir*Vana™ centrifugation protocol used to isolate total RNA/miRNA from DNA and other contaminants

Figure 2.6 Nanodrop® 1000 spectrophotometer (used in conjunction with operating software v3.8.1) manufactured by Thermo Scientific Ltd.

Figure 2.7 Extension and reverse transcription of miRNA targets using miRNA-specific stem-loop primers

Figure 2.8 Illustration outlining the process of loading sample into a TLDA card

Figure 2.9 Qiagen RT^2 Profiler array gene/control layout

Figure 2.10 Isolation of platelet-poor plasma from whole blood by centrifugation

Figure 2.11 Principles by which Proseek® (Olink, Sweeden) assay sensitivity is achieved

Figure 2.12 Diagram illustrating xCELLigence® RTCA DP instrument, E-Plate® and the principle of cellular electrical impedance measurement

Figure 2.13 Overview of the crystal violet cell adhesion/viability assay

Figure 2.14 Illustration of the Guava® easyCyte 8HT (Millipore) flow cytometer and principle of operation (inset)

Figure 2.15 Conversion of dihydroethidium to 2-hydroxyethidium by superoxide and to ethidium in the presence of reactive oxygen species

Figure 2.16 Impact-R (DiaMed), showing the cone and plate principle (inset) by which platelet adhesion and aggregation are measured under arterial flow conditions

Figure 2.17 Custom-milled brass burn weights used to inflict reproducible burn insults to LabSkin™ (Innovenn) *in vitro* 3D skin models

Figure 3.1 Diagram outlining the experimental approach taken in Chapter Three

Figure 3.2 Effect of shear stress on HAEC morphology and F-actin realignment

Figure 3.3 Effect of shear stress on endothelial nitric oxide synthase (eNOS) expression in HAECs

Figure 3.4 Effect of laminar (control) v oscillatory flow on epigenetic enzyme mRNA expression in HAECs, 24, 48 & 72 h, 10 dyne/cm^2

Figure 3.5 Effect of laminar (control) v oscillatory flow on chromatin modification factor mRNA expression in HAECs, 24, 48 & 72 h, 10 dyne/cm^2

Figure 3.6 Effect of laminar (control) v oscillatory flow on epigenetic enzyme mRNA expression in HAECs, 48 h, 10 dyne/cm^2 (n = 3)

Figure 3.7 Effect of laminar (control) v oscillatory flow on chromatin modification factor mRNA expression in HAECs, 48 h, 10 dyne/cm^2 (n = 3)

Figure 3.8 Time course of endothelial activation

Figure 4.1 Diagram outlining the experimental approach taken in Chapter Four

Figure 4.2 xCELLigence® adhesion profile of HAECs treated with varying concentrations of OMC Mg for 24 h

Figure 4.3 Crystal violet adhesion data for HAECs treated with varying concentrations of Mg (OMC only) for 24 h.

Figure 4.4 xCELLigence® adhesion profile of HAECs treated with different Mg sources (10mM) for 24 h. (First 10 h shown only)

Figure 4.5 Down-regulation of inflammatory marker genes, ICAM-1 and VCAM-1, exposed to 10mM Mg in a pro-inflammatory OSS models

Figure 4.6 HAEC magnesium receptor response to 10mM magnesium in the presence of oscillatory shear stress after 48 h

Figure 4.7 Effect of 10mM Mg on a range of putative gene targets (identified in Results Chapter Three) in the presence of oscillatory shear stress after 48 h

Figure 4.8 Effect of 10mM Mg on ROS production in HAECs exposed to TNF-α

Figure 4.9 Magnesium contribution to endothelial dysfunction

Figure 4.10 Node diagram illustrating PAK1 interactions with other proteins, including members of the Rac and Rho family

Figure 5.1 Diagram outlining the experimental approach taken in Chapter Five

Figure 5.2 Effect of hydrogel (/± OMC) v burn on wound healing mRNA expression 24 h post-burn

Figure 5.3 Effect of hydrogel (/± OMC) v burn on fibrosis mRNA expression 24 h post-burn

Figure 5.4 xCELLigence® migration profile of HAECs treated with different Mg forms (10mM) for 24 h (first 15 h shown only)

Figure 5.5 Effect of 10mM Mg on wound healing in HAECs

Figure 5.6 xCELLigence® migration profile of NHDFCs treated with different Mg forms (10mM) for 24 h. (First 15 h shown only).

Figure 5.7 Effect of 10mM Mg on wound healing in NHDFCs

Figure 5.8 xCELLigence® migration profile of HAKCs treated with different Mg forms (10mM) for 24 h. (First 15 h shown only)

Figure 5.9 Effect of 10mM Mg on wound healing in HAKCs

Figure 5.10 Effect of 10mM Mg on HAEC tube formation/sprouting

Figure 6.1 Diagram outlining the experimental approach taken in Chapter Six

Figure 6.2 Platelet adhesion and aggregation as markers of overall health in placebo and treatment groups post- 28-day intervention

Figure 6.3 Plot representations of significantly changed protein concentrations between placebo and treatment groups post-intervention

Figure 6.4 Measurement of 8-hydroxy-2'-deoxyguanosine (8-OHdG) as a biomarker for oxidative stress in placebo and treatment groups post-intervention

List of Tables

Table 1.1 Differences in tissue response to second-degree (partial) and third-degree (full-thickness) burn injuries

Table 1.2 Advantages/disadvantages of a range of alternative skin testing models

Table 2.1 Chemical make-up of magnesium forms used in this thesis

Table 2.2 OMC mineral component concentration when magnesium was normalised to 10mM

Table 2.3 Reverse transcription mastermix for miRNA Pools A & B (Applied Biosystems™)

Table 2.4 Thermocycling conditions for miRNA-specific reverse transcription reaction

Table 2.5 Component mixture for miRNA array sample when using pre-amplified product

Table 2.6 Real-time thermocycling conditions for miRNA TLDA cards

Table 2.7 Genomic elimination mix

Table 2.8 Reverse transcription mix

Table 2.9 Pre-amplification mix

Table 2.10 Thermocycling conditions for pre-amplification of cDNA for Qiagen RT^2 Profiler arrays

Table 2.11 PCR mastermix components of RT^2 Profiler arrays

Table 2.12 Thermocycling conditions for RT^2 Profiler arrays optimised for use with the Applied Biosystems 7900HT Real-Time PCR instrument

Table 2.13 PCR mix for RTR assays (Roche)

Table 2.14 ROS assay acquisition parameters for Guava® easyCyte 8HT

Table 3.1 Effect of laminar (control) v oscillatory flow on epigenetic enzyme mRNA expression in HAECs: 24 h, 10 dyne/cm^2 (n = 1)

Table 3.2 Effect of laminar (control) v oscillatory flow on epigenetic chromatin modification factor mRNA expression in HAECs: 24 h, 10 dyne/cm^2 (n = 1)

Table 3.3 Effect of laminar (control) v oscillatory flow on epigenetic enzyme mRNA expression in HAECs: 48 h, 10 dyne/cm^2 (n = 3)

Table 3.4 Effect of laminar (control) v oscillatory flow on epigenetic chromatin modification factor mRNA expression in HAECs: 48 h, 10 dyne/cm^2 (n = 3)

Table 3.5 Effect of laminar (control) v oscillatory flow on epigenetic enzyme mRNA expression in HAECs: 72 h, 10 dyne/cm^2 (n = 1)

Table 3.6 Effect of laminar (control) v oscillatory flow on epigenetic chromatin modification factor mRNA expression in HAECs: 72 h, 10 dyne/cm^2 (n = 1)

Table 3.7 Top 20 miRNA up-regulation fold changes in laminar (control) v oscillatory flow in HAECs: 24 h, 10 dyne/cm^2 (n = 1)

Table 3.8 Top 20 miRNA up-regulation fold changes in laminar (control) v oscillatory flow in HAECs: 48 h, 10 dyne/cm^2 (n = 3)

Table 3.9 Top 20 miRNA up-regulation fold changes in laminar (control) v oscillatory flow in HAECs: 72 h, 10 dyne/cm^2 (n = 1)

Table 3.10 Top 5 overlapping predicted miRNA:mRNA interactions: 24 h (n = 1)

Table 3.11 Top 12 overlapping predicted miRNA:mRNA interactions: 48 h (n = 3)

Table 3.12 Top 12 overlapping predicted miRNA:mRNA interactions: 72 h (n = 1).

Table 5.1 The Effect of Control (unburned) v Burn (untreated) on wound healing mRNA expression in a 3D skin model, 24 h post-burn (n = 3)

Table 5.2 The Effect of Control (untreated burn) v Burn (hydrogel /- OMC) on wound healing mRNA expression in 3D skin model, 24 h post-burn (n = 3)

Table 5.3 The Effect of Control (untreated burn) v Burn (hydrogel /+ OMC) on wound healing mRNA expression in 3D skin model, 24 h post-burn (n = 3)

Table 5.4 The Effect of Control (hydrogel /- OMC) v Burn (hydrogel /+ OMC) on wound healing mRNA expression in 3D skin model: 24 h post-burn (n = 3)

Table 5.5 Healthy (unburned) control v burn (no treatment) on fibrosis mRNA expression in 3D skin model, 24 h post-burn (n = 3)

Table 5.6 Effect of untreated burn (control) v hydrogel (-OMC) on fibrosis mRNA expression in 3D skin model, 24 h post-burn (n = 3)

Table 5.7 Effect of hydrogel-OMC (control) v hydrogel+OMC on fibrosis mRNA expression in 3D skin model: 24 h post-burn (n = 3)

Table 5.8 Effect of hydrogel-OMC (control) v hydrogel+OMC on fibrosis mRNA expression in 3D skin model: 24 h post-burn (n = 3)

Table 6.1 Anthropometric measurements for the OMC+BA supplement human intervention

Table 6.2 Anthropometric measurements for the OMC+BA supplement human intervention as separate groups

Abstract

Models of vascular injury and the potential therapeutic benefits of magnesium supplementation

Robert Wallace

Epigenetic modification, the accumulation of distinct chemical signatures on DNA and histones, are initially established during embryogenesis and continue to be modified by age and lifestyle choices throughout life. Expression of non-coding RNA, such as microRNA (miRNA), play a regulatory role in gene expression as well as epigenetic mechanisms. Blood vessels are readily capable of re-modelling their structures in response to hemodynamic prompts associated with variations in blood flow. Injurious oscillatory shear stress (OSS) associated with atherosclerosis, in particular, is believed to exert a damaging influence on the health and epigenetic processes of the vascular endothelium. Vascular inflammation is a key contributor to cardiovascular diseases (CVD), with inflammation and CVD risk factors closely inter-related. Atherosclerosis, the most common of the vascular inflammatory diseases, is defined as chronic, specifically affecting arterial blood vessels, and caused by dynamic dysfunction of endothelium. For the initial part of this work, we employed an endothelial cell model of OSS to investigate the relationship between miRNA expression and epigenetic mechanisms during an atherosclerotic challenge. Our results show that human aortic endothelial cells (HAECs) exhibit a clear epigenetic response to OSS in a time-dependent manner, most pronounced at 48 h.

Using our established OSS model, we next examined the anti-inflammatory response of the endothelium to a magnesium-based seawater extract in comparison to other forms of magnesium. Nutritional magnesium supplementation may act beneficially through epigenetic mechanisms, as well as traditional cellular and molecular pathways. In parallel with this, a human trial to assess the beneficial effects of a magnesium-based supplement mixture on vascular competence was conducted. Our results indicate that magnesium elicits beneficial effects on platelets and the vascular compartment through reduced platelet adhesion and aggregation.

We finally investigated the anti-inflammatory effects of magnesium supplementation on an *in vitro* dermal burn model, which included examining the ability of magnesium

to improve the angiogenic and migratory potential of endothelial cells, an essential feature of the wound healing process. Our results indicate that magnesium constitutes an important molecular constituent in this process, leading to amplified expression of a number of wound healing mechanisms and increasing response at a cellular level. As such, the inclusion of magnesium as a therapeutic aid in the stabilisation of burn injuries is a warranted addition.

Chapter One

Introduction

Excerpts from the following peer-reviewed publications have been included in this chapter:

Wallace, R.G., Twomey, L.C., Custaud, M.-A., Moyna, N., Cummins, P.M., Mangone, M. and Murphy, R.P. (2016) Potential Diagnostic and Prognostic Biomarkers of Epigenetic Drift within the Cardiovascular Compartment, *Biomed Res. Int.*

Wallace, R.G., Twomey, L.C., Custaud, M.-A., Turner, J.D., Moyna, N., Cummins, P.M. and Murphy, R.P. (2018) The role of epigenetics in cardiovascular health and ageing: A focus on physical activity and nutrition, *Mech. Ageing Dev.*

1.1 Background

Cardiovascular disease (CVD) remains a leading cause of mortality around the world, accounting for >4 million deaths annually in Europe alone, and a total cost of €210 billion in healthcare bills annually. While some aspects of developing CVD have been attributed to hereditary processes, additional risk factors include environmental and lifestyle choices. Haemodynamic forces acting within blood vessels and the response of the vessel wall play an important role in cardiovascular health.

In this respect, this literature review will (i) provide a concise overview of the cardiovascular system and its composition with respect to inflammation and atherosclerosis; (ii) review the mechanisms of arterial re-modelling and the concepts of epigenetic regulation and vascular ageing; (iii) consider the implications of dietary supplementation and exercise on epigenetic alterations; (iv) examine dermal tissue as a complex system of inflammation that incorporates the vascular unit. Finally, the primary objectives of this thesis will be outlined.

1.2 The cardiovascular system

The cardiovascular system comprises the heart, arteries, and veins, and includes approximately 5 litres of blood transported by vessels (see Figure 1.1). It is distinct from the lymphatic system, which returns excess filtered blood plasma from interstitial fluid (between cells) as lymph fluid. The cardiovascular system is responsible for distributing nutrients and oxygen around the body, removing metabolic waste products, and assisting the immune system to prevent disease. It achieves these functions by circulating blood through two distinct "loops"; a circuit through the lungs whereby gaseous exchange occurs (pulmonary circulation); and a circuit through the rest of the body providing nutrients and dissolved oxygen to cells as well as sequestering metabolic wastes to the appropriate organ for elimination (systemic circulation). The human cardiovascular system is referred to as a "closed" system, as blood remains within the network of blood vessels. Nutrients and oxygen diffuse across blood vessel layers and subsequently interact with cells.

Arteries and veins consist of three distinct layers which differ somewhat in structure according to the function of the blood vessel (see Figure 1.2):

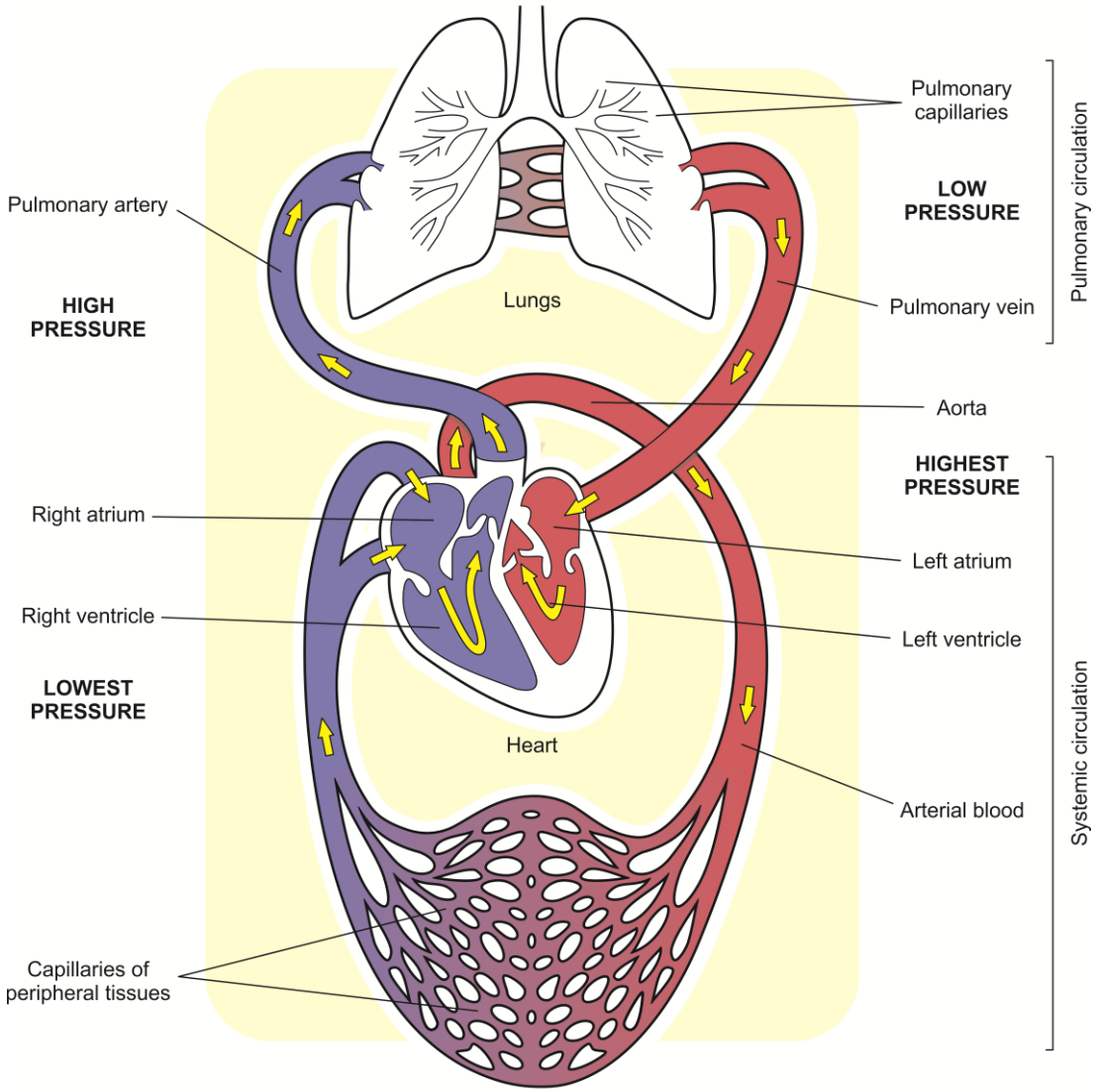

Figure 1.1 Simplified diagram of the cardiovascular system showing blood flow and relative pressure
Adapted from (Marieb, 2006)

- Tunica intima (thinnest layer): a monolayer of endothelial cells bound together by inter-endothelial junction complexes and surrounded by a thin layer of sub-endothelial connective tissue entwined with a number of circularly-arranged elastic bands called the internal elastic lamina.
- Tunica media (thickest layer in arteries): circularly-arranged elastic fibre, connective tissue, and polysaccharide substances. The second and third layers are separated by external elastic lamina. The tunica media may (especially in

arteries) contain large deposits of vascular smooth muscle tissue, which controls the internal diameter of the vessel.

- Tunica adventitia (thickest layer in veins) is made entirely of connective tissue. It also contains nerves that supply the vessel as well as nutrient capillaries (vasa vasorum) in larger blood vessels.
- Capillaries, in contrast, are simple structures, and consist of little more than a layer of endothelium resting on a basement membrane and occasional connective tissue.

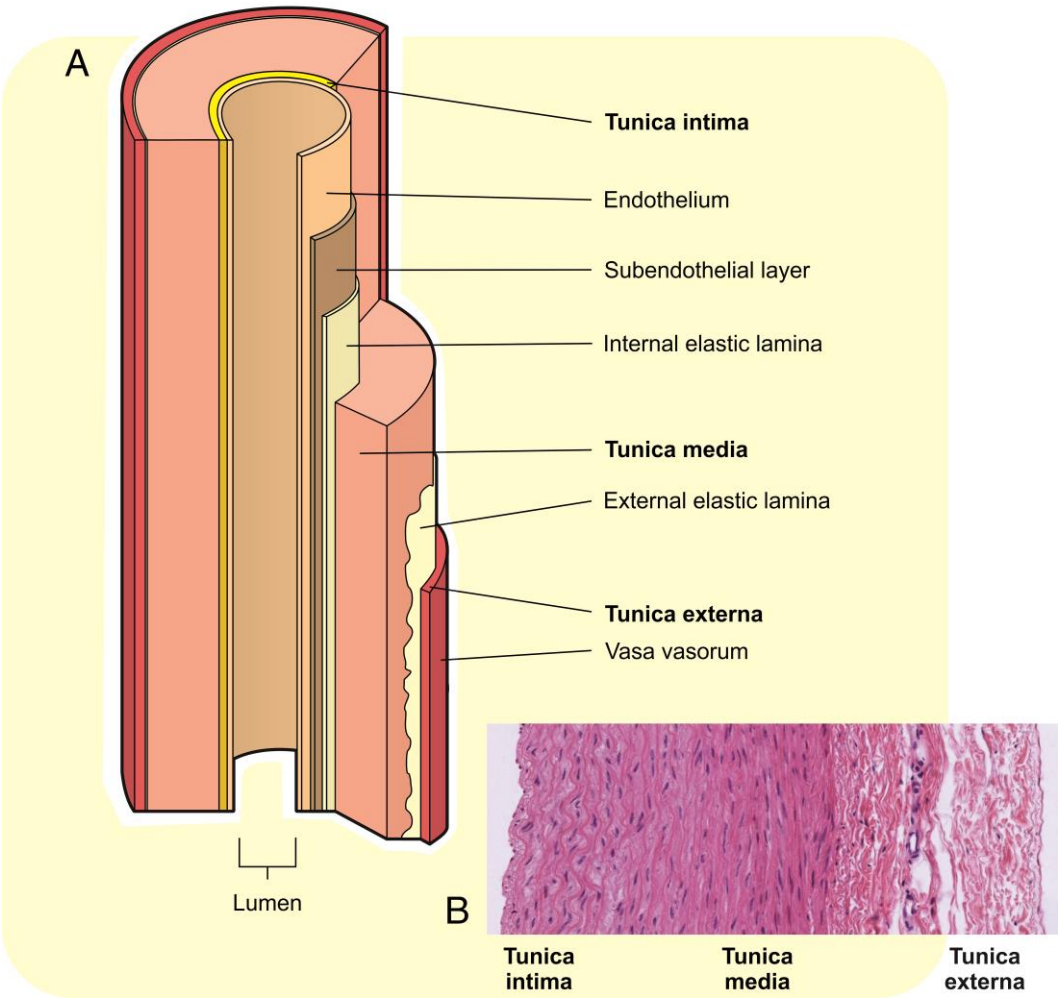

Figure 1.2 Structure of the human artery
A) Structural diagram of the human artery, highlighting the three main layers and architectural differences between them (adapted from Mescher & Junqueira 2013). B) Hematoxylin-eosin stained histological aortic section showing the three primary layers (Spitalnik, 2019)

While arteries, veins and capillaries differ in structure in order to best carry out their different functions, so too, does arterial structure diverge. The amount of

muscular/elastic tissue present in arteries varies dependent on its size and function. In larger arteries (near the heart), tunica media consists of more elastic tissue and less smooth muscle, thereby allowing the vessel to experience greater stretch, and hence, absorb the large pressure wave generated by the heart as it beats. In the smallest arteries (arterioles), tunica media consists almost entirely of smooth muscle tissue. This permits exact control over vessel diameter, which in turn, aids pressure regulation within (Waugh & Grant, 2008). Hence, rather than a static structure, the vascular system is a dynamic network, capable of adapting to the needs of the organism at the local physiological level. This standard of adaptation carries through to the cellular level, where vascular cells may develop specialised characteristics in order to best meet these requirements.

1.2.1 Blood

Blood is essentially composed of two principle components: plasma and cells. Plasma is the liquid component of blood, comprising a mixture of water (90-92%), sugars, fats, gases, hormones and proteins (eg. albumin, immunoglobulins, etc.). Other nutrients, vitamins and electrolytes are also contained within plasma. Plasma acts as a medium in which the cellular components of blood are suspended and transported. Plasma may be easily separated from whole blood by centrifugation, as cellular components sediment and plasma remains as supernatant. Plasma analysis may reveal a great deal of useful information about the health of the donor. As blood contains a number of different cell types, each with its own function, it is technically classified as a tissue. Blood cells are derived from pluripotent stem cells and are formed in red bone marrow via the highly regulated process of hematopoiesis. Hematopoietic stem cells are capable of giving rise to all other blood cells (erythrocytes, white blood cells, and platelets). These hematopoietic cells can be found circulating in blood/bone marrow in people of all ages, in addition to the umbilical cords of newborns.

1.2.2 Endothelial cells

Endothelial cells line the interior of blood vessels as a monolayer of cells around the lumen. Within the body as a whole, endothelial tissue provides signals for selective accumulation of specific tissue-resident lymphocytes. Many of these lymphocytes do

not recognise foreign antigens, but are instead activated by stress-induced "self" molecules. However, it is important to note that endothelium in different tissues is itself different, and as a result, gives rise to differing inflammatory characteristics (even if inducing agents are similar). This may be due, in a large part, to the sheer vastness of endothelium as it envelopes the entire vascular system in a monolayer of cells. So large is it, that it consists of an estimated 1×10^{13} cells and forms an organ almost 1 Kg in weight in an average adult (Sumpio *et al.*, 2002). Vascular endothelium surrounding different tissues is known to play a significant role in controlling inflammation and immune response (Strawn *et al.*, 1997). With regard to atherosclerosis, endothelium is a basic necessity of vasculature; isolating blood flow from underlying tissues. However, as a consequence of their strategic location between luminal blood flow and the underlying vessel wall (comprising smooth muscle cells and connective tissue), endothelial cells (ECs) are continually exposed to physical and chemical stimuli. It is at this interface that atherosclerosis occurs.

By providing an anti-coagulant boundary between the vessel contents (blood) and the vessel wall, blood is allowed to remain in a fluid state, with limited clot formation permitted, should vascular injury occur. This is a result of the body's necessity to achieve haemostasis, a process which recruits thrombocytes and causes bleeding to stop. ECs express a number of pro- and anti-coagulant mediators (see Figure 1.3). Differential distribution of such mediators is suggestive of the fact that ECs from different sites of the vascular tree use site-specific conditions to balance local haemostasis by altering total pro-coagulant : anti-coagulant ratios. This is further indicative of endothelial cell heterogeneity reacting to local environmental changes within vasculature (Aird, 2007a, 2007b).

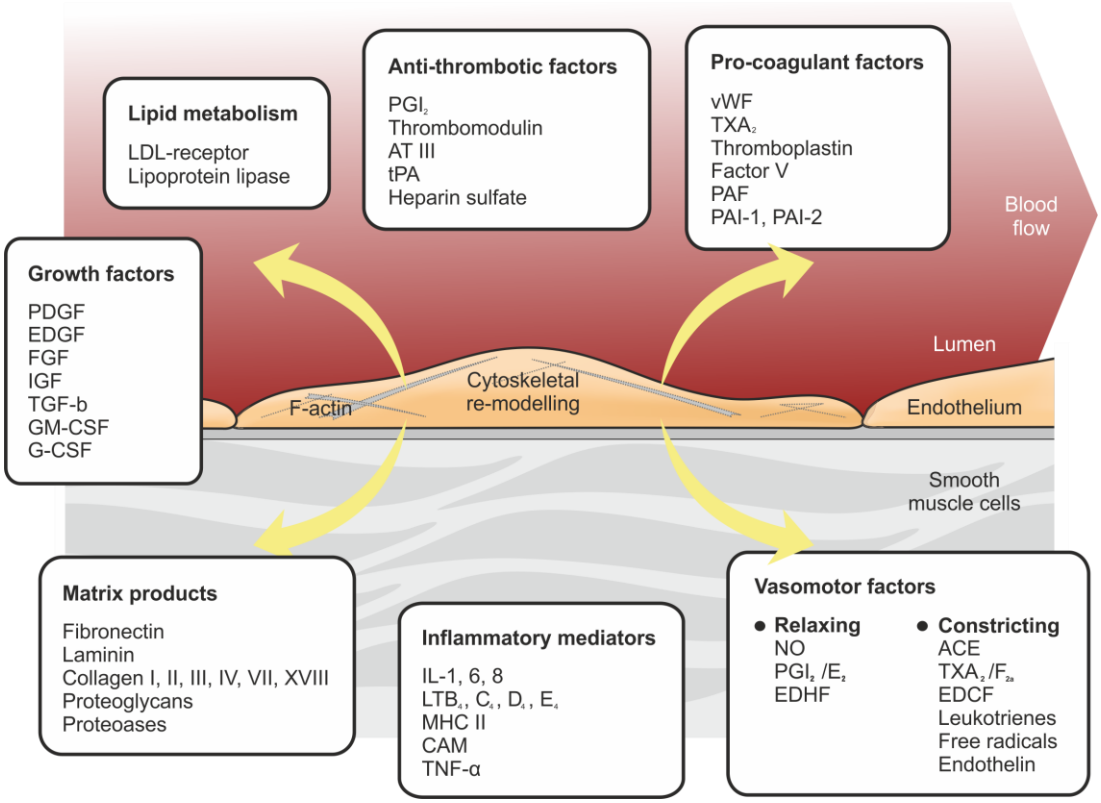

Figure 1.3 Endothelial response to the vascular environment (adapted from Sumpio *et al*. 2002)
Endothelial cells are capable of localised adaptive response to numerous stimuli, including haemodynamic force. Such responses include vasoactive substance release, and cytoskeletal re-organisation/polarisation due to complex bi-directional communication pathways.

The anti-coagulant EC barrier is highly regulated, allowing passage of select molecules through the vessel wall. Leukocytes, however, are prevented from gaining entry to the intima, as are other macromolecules. Endothelial permeability is sustained by regulated opposition of adherens and tight junctional proteins. In turn, these proteins are controlled by a number of pharmacological/physiological mediators (Alexander and Elrod, 2002). Gap junctions serve to connect vascular ECs, and allow electrochemical signals to travel along the vessel wall. Literature cites a number of different vascular functions in which these communication pathways have been implicated, including repair of endothelial lining, regulation of angiogenesis, and endothelial senescence (Pepper *et al.*, 1989). Endothelium may also effectively function as a paracrine/endocrine organ, with roles in immune response, coagulation, growth regulation, production of extracellular matrix components, and importantly, is a modulator of blood flow and blood vessel tone. This is accomplished by release of

vasoactive substances, such as prostacyclin (PGI_2), nitric oxide (NO) and platelet-activating factor (PAF) (Sumpio *et al.*, 2002). Such substances may, therefore, allow ECs to directly influence haemodynamic forces within vasculature. Importantly, research has shown that endothelial activation/dysfunction may be detected by measuring such changes in endothelium-dependent vasodilatation (Nakou *et al.*, 2008). These chemical compounds usually do not exist pre-formed in intracellular granules; rather, their major biologic effects depend on their rapid synthesis.

Atherosclerosis/inflammation is an undesirable state for vasculature, and as such, cells which comprise it take action to prevent its occurrence. Indeed, cells constantly strive to achieve homeostasis, a stable equilibrium, primarily via a number of feedback processes (Bazzoni and Dejana, 2004). In order to achieve such ends, endothelial cells modulate leukocyte interaction, and regulate cell motility (adhesion, migration, permeability and proliferation) and thus avoid development of disease. While ECs have been found to demonstrate paracrine/endocrine capacity, endothelial dysfunction results in an imbalance of vascular regulatory mechanisms; further inducing arterial wall damage. Certain areas of vasculature (particularly sites of bifurcations) are more prone to development of atherosclerosis than others (Townsend *et al.*, 2013). At atherosclerotic-prone regions, endothelial cells are exposed to cardiovascular risk factors which alter their net negative surface charge, losing their anti-thrombotic ability. Prolonged and/or repeated exposure to cardiovascular risk factors can ultimately deplete the protective effect of the endogenous anti-inflammatory system within. As a consequence, ECs may progress to senescence, lose their integrity, and detach into circulation (Ghinea *et al.*, 1987).

1.2.3 Vascular Smooth Muscle Cells (VSMCs)

Vascular smooth muscle cells comprise the majority of the vessel wall, particularly in arteries, where they must cope with larger pressures than veins. The main function of VSMCs is to regulate vascular tone by contracting or relaxing in order to change the carrying volume of blood vessels and alter local blood pressure.

It was first posited over ten years ago that intimal smooth muscle cells (SMCs) may arise from endothelium itself. Researchers theorised that embryonic aortic endothelial cells trans-differentiated into mesenchymal cells, some of which expressed smooth

muscle α-actin (SMα-actin). Characterisation of the *in vivo* phenotype of aortic ECs in chicken embryos led to an elucidation of mechanisms involved in transformation of endothelium into mesenchymal cells in thickened vessels. This thickening was believed to be a result of hemodynamic forces acting on the endothelium. Mesenchymal cells may persist either as non-muscle throughout development or alternatively convert to cells expressing SMα-actin (Arciniegas *et al.*, 2000). Further investigation revealed that mononuclear cells in blood adhere to neo-endothelial cells and migrate into the sub-endothelial space. Meanwhile, progenitor cells from blood and adventitia migrate into the intima, where they proliferate and differentiate into neo-SMCs (Xu, 2006).

1.2.4 The effect of blood pressure and pulse on vasculature

Blood pressure and pulse are key forces which exert a direct influence on vasculature, and have been associated with increased levels of inflammation (Ridker *et al.*, 2006). Blood pressure is defined as the force of the blood (both plasma and cellular components) exerted on the walls of the blood vessels (arterial walls, in the case of atherosclerosis) and is generated by the beating of the heart. Smooth muscle, present in arterial walls produces additional pressure. When the heart relaxes as part of the natural beating rhythm, pressure against arterial walls is diminished, but it is nevertheless still present. When the left ventricle of the heart beats and ejects blood into the already filled aorta, the aorta expands in order to accommodate it. The aorta then recoils due to the elastic tissue in the tunica media. This serves to push blood onwards into systemic circulation. Blood pressure consists of two measurements - systolic and diastolic pressure. Systolic pressure is defined as the pressure in the arteries when the ventricles contract. Diastolic pressure is defined as the pressure of the blood in the arteries when the ventricles are relaxed. Average healthy adult blood pressure is defined as 120/80 mmHg or 16 kPa, although it tends to rise naturally with age. Hypertension (high blood pressure) may cause damage to heart muscle over time. Heart disease then occurs and the risk of heart attack or stroke increases accordingly (Waugh and Grant, 2008). Arteries pump in conjunction with the heart, and the resultant pulse can be felt in arteries close to the surface of the skin. Pulse rate is

measured in beats per minute (BPM). Normal adult pulse rates average 60-80 beats per minute.

Blood viscosity is a significant parameter which informs the effects of blood flow on vasculature. It must also be remembered that viscosity is strongly temperature dependent, and is subject to change depending on vessel diameter. Anaemia (a decrease in red blood cell numbers/haemoglobin) is an important determinant of whole blood viscosity and frictional force of blood flow. Furthermore, it is a known contributor to endothelial cell apoptosis, and thus could potentially play an indirect role in the pathogenesis of accelerated arteriosclerosis (Boulanger *et al.*, 2007).

1.3 Vascular inflammation

Inflammation in general may be defined as a complex biological response to a reaction/infection/injury, in which part of the body becomes reddened, swollen, hot, and often painful. It may also be considered to be a protective response.

Atherosclerosis is the most common type of vascular inflammatory disease, specifically affecting arterial blood vessels. Literature describes it in two distinct ways: in both metabolic terms and as an inflammatory disease. Scientific investigation of the relationship between atherosclerosis, inflammation, and lipoprotein metabolism began in the mid-19th century. However, CVD research has increasingly focused on the role of inflammation in the development of atherosclerotic plaques. A firmly held belief that cardiovascular disease includes a genetic component has led to a rapidly expanding field of research. Sequencing of the human genome has led to greater understanding of the role of sequence variation in CVD, and has led to identification of single DNA variants that confer risk for common diseases. The possibility of epigenetic alterations (interactions between DNA and the environment) to vascular cells has been raised, due to the haemodynamic force of blood within vasculature.

Vascular inflammation is a key contributor to CVD, with inflammation and CVD risk factors closely inter-related. CVD risk factors, such as hypertension, and hypercholesterolemia are associated with higher circulating concentrations of inflammatory biomarkers (Fontes *et al.*, 2013). Atherosclerosis is the most common of the vascular inflammatory diseases. It is defined as chronic, specifically affecting

arterial blood vessels, and caused by dynamic dysfunction of endothelium. It is primarily a disease of the large and medium-sized arteries, and is the chief cause of heart disease and stroke (Lusis, 2000). Arterial structure, therefore, is an important aspect in its manifestation. Atherosclerosis may be characterised by alterations in the arterial wall, specifically accumulation/infiltration by inflammatory cells and fibrous elements (Bonaterra *et al.*, 2012). Key cells involved in atherosclerosis/vascular inflammation include arterial endothelial cells and smooth muscle cells (SMCs), which form the walls of the blood vessels.

Owing to the fact that atherosclerosis is primarily an inflammatory disease, consideration must also be given to other such disorders, and in particular, any connections they may share. Indeed, harmful effects arising from persistent inflammation have been cited as possible causes of endothelial dysfunction (Gonzalez-Gay *et al.*, 2005).

1.3.1 Cardiovascular disease – vasculature gone wrong

Cardiovascular disease (CVD) is an umbrella term for a class of diseases involving the heart and blood vessels, and consequently includes heart failure, arrhythmia, angina, hypertension, high cholesterol, and stroke amongst others. CVD accounts for 37% of deaths in the European Union (see Figure 1.4). Vascular inflammation is a key contributor to CVD, with inflammation and CVD risk factors closely inter-related. CVD risk factors, such as hypertension, and hypercholesterolemia are associated with higher circulating concentrations of inflammatory biomarkers (Fontes *et al.*, 2013). Types of CVD are varied and complex, hence there are multiple pathological mechanisms through which disease may arise. Risk factors can be divided into two distinct categories: behavioural and metabolic. Behavioural factors, which predispose individuals to CVD, include modifiable determinants, such as unhealthy diet (high cholesterol diet and salt intake, physical inactivity, over-consumption of alcohol and tobacco). Prolonged exposure to such unhealthy habits may then lead to intermediate metabolic risk factors which include high blood pressure, high serum cholesterol, raised blood glucose levels and obesity, thereby increasing chances of developing disease in the future. Among these factors, high serum cholesterol and unhealthy diet are deemed major causes of CVD (Strohacker *et al.*, 2012).

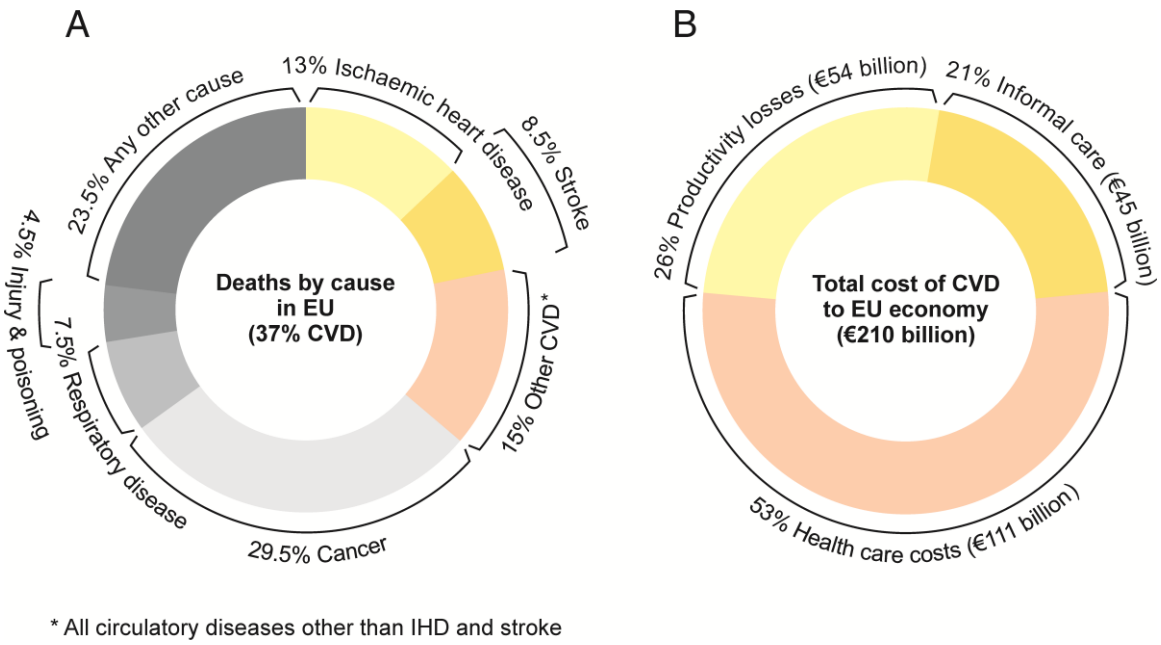

Figure 1.4 European Union CVD statistics
(A) Breakdown of mortality causes across the European Union (EU) for latest available year. (B) Breakdown of economic cost of CVD across the EU for latest available year (Wilkins *et al.*, 2017).

1.3.2 Atherosclerosis

Atherosclerosis is a chronic inflammatory disease that affects arteries through the build-up of plaque (fats, cholesterol and other substances) within the arterial wall, which can restrict blood flow. As a direct result of plaque rupture, it is a major cause of heart disease and stroke.

Arterial structure, therefore, is an important aspect in its manifestation. Atherosclerosis may be characterised by alterations in the arterial wall, specifically accumulation/infiltration by inflammatory cells and fibrous elements (see Figure 1.4). Key cells involved in atherosclerosis/vascular inflammation include arterial endothelial cells and smooth muscle cells (SMCs), which form the walls of the blood vessels.

Atherogenesis is a multi-stage inflammation process. Following injury, the resulting immune response leads to inflammation at the site. Macrophage cells are typically the

first type to respond. They act by secreting proteins (cytokines and chemokines) in order to recruit additional immune cells to the site of injury (Mohiuddin *et al.*, 2012). Indeed, leukocytes (T and B lymphocytes, natural killer cells (NK) and NKT cells, dendritic cells, mast cells and macrophages) have all been found within atherosclerotic-prone aortas. This is highly suggestive of an important role in atherogenesis (Galkina and Ley, 2007).

Formation of macrophage-derived foam cells draws a parallel with inflammatory responses in blood vessels (Kruth, 2001). Monocytes present in the blood may bind to, and subsequently move in between ECs, traversing into the sub-endothelial space, where differentiation into macrophages occurs. Literature cites increased vascular permeability as a characteristic commonly associated with inflammation, believed to be due to a highly co-ordinated loss of junctional integrity (Alexander and Elrod, 2002). Partial characterisation of the mechanisms involved in monocyte recruitment has revealed involvement of P-selectin, E-selectin, vascular cell adhesion molecule (VCAM)-1, intra-cellular adhesion molecule (ICAM)-1 and junctional adhesion molecule (JAM)-A (Galkina and Ley, 2007). Enzymes (12/15-lipoxygenase or myeloperoxidase) present in the extra-cellular space act upon the inflammatory mediator, low-density lipoprotein (LDL), to create an oxidized form (ox-LDL), which may then be taken up by macrophages via scavenger receptors (CD36 and SR-A) on their surface. Lipid homeostasis, particularly that of cholesterol, plays a critical role in foam cell formation (Yuan *et al.*, 2012). Focal build-up of cholesterol in arteries is part of the process that creates atherosclerotic plaques.

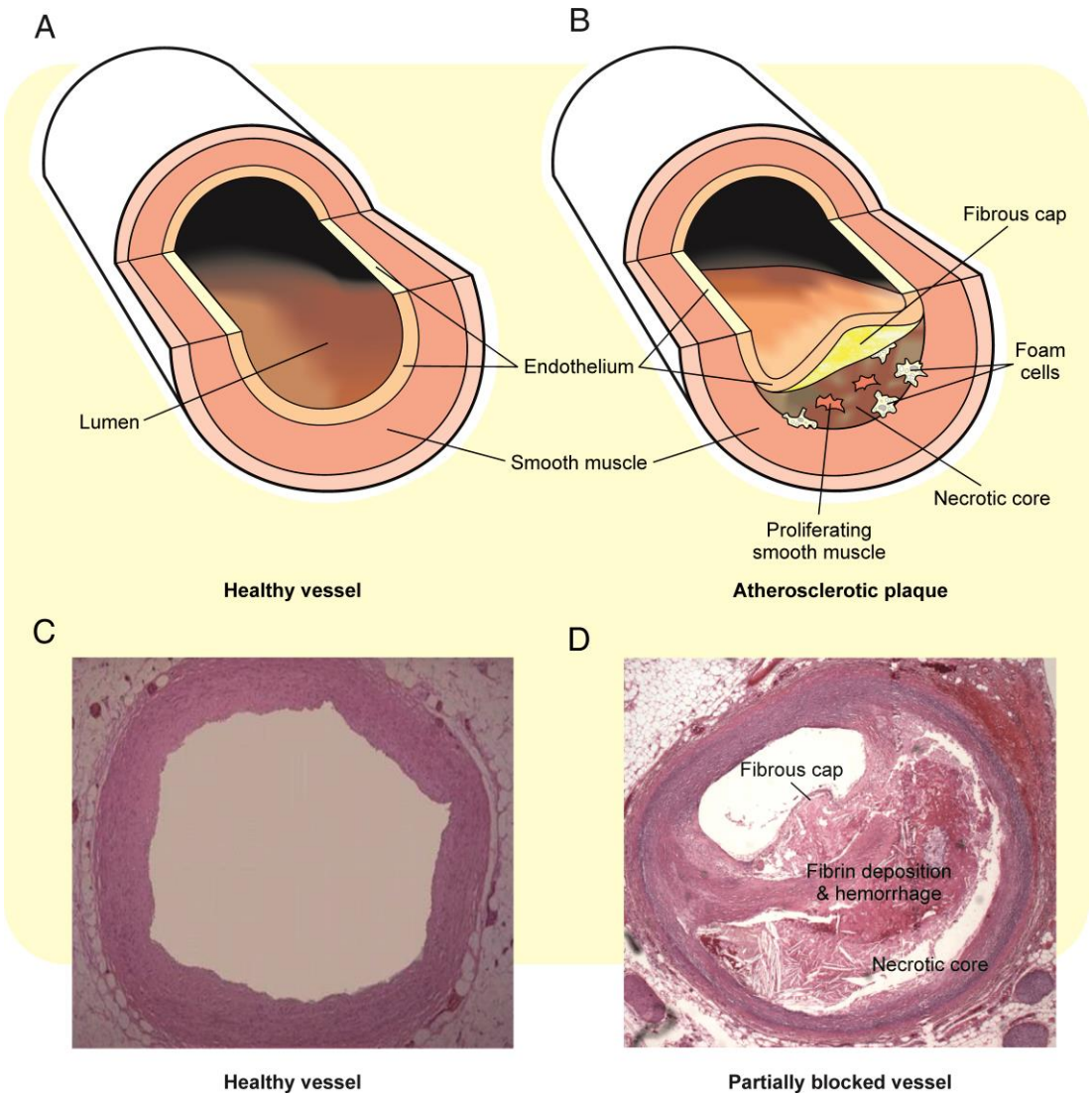

Figure 1.5 Transition between healthy and atherosclerotic vessel status
Simple diagram showing principle vessel and plaque components in healthy (A) vs atherosclerotic (B) vessels. Hematoxylin-eosin stained histological sections of the left anterior descending artery (human), showing a healthy vessel (C) and diseased vessel with narrowed lumen (D) (Ribeiro *et al.*, 2014).

Plaque build-up is achieved by cholesterol from ox-LDL particles, retained in macrophages in inclusion bodies (Muslin, 2010). Atherosclerotic lesions may contain different types of cholesterol-containing lipid particles. Lipid infusion is known to cause increased production of reactive oxygen species (ROS) and inflammation. In atherosclerosis, this is manifested in the formation of fatty streaks. Lipids may enter macrophages via a number of endocytic pathways (Kruth, 2001). Once engorged with cholesterol, the enclosed lipid droplets give the molecule a frothy/foamy appearance when examined microscopically – hence the name "foam cell".

Foam cells may undergo apoptosis. This may occur due to endoplasmic reticulum stress. Clearance of apoptotic cells by M2 macrophages occurs through a process called "efferocytosis". As the disease progresses, plaques form in the intima, swelled by large numbers of infiltrating macrophages and smooth muscle cells, topped with a fibrous cap (see Figure 1.5). Efferocytosis is impaired in advanced lesions, leading to secondary necrosis of foam cells and hence, formation of a necrotic core (Muslin, 2010). Lesions with such features are termed "vulnerable plaques" and are those which are at highest risk of rupture (Falk *et al.*, 1995).

1.3.3 Causative factors of atherosclerosis

Numerous factors have been proposed as causative agents in atherosclerotic development. Literature cites many such determinants, including high cholesterol levels and smoking, y*et al*so points to other seemingly unrelated factors which may also exert an influence on its pathogenesis. Dietary issues are among the most commonly cited, and are the largest contributors to CVD mortality (Strohacker *et al.*, 2012) (Wilkins *et al*., 2017). Numerous signalling molecules, such as inflammatory cytokines, are proposed as important factors related to atherosclerotic pathogenesis. Beyond these, literature points to other agents which may directly influence pathogenesis, one of which is exercise. It may be possible that exercise could exert some influence over plaque development. Recent research in this field has produced clear-cut results: apolipoprotein E knockout (apoE-/-) mice (with subsequent diabetic atherosclerosis) were divided into 3 groups – those which followed a strict exercise programme, those which were permitted a sedentary lifestyle, and a control group. Upon examination of blood samples and atherosclerotic plaques in the aortic root, considerable regression of atherosclerotic lesions was observed in the exercise group. Decreased concentrations of macrophages, matrix metalloproteinase-2 (MMP-2), MMP-3, MMP-8 and interleukin-6 (IL-6) in the plaques were also noted. This coincided with a concomitant increase in collagen, elastin, and tissue inhibitor of matrix metalloproteinase-2 (TIMP-2) content. Researchers cited a favourable modification in inflammatory regulators as the explanation for these results (Kadoglou *et al.*, 2013). It is clear, therefore, that exercise, while a physiological phenomenon, also exerts a chemical stimulus within the body.

It is readily apparent that while these mechanisms may exert some effect on inflammatory/atherosclerotic development/progression, they do not fully explain why atherosclerotic plaques occur in particular locations, such as sites of bifurcations. Moreover, the emergence of inflammation at sites distal from original disease is not explained using these models. The ability to interact with and adapt to the surrounding environment lies at the heart of a cell's ability to function and survive. The means by which vascular cells acclimatise to different micro-environments may present a window through which the mechanism of regional inflammatory disease may be glimpsed.

1.4 Mechanisms of arterial re-modelling

Blood vessels are readily capable of re-modelling/altering themselves in response to hemodynamic prompts associated with variations in blood flow. It must be remembered that in living organisms, vasculature is continually exposed to such natural mechanical forces. However, significant variations of flow pattern occur. In some cases, these may be pathological flow types which lead to aberrant re-modelling and development of disease status.

Assessments of cardiovascular risk (such as those based on Framingham risk scores), enable clinicians to prioritise treatment, and should be subject to evaluation before implementation. Data from studies carried out by Brindle *et al*. (2006) has shown that traditional factors, such as smoking, diet, etc. lack accuracy, and may even result in over-estimation of disease risk in low-risk populations, and *vice versa*. Involvement of hereditary factors may represent a more significant agent in both vascular re-modelling and disease development. Indeed, with regard to coronary artery disease, genome-wide association studies have led to the identification of a large number of single nucleotide polymorphisms (SNPs) associated with increased risk of developing the disease (Hernesniemi *et al.*, 2012). However, each of these approaches is based on the fundamental principle that genetic determinants lie within the static DNA code of individuals; the hypothesis being that a person may, in effect, be more susceptible to succumbing to disease, based on their unique genetic profile. Nevertheless, the genetic code of individuals has long been known to be flexible and adaptable. Such

adaptations may occur over the long term through evolution, or may occur as a more direct reaction to various stimuli by means of up/down-regulation of genes in order to best meet the demands of certain situations.

1.4.1 Influence of blood flow pattern

Individuals exhibit a clear, non-random distribution of atherosclerotic lesions within vasculature. This is especially interesting, given that the entire circulatory system is exposed to an essentially even distribution of risk factors (discussed previously). Hence, this fact further depreciates the role that such risk factors may play in disease incidence. Atherosclerotic plaques form more often at branch points or curved areas of large arteries, (i.e. regions which encounter blood flow with low mean shear stress values and cyclic reversal flow direction) (Gimbrone Jr. *et al.*, 2000). Hemodynamic forces are now widely recognised as responsible for this phenomenon. The proposal was therefore made that hemodynamic profile may stimulate endothelial phenotype to respond in a site-specific manner to such systemic risk factors (VanderLaan *et al.*, 2004). Indeed, a considerable number of studies support the theory that low levels of laminar shear stress act to promote atherogenesis. Moreover, this effect is believed to be endothelial-specific, affecting endothelial proteins (Conway and Schwartz, 2012).

As discussed previously, blood exerts a direct influence on the vasculature. This is achieved through haemodynamic interactions and is likely a key epigenetic factor in development of atherosclerosis. The pattern of blood flow throughout the cardiovascular system, by its nature, generates mechanical forces, which in turn have been found to exert a strong regulatory influence on cardiovascular physiology and pathology (Lehoux and Tedgui, 2003). Indeed, it has been proposed that such influence begins in the developing embryo, with cardiac morphogenesis. In one *in vitro* study, zebrafish embryos were used to show that cultured cardiac endothelial cells re-arranged their cytoskeletal structure and underwent a concurrent change in gene expression in response to such flow-induced forces. By occluding flow at either the cardiac inflow or outflow tracts, researchers showed that it resulted in abnormal cardiac development with strong similarities to those observed in some congenital heart defects (Hove *et al.*, 2003).

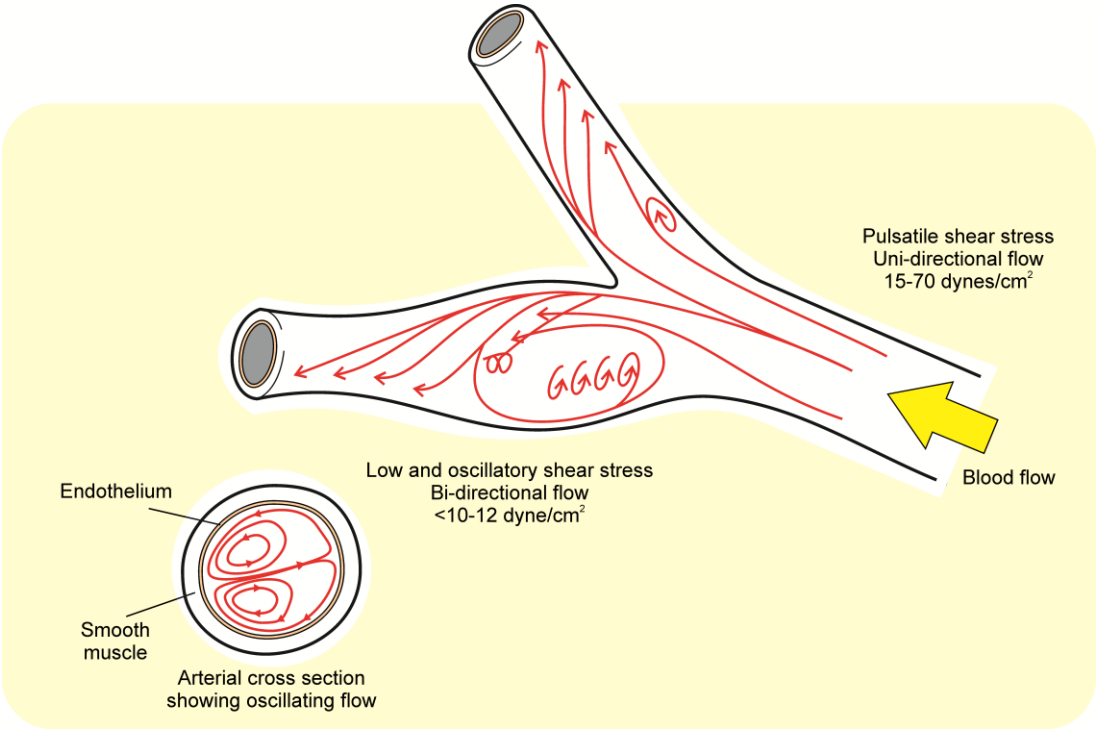

Figure 1.6 Diagram illustrating differing types of shear stress and typical forces experienced at branching points in the arterial tree
(Adapted from Chatzizisis *et al.*, (2007)

Blood flow is dominated by two distinct types:

(i) Laminar flow (smooth, orderly, unidirectional flow)

(ii) Oscillatory flow (disturbed, re-circulatory flow)

Within these, a number of sub-types (disturbed and undisturbed laminar flow, turbulent and pulsatile flow, illustrated in Figure 1.6) may more accurately reflect actual flow conditions (Chatzizisis *et al.*, 2007). In contrast to disturbed flow patterns, unidirectional laminar flow is associated with an atheroprotective effect. This type of flow occurs within straight sections of vasculature, and correlates with documented evidence of a lack of atherosclerotic development in such regions. Despite an overall steady flow, velocity within the vasculature varies continuously over time at any given point (Chatzizisis *et al.*, 2007). Flow responses are partly mediated by a raft of proteins comprised of PECAM-1, VE-cadherin and VEGFR2 at endothelial cell-cell junctions. It is notable that these proteins all clearly have additional, non-mechanical functions (Conway and Schwartz, 2012).

Thus, it becomes clear that vascular regulation by hemodynamic forces is a complex process of protein regulation, driven by genetic factors. Literature suggests a number of endothelial shear stress responsive genes. Both atheroprotective and pro-atherosclerotic gene expression by ECs have been documented. Interestingly, literature shows that in straight linear sections of arteries (laminar flow), down-regulation of pro-atherosclerotic genes occurs, leading to an atheroprotective effect, and is the major determinant in the subsequent quiescent state in these sections of vasculature (Chatzizisis *et al.*, 2007).

Mechano-transduction is essentially the conversion of a cell's mechanical stimulus into a chemical or electrical signal. In this way, the external environment may inform/affect intracellular events. Mechano-transduction may be achieved in a multitude of different ways. Indeed, vascular smooth muscle cells (VSMCs) utilise numerous sensing mechanisms to detect mechanical stimuli resulting from vascular stretch. As with most sensory systems, cells capable of mechano-sensation place an emphasis on speed and sensitivity. Mechanical forces are commonly directed to specific ion channels, which can open rapidly and amplify the signal (Gillespie and Walker, 2001).

With specific regard to atherosclerosis, the two stimuli for mechano-transduction are:

(i) Cyclical strain (circumferential strain, arising from the pulsatile nature of blood flow).

(ii) Shear stress (dragging frictional force of blood flow).

(Illustrated in Figure 1.7).

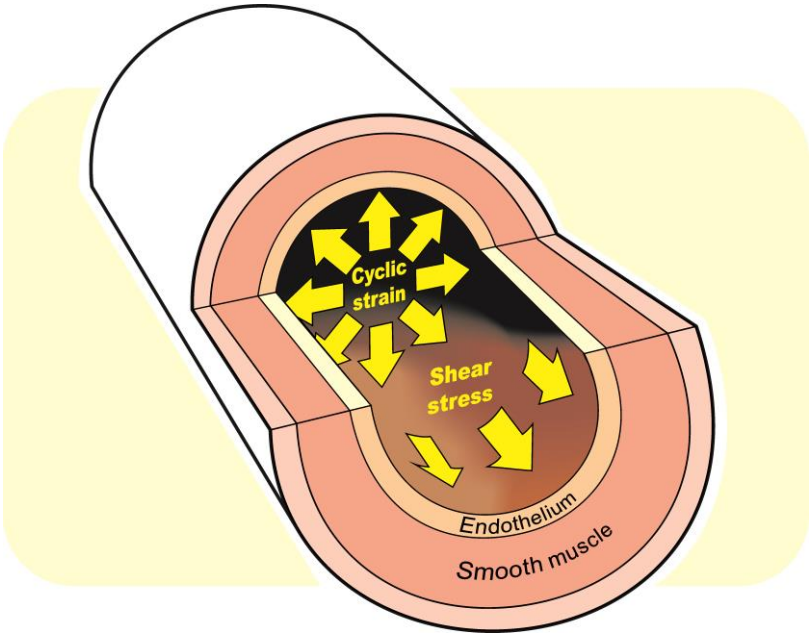

Figure 1.7 Diagram illustrating the mechano-transductive stimuli of cyclical strain and shear stress on vasculature, both of which result in modification to the arterial wall
(Adapted from Conway and Schwartz, (2012)

The pathways by which mechano-transduction occur in these systems are yet to be fully elucidated, however, both of these mechanisms play important roles in the physiological control of vascular tone, re-modelling, and initiation and progression of vascular pathologies. It is important to note that such forces may be of either physiological or physio-pathological origin. In the case of cyclical strain (vessel stretch), blood pressure is the dominant force at work. It acts to counteract the force of intraluminal pressure. Importantly, this is sensed in all cell types in the vessel (Lehoux and Tedgui, 2003). Furthermore, matrix metallo-proteinases (enzymes capable of degrading basement membrane and interstitial matrix molecules) have been implicated in this occurrence (Cummins *et al.*, 2007).

In contrast, shear stress arises from the frictional force of blood flowing against the vessel wall, and acts in parallel to the vessel surface. As a consequence, shear stress is sensed primarily by ECs. Under normal human physiological conditions, shear stress with a value of approximately 10-15 dyne/cm^2 (Lehoux and Tedgui, 2003) is opposed by tension and deformation in the endothelium (Lu and Kassab, 2011). With this in mind, it may be possible to reconcile physiological data from exercise studies with epigenetic modification.

1.5 Epigenetic regulation

Epigenetics refers to the study of changes in organisms due to modification of gene expression, rather than alteration of the genetic sequence itself. Hence, epigenetics is effectively a study of all those factors that influence gene expression, both physical and chemical, and is a natural occurrence over the lifetime of the organism in question. As epigenetic changes may be inherited, they may also influence evolution (Burggren, 2016). It is clear that variation of genetic expression introduced through epigenetic alterations may facilitate the type of phenotypic variation commonly associated with traditional evolutional theory, yet may do so over an accelerated time frame (Yan *et al.*, 2010; Heyn *et al.*, 2013).

With the genome essentially acting as a library of information, the epigenome behaves as a librarian, constantly controlling access to that information, bridging the gap between genotype and phenotype. Specific epigenomic modifications, such as transcription factor methylation binding patterns, constitute the words of this gene regulatory language, resulting in orchestrated patterns of gene activation/silencing (Yin *et al.*, 2017). Where the epigenome may be dynamically altered by external environmental influences, the underlying genome remains unaffected. This dynamic, multi-tiered interplay is controlled by a myriad of external stimuli, resulting in co-ordinated changes over time. Figure 1.8 illustrates three distinct signal levels that have been proposed (Berger *et al.*, 2009), which ultimately culminate in the generation of stable heritable epigenetic states.

This genome-epigenome interaction occurs within the chromatin environment, where spatio-temporal organisation is critical for gene expression (Toh *et al.*, 2015). Although such interactions may be classified into a number of different sub-types, the vast majority of epigenetic adaptations are regulated by DNA methylation (DNAm) and histone modification. DNAm is established through the addition of a methyl group (CH_3) on the 5th carbon of cytosine residues by the co-operative effects of DNA methyltransferase (DNMT) enzyme activity and maintained by its co-factors. The reaction is achieved with the assistance of S-adenosyl-methionine, which acts as the methyl donor (Liang *et al.*, 2002; Yin *et al.*, 2017). Methylation has been reported to be amongst the first cellular processes to occur during CVD onset (Lund *et al.*, 2004).

While cytosine methylation occurs most commonly in CpG dinucleotide sequence clusters (CpG islands) with age, cytosine methylation in GpC dinucleotides, and isolated cytosine nucleotides has also been documented (Barres *et al.*, 2009). CpG methylation level has been shown to vary in accordance with genomic location (promoter/gene body), gene transcription status (active/silenced), and cell type. In addition, hypo-methylation of regions flanking gene regulatory elements has been reported in literature (Yin *et al.*, 2017). It was assumed for many years that the role of 5-methylcytosine was to spatially and temporally fine-tune gene expression principally affecting transcription initiation mechanisms, with the consequence of either silencing or reactivating gene expression. Over the past few years, this has expanded to include many other mechanisms particularly alternative splicing and regulatory element function (van der Wijst *et al.*, 2017).

Altered chromatin structure due to covalent post-transcriptional modification (acetylation/de-acetylation, phosphorylation, and ubiquitylation) of projecting histone amino tail domains results in similarly altered gene transcription. Histone acetyl transferase (HAT) enzymes catalyse the addition of an acetyl group ($COCH_3$) from acetyl co-enzyme A to histone tails. Though they play roles in a variety of other cellular processes, HATs in this capacity encourage transcription by physically exposing chromatin to transcriptional machinery. In contrast, histone deacetylases promote gene silencing by hydrolytically removing $COCH_3$, causing histones to become more basic, condensing chromatin and thereby limiting transcriptional access (Serebryannyy *et al.*, 2016). Chromatin modifying factors (CMFs) are multi-subunit complexes reliant on ATP hydrolysis. They are capable of regulating chromatin condensation in a non-covalent manner in conjunction with other protein factors (Volokh *et al.*, 2016). Chromatin-enhancer interactions represent a critical mechanism in transcriptional control. Promoters (regions of DNA where transcription initiation occurs) and enhancers (sequences that may increase transcription of target genes) span different areas of the genome and may not lay linearly across its length. However, chromatin folding/alteration to create looping structures within the sequence may allow such distinct regions to come into close contact and facilitate enhanced transcriptional regulation.

It is apparent, therefore, that such modification leaves behind a clear epigenetic "signature" in the form of detectable and measurable changes to the molecule itself (Weidner *et al.*, 2014). Hence epigenetic adaptations may be used as markers of premature cellular ageing within the cardiovascular compartment (Marioni *et al.*, 2015). Nevertheless, the link between genetics and epigenetics is intrinsic, and goes much deeper than mere surface chemical modification of the DNA molecule. The transcriptome, and ultimately the proteome are influenced by the co-operative and cumulative effects of DNAm, and histone modification in addition to microRNA (miRNA) interactions, leading to highly contextualised gene expression with clear implications for cell differentiation and disease development (Yuan *et al.*, 2015).

The cardiovascular system is responsible for the delivery of oxygenated blood and nutrients to all tissues of the body, and is therefore central to the health of those tissues and the longevity of the organism as a whole (North and Sinclair, 2012). Vascular ageing is a process of gradual re-modelling, progressing towards an unhealthy/diseased state. It is recognised to play a central role in declining health and mortality in older people and is accompanied by well-defined changes, such as heightened inducible Nitric Oxide Synthase (iNOS) and reduced endothelial NOS (eNOS) expression (Gradinaru *et al.*, 2015; Tarantini *et al.*, 2016). Distinct from other tissues, it may be described as a function of the accumulation of chemically-aggressive ROS in combination with endothelial dysfunction, effectively lowering the threshold for disease.

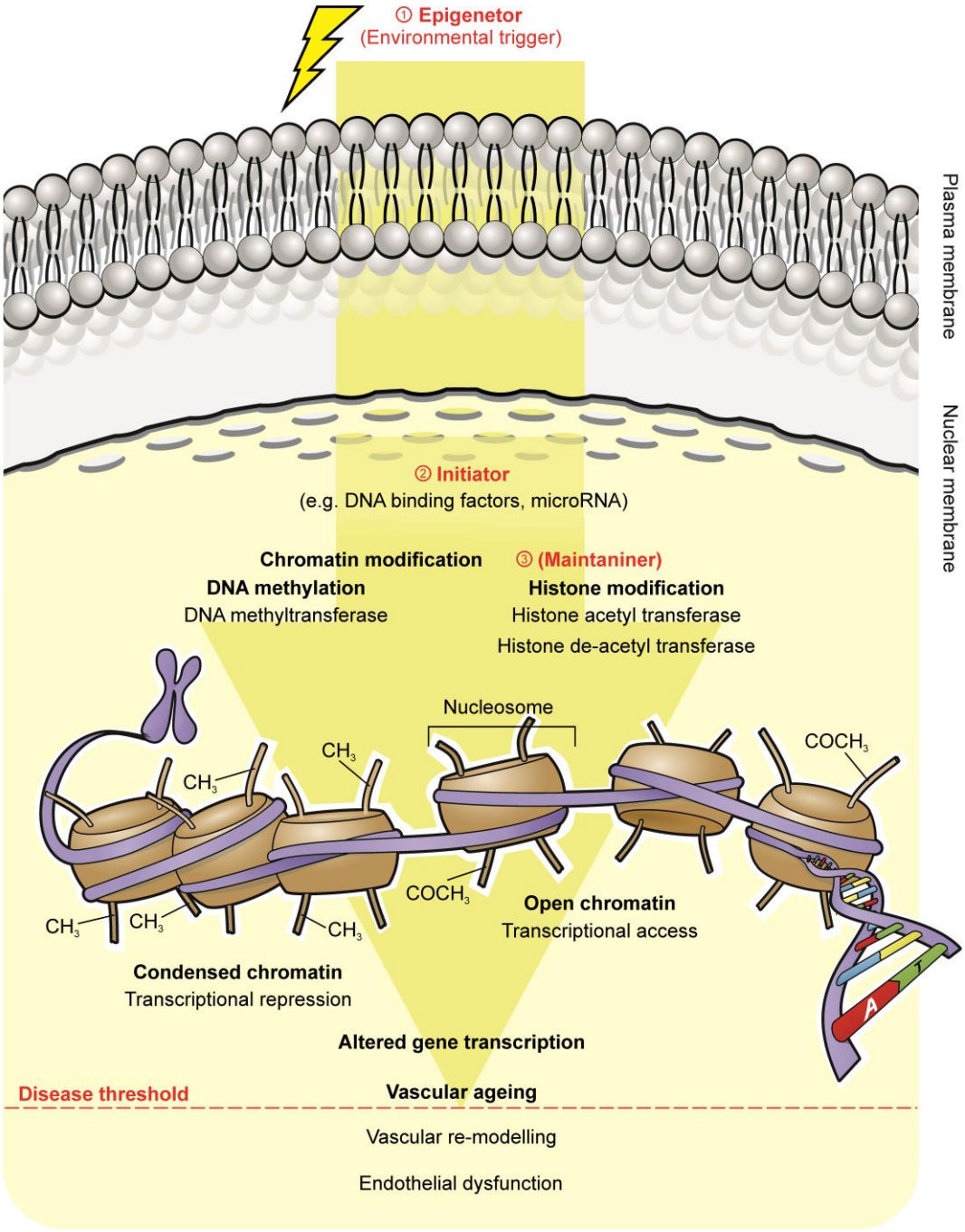

Figure 1.8 Illustration of epigenetic re-programming in vascular endothelial cells, where the extra-cellular stimulus results in modified genetic architecture, ultimately leading to altered gene transcription and lower disease threshold

1. Epigenator – environmental trigger, eg. Blood flow pattern. 2. Epigenetic initiator – translates epigenator signals to mediate establishment of local chromatin context at a particular location. 3. Epigenetic maintainer - sustains the epigenetic chromatin state.

1.5.1 The epigenetic clock and vascular ageing

Oxidative stress increases vascular permeability and promotes leukocyte adhesion. Thus, chronic low-grade inflammatory processes play a central role in the pathogenesis of a number of chronic diseases, particularly CVD. Of particular importance is the *quid pro quo* relationship between oxidative stress and inflammation, which are closely related pathophysiological processes, one of which can be easily induced by another. Thus, both processes are simultaneously found in many pathological conditions. ROS production and concomitant inflammation may promote vascular remodelling and ageing via renin-angiotensin-aldosterone and endothelin pathway activation (Savoia *et al.*, 2017). Endothelial dysfunction is characterised by reduced endothelium-dependent vasodilation of arteries, in part, from decreased bioavailability of nitric oxide (NO) (Montero *et al.*, 2015). Endothelial dysfunction has been found to occur earlier in males than females, likely due to the vasculo-protective effects of oestrogen (Celermajer *et al.*, 1994). The long-running Framingham heart study has established that vascular ageing is associated with reduced barrier function, changes in blood pressure and increased blood pressure variability; important predictors of CVD events (Franklin *et al.*, 2009). Whilst chronological age has traditionally been used as an important factor in assessment of CVD risk, biological/epigenetic age may be a much more relevant index. Biological/epigenetic age is a highly reflective measure of an individual's body and how it functions, independent of its temporal age.

Two recent influential publications have highlighted and emphasised the importance of chronic system inflammation to disease initiation and progression; the creation of a physiological 'disease environment', leading to a sequalae of aberrant permutations and combinations of epigenetic patterns (Ridker, Everett, *et al.*, 2017; Ridker, MacFadyen, *et al.*, 2017). In the CANTOS (Canakinumab Anti-inflammatory Thrombosis Outcomes Study) trial, Ridker and colleagues definitively demonstrated that lowering inflammation independently of cholesterol resulted in reduced cardiovascular risk. This has far-reaching implications and importance in developing new therapeutic strategies for the prevention, management and treatment of CVD. This paradigm shift highlights that by leveraging an entirely new way to treat patients — targeting inflammation — a significant improvement of outcomes for certain very high-risk CVD populations may be possible. The trial targeted the pro-inflammatory

cytokine interleukin-1β using the novel human monoclonal antibody, canakinumab. It is interesting to note that the expression of interleukin-1β under pathophysiological conditions is in itself regulated by epigenetic mechanisms (Hashimoto *et al.*, 2013). This ground-breaking research emphasises the concept that by targeting the epigenetics associated with chronic systemic inflammation, for example by physical activity, nutrition or pharmacological means, novel therapeutic strategies for chronic illnesses may be created.

While chronological age advances linearly, biological age may vary. Epigenetic effects, particularly methylation, may be referred to in terms of an "epigenetic clock" (Hannum *et al.*, 2013), where differences between healthy and disease states are readily identifiable over time. Epigenetic drift is a similar, but distinct term given to this phenomenon, describing changes to the epigenome over time where the parental genetic contribution pre-disposes offspring to particular health/disease outcomes. Importantly, such outcomes may subsequently be shaped by modifiable lifestyle choices. Here, chronological and biological/physiological age diverge, resulting in identifiable and measurable genetic biomarkers prior to the manifestation of markedly different health consequences. As chronological age advances, newer modifications are incorporated into the epigenome, leading to further "drift" from the original (younger) programming and mirrored in the organism's phenotype (see Figure 1.9). Hence, epigenetic drift is essentially another term for functional ageing. The robustness of this concept has been investigated by Marioni *et al*., (2016), by studying biological differences in individuals of the same chronological age to determine the influence of environmental factors on physiological ageing rates. In this study, telomere length and DNAm emerged as the two most prominent markers of biological ageing. Interestingly, while both were found to associate with age, they did so independently of each other, appearing to mark two alternate facets of the same process. Jylhava *et al*. (2017) argue that the longitudinal studies which would otherwise lend credence to either are missing. Nevertheless, there is evidence to support the value of DNAm as a prognostic biomarker: Soriano-Tarraga *et al*. (2017), for example, estimated biological age using an algorithm based on DNAm in 71 CpG sites, and accurately predicted patient outcome 3 months after ischemic stroke. Importantly, this prediction was independent of chronological age, a known risk

factor. Moreover, it firmly establishes the possibility of biological age-specific, personalised/prescriptive treatment.

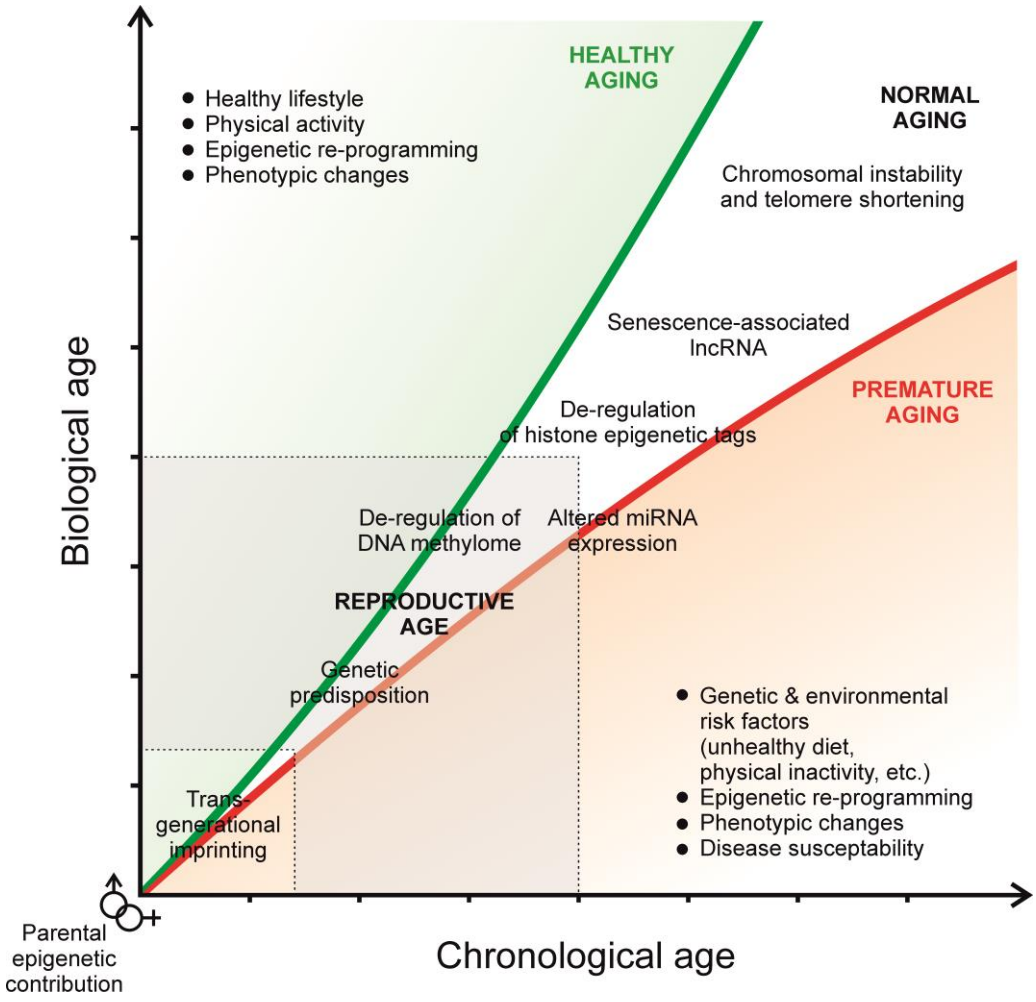

Figure 1.9 Epigenetic drift over time can result in measurable differences between physiological and chronological age
Epigenetic changes have been found to be reflective of lifestyle and may act as functional biomarkers of disease before clinical threshold is reached.

While epigenetic alterations, particularly methylation, are relatively stable, their dynamic nature dictates constant revisions. Editing/erasing of epigenetic modifications occurs in line with the hypothesis that the epigenetic clock is adjustable, and may occur by a number of different processes (see Figure 1.10). Restoration of methylated bases may occur via passive (DNA replication dependent) or active (DNA replication independent) mechanisms (Feng *et al.*, 2010). For example, active restoration sees oxidation of 5' methylcytosine residues to 5' hydroxymethylcytosine

that can be either deaminated by AID/Apobec enzymes, forming 5-hydroxymethyluracil, or oxidised further to 5-formylcytosine and 5-carboxylcytosine These residues may either then be removed by base excision repair mechanisms, or have the formyl and carboxy groups enzymatically removed (Wu and Zhang, 2010; Pfaffeneder *et al.*, 2011).

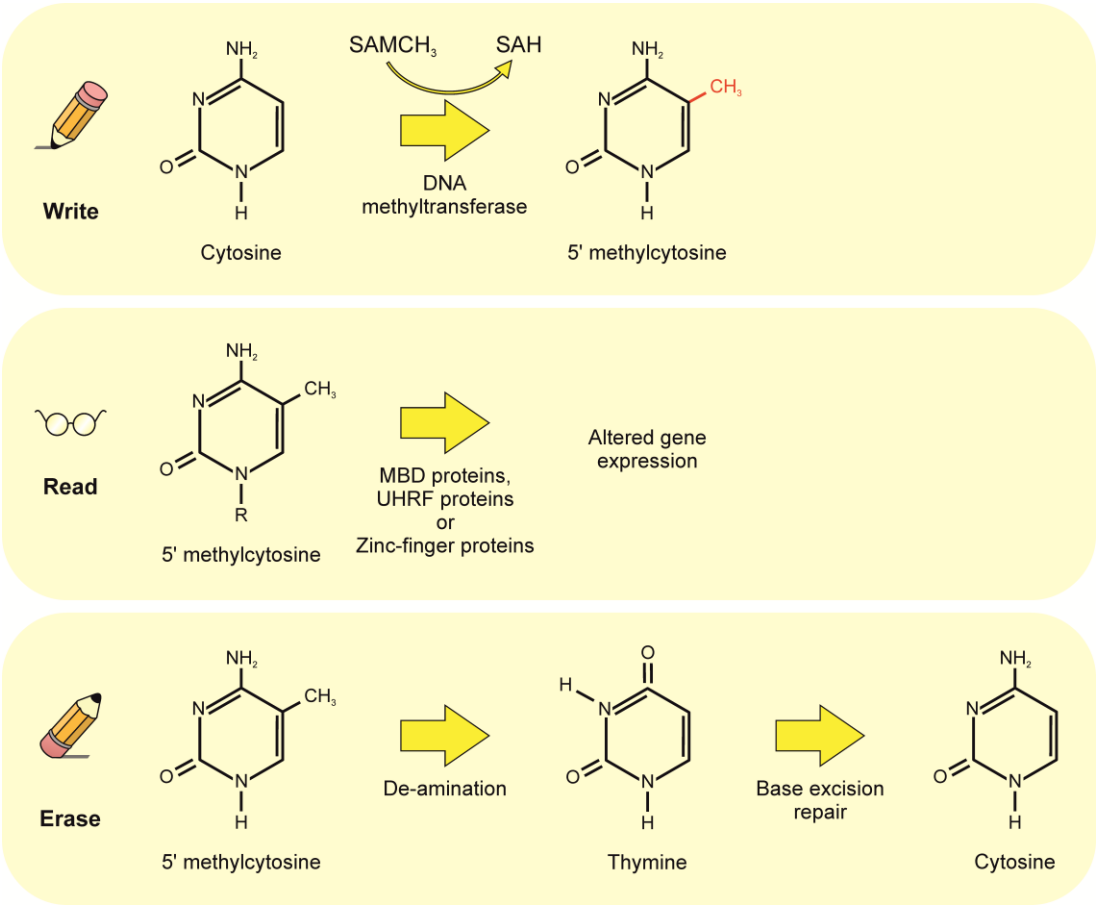

Figure 1.10 DNA methylation (writing, reading and erasing) represents one of a number of means through which epigenetic modification of DNA can occur
Methyltransferase enzymes serve to methylate cytosine residues, particularly in CpG islands. Methyl-CpG-binding domain (MBD) proteins, Ubiquitin-like, containing PHD and RING finger domain (UHRF) proteins or zinc-finger proteins may each play a role in reading methylated DNA. Deamination of 5' methylcytosines to form thymine residues that are subsequently removed via the base excision repair mechanism is one way that methylated bases may be restored.

1.5.2 Epigenetic heritability

An individual's epigenetic clock commences prior to birth, with genomic programming/imprinting of the developing embryo occurring as a result of the

amalgamation of already distinct and established parental epigenomes. Notably, the embryonic epigenome includes some regions that escape this programming (Inoue *et al.*, 2017). Nevertheless, significant regions of the epigenetic landscape are formed at this point. Lund *et al*. (2004) used genetically atherosclerosis-prone APOE-null murine models to assess the occurrence and significance of aberrant DNAm patterns during atherogenesis. Results demonstrated that clear alterations in DNAm profiles (both hyper- and hypo-methylation) were transferred to progeny, present in aortas and peripheral blood mononuclear cells, further supporting the durability and heritability of epigenetic change. Crucially, these offspring demonstrated no clinical signs of atherogenesis at the time of testing. Such multi-generational methylation transmission may be dependent on concomitant transfer of maternal transcription factors, with many developmentally important proteins displaying preference for methylated CpG sequences (Yin *et al.*, 2017).

Indeed, recent research has linked parental vitamin D deficiency with altered DNAm patterns and greater blood pressure levels in offspring. Genome-wide methylation analyses of the offspring of vitamin D-deficient rats determined hyper-methylated promoter regions of the Pannexin-1 gene. This encodes a hemichannel known to be involved in endothelial-dependent relaxation, and the authors concluded that the observed blood pressure increase was associated with impaired endothelial relaxation of large vessels (Meems *et al.*, 2016).

1.5.3 Blood-based biomarkers of epigenetic change

Blood represents an easily obtained and accepted population of cells and genetic material that readily act as biomarkers of change. The emerging field of epigenetics therefore naturally looked to blood as a means of establishing a direct link between epigenetic change and biomarker availability. To date, literature cites the development of a variety of tissue age and risk assessment tools to quantify the rate at which an individual's methylome matures over time. This is referred to as the "epigenetic age" of the individual, and is of particular relevance when considering the association between oscillatory shear stress and atherogenesis. Alterations/changes/ageing within the methylome, if detectable and verifiable, could potentially represent a novel biomarker of atherogenesis. There is, however, some

debate as to whether DNAm is the cause or consequence of ageing (Weidner *et al.*, 2014). Hannum *et al*. (2013) designed a model of epigenetic ageing using data from > 450,000 CpG loci from the whole blood of 656 individuals aged 19 to 101 years. Horvath (2013) devised a comparable procedure reliant on biomarker identification in blood and tissue samples, and expanded on the work carried out by Hannum *et al*. In contrast, Weidner *et al*., (2014), devised a similar system using just three age-related CpG markers (ITGA2B, ASPA and PDE4C). Here, the authors used bisulphite pyrosequencing to focus on those sites most associated with age prediction, selecting only those with the highest age-associated correlation. This resulted in predictions with higher precision (>5 years) than telomere attrition, the widely accepted standard of genetic age determination. While much effort has been given over to this aspect and the development of reliable techniques, investigations into the links between haemodynamic flow patterns and their effects at an epigenetic level are absent from literature.

Of the blood cell population, platelets represent perhaps the most immediate link to health in general due to their shorter ~10-day turnaround time and need for continual replacement. Therefore, their epigenetic compliment, particularly in the mitochondria, makes them ideal biomarkers of epigenetic drift. Platelet function genes may also be impacted by epigenetic modifications (Baccarelli and Byun, 2015). Although there is a known age-related increase of certain cell populations (lymphocyte/granulocytes) (Houseman *et al.*, 2012; Horvath and Ritz, 2015), the majority of epigenetic drift observed in blood is independent of differences in blood cell composition, addressing concerns that are associated with conventional blood-based biomarker efficacy (Yuan *et al.*, 2015).

1.6 MicroRNA as agents of epigenetic change

MicroRNAs (miRNA) are short, highly conserved, non-coding RNA (ncRNA) molecules, approximately 22-25 nucleotides in length (Zomer *et al.*, 2010), the actual length of which is defined by the specific argonaute involved in its genesis (Juvvuna *et al.*, 2012). Since their discovery in 1993, during experimentation on the nematode, *Caenorhabditis elegans* (*C. elegans*) (Jamaluddin *et al.*, 2011), the field of research

has expanded to encompass genome-wide studies. Current opinion hails miRNA as molecules of vast regulatory potential (Ebert and Sharp, 2012).

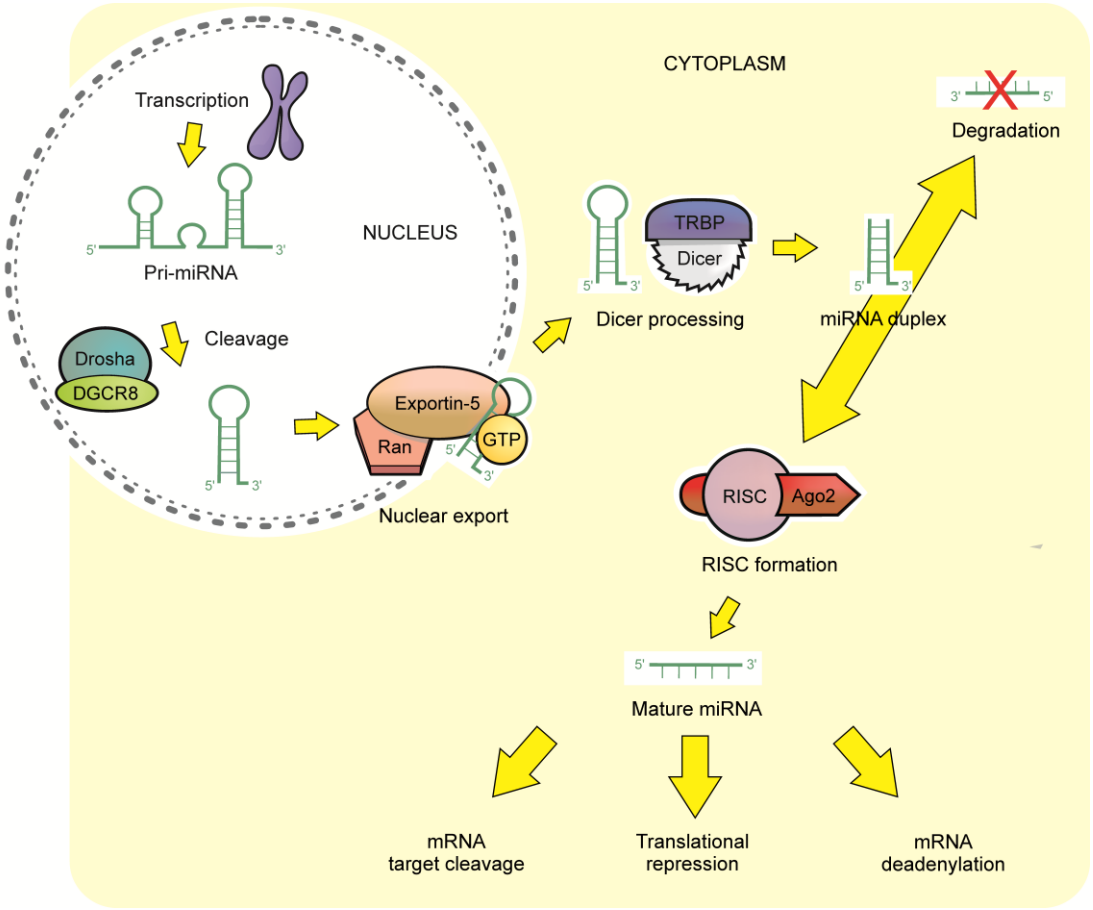

Figure 1.11 Simple diagram illustrating miRNA biogenesis and action

MicroRNA are generated through transcription by RNA polymerise II and III resulting in precursors that generate mature miRNA through a series of cleavage reactions (see Figure 1.11). It is involved in gene regulation through post-transcriptional prevention of gene expression (ie. negative control of translation). This was long believed to be solely achieved by complimentary base pairing to the 3' UTR of target mRNA, and thus preventing protein synthesis. However, new research has shown this not to be case. Binding may occur to either 3' UTR or coding regions (Fang and Rajewsky, 2011).

miRNA may be used to knock down/silence specific genes and hence, target disease caused by aberrant gene expression. P-bodies (specific cytoplasmic foci within cells)

appear to be necessary for this process, with RNA induced silencing complex (RISC) assembly, activation and hence, gene silencing occurring within these structures. Certainly, the theory facilitates miRNA sorting/shuttling events and the fact that such silencing is reversible (Macfarlane and Murphy, 2010).

MicroRNA may achieve its effect on messenger RNA during both (i) transcriptional and (ii) post-transcriptional stages:

(i) Transcriptional

MicroRNA has been shown to exert direct effects on gene expression via histone modification and DNA methylation of target genes' promoters.

(ii) Post-transcriptional

Regulation of the activities of endogenous genes is widely believed to occur through translational repression. This may be achieved by targeting specific regions within either 3' UTR or coding regions of mRNA (Fang and Rajewsky, 2011).

MicroRNA influence gene regulation by binding to the 3'UTR of multiple targeted mRNA, resulting in degradation and/or translational repression (Chen *et al.*, 2011). As such, miRNA exhibit similar gene suppression capacity to epigenetic modification. They have access to vasculature, enabling gene regulation to occur over great distances via microparticle release (and as independent entities) as they travel through the bloodstream before being incorporated into the membranes of distant cells. MicroRNA are further linked to epigenetic modification through Dicer, a key endoribonuclease enzyme involved in miRNA biogenesis. Dicer has been shown to be involved in the formation of heterochromatin structure, and which is itself post-transcriptionally regulated by histone deacetylase inhibitors (Fukagawa *et al.*, 2004; Hoffend *et al.*, 2017). MicroRNA have been shown to play a role in endothelial dysfunction, where they may also influence vascular remodelling and calcification (Alkagiet and Tziomalos, 2017). Indeed, Chen *et al*., (2011) cite miRNA-mediated epigenetic regulation as a putative mechanism involved in atherosclerosis. The inflammatory mediator, oxidised low-density lipoprotein (oxLDL), was found to up-regulate expression of miR-29b. This resulted in subsequent down-regulation of

DNMT3b in aortic SMCs and epigenetically-controlled matrix metalloproteinase (MMP-2/MMP-9) gene expression via methylation. OxLDL may itself be taken up by macrophages via scavenger receptors (CD36 and SR-A) on their surface. Focal build-up of oxLDL in arteries is involved in the initiation and progression of atherosclerotic plaque formation (Yuan *et al.*, 2012). Silent information regulator 1 (SIRT1) is a highly conserved NAD+-dependent de-acetylase enzyme also involved in this process (Yang *et al.*, 2017). Menghini *et al*. (2009) determined that miR-217 in ECs promotes endothelial senescence and down-regulates SIRT1 expression. Reduced expression of SIRT1 may heighten Autophagy protein 5 acetylation, which further controls foam cell formation, prompted by the presence of oxLDL (Yang *et al.*, 2017).

Transfection studies by Harris *et al*. (2008) have implicated miRNA-126 in suppression of VCAM-1, the monocyte recruitment molecule, discussed previously. This work further suggests that miRNA can regulate adhesion molecule expression and may provide additional control of vascular inflammation.

MicroRNA-125a-5p has been found to mediate lipid uptake and decrease TNF-α, in addition to other inflammatory cytokines, such as interleukin-2, interleukin-6, transforming growth factor-beta, in oxLDL-stimulated monocyte-derived macrophages. Thus it may, to an extent, contribute to post-transcriptional regulation of inflammatory response (Chen *et al.*, 2009).

Further to miRNA, circulating free double-stranded DNA (cfDNA) and free nucleosomes (fragments of chromatin/histone-DNA complexes) have been identified in plasma. To date, the majority of published data concerns cancer studies (Uehiro *et al.*, 2016; Rahier *et al.*, 2017). Nevertheless, elevated levels of circulating DNA are strongly associated with vasculature. During the later stages of atherosclerosis, apoptotic neutrophils release neutrophil extracellular traps (NETs). These networks of extra-cellular fibres consist of chromatin bound to granular and selected cytoplasmic proteins, and have the capability of inducing pro-inflammatory, pro-thrombotic and cytotoxic states (Borissoff *et al.*, 2013). The chromatin load of NETs is subject to the same methylation processes discussed previously, thereby raising the possibility of epigenetically-controlled gene expression. Circulating free DNA retains characteristics previously noted in genome-wide analysis of chromatin structure

(Ivanov *et al.*, 2015). Changes in histone alteration patterns in nucleosomes were found to be independent of age, making them potentially valuable biomarkers of disease (Rahier *et al.*, 2017). Given this evidence, there is a strong likelihood that cfDNA/nucleosomes will emerge as epigenetic regulators of vascular architecture and ageing.

1.7 Obesity and the effect of exercise on vasculature

Epigenetic change is brought about by external, environmental influences. To this end, lifestyle, and exercise in particular, may be considered as agents of epigenetic modification. Lifestyle and related factors are blamed for the rapid increase in obesity over the past 50 years, a phenomenon that traditional genetic variation does not explain (Waterland, 2008). A large proportion of the worldwide population are overweight, with the recent analysis ("Health Effects of Overweight and Obesity in 195 Countries over 25 Years," 2017) stating that in 2015, 603.7 million adults and 107.7 million children were obese. It is a controversial subject, but there is no doubt that it carries acute risk of related health outcomes and is of immediate public concern. Obesity, even in the absence of metabolic disorders, poses serious health risks. Body mass index (BMI) is a commonly used tool to assess obesity (Keihani *et al.*, 2015). Approximately, 70% of CVD deaths are associated with a high BMI ("Health Effects of Overweight and Obesity in 195 Countries over 25 Years," 2017). Based on longitudinal data, Quach *et al*., (2017) suggested that there was an association between BMI and increased epigenetic age, yet few studies to date have examined those changes in great depth.

A recent study by Nevalainen *et al*. (2017) used the Horvath algorithm to assess the epigenetic DNAm age of three groups: young adults (15-24 years), middle-aged (40-49 years) and nonagenarian (90 years). Results showed that greater BMI was associated with advanced epigenetic age in the blood cells of middle-aged individuals. Interestingly however, no significant correlation between BMI and increased DNAm in the nonagenarian cohort was observed. While there is the possibility that it may have been obscured by confounding factors, the authors propose that reduced growth/slowed regeneration of tissue in the nonagenarian population may explain this deceleration. This is supported in findings by Kananen *et al*. (2016), who found

multiple age-associated methylation features in a similar middle-age (40-49 years) group. Importantly, the group determined sites within a relatively narrow 9-year age range, suggestive of epigenetic clock-like activity. The authors urged caution in interpreting the data due to the fact that non-uniform DNAm patterns were detected across different cell types, at differing rates and for differing reasons. In light of these findings, cell type heterogeneity should be accounted for when screening tissue. Nevertheless, a deeper understanding of the association between BMI and epigenetic ageing may yield better treatment of obesity and ultimately maintain optimal cardiovascular health.

While BMI is a useful measure of visceral obesity, it has a number of drawbacks, primarily the fact that no distinction is made between body fat and muscle mass. Fitness, therefore, may present a more fundamental and clearer understanding of CVD genesis. As technology advances, sedentary behaviour has become increasingly prevalent as society moves away from traditional labour, leaving sport and leisure as the dominant sources of physical activity (PA). In the 21st century, PA has therefore become a modifiable lifestyle choice, with accompanying health and fitness benefits. High intensity PA is particularly beneficial for the cardiovascular system (Jiang *et al.*, 2015; Monedero *et al.*, 2015). It accordingly represents a potential epigenetic intervention point and hence, part of a possible vasculo-protective strategy. Advancing chronological age is associated with declining PA, commonly attributed to declining strength, endurance, and health status. Recent research on the Tsimané people, forager-horticulturalists of Bolivia with low incidence of heart disease and diabetes, assessed PA with respect to age and obesity. Results indicated that reduced CVD occurrence among Tsimané is unlikely due to high PA levels alone, and while possibly encompassing dietary factors, are certainly suggestive of a hereditary epigenetic mechanism. Furthermore, it is believed that reduced incidence of CVD may allow maintenance of higher activity levels into late adulthood, despite declining physical ability (Gurven *et al.*, 2013).

NO production, discussed previously as an important factor in endothelial function, has shown marked increases due to regular PA. This is achieved by increased laminar shear stress resulting in localisation of polymerase II and post-transcriptional phosphorylation of eNOS (Moore *et al.*, 2010). Shear stress-induced eNOS expression is a reversible, frequency-dependent process (Malek *et al.*, 1999).

Aberrant eNOS signalling is reported to be involved in impaired endothelial function via vascular endothelial growth factor (VEGF) and Protein kinase B interactions. This pathway gives rise to elevated homocysteine levels, a known CVD risk factor (Yan *et al.*, 2010). Crucially, links between Hyper-homocysteine and decreased methylation patterns have been reported (Jiang *et al.*, 2005).

Under normal human physiological conditions, shear stress is controlled by arterial elasticity, with a value of approximately 10-15 dyne/cm^2 (Lehoux and Tedgui, 2003). With this in mind, it may be possible to reconcile physiological data from exercise studies with epigenetic modification. Research by Benda *et al*. (2015), explored the effects of heart failure on brachial artery shear stress and blood flow pattern in lower limbs during cycle exercise using Doppler flow-mediated dilation. A marked increase in shear stress was noted in healthy control subjects and patients following the onset of moderate-intensity cycle exercise. Notably, the findings suggested a less favourable shear stress pattern in heart failure patients than control subjects, which was not attributed to workload (65 % of $\dot{V}O_2$peak) (Benda *et al.*, 2015).

Centenarians largely maintain comparatively high levels of PA and independence throughout their lives (Venturelli *et al.*, 2012). Although suggestive of impedance of the epigenetic clock, age-related decline in cardiovascular fitness and performance of centenarians is largely unknown. Lepers *et al*. (2016), report results from a study centred around centenarian athletes. While other studies have shown that athletic performance may be maintained up to 35 years of age, the 70-80 age range shows a steady decline. Lepers *et al*. (2016) states that it is never too late to become active, and hold centenarian athletic performance as evidence of such.

1.8 Nutrition as an agent of epigenetic change

Exercise/sedentary behaviour is only one aspect of lifestyle that may bring about chromatin alterations; diet is another. Human evolution is characterised by major shifts in caloric availability, and nutritional intake may lie at the heart of mechanisms that underpin prevalent metabolic diseases in modern human populations (Luca *et al*., 2010). Caloric restriction (CR) is a form of reduced food intake without malnutrition, and has been demonstrated to reduce a variety of age-related diseases, including cancer and CVD in rhesus monkeys (Colman *et al*., 2009). Maegawa *et al*., (2017) assessed

methylation-based epigenetic drift across 3 species: human, rhesus monkey and mouse. The authors found that the effects of CR were detectable in all three species, and that CR had a protective effect against DNAm as a function of age. Moreover, the authors propose that epigenetic drift is a significant determinant of mammalian lifespan. Early implementation of atherosclerotic cardiovascular disease prevention is critical, and a healthy lifestyle is encouraged, particularly for high-risk individuals (Martino *et al*., 2016). Optimising nutrition, like exercise, may serve to enhance vascular health (Han *et al*., 2017; Quach *et al*., 2017). The benefits of a high plant-based diet with lean meats and moderate consumption of alcohol are widely known. While studies relating nutrition to vascular health and epigenetics are limited, the majority have focused on epigenetic inheritance or the effect of dietary polyphenols, including resveratrol (Gallou-Kabani *et al*., 2007; Xia *et al*., 2014).

Tea and coffee are a rich source of polyphenols. A recent genome-wide DNAm investigation on tea and coffee ingestion using four European cohorts (N = 3,096) identified two differentially methylated CpG-sites (DNAJC16 and TTC17). Interestingly, this effect was only observed in women who consumed tea, not coffee, and identified regions related to known oestrogen metabolism and cancer genes (Ek *et al*., 2017). The vasculo-protective effects of oestrogen are well documented, and include promotion of endothelium replacement, inhibition of SMC proliferation and reduction of extra-cellular matrix deposition. Oestrogen is also a potent vasodilator (Woodman, 2008). Alkerwi *et al*.; (2015) found a relation between tea consumption and lower blood pressure. The tea drinkers in the study (36.3%) were largely non-smoking, younger females with better cardio-metabolic profiles. Coffee drinkers in the study had more frequent chronic pathologies. Lorenz *et al*., (2017) found that epigallocatechin-3-gallate (EGCG), a tea polyphenol, did not improve *in vivo* flow-mediated dilation in a trial of 50 healthy men and it was speculated that other tea compounds or metabolites were responsible for the observed protective effects. In contrast, separate reports document *in vitro* suppression of DNMT1 by tea polyphenols. Inhibition due to a variety of flavonoids were observed in blood DNAm data. Of these, EGCG produced the greatest suppression, with values ranging from 0.21 - 0.47μM. EGCG efficacy on DNMT-mediated DNAm was determined as independent of its own methylation and attributed largely to its direct inhibition interactions with DNMT catalytic sites. Importantly, this inhibitory activity was

strongly enhanced by the addition of Mg^{2+} in a concentration-dependent manner up to 10 mM, (highest concentration tested) (Lee *et al*., 2005).

1.9 Magnesium and cardiovascular health

The application/consumption of natural compounds, such as phenolic acids, lectins and bio-polymers, in the healthcare domain is gaining increasing attention. Magnesium (Mg) is a micro-nutrient, critically involved in membrane function, muscle contraction, protein assembly and DNA replication. It is also an essential co-factor in over 325 enzymatic reactions (Newhouse and Finstad, 2000). Mg supplementation is becoming increasingly utilised in maintaining physiological health, particularly that of the cardiovascular system (Maier, 2012). It plays a critical role in modulating vascular smooth muscle tone, endothelial cell function, and myocardial excitability and is thus central to the pathogenesis of several cardiovascular disorders such as hypertension, atherosclerosis, coronary artery disease, congestive heart failure, and cardiac arrhythmias.

The epigenetic processes discussed previously may influence health and ageing in a number of ways. Nutritional magnesium supplementation may act beneficially through epigenetic mechanisms, as well as traditional cellular and molecular pathways. Interestingly, Mg is potentially a potent epigenetic regulator via signalling through one of its receptors, namely transient receptor potential melastatin 7 (TRPM7). TRPM7 and its related magnesium receptor, TRPM6, are unique in that these extraordinary proteins comprise of two distinct functional moieties: an ion channel segment and a α-type serine/threonine kinase domain (Chubanov *et al.*, 2018). Both of these divalent cation-selective channels are activated upon reduction of cytosolic levels of Mg^{2+} and Mg·ATP. TRPM7 has been demonstrated to regulate a plethora of salient cell processes such as Mg^{2+} metabolism (Ryazanova *et al.*, 2010), Ca^{2+} signalling (Faouzi *et al.*, 2017), cell motility (Su *et al.*, 2011), proliferation (Sahni *et al.*, 2010), differentiation (Jin *et al.*, 2012), and importantly chromatin remodelling and architecture (Krapivinsky *et al.*, 2014). Genetic studies have differentiated the functional characteristics of both the ion channel segment and a α-type serine/threonine kinase domain. Inactivation of TRPM7 in mice results in early embryonic death (Jin *et al.*, 2012). Further murine studies, employing conditional

tissue-specific inactivation of TRPM7, demonstrated that TRPM7 plays a critical role in morphogenesis of various internal organs (Jin *et al.*, 2012; Sah *et al.*, 2013). In contrast to global TRPM7 null mutations, specific genetic inactivation of the kinase activity ('kinase-dead' TRPM7 mutation) does not impede embryonic development (Kaitsuka *et al.*, 2014). Interestingly, adult transgenic 'kinase-dead' TRPM7 mice are more resistant to hypomagnesmia in terms of survival, and develop a mild form of organismal Mg^{2+} deficiency (Ryazanova *et al.*, 2014). These findings highlight that the TRPM7 kinase moiety is necessary for an adaptive systemic response to Mg^{2+} deficiency and may act as a cellular epigenetic initiator, with systemic levels of magnesium being a Nutrient Epigenator. Hence, nutritional magnesium supplementation may act beneficially through epigenetic mechanisms, as well as traditional cellular and molecular pathways. This lends further credence to the possibility of using Mg as a potential therapeutic in the prevention/treatment of atherosclerosis.

This is further compounded by the fact that hypomagnesmia, present in 48% of the US population (Rosanoff *et al*., 2012), contributes to accelerated ageing, inflammation and chronic illness (Xia *et al.*, 2017). Hypomagnesemia has been stated to occur when serum Mg levels are less than 1.46 mg/L (Shrimanker and Bhattarai, 2019), although the exact figure is disputed. Hypomagnesmia has been associated with metabolic syndrome diagnosis. The concomitant presentation of several metabolic disorders in an individual, including dyslipidemia, insulin resistance, obesity and hypertension increases DM2 and CVD risk (Ma *et al.*, 1995; Rochelson *et al.*, 2007). Chronic systemic inflammation, which contributes to the development of metabolic disorders, has been inversely correlated with magnesium intakes in a cross-sectional study of 11,686 middle-aged women; the lowest prevalence of metabolic syndrome was found in the group of women with the highest quintile of magnesium intakes (median intake, 422 mg/day) (Song *et al.*, 2005).

Mg deficiency has long been linked with vascular compromise/permeability *in vivo*, through ROS and cytokine signalling (Wiles *et al.*, 1997). Moreover, it has been shown to result in increased oxidative stress in ECs cultured in low-Mg environments and activation of NF-κB (Altura *et al.*, 2014). Interestingly, supplementation with Mg sulphate has demonstrated suppressed inflammatory responses through the NF-κB pathway (Rochelson *et al.*, 2007). A recent report by Almousa *et al*. (2018) supports

this, demonstrating that high Mg ($MgSO_4$) concentrations resulted in a reduced HUVEC response to inflammatory stimulus. Low Mg concentrations, in contrast, resulted in increased expression of adhesion molecules and inflammatory cytokines (including in the absence of inflammatory stimulus) that enhanced binding of monocytes to ECs. Zierler *et al*. (2017) suggest that the TRPM7 kinase could act upstream of Annexin-A1, a potent anti-inflammatory agent, thereby regulating immune response through NF-κB.

The daily recommended Mg dose has been approximated at ≥ 300 mg/day, but is age/life-stage/gender dependent (Jahnen-Dechent and Ketteler, 2012), and exhibits variable distribution throughout the body (see Figure 1.12). A wide variety of magnesium sources are available as over-the-counter dietary supplements. These are available in organic (eg. citrates, lactates, gluconates) and inorganic forms (eg. oxides, carbonates, chlorides, hydroxides), in addition to magnesium complexes/chelates (eg. amino acid chelates). The effectiveness of these may depend upon their relative bioavailability (Firoz and Graber, 2001; Coudray *et al.*, 2005). Dissociation of Mg compounds may also play a role in this. $MgCl_2$, for example, is highly soluble in water (90% of cytoplasm) where it dissociates into ions: a cation of magnesium (Mg^{2+}) and two anions of chloride (Cl^-). Approximately 24-76% of dietary Mg is absorbed by the gut; the remainder is discarded in faeces (Graham *et al*. 1960).

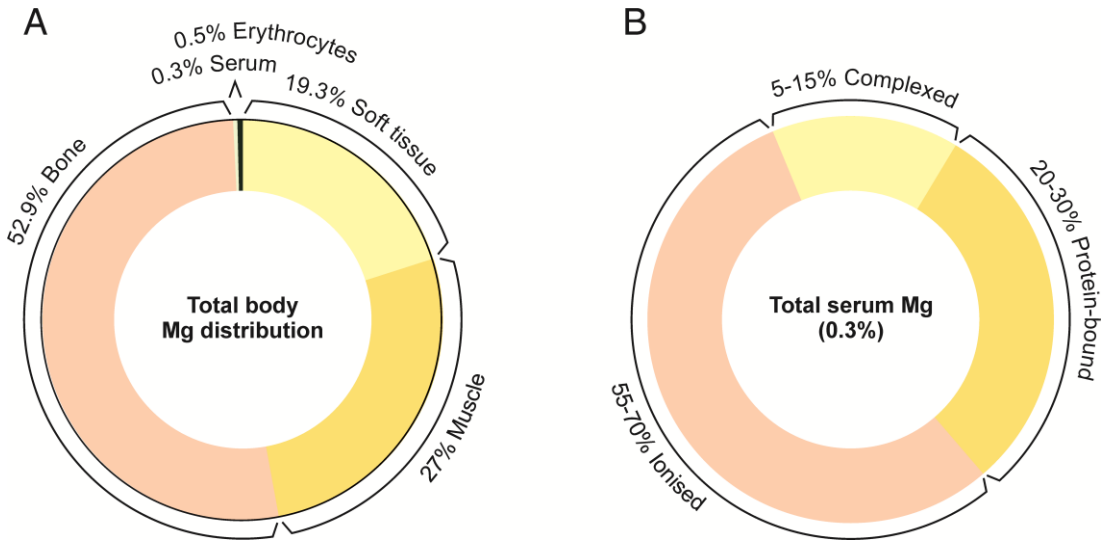

Figure 1.12 Total Mg distribution
(A) Total body Mg distribution, (B) Total serum Mg levels in humans. Mg is mostly sequestered in bone, muscle and soft tissue**.** Total serum Mg levels account for only ~0.3% of total body Mg. Ranges are provided due to differing measurement methods, resulting in variable readings (Jahnen-Dechent and Ketteler, 2012).

1.10 Complex systems as models of inflammation

Literature has shown the cardiovascular system and its components to demonstrate complex reactions at the onset of inflammation. These range from adhesion of monocytes and lymphocytes on the endothelial surface to epigenetic alterations/vascular ageing as a result of environmental factors that include magnesium supplementation. In this section of the review, literature surrounding dermal tissue, as an additional and more complex model of inflammation that incorporates the vascular component, will be evaluated.

1.10.1 An overview of human dermal tissue and its response to injury

The skin's primary function is to protect the body from exogenous environmental influences. It is comprised of two major layers – the epidermis and dermis, with each further divided into morphologically-distinct sub-layers. The stratum corneum (corneocytes surrounded by lipid regions) acts as the main barrier, and comprises the outermost layer of epidermis. Blood vessels are located immediately below this in the dermis. Hence, for the absorption of trans-dermal Mg under normal circumstances, it

must first permeate the stratum corneum. Once this is achieved, Mg may then be transported in circulation (Kass *et al.*, 2017).

Epidermal keratinocytes originate in the stratum basale and transition up through the layers of the epidermis (Figure 1.13). During this movement, they undergo gradual differentiation and morphology changes until they reach the stratum corneum, where they form a layer of nucleus-free, flat, and highly keratinised squamous cells. This layer forms an effective barrier to the entry of infectious agents into the body and helps to limit moisture loss. Trans-epidermal water loss, (TEWL), along with changes in pH are characteristic of skin barrier loss and thermal burn injury (Duffy *et al.*, 2017).

Normal Human Dermal Fibroblasts (NHDF) are responsible for producing the extra-cellular matrix forming the connective tissue of the skin, and play a crucial role during wound healing. NHDFs are an adherent cell type, which over time form a confluent, contact-inhibited monolayer. Fibroblast and keratinocyte interaction plays a critical role in preserving skin integrity under both normal and pathological conditions (Carr *et al.*, 2017). Experimentally, keratinocyte-conditioned medium has been shown to suppress type-1 and -3 collagen expression in fibroblast cells (Ghaffari *et al.*, 2009).

The first study to investigate trans-dermal Mg absorbency in humans was only recently published by Kass *et al*. (2017). There, the authors examined serum and urinary Mg levels following treatment with 56 mg/day Mg^{2+}-/placebo- infused cream, reporting statistically significant increases in serum Mg levels in a sub-group of non-athletes. However, a thermal burn insult may result in altered skin absorbance properties. A compromised stratum corneum results in impaired epithelial permeability, particularly at the burn margin, as demonstrated by Plichta *et al*. (2014) using murine models. Burn injuries may exert catastrophic influences on human life, suffering, disability, and financial loss.

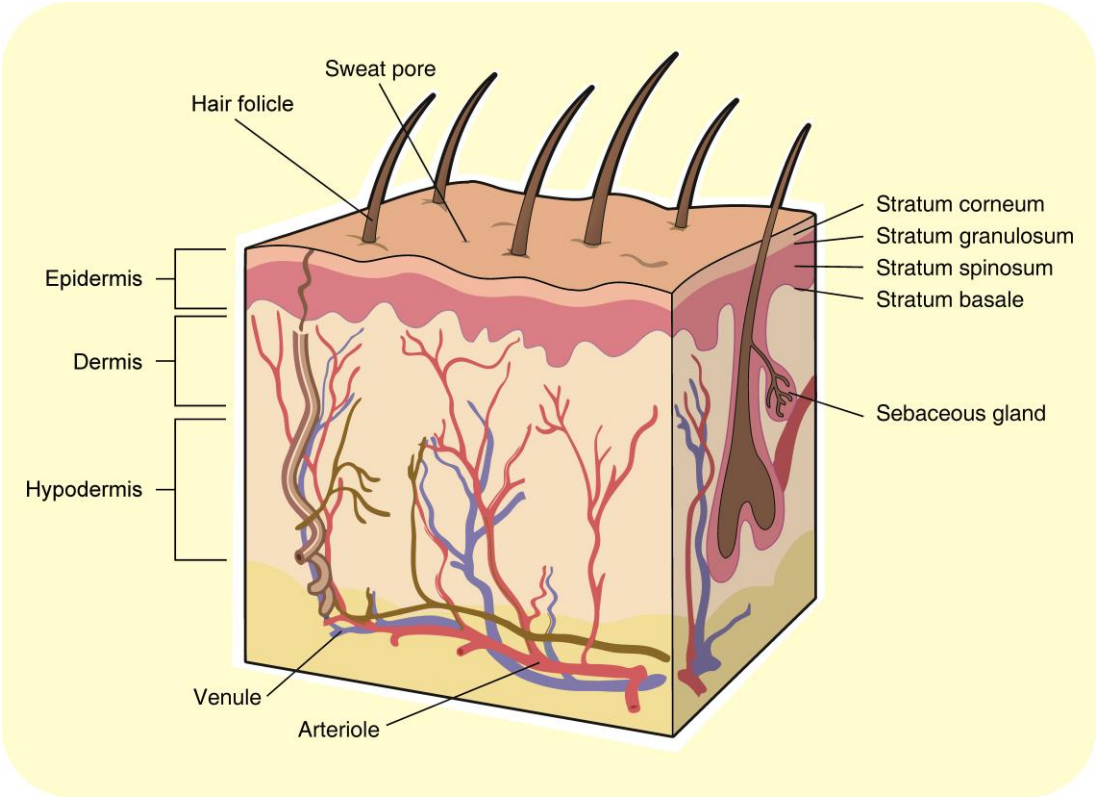

Figure 1.13 Diagram of healthy skin, indicating morphologically-distinct sub layers
(Adapted from www.dreamstime.com/stock_image)

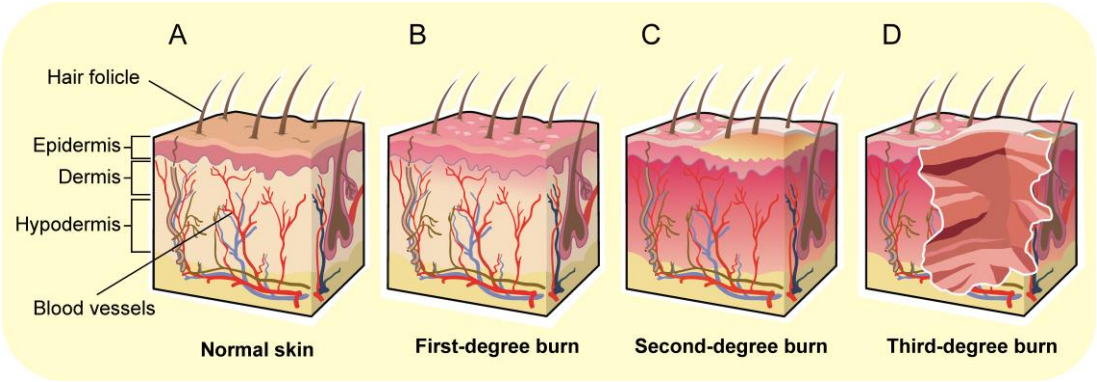

Figure 1.14 Diagram illustrating skin burn damage progression from healthy skin through to third-degree burn
(Adapted from www.dreamstime.com/stock_image)
Burn depth refers to the amount of skin, and possibly other tissue, damaged or destroyed, and may be categorised as follows: (B) First-degree burns affect only superficial skin layers. (C) Second-degree (partial-thickness) burns extend into some of the underlying dermal layer. (D) Third-degree (full-thickness) burns are those where the injury extends to all skin layers. Temperature and exposure duration are a important determining factors.

Wound healing is a dynamic, complex mechanism involving numerous cell types and signalling mediators, and occurs over four distinct but overlapping stages: hemostasis, inflammation, proliferation, and re-modelling. Numerous additional factors influence these processes - nutrition, age, oxygenation, surgical techniques, and pre-existing medical conditions, such as diabetes or infection may all contribute to wound healing and its complications (Schiff, 2009). A recent study used NDFCs to examine the effect of natural bio-molecules (lectins and polysaccharides) on cell migration/wound closure (de Sousa *et al.*, 2019). Of those tested, only Frutalin (a breadfruit lectin) stimulated NDFC migration *in vitro*. Burn injuries differ significantly from other wound types due to the application of heat (see Figure 1.14), and also by severity (see Table 1.1), yet the induced inflammatory response is the same for all traumatic wounds. This response may be further sub-divided into (i) cellular and (ii) vascular response:

(i) Neutrophils and monocytes migrate to the inflammatory site, before replacement by macrophage cells recruited through mast cell releasate (TNF, histamine, proteases, leukotreins and cytokines) in addition to chemotactic factors (including kallikreins and fibrin peptides) released from the coagulation process itself. This aids phagocytosis and cleaning of dead tissue and toxins released by burned tissue.

(ii) Localised vasodilation occurs immediately following burn injury. Increased endothelial permeability caused by the effects of inflammatory mediators leads to leakage of fluid into the interstitial space. Such permeability separates burn injuries from other traumatic wound types (Tiwari, 2012; Zhao *et al.*, 2015; Rae *et al.*, 2016).

Table 1.1 Differences in tissue response to second-degree (partial) and third-degree (full-thickness) burn injuries

	Second-degree burn (Partial thickness burn)	Third-degree burn (Full-thickness burn)
Tissue perfusion	Initial vasoconstriction causing transient decreased dermal blood flow.	Vascular occlusion causing prolonged decrease in blood flow.
Capillary permeability	Increased permeability after dermal vessel injury.	Increased after injury to dermal and sub-dermal vessels.
Edema formation	In dermis and in junction between dermis & epidermis.	In dermis & sub-dermis.
Interstitial change	Loss of interstitial matrix in burned areas. Tissue integrity maintained in non-burned dermis.	Loss of interstitial integrity & damage to matrix components, hyaluronic acid & collagen scaffolding.
Interstitial pressure	Mild decrease in injured dermis.	Marked decrease in injured dermis.
Lymphatics	Preserved function, allowing for rapid edema clearance & lost proteins.	Damaged with severely decreased clearance of edema & lost proteins.

Individuals exposed to severe burns (≥ 30 per cent of total body surface area) develop hypomagnesmia and hypocalcemia, as well as hypoparathyroidism and renal resistance to the administration of exogenous parathyroid hormone. A large portion of mineral loss occurs through cutaneous exudate, and correlates with burn severity/area. This is largely due to increased endothelial permeability, with extensive loss of plasma leading to hypovolemic shock (Berger *et al.*, 1997; Klein and Herndon, 1998; Tiwari, 2012; Rae *et al.*, 2016). Intra-cellular Mg uptake may occur as a result of the increased metabolic rate observed in burn patients in order to support the increased energy requirements of cells (Klein and Herndon, 1998). Hence, nutrition is an important factor in recovery. Hypocalcemia is a product of bone resorption, resulting from differentiation of bone marrow stem cells into osteoclasts via activation of NF-κB and RANKL (Klein *et al.*, 1997; Klein, 2011). The close relationship between Mg and Ca, was not hypothesised to play a role in this, however.

1.10.2 Burn modelling as an experimental approach

Given the complex nature of wound healing, and the serious health implications of burn injuries, it is no surprise that researchers have turned to more complex models to further investigate possible treatments/therapies. Literature shows that the majority of

dermal burn research is conducted using *in vivo* murine and porcine models. Typical protocols use anesthetised animals subjected to sham and thermal/scald burn injuries for a specific duration (typically 10 sec.). This generates an insensate third-degree full-thickness burn, which may be sampled 24-96 h post-burn (Plichta *et al.*, 2014; Andrews *et al.*, 2016). The ability to create reproducible and consistent burns is a key factor in any such experiment. Punch biopsy with accompanying histological analysis is a widely accepted method of assessing burn depth, and a host of different analysis methods are described, including thermography, etc.

Table 1.2 Advantages/disadvantages of a range of alternative skin testing models [adapted from Abd *et al.*, (2016)]

	Advantages	**Disadvantages**
Human skin ***in vivo, ex vivo***	Most biologically relevant. Ex vivo is best surrogate.	Often precluded for ethical reasons. Variability.
Animal skin **eg. porcine, murine**	Reasonably easy to obtain animal skin, particularly ex vivo.	Different barrier properties. Variability. Ethical considerations.
Artificial membranes **eg. lipid-based**	Useful for studying basic diffusion mechanisms. Consistent & homogeneous.	No physiologically representative of human skin.
***In vitro* skin models** **eg. LabSkin**	Can be engineered to mimic healthy/disease states. Built-in barrier properties. Metabolism can be sustained.	Usually more permeable than human skin. General lack of cell diversity.

Nevertheless, due to high costs and ethical considerations associated with animal models, alternatives to *in vivo* testing are also used (Table 1.2). Artificial membranes are commercially available/constructible, including lipid-based models and simple polymeric models, and are distinct from nanocellulose and other membranes used as trans-dermal drug delivery patches (Abd *et al.*, 2016; Morais *et al.*, 2019).

Living skin equivalents (LSEs) take this concept further, with physiologically-relevant *in vitro* models that can be engineered to mimic specific healthy/disease states. Moreover, they can be cultured/maintained over time in a way that *ex vivo* mammalian tissue cannot – tissue-derived cells slowly lose their viability and metabolism is reduced (Mitchell *et al.*, 2016). Such LSEs have been shown to closely resemble human skin by histological analysis, immunostaining, TEM and scanning electron

microscopy after transplantation to athymic murine models for evaluation of regenerative and clinical performance (Mazlyzam *et al.*, 2007). If used as replacement tissue, such dermal substitutes re-vascularise in two to three weeks from the graft bed and must subsequently receive an epidermal graft to complete the recovery (Braye *et al.*, 2005). LSEs are commercially available for experimental purposes. Alternatively, they may be self-engineered using cell types with a final architecture tailored to meet specific experimental demands (Mi *et al.*, 2018). While imperfect and limited, such models allow the study of burn and healing processes in depth, in addition to the performance properties of potential therapeutics.

1.10.3 Burn recovery

The process of re-epithelialisation begins a few hours post-burn as keratinocytes migrate from undamaged dermis. Re-epithelialisation of second-degree burns typically requires 5-7 days to fully cover the wound, with third-degree burns requiring much longer. Basement membrane formation between dermal and epidermal layers occurs after this process, with angiogenesis and fibrogenesis further aiding dermal reconstruction (Tiwari, 2012) (see Figure 1.15).

Angiogenesis, the formation of new blood vessels from a pre-existing vasculature, is an important natural process involving the migration, growth and differentiation of endothelial cells. It is a critical process of growth and development, as well as of wound healing (Iruela-Arispe and Dvorak, 1997; Dvashi *et al.*, 2014). Angiogenesis is initiated by the release of pro-angiogeneic factors that attract inflammatory and ECs, promoting their proliferation. ECs respond by secreting matrix metallo-proteinases (MMPs). MMPs comprise a family of zinc-dependent endopeptidases capable of proteolytically degrading ECM proteins and remodelling basement membranes (Rundhaug, 2005; Van Lint and Libert, 2007). Thus, digestion of blood vessel walls occurs and EC migration toward the site of the angiogenic stimuli is permitted. As a result of this and continued proliferation and migration, ECs form capillary tubes and ultimately new blood vessels (Iruela-Arispe and Dvorak, 1997). This occurs with concomitant re-epithelialisation of the wound site (Park and Park, 2018). There is some evidence to suggest that Mg could play a role in angiogenesis through the TRPM7 receptor. Literature shows that while MMP production remained unaffected,

magnesium deficiency/TRPM7 silencing impaired EC migration and inhibited growth by arresting cells in the G_0/G_1 and G_2/M phases of the cell cycle. TRPM7 down-regulation may mediate low Mg-induced inhibition of cell growth and migration. This points to Mg and TRPM7 as modulators of the angiogenic phenotype of microvascular endothelial cells (Baldoli and Maier, 2012).

Scarring occurs in the third phase of healing, where fibrous structural proteins (collagen and elastin) are laid down as ECM around epithelial, ECs and VSMCs. It is this ECM that is re-modelled into scar tissue, when fibroblast cells acquire the myofibroblast phenotype responsible for scar contraction.

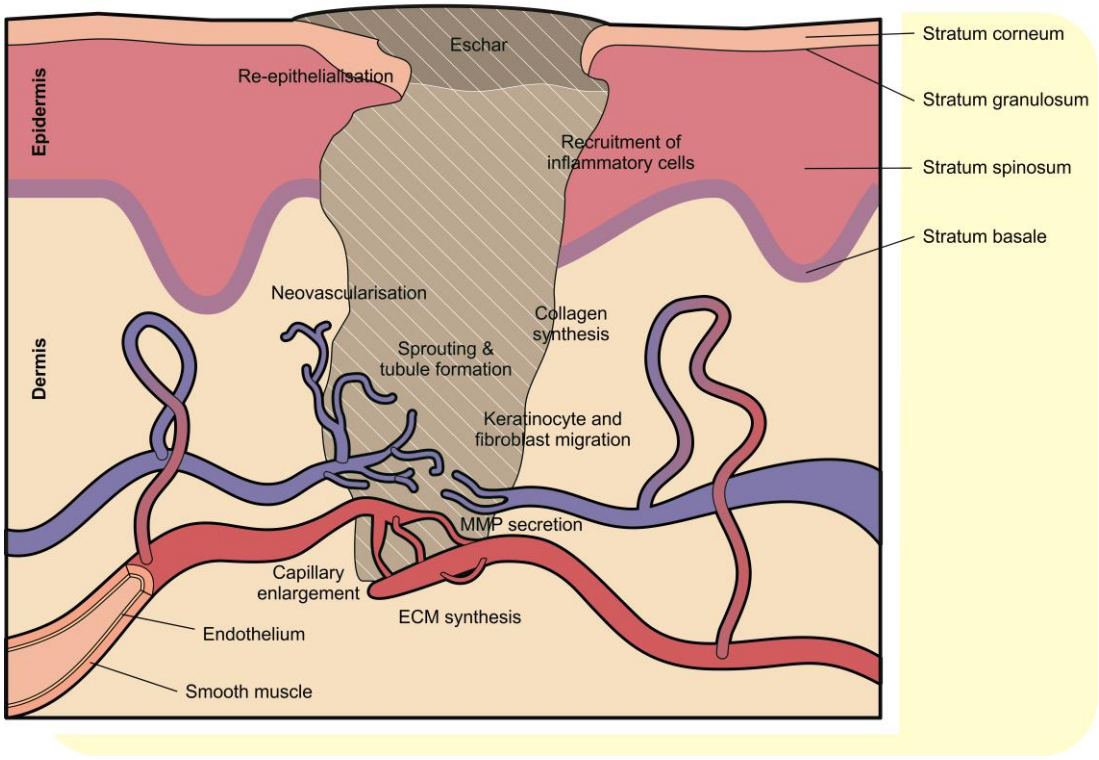

Figure 1.15 Burn wound healing and angiogenesis following inflammatory phase

1.10.4 Burn Dressings as Therapeutic Delivery Agents

Dressings are typically used to facilitate repair/regeneration of damaged tissue. These form a physical barrier between the damage site and external environment, though preferably must remain permeable to air. However, no ideal dressing exists in clinical practice. Infection remains the principal cause of complications in burn injuries, though sterilisation of the burn site occurs naturally as a result of high heat. Hence, infection usually occurs after migration of organisms deep seated in the epithelial appendages of hair follicles and sebaceous glands (Adamian *et al.*, 2004; Tiwari,

2012; Glik *et al.*, 2018). Such dressings may be broadly described as either (i) passive or (ii) active:

(i) Passive dressings protect the wound.

(ii) Active dressings promote healing in addition to protecting the wound. They interact with the wound bed components to enhance wound healing. They may be anti-microbial, absorbent, improve moisture retention, aid collagen deposition, etc.

Modern dressings merge a number of technologies together, with the overarching aim to achieve skin regeneration, not skin repair (Madaghiele *et al.*, 2014). They must overcome individual component side-effects/interactions in order to elicit a beneficial result and minimise scarring. For example, while topical anti-microbial substances allow control of bacterial load, they may also result in cytotoxicity and impede healing rate (Slaviero *et al.*, 2018). Hydrogels and spongy membrane scaffolds are an example of active dressings. They have been used as therapeutic delivery mechanisms for cutaneous wound healing and burn treatment. Hydrogels are hydrophilic cross-linked polymeric chain structures, and may be composed of hydrocolloids, alginates, hydrogels, collagen or hyaluronic acid (Dhaliwal and Lopez, 2018). They typically exhibit swelling capacity, drug compatibility, safety, low toxicity, shelf stability and high purity. Additional essential requirements include bio-compatibility and mechanical strength (de Sousa *et al.*, 2019). Literature cites numerous studies involving the application of drug-/treatment-infused hydrogels on skin as potential therapeutics (Madaghiele *et al.*, 2014; Huang *et al.*, 2018).

First-aid, packaging and transportation of the burn-injured patient to hospital is the most important contribution to the successful management and outcome. In this respect, use of hydrogels as a pre-hospital treatment has reportedly increased in the last decade, where 39% of emergency medical services in the United Kingdom applied hydrogel dressings (e.g., Water-Jel, Water-Jel Technologies, Carlstadt, NJ, USA; Burnshield, Levtrade, Johannesburg, South Africa) (Allison, 2002). This figure is disputed by (Goodwin *et al.*, 2016), whose systematic review assessed supporting evidence for the clinical use of hydrogel dressings and found hydrogel usage to be much less prolific.

1.11 Study hypotheses and objectives

Vascular inflammation is a key contributor to CVD, with inflammation and CVD risk factors closely inter-related. Atherosclerosis, the most common of the vascular inflammatory diseases, specifically affects arterial blood vessels, and is caused by dynamic endothelial dysfunction. Epigenetic modification, the accumulation of distinct chemical signatures on DNA and histones, are initially established during embryogenesis and continue to be modified by age and lifestyle choices throughout life. Injurious oscillatory shear stress (OSS), associated with atherosclerosis in particular, is believed to exert a damaging influence on the health and epigenetic processes of the vascular endothelium. Literature suggests a number of possible regulatory elements that control these epigenetic processes. Evidence shows that expression of non-coding RNA, such as miRNA, may regulate gene expression as well as epigenetic mechanisms. In addition, nutritional Mg supplementation may act beneficially through epigenetic mechanisms, as well as traditional cellular and molecular pathways. While knowledge of epigenetic processes as a whole has expanded considerably in recent years, the juncture between vascular inflammation, epigenetics and magnesium remains undefined and underexplored. Hence, the following objectives are set out in this thesis:

1.11.1 Study 1: Profiling the epigenetic effects of oscillatory shear stress on vascular endothelium

This thesis will first establish a model of vascular oscillatory shear stress, through which, a number of key genes and mechanisms involved in epigenetically-regulated vascular ageing may be identified.

1.11.2 Study 2: Exploring the use of magnesium as an anti-inflammatory agent

While the effects of Mg on the endothelium using *in vivo* and *in vitro* models have been widely published, no such investigations have been carried out using a dynamic model of shear stress. Hence, the use of Mg as a therapeutic agent to combat inflammatory response/atherogenesis will be investigated.

1.11.3 Study 3: Exploring the use of magnesium as an anti-inflammatory agent in a multicellular model of inflammation

An *in vitro* skin burn model will be developed as a more complex model, through which, a magnesium-infused hydrogel therapeutic will be tested for anti-inflammatory properties. Skin cells (Normal Human Dermal Fibroblast cells and Adult Human Dermal Keratinocyte cells) will be assessed in conjunction with Human Aortic Endothelial cells in order to ascertain the effect of Mg on wound healing and angiogenesis.

1.11.4 Study 4: Investigating the systemic circulatory effects of Mg supplementation explored as a human trial

A 28-day human trial to assess the effects of a magnesium-based supplement mixture on vascular competence will be conducted. In this way, the effect of Mg in systemic circulation will be assessed using platelet function as a measure of cardiovascular competence. Analysis of circulatory biomarker proteins related to low-grade inflammation and vascular reactivity will enable the sensitive determination of any protective impact that such supplementation may yield.

In completing these objectives, a comprehensive picture of the role of magnesium as a potential anti-inflammatory agent will be drawn, its role as a possible epigenetic regulatory element will be explored, and the inclusion of magnesium as a therapeutic aid in the stabilisation of burn injuries will be assessed.

Chapter Two

Materials and methods

2.1 Materials

2.1.1 Reagents, chemicals and consumables

Acea Biosicences Inc., (CA, USA):

05665817001	xCELLigence® CIM-Plate® 16 (6)
05469830001	xCELLigence® E-Plate® 16 (6)

Becton, Dickinson and Company, (NJ, USA)

369714	Blood collection vacutainer (sodium citrate) 4.5 mL

Cloud Clone, USA

CEA660Ge	8-Hydroxydeoxyguanosine (8-OHdG) ELISA kit

Digital Bio, Nano-EnTek, (South Korea):

AD4K-200	AccuChip™ 4X Kit

Eppendorf (Hamburg, Germany):

0030121589	Eppendorf Safe-Lock Tubes, 1.5 mL, Biopur®

Innoven, (Yorkshire, UK):

LS4.5	LabSkin™ *in vitro* 3D skin model

Integrated BioDiagnostics (Ibidi®) GmbH, (Martinsried, Munich, Germany):

81516	Ibidi® µ-slide Angiogenesis
80182	Ibidi® µ-slide $I^{0.6}$ luer

InvivoGen, (CA, USA):

ant-pm-1	Primocin™ anti-microbial agent

Lennox Laboratory Supplies Ltd., (Dublin, Ireland):

SI-033-0716	99+% Industrial Methylated Spirits (IMS)

Lonza, (Maryland, USA):

00192627	Adult Human Dermal Keratinocyte Cells (Lot# 0000249305)
BE17-512F	Dulbecco's Phosphate Buffered Saline (Ca- and Mg-free)
	Human Aortic Endothelial Cells
CC-2511	Normal Human Dermal Fibroblast Cells (Lot# 0000465422)

Merck Millipore, (Massachusetts, USA):

4500-0025	Guava easycheck™ kit Lot #15-0304
4200-0140	Instrument cleaning fluid (ICF) Lot #3166056

Neal's Yard, (London, UK):

Human trial supplements active (OMC and *Boswellia serrata* extract)

Human trial supplements placebo (glycerin)

Full components for both listed in Appendix B

Promocell, (Heidelberg, Germany):

C-29910	Cryo-SFM serum-free medium for cryopreservation
C-97237	Customer Formulation Endothelial Cell Growth Medium MV (Mg-free)
C-97238	Customer Formulation Fibroblast Growth Medium (Mg-free)
C-97239	Customer Formulation Keratinocyte Growth Medium (Mg-free)
C-22020	Endothelial Cell Growth Medium MV; Endothelial Cell Growth Medium MV Supplement Mix: (Fetal Calf Serum (FCS) 5.0% (v/v), Endothelial Cell Growth Supplement (ECGS) 0.4% (v/v), Endothelial Growth Factor (EGF)
C-2121	Endothelial Cell Growth Medium MV II Kit
C-23120	Fibroblast Growth Medium II Kit
C-20111	Keratinocyte Growth Medium II Kit

Roche Diagnostics (Basel, Switzerland):

100144495	AURKB RealTime Ready Catalogue Assay

10014486	BRD7 RealTime Ready Catalogue Assay
100144529	DOT1L RealTime Ready Catalogue Assay
06402682001	FastStart Essential DNA Probes Master
100073	GAPDH RealTime Ready Catalogue Assay
04729692001	LightCycler® 480 plates (96-well)
100144510	NCOA3 RealTime Ready Catalogue Assay
100144501	PAK1 RealTime Ready Catalogue Assay
100139772	SETD6 RealTime Ready Catalogue Assay
04379012001	Transcriptor First Strand cDNA Synthesis Kit
100100763	TRPM6 RealTime Ready Catalogue Assay
100100772	TRPM7 RealTime Ready Catalogue Assay

Sigma Chemical Company Ltd., (Dorset, UK):

A2152-50G	Bovine serum albumin (BSA)
C-2432	Chloroform (99+%)
C-3886	Crystal violet
37291-25MG	Dihyroethidium
S-002M	Dimethyl sulfoxide (DMSO)
D8537	Dulbecco's Phosphate Buffered Saline
E7023	Ethanol (99+%)
F2442-50ML	Fetal Bovine Serum (FBS)
M0088000	Magnesium aspartate dihydrate
M1028-100ML	Magnesium chloride ($MgCl_2$) Lot#SLBR8048V
E0282-1ML	MaxGel™ ECM
MG500-500ML	May–Grünwald stain
P4417-100TAB	Phosphate buffered saline (PBS) tablets
P6148-500G	Paraformaldehyde
L3771-500G	Sodium dodecyl sulphate (SDS)
H8916	Human recombinant TNF-α
X100	Triton
T4174-100ML	Trypsin-EDTA (10X)
T8154	Trypan Blue

P1379-500ML	Tween 20
W4502-1L	Water (molecular biology reagent)
Primer sequences:	
GAPDH Forward	5' GAGTCAACGGATTTGGTCGT 3'
GAPDH Reverse	5' TTGATTTTGGAGGGATCTCG 3'
ICAM-1 Forward	5' AGAGACCCCGTTGCCTAAAA 3'
ICAM-1 Reverse	5' CAGTACACGGTGAGGAAGGT 3'
VCAM-1 Forward	5' GCTCTGTCACTGTAAGCTGC 3'
VCAM-1 Reverse	5' CTGCCTTTGTTTGGGTTCGA 3'

Sarstedt AG & Co. (Nümbrecht, Germany):

72.737.002	0.2 mL PCR tubes
72.735.002	0.5 mL PCR tubes
72.706.200	1.5 mL microtubes
72.695.500	2 mL microtubes
62.554.502	15 mL centrifuge tubes
62.559.001	50 mL centrifuge tubes
86.1254.001	10 mL serological pipettes
83.3902	100 x 20 mm tissue culture dishes
83.3920	6-well tissue culture plates
83.3921	12-well tissue culture plates
83.3922	24-well tissue culture plates
83.3924	96-well tissue culture plates
82.1582	96-well round-bottom plates
83.1830	Cell scrapers
72.380.992	CryoPure tubes
83.1826.001	Filtopur 0.2 μm syringe filters

STARLAB GmbH, (Hamburg, Germany):

S1121-3810	10 μL filtered pipette tips
S1120-1810	20 μL filtered pipette tips
S1120-8810	200 μL filtered pipette tips

S1120-9810	300 µL filtered pipette tips
S1126-7810	1000 µL filtered pipette tips

Thermo Fisher Scientific Ltd., Massachusetts, USA):

AM9890	DNAZap® (Ambion)
4368814	High Capacity miRNA cDNA reverse transcription Kit
33-32-P/25	Integra® disposable biopsy punches, 3.0 mm (Miltex®)
R415	Rhodamine Phalloidin (Invitrogen)
AM9780	RNaseZap® (Ambion)
4399966	Megaplex™ RT Primers Human (Pool A) v2.1
4444745	Megaplex™ RT Primers Human (Pool B) v3.0
4399233	Megaplex™ PreAmp Primers, Human (Pool A) v2.1
4444303	Megaplex™ PreAmp Primers, Human (Pool B) v3.0
AM1560	*mir*Vana™ miRNA isolation kit (Invitrogen)
4428123	TaqMan® Array Human MicroRNA A Card v3.0
4398978	TaqMan® Array Human MicroRNA B Card v 2.1
4391128	TaqMan® Pre Amp Master Mix 2X
4440040	Taqman® Universal Master Mix II, no UNG
AM9849	TE buffer, pH 8.0, RNase-free
15596018	Trizol™ reagent

Qiagen GmbH, (Hilden, Germany):

330401	RT^2 First Strand Kit (12)
330451	RT^2 Pre-Amp cDNA Synthesis Kit (12)
330523	RT^2 SYBR® Green ROX™ qPCR Mastermix (24)
PBH-086Z	RT^2 Pre-Amp Pathway Primer Mix (Human chromatin remodelling factors)
PBH-085Z	RT^2 Pre-Amp Pathway Primer Mix (Human epigenetic chromatin modification enzymes)
PBH-121Z	RT^2 Pre-Amp Pathway Primer Mix (Human wound healing)
PAHS-086ZC	RT^2 Profiler PCR array (Human chromatin remodelling factors)

PAHS-085ZC	RT^2 Profiler PCR array (Human epigenetic chromatin modification enzymes)
PAHS-121ZC	RT^2 Profiler PCR array (Human wound healing)

2.1.2 Instrumentation and Apparatus

Acea Biosicences Inc., (CA, USA):

3X16 instrument	xCELLigence® Real-Time Cell Analyser (RTCA) DP

Biotek, (Vermont, USA):

ELx800 microplate reader

Bio-Rad, (CA, USA):

Mini Protean Tetra Cell Western Blot system

MJ Mini Thermal Cycler

Carl Zeiss (Oberkochen, Germany):

Zeiss 710 Confocal Microscope

Digital Bio, Nano-EnTek, (South Korea):

Advanced Detection and Accurate Measurement ($ADAM^{MC}$) counter

AD4K-200	Accuchip 4x Kit

Eppendorf, (Cambridge, UK):

Centrifuge 5415 D; Centrifuge 5430 R; Centrifuge 5810 R

Global Medical Instrumentation Inc., (MN, USA):

Mikro 200R micro-centrifuge

Integrated BioDiagnostics (Ibidi®) GmbH, (Martinsried, Munich, Germany):

10962	Perfusion set (red)
10903	Pump and fluidic system v1.1 Software: PumpControl v1.5.0
80008	Olaf Humidifying Chamber

Leica Microsystems, (Wetzlar, Germany):

13613210	Leica DM500 microscope with ICC50 camera module Software: Leica Application Suite EZ v.3.4.0

Merck Millipore,(Massachusetts, USA):

Guava® easyCyte 8HT Benchtop Flow Cytometer

Software: guavaSoft inCyte v2.7

Nalgene, (Rochester, NY, USA):

Mr. Frosty™ Cryo-freezing container

Nikon, (Shinagawa, Tokyo, Japan):

Eclipse TS100 phase-contrast microscope

Sanyo, (Osaka, Japan):

MDF-U7386S	Ultra-Low Temperature Freezer (-80°C)

Stuart Scientific Ltd, (Staffordshire, UK):

SA8	Vortex
SSM1	Orbital Shaker
SSL4	See-Saw Rocker
SBH130D	Block Heater

Taylor-Wharton Cryogenics, (Borehamwood, UK):

35VHCB-11M	VHC35 Liquid nitrogen storage container

Thermo Fisher Scientific Ltd., Massachusetts, USA):

4330966 7900HT Fast Real-Time PCR System (Applied Biosystems)

51022886 HERAsafe™ KS-18 Class II Biological Safety cabinet

51022391 HeraCell™ 150 incubator

NanoDrop 1000 spectrophotometer

2.1.3 Preparation of stock solutions and buffers

Table 2.1 Chemical make-up of magnesium forms used in this thesis

Magnesium type	Chemical formula	Mol. Weight (g/mol)
OMC (free Mg)	Mg^{2+}	24.305
Magnesium chloride	$MgCl_2$	95.211
Magnesium aspartate dihydrate	$C_8H_{12}MgN_2O_8 \cdot 2H_2O$	288.494

2.1.3.1 Magnesium dilutions

Magnesium dilutions were based on molecular weights, as indicated in Table 2.1, with consequential mineral concentrations for OMC detailed in Table 2.2.

Note that for xCELLigence® adhesion and migration experiments, concentrations were doubled or tripled respectively, allowing for the addition of a cell suspension bringing the final concentration to precisely that required.

Table 2.2 OMC mineral component concentration when magnesium was normalised to 10mM (based on certificate of analysis, Questor Centre, Queens University, Belfast, March 2017, Appendix A)

Mineral	Concentration (mM)
Magnesium	10.000
Potassium	2.300
Sodium	1.730
Boron	0.065
Calcium	0.003
Other trace elements	0.000

2.2 Methods

2.2.1 Cells and culturing techniques

For the entirety of this study, the cell types used were as follows: Human Aortic Endothelial Cells (HAECs), Normal Human Dermal Fibroblast cells (NHDFs), Human Dermal Keratinocyte Cells (HDKCs). All cell types were maintained in a 37°C humidified atmosphere containing 5% CO_2 (Freshney, 2016). HAECs, NHDFs and HDKCs were purchased from PromoCell GmbH (Heidelberg, Germany). All cell culturing techniques were conducted in a highly clean, sterile environment, using a HERAsafe KS-18 Class II Biological Safety cabinet. Cells were routinely visualised using a Nikon Eclipse TS100 phase-contrast microscope.

2.2.1.1 Culture of Human Aortic Endothelial Cells (HAECs)

HAECs are a strongly adherent cell type, which over time form a confluent, contact-inhibited monolayer with distinct cobblestone morphology (see Figure 2.1). HAECs were maintained in Endothelial cell growth medium MV, supplemented with a separate Endothelial SupplementMix® of growth factors containing ECGS/H 0.4% (v/v), FBS 5.0% (v/v), Endothelial Growth Factor 10 ng/ml, hydrocortisone 1 μg/mL. 100 μg/mL Primocin™ antibiotic was added to guard against fungal and bacterial infection. Cells between passages 10-12 were used for experimental purposes and were maintained in a humidified atmosphere of 5% CO_2/95% air at 37°C. (Freshney *et al*., 2011).

2.2.1.2 Culture of Normal Human Dermal Fibroblast Cells (NHDFs)

NHDFs are larger, and exhibit an elongated appearance in comparison to HAECs. They were maintained in Fibroblast growth medium, supplemented with a separate Fibroblast SupplementMix®. 100 μg/mL Primocin™ antibiotic was added to guard against fungal and bacterial infection. Cells between passages 10-12 were used for experimental purposes and were maintained in a humidified atmosphere of 5% CO_2/95% air at 37°C.

2.2.1.3 Culture of Human Epidermal Keratinocyte Cells (HEKCs)

HEKCs are morphologically smaller (15-50 μm) than HAECs. They were maintained in Keratinocyte Growth Medium, supplemented with separate Keratinocyte SupplementMix®. 100 μg/mL Primocin™ antibiotic was added to guard against fungal and bacterial infection. Cells between passages 10-12 were used for experimental purposes and were maintained in a humidified atmosphere of 5% CO_2/95% air at 37°C.

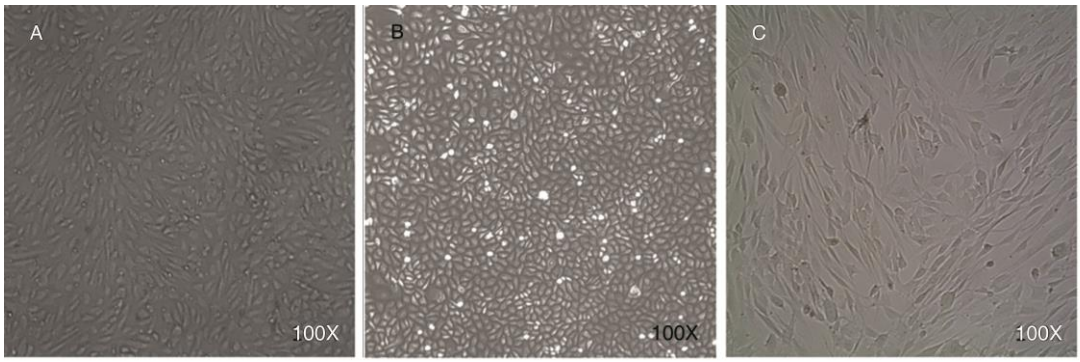

Figure 2.1 Phase contrast microscopy images (100X magnification) of cells used throughout this thesis
(A) Human Aortic Endothelial cells; (B) Human Epidermal Keratinocyte Cells; (C) Normal Human Dermal Fibroblast cells.

2.2.1.4 LabSkin™ 3D skin model

LabSkin™ 3D skin models were purchased from Innovenn Ltd. (York, England). These consisted of fully-differentiated epidermal strata, consisting of dermal fibroblast cells and keratinocytes supported by a fibrin matrix. The model was capable of permitting micro-organisms to be grown on its surface, mimicking infection or the skin's natural microflora. While microbiological loading/testing was not carried out in this instance, the natural barrier function of the model permitted the assessment of skin care ingredients and formulations not possible using standard 2D *in vitro* cell culturing techniques.

Upon arrival, the 4.5 cm^2 inserts were transferred from transport/maintenance culture medium into fresh, warm cell culture medium in deeper 6-well culture plates. The models were allowed to equilibrate overnight at 37°C in a 5% CO_2 atmosphere. Media was changed after 24 h and after a 6-h period during which models could acclimatise,

experiments were begun. Normal cell culture equipment and aseptic technique were adapted to maintain the model for its 10-day life expectancy. (Duffy *et al.*, 2017).

2.2.1.5 Trypsinisation of cells

Trypsinisation of adherent cells was required for the purposes of sub-culturing and experimental setup. For trypsinisation, cells were passaged at 70-90% confluence. All necessary solutions (PBS, trypsin and culture medium) were warmed to 37°C in a water bath beforehand. Growth medium was removed from culture dishes, and cells gently washed 2-3 times in sterile PBS with a swirling motion in order to remove macroglobulin and other trypsin inhibitors present in the culture medium serum. Approximately 100 µL of trypsin-EDTA (10% (v/v) in PBS) per cm^2 culture dish surface was subsequently added to the cells and incubated at 37°C for 5 min. When approximately 50% of cells appeared loose, the cell culture dish was firmly tapped on the side to remove remaining cells from the dish surface. Trypsinisation was halted upon addition of an equal volume of fresh growth medium containing FBS, and cells collected from suspension by centrifugation at 400 x g for 5 min. at room temperature. Cells were re-suspended in growth medium and counted using either a Neubauer chamber haemocytometer or Advanced Detection and Accurate Measurement ($ADAM^{MC}$) counter. Cells were typically split at a 1 in 3 ratio.

Note: For all magnesium-sensitive experiments, cells were washed with Mg-free PBS (Lonza), and trypsinised using trypsin-EDTA (Sigma Aldrich) diluted in Mg-free PBS.

2.2.1.6 Cryogenic preservation and recovery of cells

For long term storage, cells were maintained in a liquid N cryo-freezer unit (Taylor-Wharton, USA). Following trypsinisation, cells were centrifuged at 400 x g for 5 min. at room temperature, and the supernatant removed. The cell pellet was re-suspended in 5.4 mL freezing medium containing 20% (v/v) FBS, dimethylsulphoxide (DMSO) 10% (v/v). 1.8 mL aliquots were transferred to sterile cryo-vials, then placed in a Mr Frosty™ (Nalgene, USA) cryo-freezing unit (containing isopropanol) in a –80°C freezer. This created an environment in which a controlled rate of decrease in

temperature (approximately –1°C/min.) could occur. Following overnight freezing at –80°C, cryo-vials were transferred to the cryo-freezer unit.

For recovery of cells, cryo-vials were thawed rapidly in a 37°C water bath and added to a 58 cm^2 cell culture dish containing 5 mL pre-warmed (37°C) growth medium to dilute the DMSO. After 24 h incubation, medium was removed, cells were washed once in sterile PBS, and 7 mL fresh growth medium added (to eliminate any remaining DMSO, and ensure unimpaired growth).

2.2.2 Cell counting

For experimental purposes and healthy cell growth, cells were seeded at precise numbers and densities. This practice ensured consistency between experimental procedures. In order to achieve accurate and rapid cell counts, one of two methods were used: either a Neubauer chamber haemocytometer, or the ADAM^{MC} electronic cell counter (Digital Bio, Korea). Counting methods were incorporated in all experimental procedures.

2.2.2.1 ADAM^{MC} cell counter (Digital Bio, Korea)

The ADAM^{MC} Counter utilised a precision microscope with integrated fluroscent staining and image analysis software to generate cell counts. Cells were mixed with Propidium Iodide (PI), which intercalated with DNA, staining nuclei of cells that were either non-viable or which had been lysed. It could not penetrate the membrane of intact, viable cells (see Figure 2.2).

Approximately 20 µL cell suspension was mixed with 20 µL T solution (containing PI and lysis buffer) and transferred (~30 µL) by capillary action into the ‘T’ channel of a disposable microfluidic chip, giving a total cell count. Similarly, 20 µL cell suspension was mixed with 20 µL N solution (containing PI, no lysis buffer), transferred to the ‘N’ channel, yielding a total non-viable cell count. Each N/T channel contained 22 grids, which were automatically counted, averaged and the resulting cell density ‘N’ subtracted from ‘T’, giving a viable cell count/ml cell suspension. Results were displayed on the front of the instrument.

2.2.2.2 Haemocytometer

Haemocytometer counting allowed not only counting of cells in suspension, but also determination of the percentage of viable (intact) cells using the dye exclusion method. Dilution factor was typically 1:2.

Determination of the approximate number of viable cells by dye exclusion involved mixing an aliquot of cells with a volume of buffer or balanced saline, containing a water-soluble (membrane lipid-insoluble) dye (trypan blue), visible when it leaked into cells with damaged plasma membranes. Such cells within the grid (which were faint or dark blue in appearance) were counted as dead cells.

The number of cells was calculated using the following equation:

$$Cell\ number\ per\ mL = \frac{G_1 + G_2 + G_3 + G_4 + G_5}{5}) \ (2) \ (10^4)$$

Where G represents each individual grid.

To check cell viability, the following calculation was performed:

$$Viable\ cells\ per\ mL = \frac{Live\ cells\ (not\ including\ trypan\ blue\ cells)}{Total\ count\ (inc.\ those\ with\ trypan\ blue)}$$

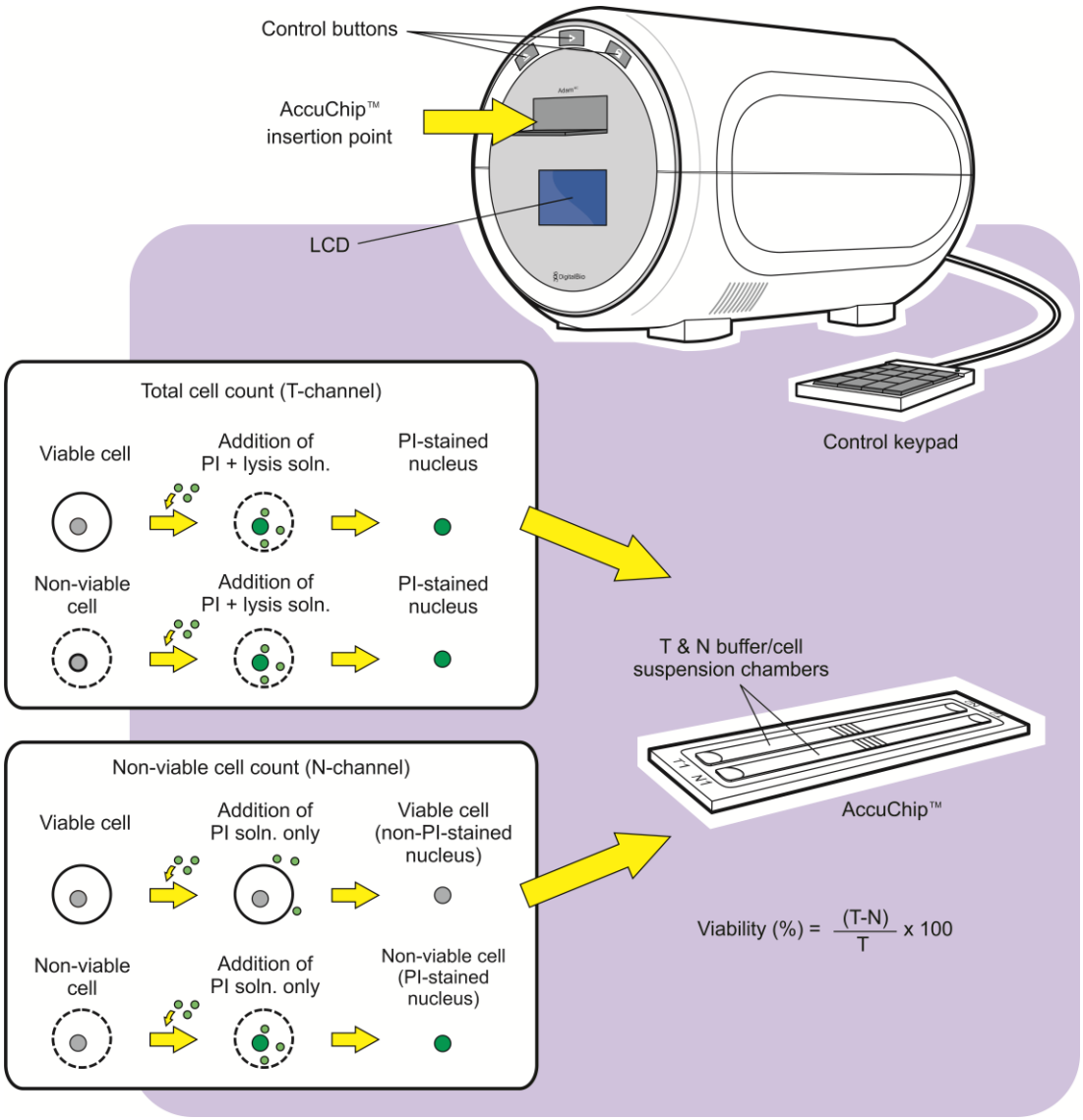

Figure 2.2 ADAM^{MC} electronic cell counter and AccuChip™ system principle of operation
Inset shows propidium iodide nuclear stain used to differentiate between viable and dead cells. Manufactured by Digital-Bio, Korea. (Adapted from www.nanoentek.com)

2.2.3 Ibidi® (Integrated BioDiagnostics®) cell perfusion system

The Ibidi® perfused flow system was used to mimic blood flow over cells under *in vitro* conditions. ECs were exposed to precisely-controlled continuous unidirectional shear stress on proprietary Ibidi® μ-slides. This allowed either harvesting of cells for quantitive Real-Time PCR (qRT-PCR) measurement of miRNA expression levels experiments, or fixation for immunocytochemical staining under flow conditions.

Due to the temperature dependency of gas solubility in water and plastic, when stored at room temperature, gases solved in plastic and liquids at lower temperatures are released when heated up. In the incubator, air bubbles would then emerge inside slides and tubing that may result in damage to adherent cells. Therefore, before use, sterile slides, tubes and media were acclimatised in the incubator overnight at 37°C in order to remove any gases present. While de-gasing occurred, HAECs were diluted to a density of $1x10^6$ cells/mL, with 200 µL of this dilution applied into the hollow chambers of each slide. HAECs were permitted time to adhere and grow to confluency, before µ-slides were connected to the pump system, via its luer connectors, in accordance with manufacturer's instructions (see Figure 2.3). During this procedure, care was taken to avoid the introduction of air bubbles into the system, which could have resulted in damage to seeded cells. Cells were subsequently exposed to various levels of shear stress (dyne/cm^2) for various time intervals. Control slides containing un-sheared "static" ECs were cultured in the same incubator. Following experiments, both sheared and static slides were fixed and ready for immunocytochemical staining. (Mack *et al.*, 2017).

For experiments requiring the application of oscillatory flow patterns, two fluidic units (master and slave) were connected in sequence. Oscillating flow was permissible on the slave unit only.

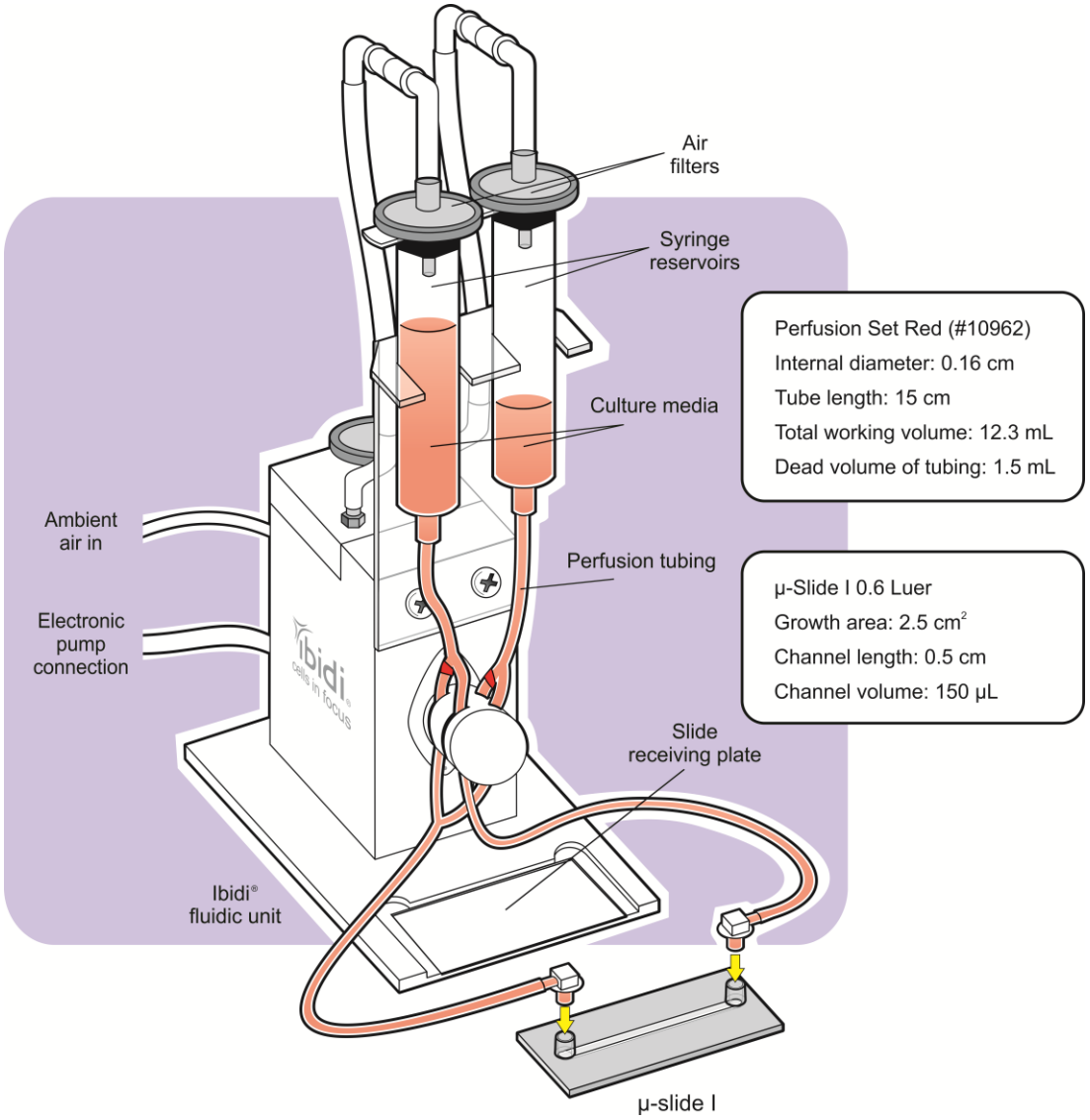

Figure 2.3 Ibidi® fluidic unit, perfusion tubing, and µ-slides used for simulation of various physiological vascular conditions (continuous unidirectional, oscillating, and pulsatile flow) *in vitro*
Two fluidic units connected in series were required to produce oscillatory flow patterns. Manufactured by Ibidi GmbH, Germany.

2.2.4 Analysis of RNA expression

2.2.4.1 RNA isolation

Working in an RNase-free environment is essential when isolating and manipulating RNA. RNA is a relatively fragile molecule, easily degraded by ubiquitous RNase enzymes. Thus, stringent measures are required to avoid this potential hazard. RNases may be introduced accidentally into the RNA preparation at any point in the procedure through improper technique. RNase-Zap® (Ambion) was used to remove RNase

contamination from surfaces. Nevertheless, due to its ubiquitous and difficult to eliminate nature, prevention of its introduction was deemed essential. Good aseptic technique, along with the use of disposable gloves and sterile filter tips were required to achieve this.

RNA was extracted for the purposes of investigating gene expression. Two different techniques were used to extract RNA from varying experimental setups:

1. TRIzol® RNA extraction (Thermo Fisher)
2. *mir*Vana™ miRNA isolation kit (Invitrogen)

2.2.4.2 TRIzol® RNA extraction (guanidinium thiocyanate-phenol-chloroform extraction) from 3D skin model biopsies and 2D monocultures

TRIzol® is a ready-to-use reagent for isolation of total RNA from cells and tissues, maintaining RNA integrity whilst disrupting cells and dissolving cell components (Chomczynski and Sacchi, 1987, 2006). Samples were stored on ice for 5 min. to allow complete dissociation of complexes.

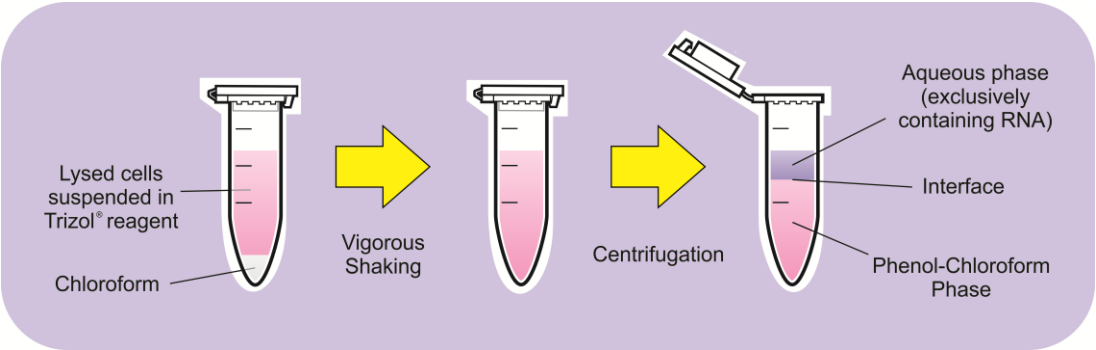

Figure 2.4 Illustration of phase separation during TRIzol® RNA extraction

For every 1 mL of TRIzol® used, 0.2 mL chloroform was added, with samples then vigorously shaken for 15 sec. Samples were incubated for 10 min. at room temperature and centrifuged at 16650 g at 4°C for 20 min. As Figure 2.5 illustrates, the mixture separated into a lower pink phenol-chloroform phase, an interphase and an upper colourless phase (where the RNA resided). To precipitate RNA, the upper phase was transferred to a fresh Eppendorf tube, where 500 µL of isopropanol for

every 1 mL of upper phase is added. This was inverted 5-8 times and incubated at -20°C overnight. The following day, samples were incubated at room temperature for 10 min. and centrifuged at 13000 RPM for 15 min. at 4°C. Supernatant was discarded, and the RNA pellet was washed in 1 mL of 75% ethanol in RNase -free dH_2O. Eppendorf tubes were vigorously shaken, and centrifuged at 13000 RPM for 10 min. at 4°C. Ethanol was aspirated and the pellet was air-dried before being re-suspended in 50 µL of nuclease-free H_2O. RNA was incubated at 60°C for 10 min. and immediately kept on ice before quantification using the NanoDrop® 1000 system. Otherwise, RNA was stored at -80°C.

2.2.4.3 *mir*Vana™ miRNA isolation kit

MicroRNA was isolated from samples using the *mir*Vana™ miRNA isolation kit (Invitrogen), a system that combined organic extraction and centrifuge-based filtration techniques. Total RNA was also isolated from small-volume samples using the kit. Stimulated cells in Ibidi® µ-slides were placed on ice and washed three times with ice-cold PBS by gentle flushing through the slide. PBS was fully aspirated at the end of the third wash. Cells (still attached to slides) were then disrupted using a denaturing lysis solution. Lysate was collected and transferred to a spin column. An additive solution, included with the kit, was then combined with the lysate, which served to stabilise RNA, and concomitantly inactivate RNases.

Extraction utilised acid phenol:chloroform and centrifugation at 10,000 g to remove other cellular components, leaving a semi-pure RNA sample. This was then further purified in the glass-fibre filter by additional centrifugation steps, before elution to yield pure samples of total RNA (see Figure 2.5). No RNA preservatives were added. RNA was quantified and qualified on a NanoDrop® 1000 Spectrophotometer. Samples were then stored at -80°C before transcription into complimentary DNA (cDNA).

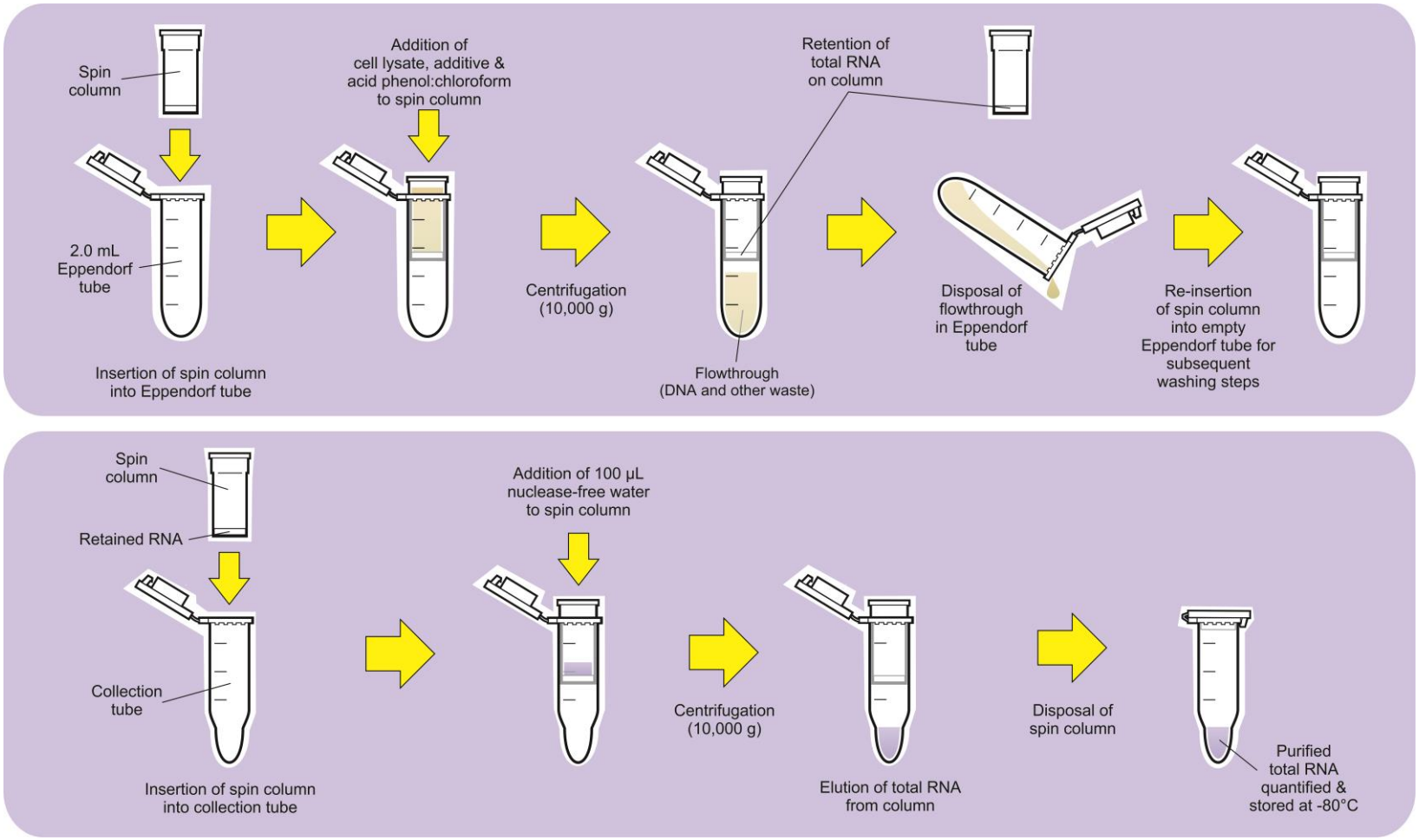

Figure 2.5 Diagram illustrating the main steps of the *mir*Vana™ centrifugation protocol used to isolate total RNA/miRNA from DNA and other contaminants

2.2.4.4 Quantification of RNA by NanoDrop® 1000 spectrophotometer

In order to determine RNA concentration in each sample, a NanoDrop® 1000 spectrophotometer (Thermo Scientific) was used. The instrument was controlled through use of specific PC-based software. After selecting the appropriate measurement parameter under software settings (RNA-40), the instrument was calibrated using 1.2 µL RNase-free water, then blanked using 1.2 µL 100% ethanol (in the case of the mirVana™ kit). Undiluted 1.2 µL sample was subsequently pipetted onto the lower measuring pedestal (see Figure 2.6). The pathlength between upper and lower pedestals was computer-controlled to 0.1 cm. Sample absorbance was read at wavelengths of 260/280 nm and 260/230 nm, and analysed by determining the ratio between each.

260/280 nm: A ratio of approximately 2.0 was regarded as highly purified RNA.

260/230 nm: A secondary measure of nucleic acid purity; a ratio of 1.8-2.2 was regarded as highly purified RNA. Lower ratios indicated the presence of protein; higher ratios implied the presence of organic reagents.

RNA concentration (ng/µL) was calculated using Beer's law, based on absorbance at 260 nm:

$$\text{Absorbance} = (E)\,(b)\,(c)$$

Where E is the wavelength-dependent molar absorptivity coefficient (or extinction coefficient) with units of l/mol-cm, b is the path length (0.1 cm), and c is the analyte concentration in Moles.

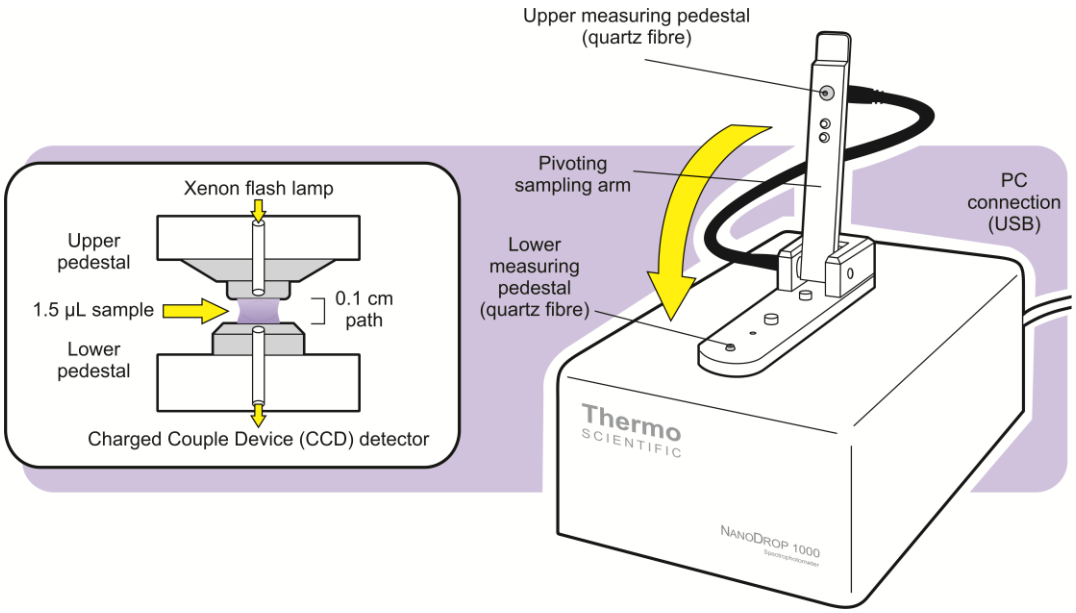

Figure 2.6 Nanodrop® 1000 spectrophotometer (used in conjunction with operating software v3.8.1) manufactured by Thermo Scientific Ltd.
Inset shows sample pedestal and light path. Xenon flash lamp light source; 2048-element linear silicon Charged Couple Device (CCD) array detector; 220-750 nm wavelength range. Manufactured by Thermo, UK.

2.2.5 Polymerase Chain Reaction (PCR) techniques

Polymerase Chain Reaction **(**PCR) is a process used to amplify specific sequences of DNA at an exponential rate for use in a variety of applications. Standard "bench-top" PCR was used for synthesising complementary DNA (cDNA) using a bench-top thermocycler (BioRad, USA).

Quantitative Real-Time PCR (qRT-PCR) reactions followed the standardised principles of PCR. It was used to amplify target DNA with a view to simultaneously quantifying the targeted DNA sequence as it accumulated during the reaction. This technique was used for both miRNA profiling and gene expression work and was facilitated by the use of Taqman hydrolysis probes or SYBR green dye respectively. Specific applications necessitated the use of a variety of different reverse-transcription/pre-amplification kits (detailed below), but all followed the same basic principals. All qRT-PCR was performed on either a 7900HT Fast Real-Time PCR System (Applied Biosystems) or Lightcycler®96 (Roche), depending on the plate format or specific chemistry of the assay.

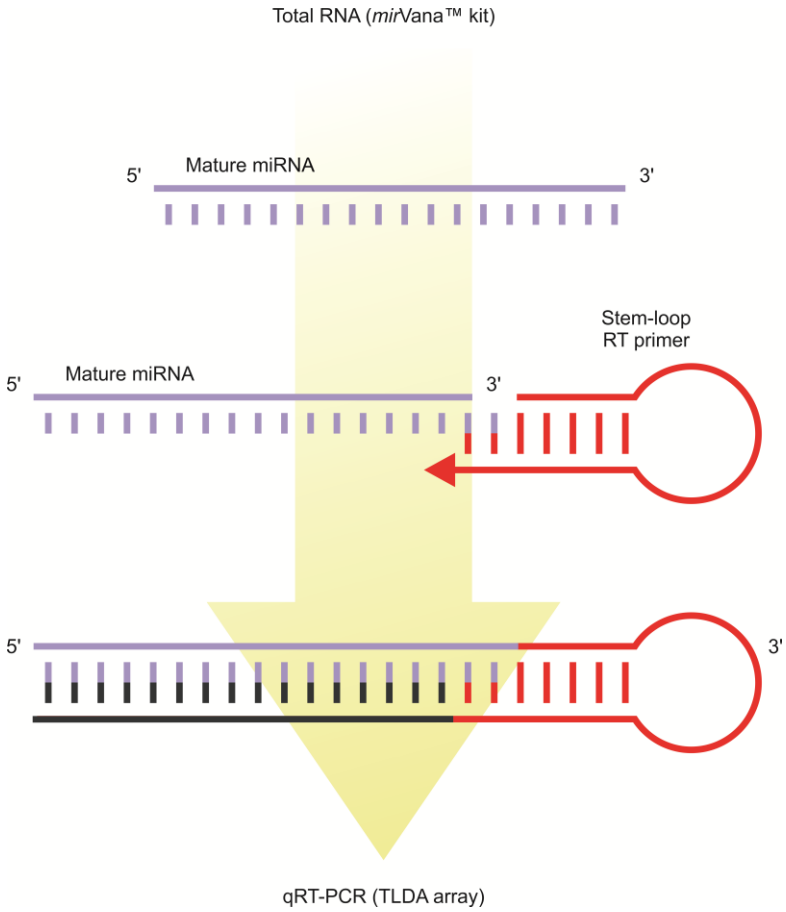

Figure 2.7 Extension and reverse transcription of miRNA targets using miRNA-specific stem-loop primers
(Adapted from Life Technologies, 2013)

2.2.5.1 Reverse transcription of miRNA

Reverse transcription (RT) is a process used to convert single-stranded RNA into double-stranded complementary DNA (cDNA). In order to accurately amplify, both standard and quantitative PCR techniques require the presence of a template that is at least twice the length of the forward/reverse primers used (~ 20 nucleotides). Consequently, the minimum length of the target should generally be ≥ 40 nucleotides. MicroRNA strands (~ 18-23 nucleotides) were therefore much too short to successfully amplify using standard reverse transcription techniques. Hence, the process was achieved using primers with a highly stable stem-loop configuration to lengthen the cDNA target. The forward primer increased length and used nucleotides designed to optimise its melting temperature. Assay specificity was greatly increased

by the positioning of the probe sequence; optimisation was achieved by binding with as much of the original miRNA sequence as possible. Optimisation of the probe melting temperature was enhanced by the addition of a minor groove binding moiety (Kramer, 2011).

2.2.5.2 Reverse transcription/cDNA synthesis for miRNA TLDA arrays

The Taqman® miRNA RT kit (Applied Biosystems™) was used to synthesise single-stranded cDNA. This employed stem-loop primers, ensuring that complimentary DNA from mature miRNA was synthesised only, while precursor miRNA was ignored. In order to create a comprehensive profile for both Pool A and B, two reactions were used. These utilised RNA-specific primer populations for the precise pool in question. MicroRNA was isolated using the *mir*Vana™ kit (see section 2.2.4.3), and as Figure 2.7 illustrates, formed the starting material for the subsequent reverse transcription reaction.

The RT reaction had a final volume of 7.5 µL and contained:

- 3 µL (1-350 ng) total RNA
- 4.5 µL of RT master mix

The master mix was made up as shown in Table 2.3 in a 2 mL nuclease-free tube.

Table 2.3 Reverse transcription mastermix for miRNA Pools A & B (Applied Biosystems™)

RT reaction mix component	Volume required for 1 sample (µL)
Megaplex™ RT primers (Pool A or B) 10X	0.8
dNTPs (100 mM)	0.2
Multiscribe reverse transcriptase (50 U/µL)	1.5
RT buffer (10X)	0.8
$MgCl_2$	0.9
RNase inhibitor (20 U/µL)	0.1
Nuclease-free water	0.2
Total	**4.5**

Samples were mixed by gentle pipetting and incubated on ice for 5 min. Samples were then run on the PCR thermocycler under the conditions found in Table 2.4.

Table 2.4 Thermocycling conditions for miRNA-specific reverse transcription reaction

Stage	Temperature (°C)	Duration (min.)
Cycle (40)	16	2
	42	1
	50	1
Hold	85	5
Hold	4	∞

2.2.5.3 Taqman® miRNA arrays

The presence of the target was detected in real-time through cleavage of the TaqMan® hydrolysis probe by polymerase 5'-3' activity. The master mix for the TLDA cards (A and B) was made up as shown in Table 2.5 for pre-amplified cDNA.

Table 2.5 Component mixture for miRNA array sample when using pre-amplified product

Component	Volume for One Array (µL)
TaqMan® Universal PCR MasterMix	450
Diluted Pre-Amp Product	9
Nuclease-Free Water	441
Total	**900**

Samples were mixed by gentle pipetting and centrifuged briefly. TLDAs were allowed to come to room temperature before adding 100 µL of the mix into each loading reservoir. Arrays were then centrifuged twice for 1 min at 1000 RPM in order to draw sample into each of the 384 wells of the card (see Figure 2.8). The TLDA card was then sealed and the loading chambers removed using scissors. The card was then run

on the Applied Biosystems® 7900HT Fast Real-Time PCR System using the parameters contained within the Sequence Detection Systems (SDS) setup file on the supplied CD as shown in Table 2.6.

Table 2.6 Real-time thermocycling conditions for miRNA TLDA cards

Number of Cycles	Temperature (°C)	Duration (min.)
40	50	2
	94.5	10
	97	0.5
	59.7	1

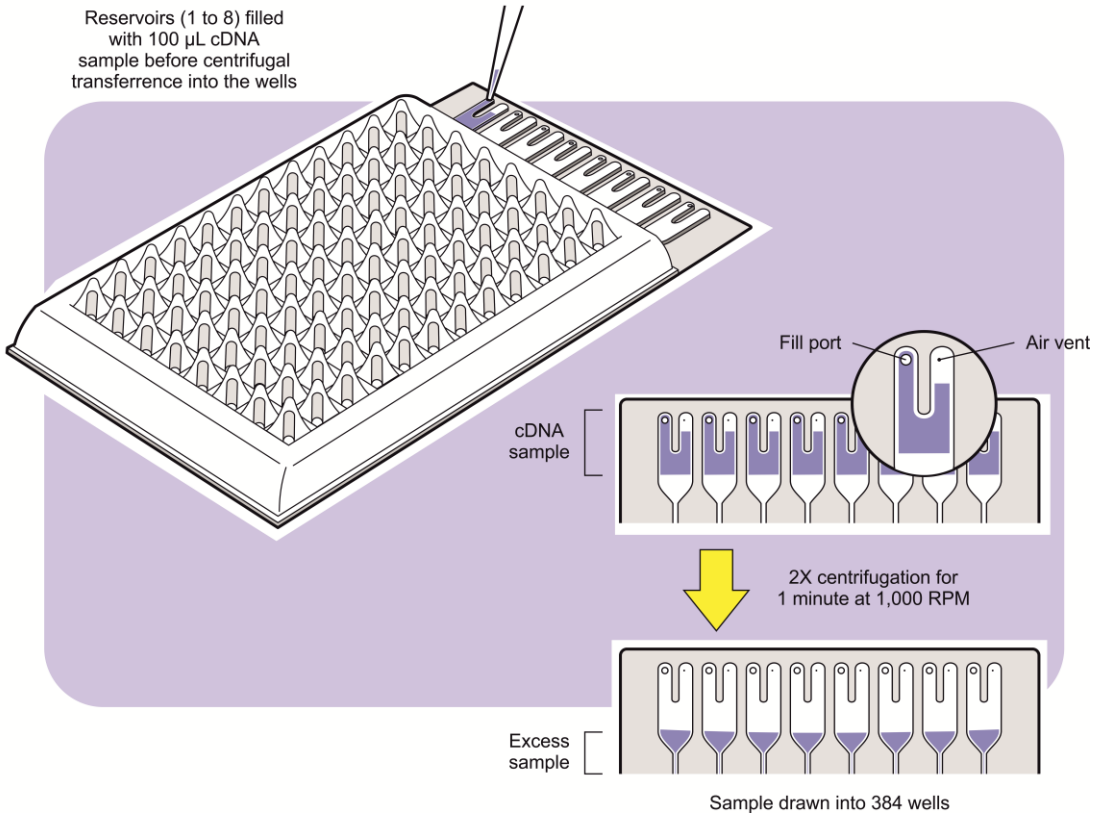

Figure 2.8 Illustration outlining the process of loading sample into a TLDA card

2.2.5.4 Pre-amplification and cDNA synthesis of RNA for analysis using Qiagen RT^2 Profiler arrays

Due to the very small quantities of total RNA obtainable from Ibidi® µ-slides, cDNA was pre-amplified using the RT^2 Pre-Amp cDNA Synthesis kit (Qiagen) prior to real-time PCR analysis. This kit enabled both first strand synthesis and pre-amplification of specific gene targets present on 96-well RT^2 Profiler arrays.

The RT^2 Pre-Amp cDNA Synthesis Kit and RT^2 Pre-Amp Pathway Primer Mix (specific for the array in use) were sufficient to generate template for gene expression analysis from as little as 1–100 ng total RNA. Therefore, following quantification, RNA samples were normalised by dilution to allow consistent and equal loading into all arrays, and hence, facilitate analysis. The optimal amount of starting material was dependant on the relative abundance of the transcripts of interest. As lower abundance transcripts would require more RNA and higher abundance transcripts would require less RNA, greater amounts of input total RNA would yield a greater number of positive calls; ie. genes expressed in the linear dynamic range of the method. Therefore, the maximum permissible amount of starting material was chosen from the range of isolated samples.

2.2.5.5 Genomic DNA elimination

Elimination of genomic DNA was essential in order to obtain optimal real-time gene expression data, as it could potentially result in false positive signals and inhibition of reverse transcriptase/DNA polymerase enzymes, ultimately leading to lower than expected efficiency and PCR sensitivity reduction. The inclusion of a genomic elimination step in addition to the stringent RNA isolation protocols of the *mir*Vana™ kit was therefore a required procedure. This pre-emptive step involved the incubation of each RNA sample with a DNA-degrading enzyme in a buffer mix for 42°C for 5 min. (see Table 2.7).

Table 2.7 Genomic elimination mix

Component	Amount for 1 sample
RNA	1-100 ng
Genomic elimination buffer	2 µL
Nuclease-free water	Variable
Total	**10 µL**

Each RT^2 array contained a designated well (see Figure 2.9) specifically designed to test for the presence of such genomic contamination. CT values of 30 after pre-amplification were recommended as the value above which DNA contamination should be addressed.

2.2.5.6 Reverse transcription of RNA for analysis using Qiagen RT^2 Profiler arrays

10 µL of genomic elimination mix was added to the reverse transcription mix (outlined in Table 2.8) and allowed to incubate at 42°C for 30 min. Once complete, the reaction was stopped by heating to 95°C and cooled to ~4°C on ice. The reverse transcription step included the addition of a positive control (P2) to each sample. When analysed by real-time PCR, these controls enabled the determination of whether the various reaction components/conditions operated properly.

Table 2.8 Reverse transcription mix

Component	Volume (µL)
5X buffer (BC3)	4
Control (P2)	1
cDNA synthesis enzyme mix	1
RNase inhibitor	1
RNase-free water	3
Total	**10**

2.2.5.7 Pre-Amplification of cDNA for analysis using Qiagen RT^2 Profiler arrays

Once transcribed from RNA to cDNA, pre-amplification was initiated. The RT^2 Pre-Amp Pathway Primer Mix used was specific for the particular RT^2 Profiler PCR Array in use (eg. Epigenetic enzymes array, or wound healing array). During this initial amplification step, the Pathway Primer Mix enabled amplification of cDNA specific for those genes targeted by that array. 5 µL cDNA synthesis reaction was added to 20 µL pre-amp mix (see Table 2.9), after which, the contents were gently mixed and transferred to the thermocycler for PCR.

Table 2.9 Pre-amplification mix

Component	Volume (µL)
RT^2 Pre-amp PCR mastermix	12.5
RT^2 Pre-amp pathway primer mix	7.5
Total	**20.0**

As Table 2.10 indicates, the RT^2 kit utilised hot-start *Taq*-polymerase, hence the high starting temperature required to activate the enzyme. Following PCR, 2 µL side reaction reducer solution was added. This was incubated at 37°C for 15 min., with the degrading enzyme then de-activated by heating to 95°C for 5 min. 84 µL nuclease-free water was immediately added, bringing total volume to 109 µL. Pre-amplified cDNA samples were then stored at -80°C until required.

Table 2.10 Thermocycling conditions for pre-amplification of cDNA for Qiagen RT^2 Profiler arrays

Cycles	Duration	Temperature (°C)
1	10 min.	95
12	15 seconds	95
	2 min.	60
Hold	∞	4

All RT^2 Profiler arrays used in experiments in this thesis were in a 96-well format. As Figure 2.9 illustrates, each array comprised 84 pathway-specific and 5 housekeeping primer assays, thereby allowing a comprehensive set of data to be obtained from a single sample on a single plate. Each array also contained a genomic control well in addition to triplicate reverse transcription and positive PCR controls. All genes are listed in Appendix A.

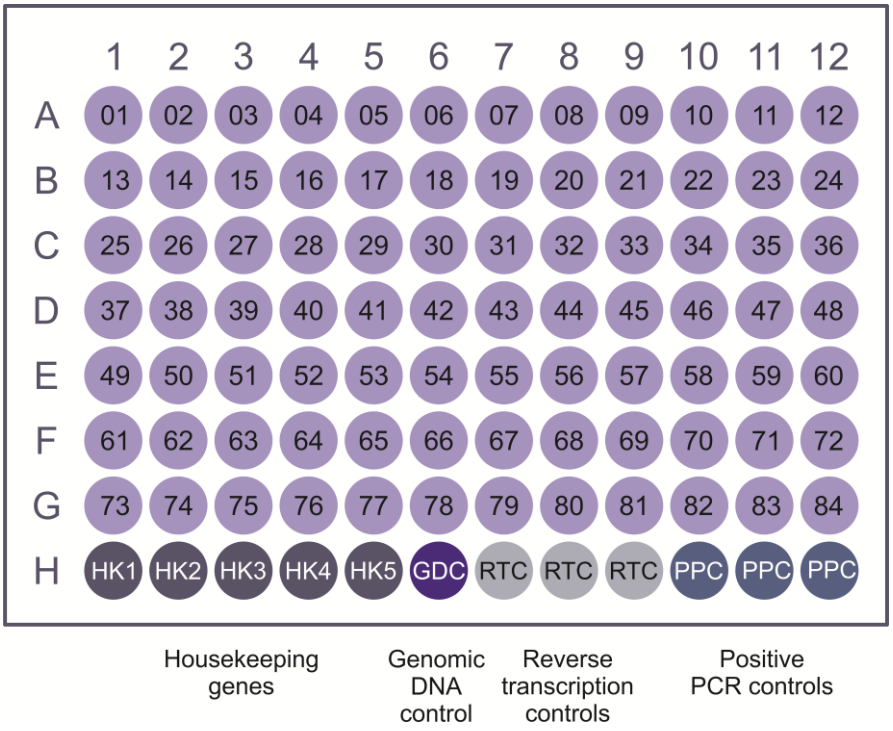

Figure 2.9 Qiagen RT^2 Profiler array gene/control layout

Table 2.11 PCR mastermix components of RT^2 Profiler arrays

Component	Volume (µL)
2X SYBR Green mastermix	1275
Pre-amp reaction	102
RNase-free water	1173
Total	**2550**

As in the reverse transcription step, hot-start *Taq* polymerase required a temperature of 95°C to activate the enzyme. 25 µL mastermix solution (see Table 2.11) was added to each well of the 96-well plate before sealing using optical film to prevent evaporation. Plates were centrifuged at 10,000 g for 1 min. in order to remove bubbles and ensure that all contents resided in the bottom of each well. Thermocycling conditions specific for the Applied Biosystems 7900HT Real-Time PCR instrument were used (see Table 2.12).

Table 2.12 Thermocycling conditions for RT2 Profiler arrays optimised for use with the Applied Biosystems 7900HT Real-Time PCR instrument

Cycles	Duration	Temperature (°C)
1	10 min.	95
40	15 sec	95
	1 min.	60

2.2.5.8 qRT-PCR using RealTime Ready (RTR) assays (Roche, Switzerland)

Single-gene expression quantification was carried out using qRT-PCR RealTime Ready (RTR) hydrolysis probes (Roche, Switzerland). Each RTR assay contained gene-specific primers for the target gene and a Universal Probe Library probe, a short FAM-labelled hydrolysis probe with locked nucleic acid. PCR mixes were prepared in PCR tubes on ice. PCR reaction mix components are listed in Table 2.13. 15 µL of the PCR mix was placed into each well of the LightCycler®96 multi-well plates. 5 µL of template cDNA was added to make a 20 µL reaction. 96-well plates were centrifuged for 2 min. at 1500 g in a swing-out bucket and placed into the LightCyler®96. Using the PCR program described according to manufacturer's instructions, the reaction was performed. LightCyler®96 software was used to analyse relative quantification of target genes.

Table 2.13 PCR mix for RTR assays (Roche)

Component	Concentration	Volume (µL)
PCR-grade water	-	4
Probes master	2X	10
RTR mix	20X	1
Total volume	**-**	**15**

2.2.6 qRT-PCR data and bioinformatical analysis

In order to accurately process and interpret data generated by qRT-PCR, cyclic threshold (Ct) values were filtered and interrogated by statistical analyses. This was achieved in a number of ways, depending on the assay type and format, as detailed in this section.

2.2.6.1 qRT-PCR gene analysis and QC for RT^2 arrays

RT^2 Profiler PCR Arrays facilitated analysis of gene panels related to wound healing, fibrosis and associated biological pathways. The Qiagen PCR Array Data Analysis web portal was used to interpret replicate (n = 3) qRT-PCR data. Any Ct value equal to 35 was considered a negative call. RT^2 Profiler arrays incorporated a number of controls, including genomic and reverse transcription controls. A panel of endogenous controls were used to normalise data (Ct Gene of Interest – Ct Average of endogenous controls). Biological replicates were performed, and the average ΔCt value of each gene was calculated across those replicate arrays for each treatment group. ΔΔCt for each gene were calculated across two groups/arrays. ΔΔCt = ΔCt (Group 2) - ΔCt (Group 1). Group 1 was the control and Group 2 was the experimental. Fold-change for each gene from Group 1 to Group 2 was calculated as $2^{(-\Delta\Delta Ct)}$. If the fold-change was greater than 1, the result was reported as a fold up-regulation.

2.2.6.2 Data Filtration for miRNA/mRNA Analysis

Data were filtered for differentially-expressed mRNA and miRNA. MicroRNA SDS files were initially analysed using ExpressionSuite V1.1 analysis software. Normalised values were calculated and ranked while unexpressed targets were eliminated. Normalised Ct values for each target were then aligned with both experimental parameters (laminar & oscillatory) for both mRNA and miRNA.

2.2.6.3 Joint miRNA/mRNA Analysis

miRNA and mRNA were analysed using MirTarVis+ software V. 0.8.11, a web-based interactive visual analytics tool for miRNA target prediction and integrative analyses of multiple prediction results by comparing overlapping results of interrogations. Datasets were analysed using a paired two-sample t-test. For initial experiments, statistical analyses were not applicable. However, subsequent datasets (n = 3) were subjected to Student's t-test and filtered by P value. Software searches for possible miRNA-target pairs for the filtered data.

miRTarVis+ supported two sequence-based prediction algorithms (TargetScan and microRNA.org) and four expression profile-based prediction algorithms (correlation analysis, mutual information, GenMiR++, and MINE analysis).

2.2.7 Analysis of protein biomarkers in platelet-poor plasma

Platelet-poor plasma samples were analysed for inflammatory protein biomarkers in collaboration with Olink, Sweden using the Proseek® technique. Whole blood samples were taken from female participants following the provision of informed consent (see section 2.2.9).

2.2.7.1 Isolation of platelet-poor plasma from whole blood

Platelet-free plasma was isolated from whole blood using a double centrifugation method (see Figure 2.10). Whole blood was collected in 4.5 mL vacutainers containing sodium citrate (anti-coagulant). Samples were mixed by gentle inversion to ensure even distribution of anti-coagulant. Within 15 min. of collection, samples

were centrifuged at 1550 RCF for 20 min. at room temperature (20-22°C) to pellet the cell portion. The plasma supernatant was carefully aspirated to a fresh tube and centrifuged again at 13,000 RCF for 2 min. to remove any contaminating cells or debris. Platelet-poor plasma was then collected and portioned into 250 µL aliquots in Sarstedt screw cap tubes, snap frozen in liquid nitrogen and then stored at -80°C until further analysis.

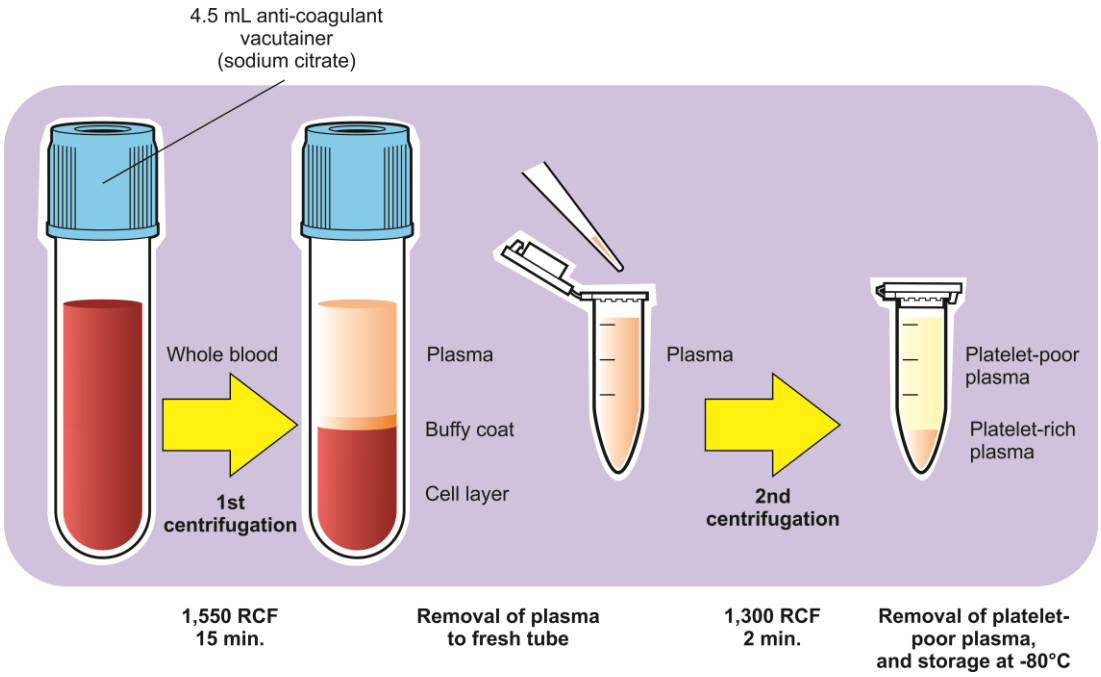

Figure 2.10 Isolation of platelet-poor plasma from whole blood by centrifugation

2.2.7.2 Human Protein Biomarker Assay - Proseek® Multiplex Immunoassay* (* as performed in collaboration with Olink, Sweden)

The Proseek® multiplex immunoassay was a high-throughput assay, enabling analysis of 92 inflammation-related protein biomarkers using 1 µL of sample. The hybrid technique combined the high specificity of dual antibody binding with that of complimentary base pairing and the sensitivity that PCR allows. This technique was termed "Proximity Extension Assay" (PEA) technology (see Figure 2.11).

A pair of oligonucleotide-labelled antibodies (Proseek® probes) specific for each biomarker were allowed to bind to each target protein in the sample. When two Proseek® probes were in close proximity, a new PCR target sequence was created by

a proximity-depended DNA polymerisation reaction. Each oligonucleotide pair held a unique DNA sequence enabling hybridisation only to each other. This sequence may subsequently be detected by qRT-PCR and quantified.

2.2.7.3 Proseek® (Olink, Sweden) Sample Preparation

20 µL of each platelet-poor plasma sample was aliquoted into a well on a 96-well plate and shipped to Olink Bioscience on dry ice. Proseek® assays were performed by Olink Bioscience (Upsala, Sweden) to evaluate the expression of potential inflammatory biomarkers (see Appendix A for full biomarker lists).

Briefly, samples were incubated with oligonucleotide-conjugated antibodies (illustrated in Figure 2.11), facilitating a hybrid immuno/PCR technique that permitted a high level of specificity using minimal sample volume (1 uL). Results provided by the company were expressed in normalised protein expression (NPX) values on a log2 scale, hence a high value corresponded to a high protein expression and vice versa with a low value. Limit of detection (mean negative control plus 3 x standard deviation) was determined for each biomarker for each sample. The provided data were made linear using the formula:

$$2^{NPX} = \text{linear NPX}$$

Linear NPX data were checked for normal distribution using the Shapiro-Wilke test for small sample sizes and mixed ANOVA were performed.

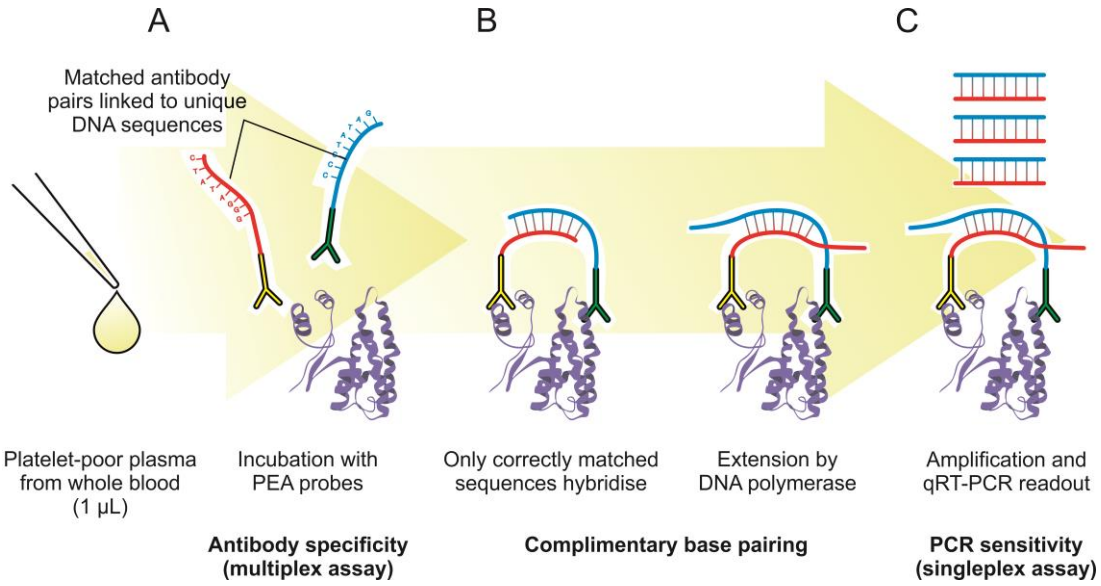

Figure 2.11 Principles by which Proseek® (Olink, Sweeden) assay sensitivity is achieved
(Adapted from www.olink.com). (A) Two Proseek® probes (oligonucleotide labelled antibodies) bind to the target protein in the sample; (B) The close proximity of the probes results in the formation of a PCR template sequence by proximity-dependent DNA polymerisation; (C) The resulting sequence is detected and quantified using standard qRT-PCR

2.2.8 Whole cell analysis techniques

2.2.8.1 Immunocytochemistry

Preparation for immunocytochemical staining under flow conditions required extreme care, as cells remained confined within the narrow parameters of Ibidi® µ-slides. All solutions were added drop by drop into one side, and were carefully pipetted out of the other side. As during the initial setup of the apparatus, care was taken to avoid the harmful introduction of air bubbles.

Prior to staining, cells were fixed in order to preserve cell structure, particularly as the cytoskeleton is dynamic and sensitive to changes to both chemical and mechanical environments. In order to determine localisation of F-actin within cells, and its association with shear stress, HAECs were washed 3 times in PBS and fixed with 3% (v/v) formaldehyde for 15 min. Fixed cells were subsequently washed in PBS 3 times; with 0.2% (v/v) Triton X-100 for 15 min, following which, cells were again washed 3 times. Cells were blocked for 30 min. in PBS containing 5% (w/v) BSA solution. After blocking, cells were stained for F-actin, by adding a 1:40 dilution of Rhodamine

Phalliodin (Invetrogen) for 20 min. Samples were then washed for a final time, before visualisation by fluorescent confocal microscopy.

2.2.8.2 Confocal Microscopy using the Zeiss 710

Confocal microscopy is a specialised optical imaging technique used to increase optical resolution and contrast through use of point illumination and a spatial pinhole to eliminate out-of-focus “hazy” light in specimens of greater thickness than the focal plane, such as cells. "Haze" is commonly associated with traditional fluorescent microscopy. Confocal laser scanning microscopes use multiple mirrors (typically 2 or 3 scanning linearly along x and y axes) to scan the laser across the sample and "de-scan" the image across a fixed pinhole and detector. Sample images were acquired using the 561nm laser. The live scanning option was used to focus the image prior to acquisition. Care was taken to shield samples from the laser as much as possible prior to acquisition in order to prevent bleaching of the fluorophore and a reduction in image quality.

2.2.8.3 xCELLigence® Real Time Cell Analysis

The xCELLigence® RTCA DP instrument used non-invasive electrical impedance monitoring to quantify cell proliferation, morphology change, and cell attachment without the incorporation of labels. The system permitted real-time measurement of cell adhesion using proprietary E-plates®, and cell invasion and migration (CIM) using an electronically integrated Boyden chamber (CIM-Plate 16®). The instrument was placed in a standard CO_2 cell culture incubator and powered and controlled via a cable connected to the control unit (a laptop PC) housed outside the incubator.

Gold micro-electrodes were fused to the bottom surface of a microtiter plate well (see Figure 2.11). When submersed in an electrically conductive solution (such as standard tissue culture medium), an electrical circuit was created, where an electrical potential was passed across the electrodes. Cells on the surface of the electrodes altered the local ionic environment at the electrode/solution interface leading to increased electrode impedance. The more cells attached, or the stronger the attachment, the higher the impedance. Impedance was measured using a dimensionless parameter

termed “Cell Index” (CI), derived from the relative change in electrical impedance. The magnitude of impedance was dependent on cell number, size and shape, and the cell-substrate attachment quality. Importantly, neither the gold micro-electrode surfaces nor the applied electric potential (22 mV) exerted any known effect on cell health or behaviour (Ke *et al.*, 2011; Chollangi *et al.*, 2018).

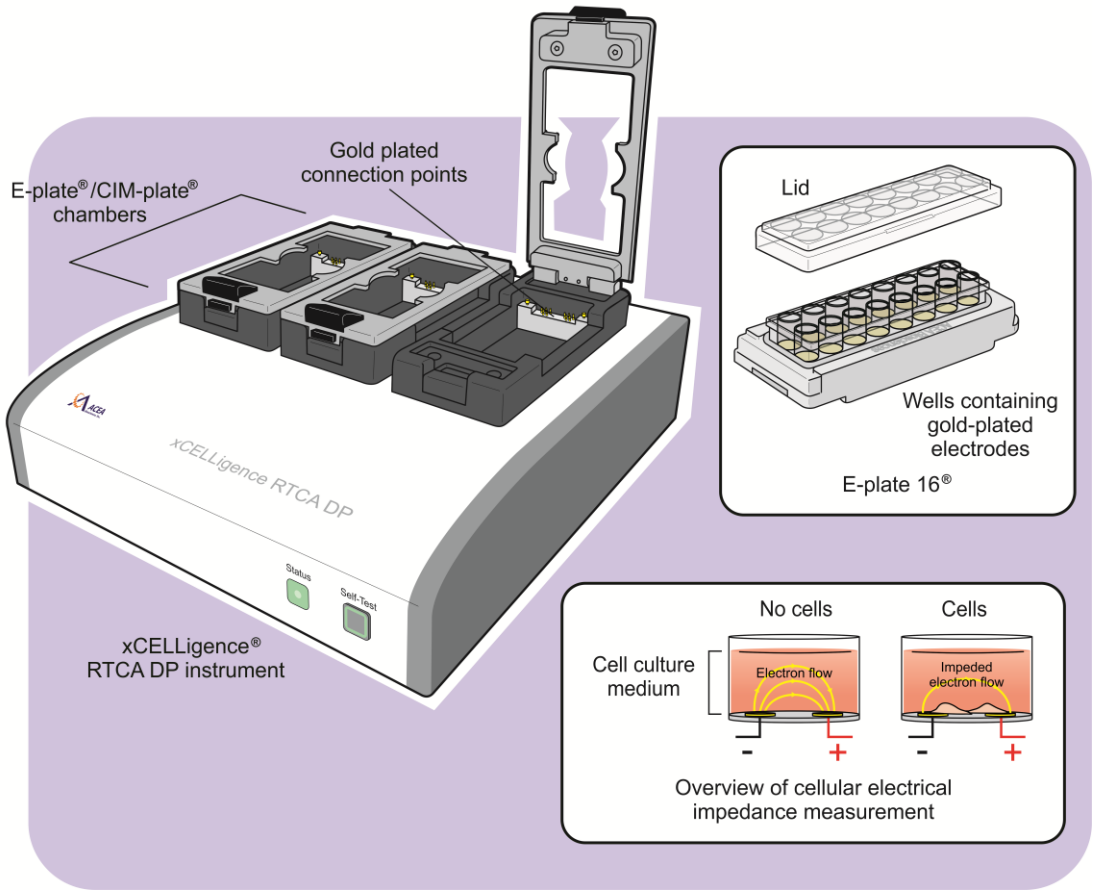

Figure 2.12 Diagram illustrating xCELLigence® RTCA DP instrument, E-Plate® and the principle of cellular electrical impedance measurement
(Adapted from https://www.aceabio.com/products/icelligence/). E-plates® contain gold micro-electrodes embedded in well bottoms/substrate. As cells adhere to the substrate, electrical impedance increases. The cell index (CI) value at each time point is defined as (Rn-Rb)/15; where Rn is the cell-electrode impedance of the well when it contains cells and Rb is the background impedance of the well with media alone. CIM-Plates® (not illustrated) operate in a similar manner, but instead use dual chambers (upper and lower) with an electrode-embedded membrane in between. Cells seeded onto the membrane migrate through it towards a chemi-attractant, thereby reducing electrical impedance. Manufactured by Acea Biosicences Inc., USA.

2.2.8.4 xCELLigence® adhesion assays

E-Plates are single-use, disposable devices used for performing cell-based assays on the xCELLigence® system. Each individual well on an E-Plate 16® incorporates a sensor electrode array that allows cells in the well to be monitored and assayed (see Figure 2.12).

1) Using a multi-channel pipette, 100 µL of culture medium was added to each well of the E-Plate 16®. The introduction of air bubbles was avoided, as was accidental damage to electrodes by touching them with the pipette tip. Approximately 300 µL of de-ionized water was then added to the troughs surrounding the wells in order to maintain humidity within the plate. The plate was then allowed to equilibrate in the laminar flow cabinet for 30 min.

2) While the plate was incubating, experimental parameters were set up on the RTCA software as follows:

- Experimental Notes tab: Experimental information, purpose, name etc. were entered.
- Layout tab: Cell number, type, treatment etc. within each individual well were entered, thereby determining whether individual or duplicate well analyses were performed.
- Schedule tab: Experiment length and interval timing between sweeps were determined by these settings.

Step one: Initial background reading.

Step two: for a typical adhesion/proliferation experiment, 96 sweeps at 15 min. intervals were selected. This gives monitoring of adhesion over a 24 h period. A sub step was then added which runs automatically after step two. In this sub step, reading intervals were set at 30 min. and 192 sweeps, allowing proliferation monitoring for a 4-day period.

3) The equilibrated E-Plate® was then inserted into the dock cradle ensuring it was aligned correctly. The programme was begun by initiating step one (background reading).

4) The plate was removed and 100 µL of cell suspension was added (100 µL of media for the no cell controls). The plate was left for 30 min. in the laminar for cells to settle, with the plate gently tapped to help with even distribution of cells.

5) Following incubation, the plate was re-inserted to the cradle for the final time and step two was initiated.

2.2.8.5 xCELLigence® cell migration assay

Cellular Invasion and Migration (CIM)-Plates® are single use, disposable apparatuses used for performing cell invasion and cell migration assays on the xCELLigence® instrument. Each CIM-Plate 16® comprises a plate cover (lid), and upper chamber and lower chambers.

The upper chamber consisted of 16 wells, each sealed at the bottom with a microporous polyethylene terephthalate (PET) membrane containing micro-fabricated gold electrode arrays on the bottom side of the membrane.

The median pore size of this membrane was 8 µm. The lower chamber contained 16 corresponding wells, each of which served as a reservoir for media and any chemo-attractant for cells in corresponding upper chambers.

1) In the laminar flow cabinet, the plate was oriented correctly using the supplied plate-holder apparatus. Using a multichannel pipette, 160 µL of full serum media was added to sample wells. 160 µL of serum-free medium was used in 2 of the 16 wells to act as a negative control.

2) The upper (electrode containing) chamber was then clicked in place on top of the lower chamber.

3) 50 µL of serum-free media was added to each well of the upper chamber

4) The assembled CIM-Plate® was then loaded into the xCELLigence® system cradle and allowed to equilibrate for one hour.

5) During the incubation time, the experiment was set up on the RTCA software as described for the cell adhesion/proliferation experiment.

6) Following one h equilibration, the one-min. background reading was performed.

7) 100 µL of cell suspension was then added to each well and 100 µL of media for the no-cell control. The plate was left for 30 min. in the laminar flow cabinet following addition of cells. Following incubation, the plate was again loaded into the cradle and step 2 was initiated.

2.2.8.6 Crystal violet adhesion assay

The crystal violet adhesion assay is a simple technique used to determine adhesion/cell viability of adherent cells by staining and measuring absorbance at ƛ 562 nm, where absorbance is proportional to concentration. A number of wash steps ensure that dead/non-adherent cells are removed, hence only those living/adhered to the well are stained (see Figure 2.13)

Trypsinised cells ($2.5*10^5$ cells/mL) were added to pre-prepared wells of a 96-well plate (50 µL medium, warmed to 37°C) before being brought to a final volume of 200 µL and left overnight. The experimental procedure was performed in triplicate for a pre-determined number of time points, and based on a modified protocol by (Feoktistova *et al.*, 2016).

Following overnight incubation, cell culture medium was replaced with fresh medium containing the cell stimulus/treatment (OMC Mg), and establishing (t)=0 min. At each ensuing timepoint, the plate corresponding to said timepoint was removed from the incubator, the medium was removed and the well washed with PBS. 100 µL of 3.75% formaldehyde was added to each well and allowed to incubate for 15 mins. at room temperature. Wells were again washed with PBS prior to the addition of 100 µL of a 5 mg/mL crystal violet solution and a 5 min. incubation at room temperature. Following another brief wash, plates were inverted and allowed to air dry for 10 mins.

Once completely dry, 50 µL of a 2% SDS solution was added to each well and the plate was incubated for 30 min. at room temperature. Absorbance values (ƛ 562 nm) for each well were obtained on an ELx800 Microplate Reader (BioTek) and treated samples were compared against untreated controls.

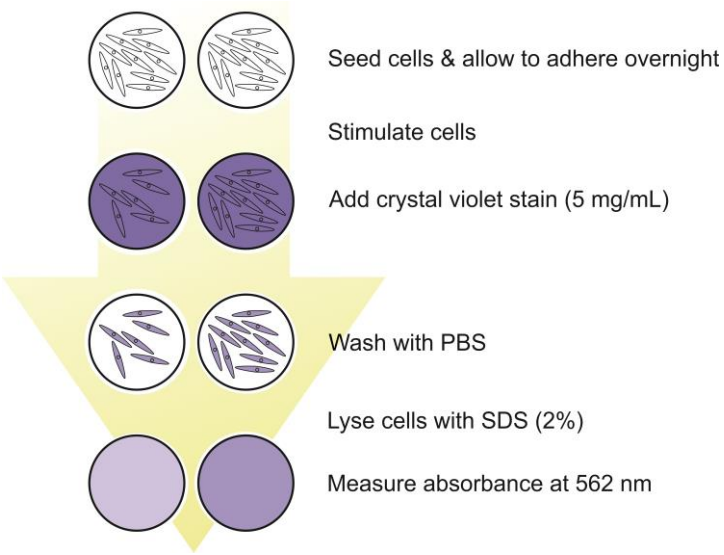

Figure 2.13 Overview of the crystal violet cell adhesion/viability assay
(Adapted from Feoktistova, Geserick & Leverkus 2016)

2.2.8.7 Wound healing cell migration assay

The *in vitro* wound healing assay is a simple method based on the principle that upon creation of an artificial gap in a confluent monolayer of cells, those cells on the edge of the gap will migrate/proliferate toward the opening to close the "wound" until new cell–cell contacts are established (Liang *et al.*, 2007).

Confluent monolayers of cells were scratched with a sterile 200 µL pipette tip using firm, even pressure. Cells were washed with warm PBS, removing damaged cells and debris, before adding the treated medium. A Leica DM500 microscope with ICC50 camera module was used to capture 40X images at 6 h regular intervals during wound closure, with Image J software (National Institutes for Health, USA) and the Angiogenesis Analyzer macro plugin subsequently used to determine the rate by measuring the changes in the gap area. Measurements were reported in pixels.

2.2.8.8 Angiogenic tube formation assay

The tube formation assay is a tool for angiogenesis quantification. It is based on the principle that cells differentiate morphologically to form capillary-like tubes within 24 h by first adhering to a substrate and then migrating towards each other.

MaxGel™ ECM (Sigma Aldrich) was thawed slowly on ice overnight, before pre-coating Ibidi® Angiogenesis μ-slides and allowed to solidify at 37°C in a sterile incubator. This formed a basement membrane-like surface in each 4 mm well. A 50 μL 2 x 10^5 cells/mL HAEC suspension was subsequently used to seed on top of this. Cells were observed and imaged in 6-h intervals. A Leica DM500 microscope with ICC50 camera module was used to capture 100X images at 6 h regular intervals during this process, with Image J (National Institutes for Health, USA) software and the MRI Wound Healing Tool.ijm macro plugin subsequently used to quantify the rate by measuring tube length. Measurements were reported in pixels.

2.2.8.9 Determination of Reactive Oxygen Species (ROS) by flow cytometry using dihydroethidium (DHE) staining

Traditional flow cytometry is a sensitive laser-based, biophysical technique that operates by suspending cells in a stream of fluid and passing it by an electronic detection apparatus. Thus, quantitative properties of single cells may be acquired, one cell at a time, for up to thousands of particles (events) per second. Laser light of a single wavelength is directed onto the hydrodynamically-focused stream of fluid. Detectors are aimed at the point where the stream passes through the light beam. They are:

- In-line with the light beam (to detect forward scatter)
- perpendicular to the light beam (to detect side scatter)

Forward scatter corresponds with cell volume and side scatter corresponds with cell granularity (ie. inner complexity of the cell). The Guava® easyCyte 8HT (Millipore) uses a micro-capillary flow cell, and is capable of obtaining samples from 96-well microtitre plates. It uses a lower volume of sample than traditional flow cytometry, and does not require the use of sheath fluid to achieve cell/particle separation (see Figure 2.14). Use of lasers to interrogate samples and photomultipliers to detect resultant signals remain as those used in traditional flow cytometers.

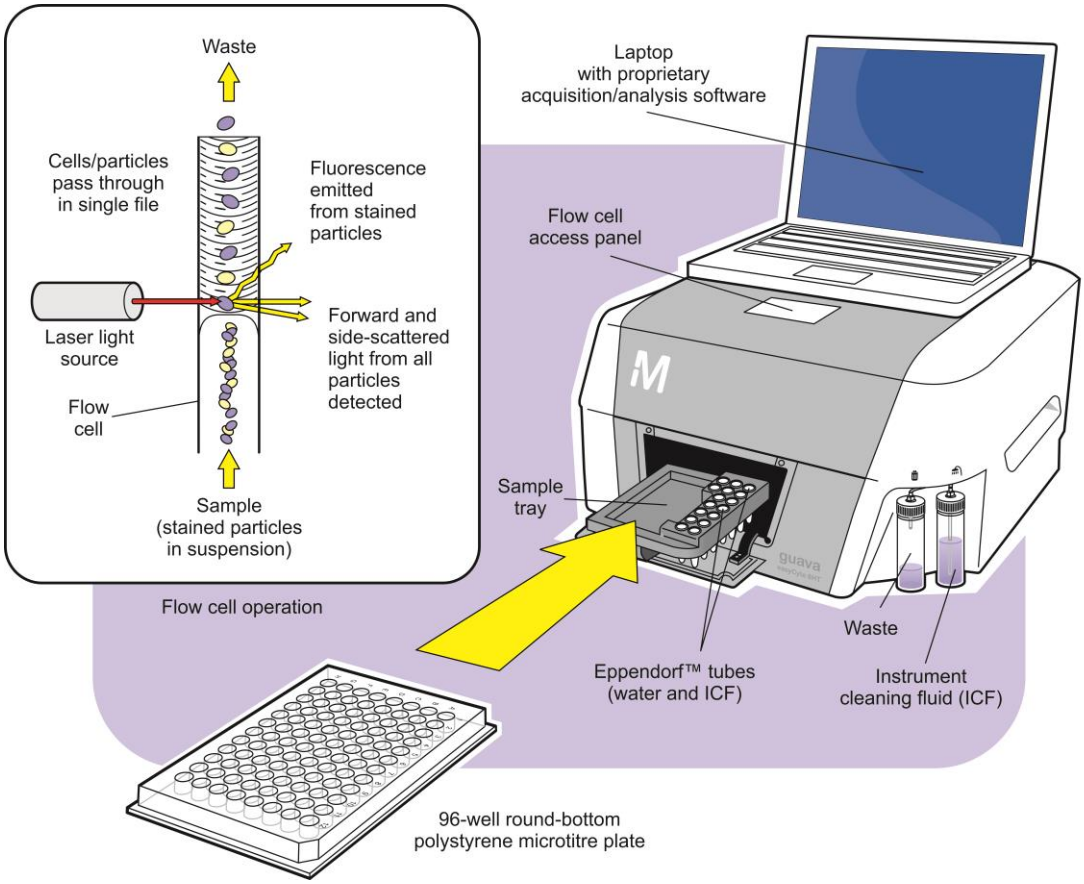

Figure 2.14 Illustration of the Guava® easyCyte 8HT (Millipore) flow cytometer and principle of operation (inset)
Software used: guavaSoft inCyte v2.7.

Dihydroethidium (DHE) is a redox-sensitive probe used to label live cells and measure production of ROS, in particular superoxide. DHE is oxidised by reactive oxygen and nitrogen species (e.g. superoxide, hydrogen peroxide, hydroxyl radical) to form ethidium (see Figure 2.15).

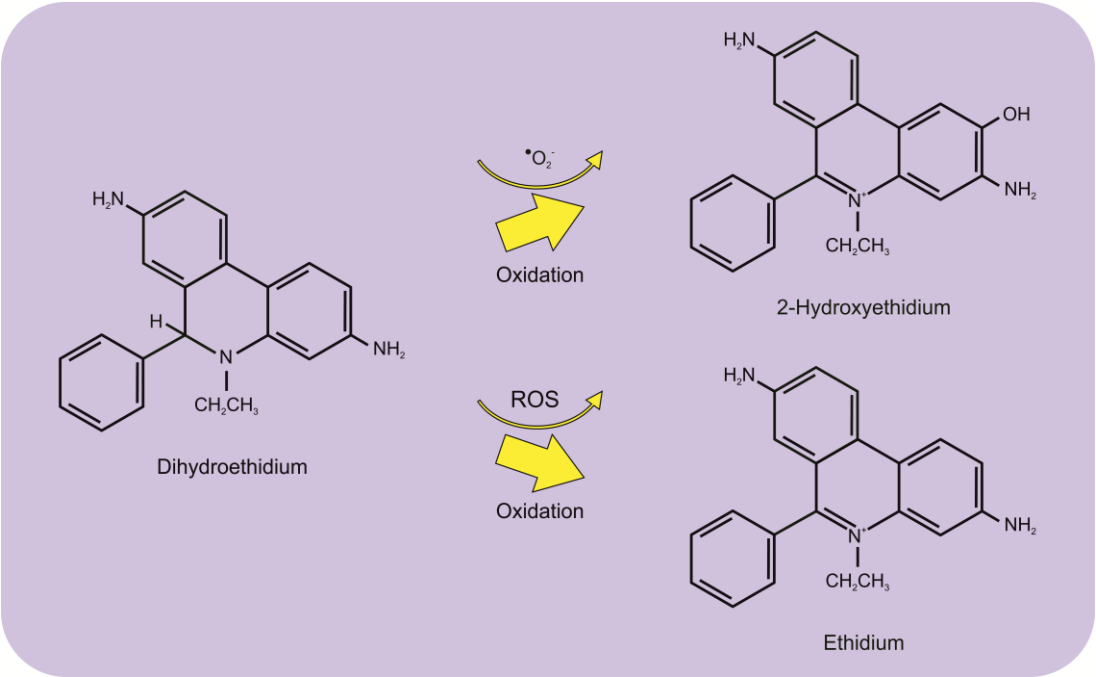

Figure 2.15 Conversion of dihydroethidium to 2-hydroxyethidium by superoxide and to ethidium in the presence of reactive oxygen species

The experimental setup was adapted from a protocol established by Munhoz *et al.* (2016). Briefly, cells were stimulated with the inflammatory cytokine, tumor necrosis factor alpha (TNF-α) (0, 10 and 100 ng/mL) for 12 h in order to induce an increase in ROS. Cells were stained with 3 μM DHE 30 min prior to completion of the treatment incubation period. Additional cultures of untreated cells were employed as unstained controls, with 1% hydrogen peroxide (H_2O_2) used to demonstrate a positive control. Cells were trypsinised and pelleted before being washed in warmed PBS. Cells were re-centrifuged and the pellet re-suspended in 600 μL of Mg-free medium before being transferred to a round-bottomed 96-well plate. Samples were subsequently analysed in triplicate by flow cytometry. The following settings were applied:

Table 2.14 ROS assay acquisition parameters for Guava ® easyCyte 8HT

Number of events	10,000
Time to acquire:	240 sec.
Sample volume	0.2 mL
Channel	Red 2

2.2.8.10 Determination of oxidative stress in plasma samples by ELISA using 8-hydroxydeoxyguanosine (8-OHdG)

The reactive nature of ROS may result in oxidative damage to cell membranes, protein and DNA. 8-hydroxydeoxyguanosine (8-OHdG), an oxidised nucleoside of DNA resulting from a hydroxyl radical attack on guanine, is the most frequently detected and studied DNA lesion (Wu *et al.*, 2004). It is used as a biomarker of oxidative DNA damage caused by ROS. An enzyme-linked immunosorbent assay (ELISA) was used for quantification of 8-OHdG in human plasma samples. This kit employed the competitive inhibition ELISA method to achieve a detection range of 74.07-6,000 pg/mL.

The ELISA kit was designed to measure antigens from serum, plasma and other biological fluids, and their specificity and calibration was confirmed by the manufacturer. Materials provided in the kit included a pre-coated 96-well microtitre plate, standard, standard diluent, assay diluent, detector antibody, TMB substrate, stop solution, wash buffer concentrate and detection reagent (biotin-labelled antigen). PBS (pH7.0-7.2) was required to dilute the wash buffer concentrate.

Specific 8-OHdG capture antibody was pre-coated onto each well surface. 50 µL plasma sample (containing the antigen/analyte to be tested) was added along with an equal volume of biotin-labelled antigen detector. Sample antigen and biotin-labelled antigen competitively bound to the capture antibody on the well surface. Following incubation, any unbounded conjugate was washed off. 100 µL horseradish peroxidase (HRP)-avidin conjugate was then added. After 20 min. room temperature incubation and washing, 90 µL tetramethylbenzidine (TMB) substrate solution was added. TMB substrate became blue in colour following catalysation of peroxidase by HRP, and turned yellow following the addition of 50 µL stop solution (2n H2SO4).

The greater the concentration of analyte (8-OHdG) in the sample, the more capture antibody active sites were taken up by it. Hence, there were fewer active sites available to bind competitor enzyme-labelled antigen molecules. HRP-avidin conjugate only bound to enzyme-labelled antigens. As a result, intensity of the colour in each well was inversely proportional to the concentration of analyte. Sample

readings (λ 450 nm) were compared against standards (0, 74.07, 222.22, 666.67, 2000 and 6000 pg/mL) ran on the same plate.

2.2.8.11 Assessment of platelet adhesion and aggregation by Impact-R cone and plate analysis

The Impact-R device (DiaMed) was used to assess platelet function (adhesion and aggregation) in an anti-coagulated whole blood aliquot (130 µL) under near-physiological conditions. Blood samples drawn into sodium citrate vacutainers were analysed 1-hour post-draw. The system, components and principle of operation are illustrated in Figure 2.16. Samples were washed with PBS prior to staining with May–Grünwald stain.

Adhered platelets were quantified by image analysis software, using random, representative images of the plate surface. Averaged results were expressed as a percentage of the plate surface area covered by aggregates (SC %) as an index of platelet adhesion, and average aggregate size (AS μm^2) as an index of aggregation.

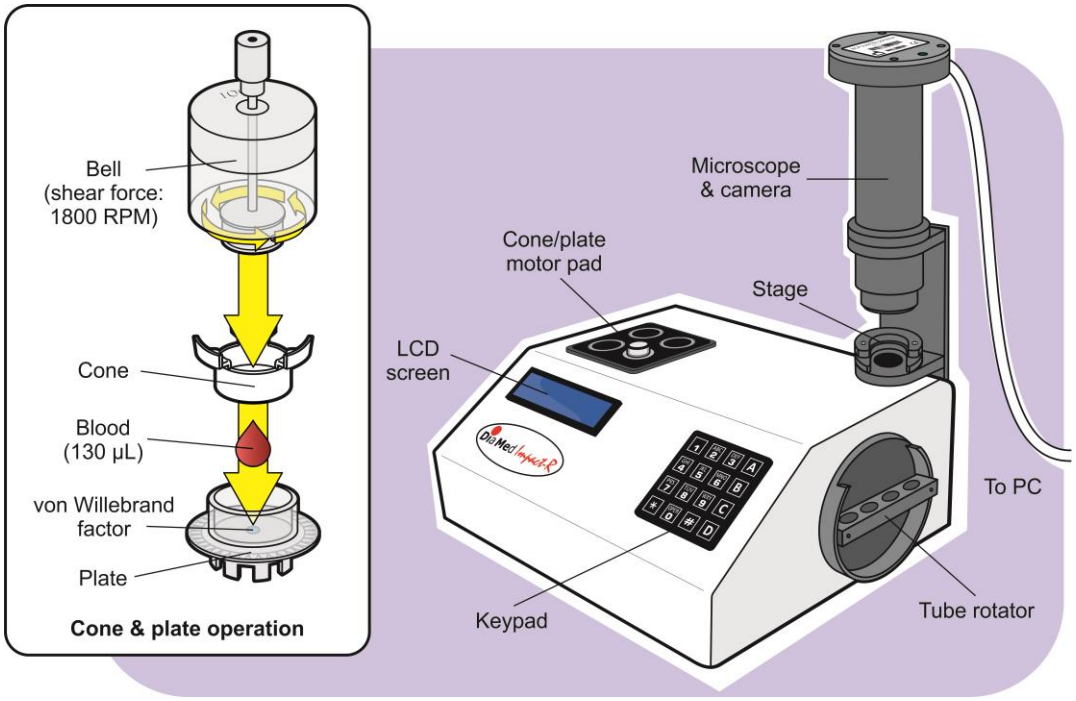

Figure 2.16 Impact-R (DiaMed), showing the cone and plate principle (inset) by which platelet adhesion and aggregation are measured under arterial flow conditions
Software used: DiaMed Impact-R v1.31

2.2.8.12 Application of burn insult to *in vitro* 3D skin model

In vitro burn insults were applied using a modified animal model protocol by Plichta *et al*. (2014). Custom 3.66 g brass weights were milled from brass stock with a surface contact area of 10 mm and a protrusion for handling with tweezers (see Figure 2.17). Weights were heated to 100°C on a heating block (Stuart) and temperature checked using an infrared thermometer. Skin models (in well-insert baskets) were removed from 6-well plates and quickly placed onto a plastic surface in a laminar cabinet to avoid heat dissipation. Brass weights were removed from the heating block using tweezers and immediately placed on the centre of each 2.5 cm model for 10 seconds. After 10 seconds, the brass weight was removed and the appropriate treatment was topically applied. Each treatment consisted of custom-cut 2.5 cm gauze disks soaked in the appropriate therapy. Models were returned to the incubator for 24 and 48 h, after which time, models were sampled for subsequent analysis.

Skin biopsies were taken from the model using Integra® 3 mm disposable biopsy punches (Fisher Scientific Ltd.) post-treatment. Biopsies were immediately snap-

frozen in liquid N, before storage at -80°C. RNA was subsequently harvested from biopsy samples using the TRIzol® islolation method as described in section 2.2.4.2. Genetic material was investigated using RT^2 Profiler arrays (Qiagen) containing primers for wound-healing and fibrosis associated genes (see Appendix A for complete gene list).

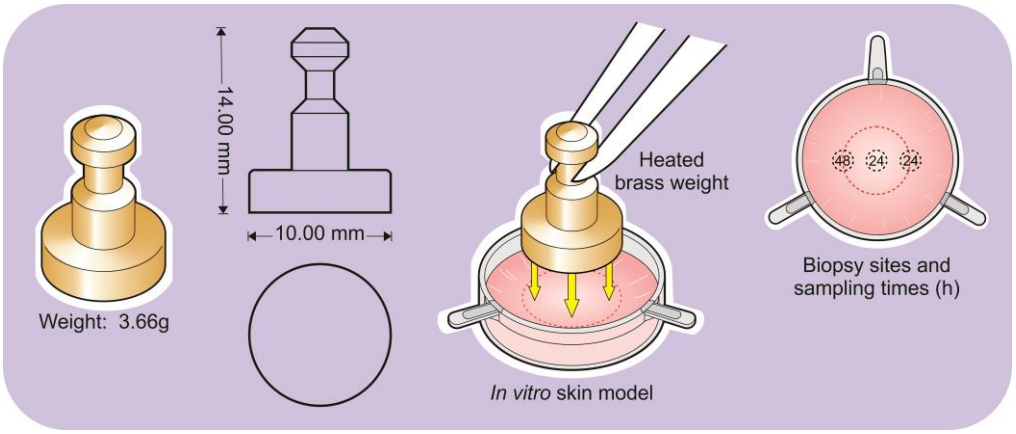

Figure 2.17 Custom-milled brass burn weights used to inflict reproducible burn insults to LabSkin™ (Innovenn) in vitro 3D skin models
3.0 mm biopsies were taken from the model in the centre and along the burn margin as indicated.

2.2.9 Human Intervention

Neal's Yard Remedies, UK, produced a functional food supplement drink, consisting of two functional health components (1) OMC and (2) *Boswellia serrata* extract. (Full details of both active and placebo are listed in Appendix B). The purpose of this study was to examine the potential anti-oxidative and anti-inflammatory effects of these two natural products in addition to platelet activity in a cohort of 45-65 year old healthy females.

Briefly, 16 healthy females (45-65 years) participated in the 28-day study, and were randomly assigned a placebo (glycerine) or active supplement. All subjects provided informed consent in compliance with the Helsinki Declaration. The experimental protocol was approved by DCU Ethics Committee. All subjects were required to adhere to the same pre-testing protocol; no strenuous exercise 24 h pre-testing, no consumption of alcohol 48 h prior and be drug naïve to participate. Prior to testing all subjects completed a survey to ensure suitability for testing and signed consent forms

(see Appendix B). On the extremely low chance that an incidental finding was discovered that could have implications on a subjects' health, the volunteer was to be informed in accordance with best practice, guidelines and protocol laid out by Wolf *et al.*, (2008).

Blood was drawn immediately prior to, and after, the 28-day supplementation period (active versus placebo control) and functional analysis was carried out using the Impact-R system as detailed in section 2.2.8.11. Vacutainers containing sodium citrate anti-coagulant were used for functional studies. Proseek® (Olink, Sweden) multiplex immunoassays were used to assess protein biomarkers, as detailed in section 2.2.7.3. Plasma ROS levels were ascertained using an 8-OHdG ELISA kit (Cloudcone, USA), detailed in section 2.2.8.10.

Statistical analyses were carried out using SPSS v24. One-way analysis of co-variance (ANCOVA) was used to compare post-intervention values differed between placebo and treatment groups, while controlling for differences observed at baseline. This was achieved by the generation of estimated marginal means, statistically eliminating the effect of "pre"-intervention effects. Levene's test and normality checks were carried out and the assumptions met. Post hoc tests (Bonferonni) were used to determine the significance of observed differences.

Chapter Three
Genetic and epigenetic response of HAECs to oscillatory shear stress

3.1 Introduction

Structurally, endothelial cells (ECs) are flat and squamous. Under the influence of haemodynamic force, these cells have the ability to alter their morphology to re-align (polarise) in the direction of blood flow. Cellular thickness ranges from 0.1 μm in capillaries to 1.0 μm in the aorta, where blood flow is comparatively much stronger. ECs frequently exist in a quiescent state, i.e. non-proliferating, with an average lifespan of approximately one year (Aird, 2007). A number of cellular characteristics are associated with this adaptive polarisation, including modifications to the plasma membrane, resulting in a more defined and distinct structure. Cell shape, too, is altered; becoming elongated. Critically, blood flow, encourages the development of strong attachments to neighbouring cells, in addition to underlying basement membranes (Nelson, 2003). Hence, the endothelium provides an anti-coagulant barrier between the vessel contents (blood) and the underlying vessel wall. The ability of ECs to polarise in this fashion necessitates extensive re-modelling of cytoskeletal structure and cell-cell junctions to attain a long, cuboidal morphology that aligns in the direction of blood flow (Desai *et al*., 2008; Zhang *et al.*, 2005).

As discussed in Chapter One, blood exerts a direct influence on the vasculature. This is achieved through haemodynamic interactions and is likely a key epigenetic factor in development of atherosclerosis. The pattern of blood flow throughout the cardiovascular system, by its nature, generates mechanical forces that, in turn, have been found to exert a strong regulatory influence on cardiovascular physiology and pathology (Lehoux and Tedgui 2003; Davies 2009). Unidirectional laminar flow is associated with an athero-protective effect. This type of flow occurs within straight sections of vasculature, and correlates with documented evidence of a lack of atherosclerotic development in such regions. In contrast, turbulent, oscillatory flow is associated with onset of vascular lesions. Despite an overall steady flow, velocity within the vasculature varies continuously over time at any given point (Chatzizisis, Coskun *et al*. 2007).

DNA methylation is an example of the type of independent epigenetic modification associated with such hemodynamic variations in blood flow. While little is known of the environmental-chromatin interaction, mechanical signals received at the mechano-sensitive plasma membrane (such as focal adhesions) are believed to be transferred

via a protein-driven nucleo-skeletal link, permitting functional chromatin organisation in the nucleus (Iyer *et al.*, 2012). DNA methylation-derived measurements have been found to predict mortality independently of health status and other known genetic factors (Marioni *et al.*, 2015). As with most sensory systems, cells capable of mechano-sensation place an emphasis on speed and sensitivity. Epigenetic changes have been found to be reflective of lifestyle, and may act as functional biomarkers of disease before clinical threshold is reached. Significant variations of flow pattern occur, such as those produced in response to either exercise or sedentary behaviour. **In this respect, the hypothesis that oscillatory shear stress results in epigenetic modification/alteration of HAECs towards a pro-atherosclerotic profile was investigated.**

HAECs were exposed to varying durations of shear stress (0-72 h), at 10 dyne/cm^2 in both laminar and oscillatory flow patterns using the Ibidi® perfusion system. Cells were subsequently harvested for total RNA and miRNA from resulting lysates using the mirVana® RNA isolation kit (Life Technologies). Total RNA was pre-amplified using the appropriate pathway-specific RT² PreAMP Primer Mix (Qiagen) before undergoing reverse transcription. Samples were amplified using qRT-PCR-based RT^2 Profiler arrays (Qiagen), and analysed using appropriate software. MicroRNA was reverse transcribed and run on TLDA arrays (Life Technologies). Bioinformatic analysis of mRNA:miRNA expression patterns was conducted using MirTarVis+ open-access software v 0.8.11, in conjunction with correlation analysis, mutual information, MINE, GenMir++, TargetScan and microRNA.org algorithms/databases.

3.1.1 Study aims

In this chapter, the physiological effects of laminar and oscillatory shear stress on the epigenetic adaptability of HAECs was investigated. Hence, the overall aims of this chapter include:

- To establish and verify a pro-inflammatory, pro-atherosclerotic phenotypic model of the endothelial vasculature based on oscillatory shear stress.
- To establish and verify a comparable, healthy phenotypic model of the endothelial vasculature based on laminar shear stress.

- To compare differential epigenetic factor expression between the two model systems and identify putative genes involved in pro-inflammatory atherogenesis.
- To compare differential miRNA expression patterns with epigenetic mRNA and identify key regulators of vascular re-modelling.

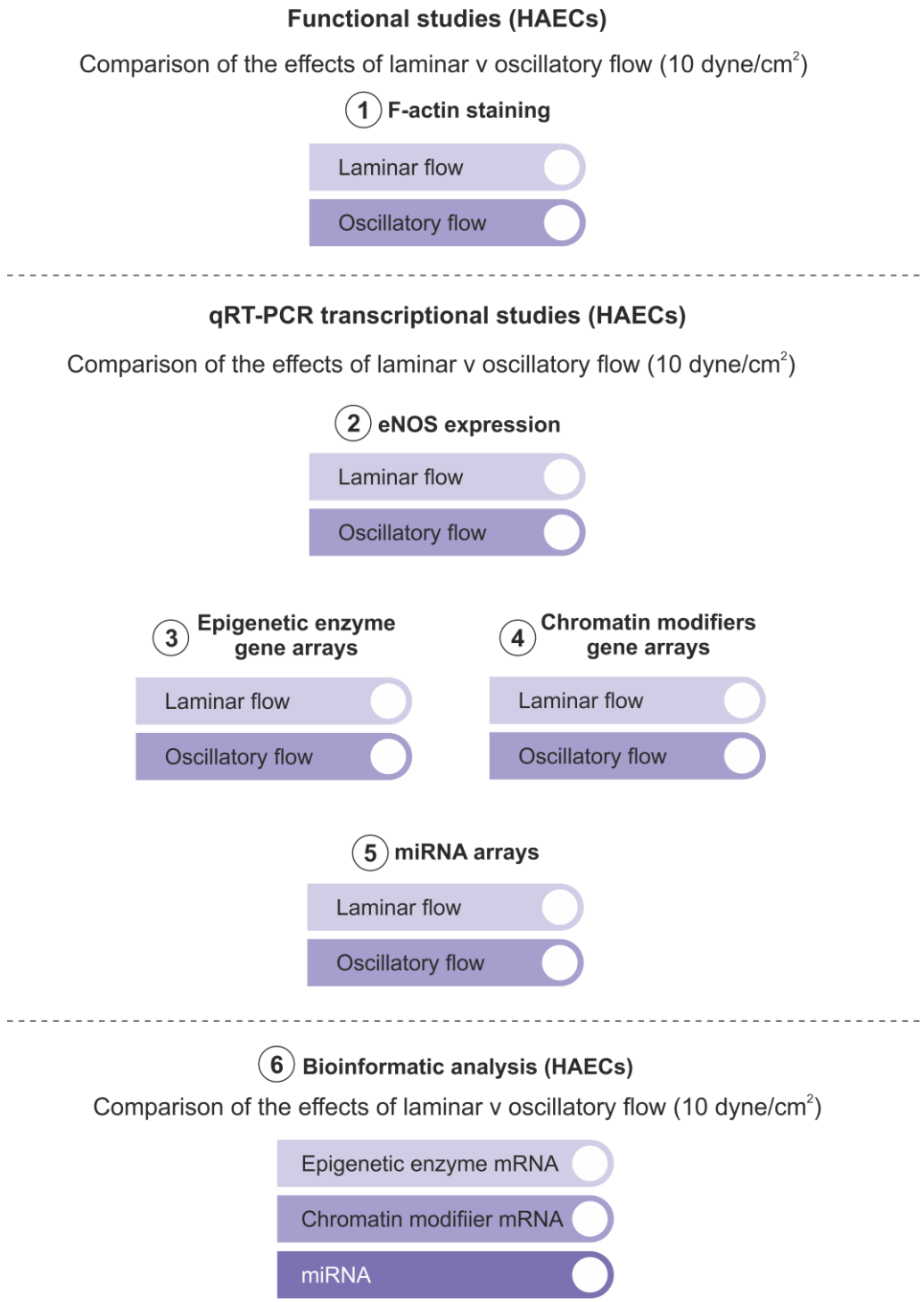

Figure 3.1 Diagram outlining the experimental approach taken in this chapter

3.2 Results

3.2.1 Suitability of the Ibidi® perfusion system as a method of mimicking the *in vivo* shear condition in HAECs

HAECs were exposed to static, laminar (10 dyne/cm^2) and oscillatory flow (±10 dyne/cm^2) for 24 h, followed by F-actin staining using phalloidin (543 nm) and subsequent examination of Ibidi μ-slides by fluorescent confocal microscopy (Figure 3.2).

Examination of Ibidi μ-slides by confocal microscopy revealed that laminar shear stress resulted in visible polarisation of HAECs in the direction of media flow (Figure 3.2C), whilst oscillatory flow yielded a "cobblestone" morphology over the same duration (Figure 3.2B). Such polarisation is associated with normal, healthy vasculature, whereas oscillatory shear stress is associated with the disease phenotype (Green *et al.*, 2018). The observed cobblestone morphology was deemed physiologically representative of this, and hence suitable for further experimentation to verify an increase in inflammatory markers.

Both outcomes served as a positive indicator of shear stress-mediated changes to endothelium. Once the cells were satisfactorily shown to respond to shear through use of the Ibidi® perfusion system, appropriate experiments were then undertaken to further examine mechano-regulated epigenetic changes.

3.2.2 Inflammatory response of HAECs to oscillatory shear stress.

HAECs were exposed to static, laminar (10 dyne/cm^2) and oscillatory flow (±10 dyne/cm^2) for 24, 48 and 72 h, prior to whole cell mRNA harvesting and subsequent qRT-PCR for endothelial Nitric Oxide Synthase (eNOS) expression (Figure 3.3).

Exposure of HAECs to shear stress for durations less than 24 h resulted in an inflammatory response regardless of flow pattern, in line with the model of endothelial activation previously described by Hahn and Schwartz (2009). In this model, laminar shear stress results in an acute inflammatory profile that is quickly resolved as athero-

protective mechanisms inherent within the cell are activated, whilst with oscillatory shear stress, such mechanisms remain deactivated and the inflammatory response persists.

Nitric oxide (NO) induces dilation of blood vessels in response to laminar shear stress and is a necessary factor for continued health of the vascular system. Inhibition of eNOS causes reduced NO production, ultimately leading to endothelial dysfunction. This phenomenon is clearly illustrated in Figure 3.3. Both laminar and oscillatory conditions initially expressed low levels of eNOS, but only the laminar shear condition underwent a restoration back to healthy levels. HAECs exposed to oscillatory shear stress, in contrast, continued to express low levels of eNOS and to exhibit an inflammatory profile up to 72 h.

3.2.3 Impact of 24 h oscillatory flow on epigenetic gene expression in HAECs

HAECs were exposed to laminar (10 dyne/cm^2) and oscillatory flow (±10 dyne/cm^2) for 24 h, prior to whole cell mRNA harvesting. Samples were subsequently analysed by qRT-PCR using gene arrays specific for epigenetic enzyme and chromatin modification factor expression (Figures 3.4(i) and 3.5(i), respectively; n=1).

At 24 h, normalised epigenetic enzyme gene array analysis revealed thirty seven marginally (2.0-5.0 fold) up-regulated genes relating to epigenetic enzymes in response to oscillatory flow, whilst only two (SETD6 and KDM4C) exhibited down-regulation (-4.77 and -7.50, respectively) (Table 3.1).

In comparison, at the same timepoint, the chromatin modification factor panel showed comparatively little change in response to oscillatory flow, with only one up-regulated gene (PHF21B, 5.37-fold) and two down-regulated genes (BRDT, -5.04-fold and PHF1, -2.04-fold) from the panel of 84 (Table 3.2).

3.2.4 Impact of 48 h oscillatory flow on epigenetic gene expression in HAECs

HAECs were exposed to laminar (10 dyne/cm^2) and oscillatory flow (±10 dyne/cm^2) for 48 h, prior to whole cell mRNA harvesting. Samples were subsequently analysed

by qRT-PCR using gene arrays specific for epigenetic enzyme and chromatin modification factor expression (Figures 3.4(ii) and 3.5(ii), respectively; n=1).

Due to cost constraints, array analyses were initially performed as single replicates, with the timepoint of most interest investigated further. Initial n = 1 data revealed that the 48 h timepoint yielded the overall largest number of gene expression changes of the 3 timepoints analysed. It was therefore decided to increase the number of biological replicates at 48 h to n = 3 (see Figures 3.6 and 3.7). In this regard, the resultant epigenetic enzyme panel analysis showed a small number of up-regulated genes, but overall yielded a larger number of down-regulated genes in response to oscillatory flow (see Table 3.3).

Observed chromatin modification factor expression changes for the same 48 h timepoint were again fewer in number in comparison to the epigenetic enzymes data. Five genes were down-regulated in response to oscillatory shear stress (see Table 3.4).

3.2.5 Impact of 72 h oscillatory flow on epigenetic gene expression in HAECs

HAECs were exposed to laminar (10 dyne/cm^2) and oscillatory flow (±10 dyne/cm^2) for 72 h, prior to whole cell mRNA harvesting. Samples were subsequently analysed by qRT-PCR using gene arrays specific for epigenetic enzyme and chromatin modification factor expression (Figures 3.4(iii) and 3.5(iii), respectively; n = 1).

Figure 3.4 shows that exposure to oscillatory flow for 72 h using the Ibidi® system resulted in overall fewer genes demonstrating changes in epigenetic enzyme gene expression in comparison to the 48 h timepoint. The six up-regulated and three down-regulated genes are detailed in Table 3.5, where transcriptional changes in the range of +8.8 to -4.01-fold are recorded.

Figure 3.5 shows that chromatin modification factor gene expression also exhibited a reduction in the overall number of genes that responded to OSS after 72 h in comparison with the previous 48 h. Table 3.6 details the ten genes exhibiting up-regulation (2.13 - 84.19-fold) detected. No down-regulated genes were detected.

3.2.6 Impact of oscillatory flow on miRNA gene expression in HAECs

HAECs were exposed to laminar (10 dyne/cm^2) and oscillatory flow (±10 dyne/cm^2) for 24-72 h, prior to whole cell miRNA harvesting from resulting lysates using the *mir*Vana® miRNA isolation kit (Ambion). Total miRNA was pre-amplified using the appropriate Megaplex™ pre-amp primer mix (Life Technologies). MicroRNA was reverse transcribed and run on TLDA cards A and B (Life Technologies). Data were analysed using ExpressionSuite v.1.1.

Tables 3.7, 3.8 and 3.9 show the top twenty miRNA for which expression changes were observed at the 24, 48 and 72 h timepoints respectively. Table 3.7 shows that of the top twenty miRNA up-regulated in response to oscillatory shear stress after 24 h, the top 4 are members of the let-7 family. Table 3.8 shows that after 48 h, let-7 miRNA were again relatively highly expressed, but comprised fewer of the up-regulated miRNA overall, and were interspersed among other miRNA forms in the top 20. Fold change was notably increased at this timepoint, however. After 72 h, extremely high levels of miRNA fold change (>50) were observed in HAECs, suggesting a build-up within the closed microfluidic system over time (see Table 3.9).

3.2.7 Bioinformatic analysis of mMR:miRNA expression patterns: 24 h

HAECs were exposed to laminar (10 dyne/cm^2) and oscillatory flow (±10 dyne/cm^2) for 24 h, prior to whole cell mRNA and miRNA harvesting. Samples previously interrogated by qRT-PCR gene array and TLDA cards A and B, were re-analysed using MirTarVis+ software (V. 0.8.11) for possible miRNA-target pairs. (Table 3.10; n = 1).

Table 3.10 shows that overlapping predicted interactions between Correlation analysis, MINE, GenMir++, TargetScan and microRNA.org online databases revealed that four of the twelve members of the let-7 miRNA family likely interact with five epigenetically regulated genes in HAECs. These specifically related to genes controlling cytoskeletal re-modelling (PAK1) and known inflammatory pathways (NCOA1, USP21, RNF20).

3.2.8 Bioinformatic analysis of n = 3 mRNA:miRNA expression patterns: 48 h

HAECs were exposed to laminar (10 dyne/cm^2) and oscillatory flow (±10 dyne/cm^2) for 48 h, prior to whole cell mRNA and miRNA harvesting. Samples previously interrogated by qRT-PCR gene array and TLDA, were re-analysed using MirTarVis+ software (V. 0.8.11) for possible miRNA-target pairs. (Table 3.11; n = 3)

Overlapping predicted interactions between Correlation analysis, GenMir++, TargetScan and microRNA.org online databases yielded a similar cohort of interactions to that of the 24 h timepoint, but with statistical relevance. As with the 24 h timepoint, a large number of miRNA from the let-7 family were proposed as likely candidates for interaction with a range of epigenetic mRNA counterparts (see Figure 3.7).

3.2.8 Bioinformatic analysis of mRNA:miRNA expression patterns: 72h

HAECs were exposed to laminar (10 dyne/cm^2) and oscillatory flow (±10 dyne/cm^2) for 72 h, prior to whole cell mRNA and miRNA harvesting. Samples previously interrogated by qRT-PCR gene array and TLDA, were re-analysed using MirTarVis+ software (V. 0.8.11) for possible miRNA-target pairs (see Table 3.12; n = 1).

As with the previous two timepoints (24 and 48 h), analysis of the 72 h timepoint yielded a similarly narrow band of let-7 miRNA with putative epigenetic mRNA interactions. Notably, many of the same miRNA:mRNA interactions (such as hsa-let-7b-002619:NCOA3) were suggested by the software package.

Figures 3.1-3.6

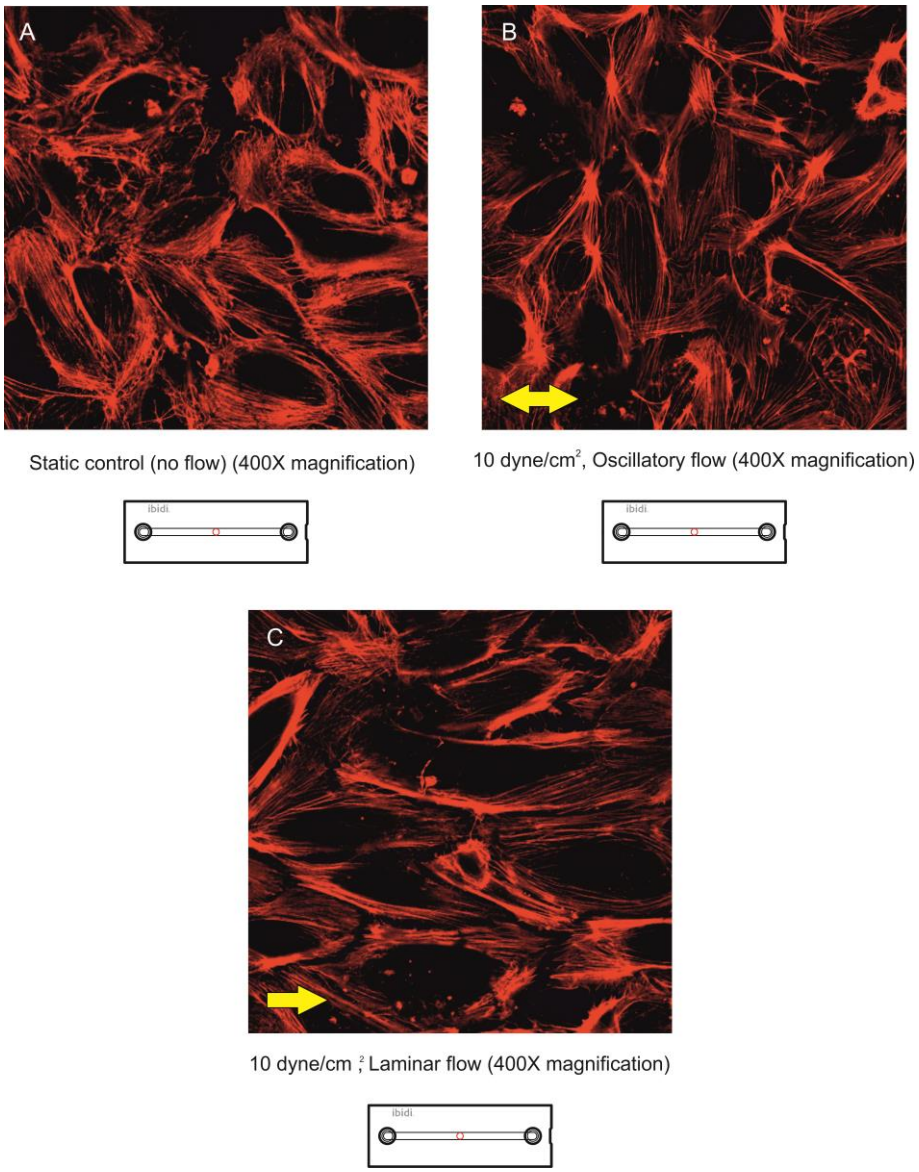

Figure 3.2 Effect of shear stress on HAEC morphology and F-actin realignment HAECs were exposed to (A) static, (B) ±10 dyne/cm^2 oscillatory shear and (C) 10 dyne/cm^2 laminar shear for 24 h using the Ibidi® perfusion system. Cellular localisation of F-actin was detected by confocal microscopy and immunofluorescent imaging (phalloidin stain, ƛ543 nm). F-actin filaments noticeably re-aligned in the direction of the shear vector. Arrows show direction of media flow, and red circles indicate μ-slide format and area imaged. (n = 3).

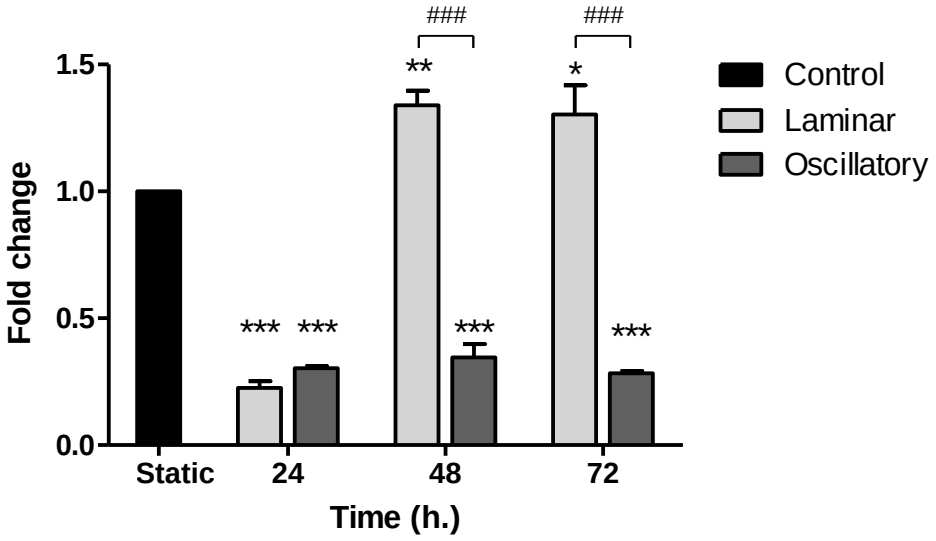

Figure 3.3 Effect of shear stress on endothelial nitric oxide synthase (eNOS) expression in HAECs Confluent HAECs were exposed to laminar and oscillatory shear stress (10 dyne/cm^2) for 24, 48 and 72 h using the Ibidi® perfusion system, after which, whole mRNA was harvested and subjected to analysis by qRT-PCR. Histograms represent mRNA expression fold changes. Results are averaged from three independent experiments (n = 3). *P≤0.05, **≤0.01, ***P≤0.001 versus control, ###P≤0.001 versus laminar.

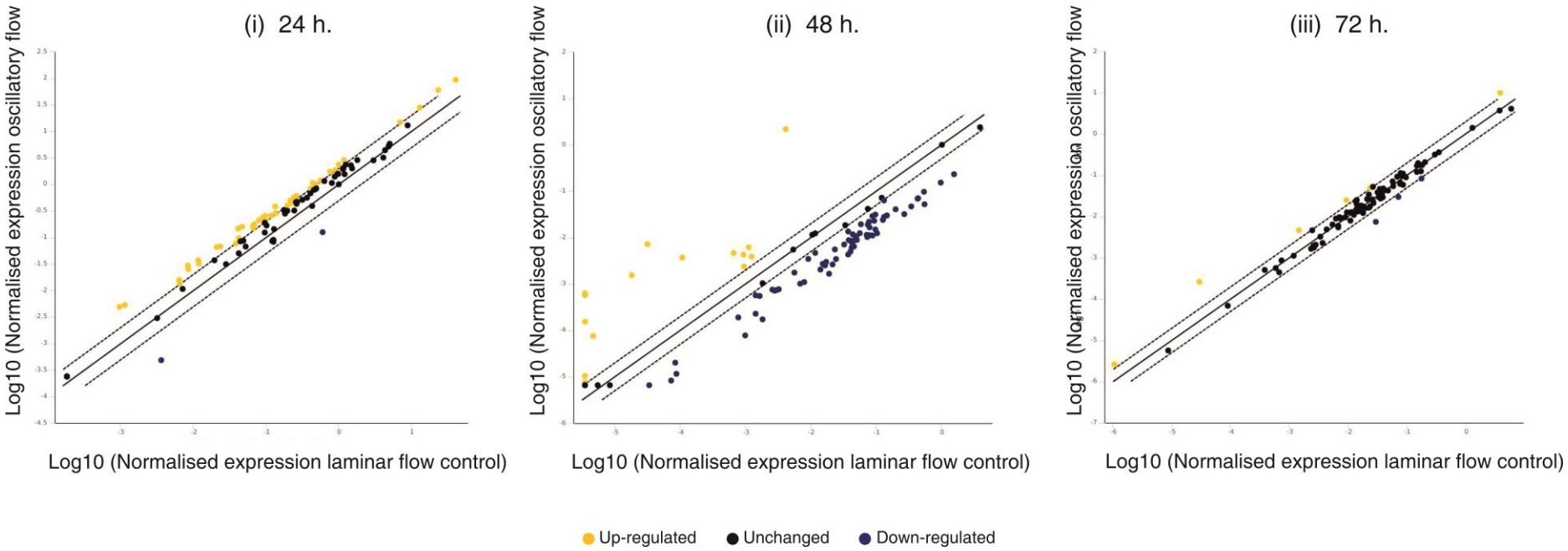

Figure 3.4 Effect of laminar (control) v oscillatory flow on epigenetic enzyme mRNA expression in HAECs, 24, 48 & 72 h., 10 dyne/cm2
Scatter plot represents normalised gene expression for all genes present on the array. The central line indicates unchanged gene expression. Dotted lines indicate selected fold regulation threshold. Data points beyond these represent genes that meet the selected 2-fold regulation threshold. Pre-amplification using the appropriate pathway-specific RT² PreAmp Primer Mix was applied and appropriate corrections made using proprietary Qiagen RT2 analysis software. CT cut-off was set at 35. CT values for endogenous control genes were geometrically averaged and used in ΔΔCT calculations. (n = 1 for each array).

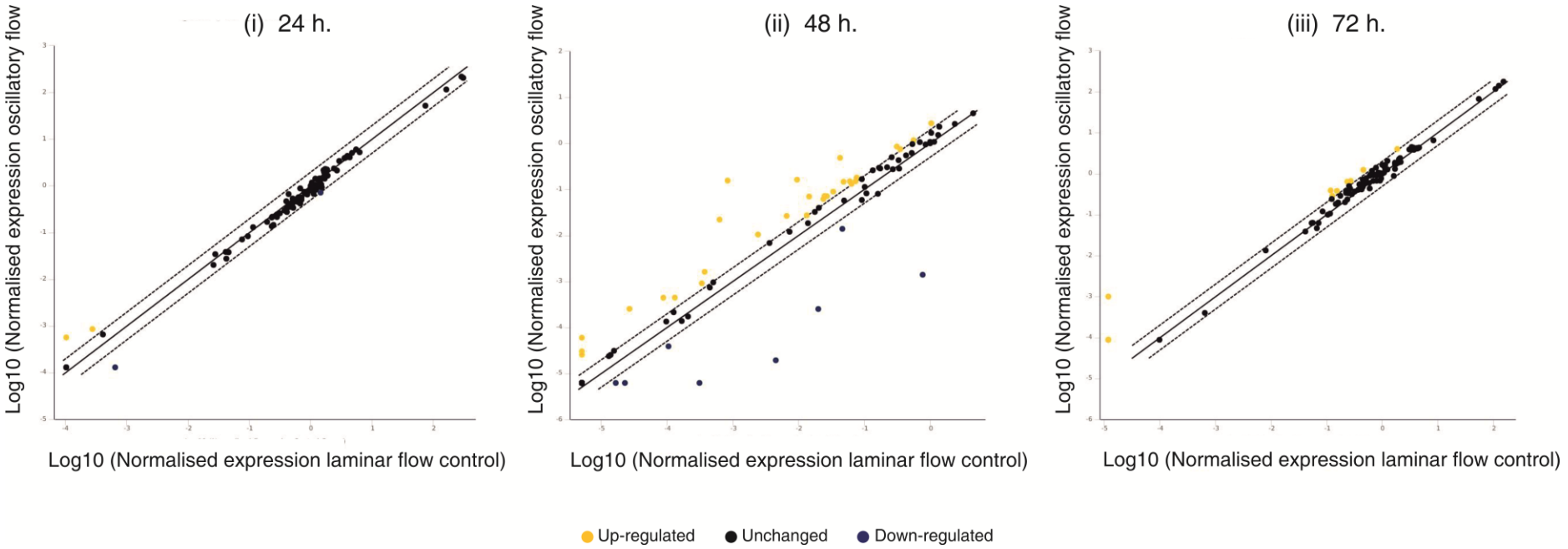

Figure 3.5 Effect of laminar (control) v oscillatory flow on chromatin modification factor mRNA expression in HAECs, 24, 48 & 72 h., 10 dyne/cm^2

Scatter plot represents normalised gene expression for all genes present on the array. The central line indicates unchanged gene expression. Dotted lines indicate selected fold regulation threshold. Data points beyond these represent genes that meet the selected 2-fold regulation threshold. Pre-amplification using the appropriate pathway-specific RT^2 PreAmp Primer Mix was applied and appropriate corrections made using proprietary Qiagen RT2 analysis software. CT cut-off was set at 35. CT values for endogenous control genes were geometrically averaged and used in ΔΔCT calculations. (n = 1 for each array).

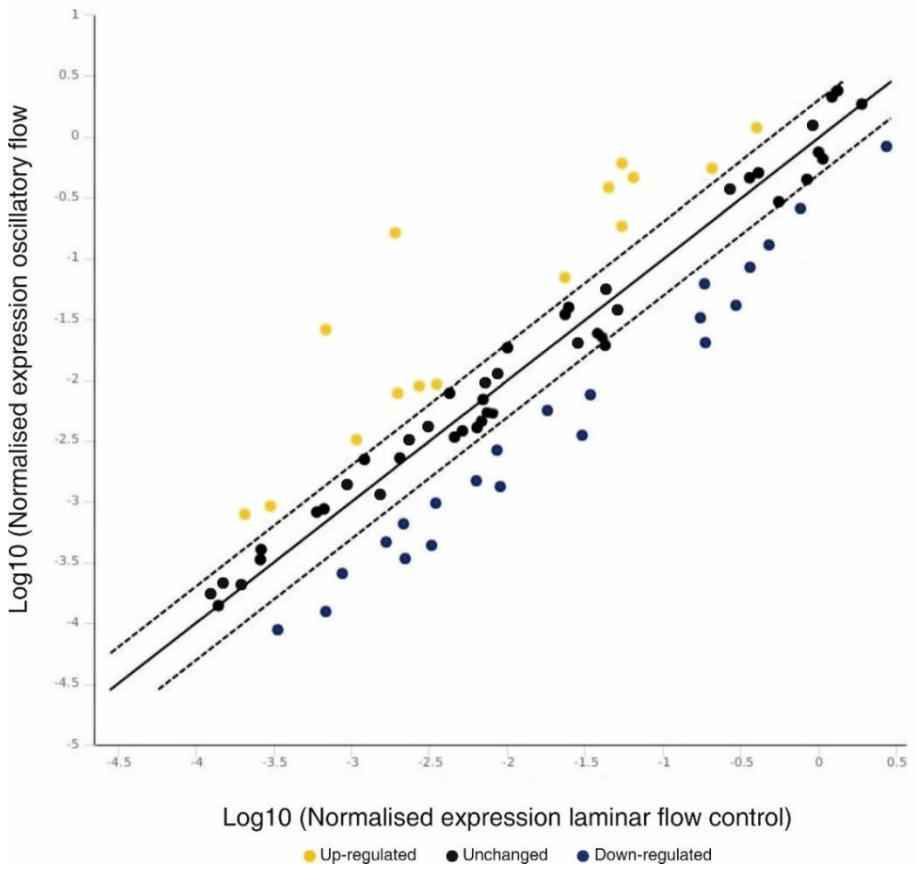

Figure 3.6 Effect of laminar (control) v oscillatory flow on epigenetic enzyme mRNA expression in HAECs, 48 h, 10 dyne/cm^2 (n = 3)

Scatter plot represents normalised gene expression for all genes present on the array. The central line indicates unchanged gene expression. Dotted lines indicate selected fold regulation threshold. Data points beyond these represent genes that meet the selected 2-fold regulation threshold. Pre-amplification using the appropriate pathway-specific RT^2 PreAmp Primer Mix was applied and appropriate corrections made using proprietary Qiagen RT^2 analysis software. CT cut-off was set at 35. CT values for endogenous control genes were geometrically averaged and used in ΔΔCT calculations.

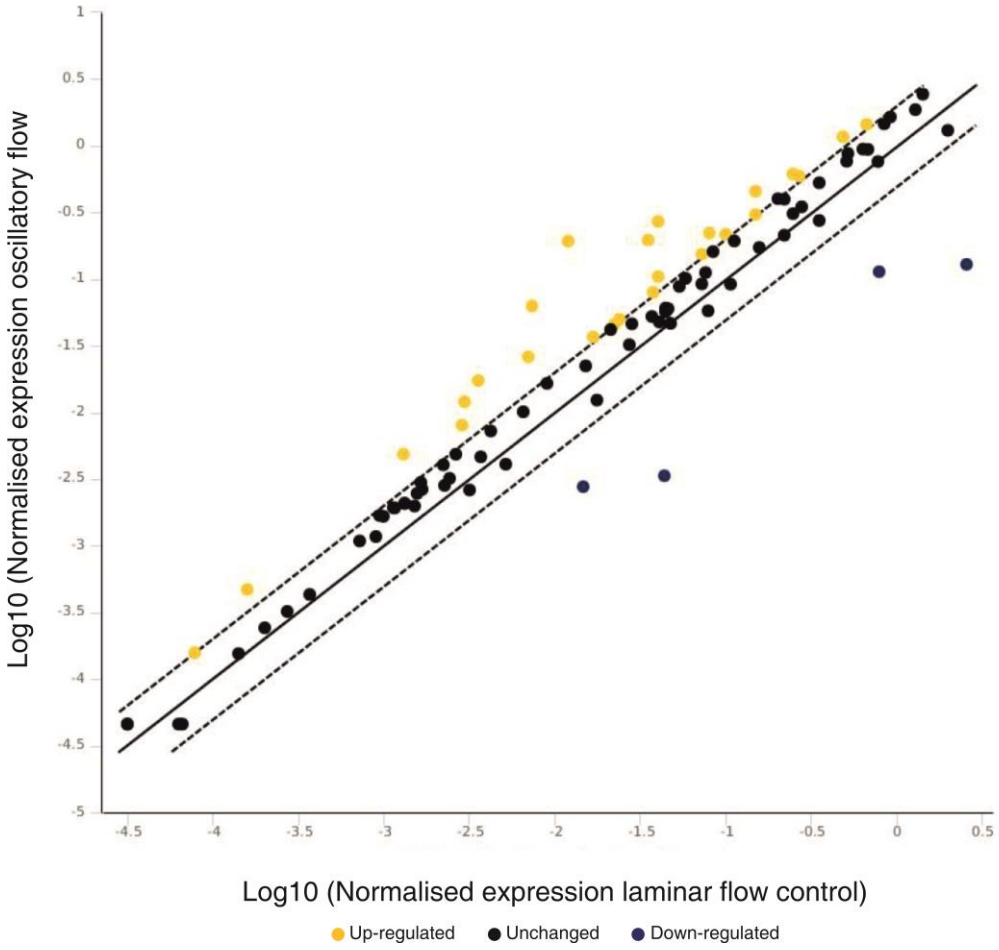

Figure 3.7 Effect of laminar (control) v oscillatory flow on chromatin modification factor mRNA expression in HAECs, 48 h, 10 dyne/cm^2 (n = 3)
Scatter plot represents normalised gene expression for all genes present on the array. The central line indicates unchanged gene expression. Dotted lines indicate selected fold regulation threshold. Data points beyond these represent genes that meet the selected 2-fold regulation threshold. Pre-amplification using the appropriate pathway-specific RT² PreAmp Primer Mix was applied and appropriate corrections made using proprietary Qiagen RT^2 analysis software. CT cut-off was set at 35. CT values for endogenous control genes were geometrically averaged and used in ΔΔCT calculations.

Tables 3.1-3.12

Table 3.1 Effect of laminar (control) v oscillatory flow on epigenetic enzyme mRNA expression in HAECs: 24 h, 10 dyne/cm^2 (n = 1)

Gene	Fold regulation	Gene	Fold regulation
PRMT6	5.00	WHSC1	2.32
ESCO2	4.65	KAT6B	2.31
KMT2E	3.55	SETD1A	2.30
KMT2A	3.46	HDAC7	2.28
SETD4	3.38	NCOA6	2.28
PAK1	3.17	KDM6B	2.23
HDAC10	3.12	KAT6A	2.16
HDAC11	2.93	USP21	2.15
SETD5	2.87	KDM1A	2.10
KDM5C	2.85	AURKB	2.08
KMT2C	2.69	HDAC6	2.08
PRMT7	2.61	SETD2	2.07
NSD1	2.60	KDM5B	2.04
DOT1L	2.56	DNMT3A	2.03
SETD7	2.56	KAT2A	2.03
HDAC3	2.50	USP16	2.03
SETDB2	2.46	RNF2	2.01
HAT1	2.42	KDM4C	-4.77
MBD2	2.39	SETD6	-7.50
UBE2B	2.32	-	-

Table 3.2 Effect of laminar (control) v oscillatory flow on epigenetic chromatin modification factor mRNA expression in HAECs: 24 h, 10 dyne/cm^2 (n = 1)

Gene	Fold regulation
PHF21B	5.37
PHF1	-2.04
BRDT	-5.04

Table 3.3 Effect of laminar (control) v oscillatory flow on epigenetic enzyme mRNA expression in HAECs: 48 h, 10 dyne/cm^2 (n = 3)

Gene	Fold regulation	p-value	Gene	Fold regulation	p-value
SETD5	227.56	0.025	RPS6KA3	-4.72	0.030
KMT2A	180.21	0.050	HDAC2	-4.79	0.025
AURKA	165.17	0.041	KAT7	-4.79	0.028
KMT2E	163.59	0.034	CIITA	-5.14	0.046
KAT6B	85.37	0.037	RNF20	-5.17	0.039
KDM6B	43.72	0.046	SETD8	-5.23	0.050
NSD1	34.33	0.050	PRMT1	-5.46	0.050
ESCO2	15.92	0.023	PRMT3	-5.56	0.027
DOT1L	7.01	0.048	NCOA1	-5.62	0.024
HDAC3	5.51	0.018	USP21	-5.68	0.013
KAT6A	4.66	0.037	MYSM1	-5.75	0.041
HDAC6	3.14	0.050	AURKB	-6.17	0.037
KMT2C	2.97	0.028	PRMT2	-6.17	0.046
KDM5C	2.53	0.050	CARM1	-6.18	0.050
HDAC11	2.17	0.037	UBE2A	-6.33	0.034
USP22	-2.08	0.044	ATF2	-6.44	0.041
CDYL	-2.48	0.027	SETD1B	-6.44	0.046
SETDB2	-2.52	0.019	RNF2	-6.53	0.049
SETD4	-2.64	0.050	SUV39H1	-6.69	0.040
PRMT5	-2.76	0.048	RPS6KA5	-6.83	0.016
HDAC5	-2.97	0.030	DNMT3A	-6.88	0.037
DNMT3B	-3.00	0.030	KAT8	-6.97	0.024
HDAC9	-3.01	0.041	WHSC1	-6.97	0.050
KDM5B	-3.05	0.050	USP16	-7.01	0.042
CSRP2BP	-3.14	0.046	SETDB1	-7.08	0.035
SETD3	-3.50	0.020	NEK6	-7.19	0.021
SUV420H1	-3.72	0.031	HDAC10	-7.2	0.045
ESCO1	-3.90	0.049	DNMT1	-7.84	0.037
KDM1A	-3.90	0.037	KDM4C	-7.97	0.039
KDM4A	-4.01	0.032	KAT2B	-8.05	0.041
AURKC	-4.04	0.050	KAT2A	-8.32	0.027
HDAC4	-4.20	0.016	HDAC1	-8.35	0.033
HAT1	-4.32	0.039	KAT5	-8.52	0.046
SETD7	-4.51	0.028	UBE2B	-10.31	0.050
HDAC8	-4.56	0.047	DZIP3	-10.51	0.046
SETD2	-4.62	0.045	SMYD3	-11.49	0.015
EHMT2	-4.65	0.033	SETD6	-12.76	0.036

Table 3.4 Effect of laminar (control) v oscillatory flow on epigenetic chromatin modification factor mRNA expression in HAECs: 48 h, 10 dyne/cm^2 (n = 3)

Gene	Fold change	p-value
BRD7	18.86	0.045
PHF2	14.74	0.040
CHD6	12.12	0.043
BRWD1	9.24	0.020
FHF2	8.45	0.023
CTBP1	7.25	0.047
SMARCA	7.22	0.021
BAZ2A	6.86	0.016
MBD4	6.69	0.025
MBD2	5.66	0.028
PPC	5.23	0.050
CDYL	4.26	0.028
ING1	4.18	0.026
ING4	3.85	0.034
CHD7	3.75	0.049
CTCF	3.43	0.035
CBX7	2.22	0.038
CDYL2	2.12	0.011
CHD8	2.11	0.026
PHF6	2.05	0.035
PHF5A	-4.29	0.058
CTBP2	-8.48	0.028
ZMYND8	-10.64	0.023
SPEN	-43.64	0.031

Table 3.5 Effect of laminar (control) v oscillatory flow on epigenetic enzyme mRNA expression in HAECs: 72 h, 10 dyne/cm^2 (n = 1)

Gene	Fold change
AURKB	8.80
PAK1	3.21
MYSM1	2.68
ASH1L	2.48
PRMT8	2.48
SUV420H1	2.08
SETD8	-2.14
KDM4C	-2.39
KAT6B	-4.01

Table 3.6 Effect of laminar (control) v oscillatory flow on epigenetic chromatin modification factor mRNA expression in HAECs: 72 h, 10 dyne/cm^2 (n = 1)

Gene	Fold change
BRDT	84.19
ARID1A	7.41
PHF21B	7.41
CHD9	3.30
BAZ1A	2.72
PHF3	2.71
CHD1	2.49
BAZ2B	2.46
CHD7	2.26
CBX3	2.13

Table 3.7 Top 20 miRNA up-regulation fold changes in laminar (control) v oscillatory flow in HAECs: 24 h, 10 dyne/cm^2 (n = 1)

miRNA	Fold change
hsa-let-7a-000377	7.746
hsa-let-7c-000379	7.604
hsa-let-7d-002283	5.338
hsa-let-7g-002282	3.861
hsa-miR-15a-000389	3.675
hsa-miR-138-002284	3.668
hsa-miR-139-5p-002289	3.648
hsa-miR-143-002249	3.590
hsa-miR-149-002255	3.582
hsa-miR-152-000475	3.456
hsa-miR-154-000477	3.331
hsa-miR-155-002623	3.312
hsa-miR-15a-000389	3.311
hsa-miR-15b-000390	3.141
hsa-miR-16-000391	3.032
hsa-miR-17-002308	2.782
hsa-miR-181a-000480	2.649
hsa-miR-181c-000482	2.627
hsa-miR-182-002334	2.484
hsa-miR-185-002271	2.456

Table 3.8 Top 20 miRNA up-regulation fold changes in laminar (control) v oscillatory flow in HAECs: 48 h, 10 dyne/cm^2 (n = 3)

miRNA	Fold change	P-value
hsa-let-7f-000382	26.294	0.032
hsa-miR-1250-002887	26.100	0.042
hsa-miR-26a-2#-002115	23.029	0.017
hsa-miR-301b-002392	20.365	0.05
hsa-miR-149-002255	18.332	0.05
hsa-miR-106b-000442	18.564	0.036
hsa-miR-26a-2#-002115	18.291	0.019
hsa-let-7c-000379	12.388	0.074
hsa-miR-372-000560	10.334	0.027
hsa-miR-371-3p-002124	10.285	0.05
hsa-miR-130b-000456	10.347	0.020
hsa-miR-148b#-002160	10.294	0.041
hsa-let-7g-002282	9.921	0.05
hsa-miR-554-001522	9.843	0.011
hsa-miR-328-000543	7.127	0.026
hsa-miR-148b#-002160	6.223	0.039
hsa-miR-550-002410	3.836	0.042
hsa-miR-103-000439	3.813	0.023
hsa-miR-15b-000390	3.754	0.05
hsa-miR-302b#-002119	3.529	0.025

Table 3.9 Top 20 miRNA up-regulation fold changes in laminar (control) v oscillatory flow in HAECs: 72 h, 10 dyne/cm^2 (n = 1)

miRNA	Fold Regulation
hsa-miR-614-001587	54.231
hsa-miR-301b-002392	43.828
hsa-let-7g-002282	42.924
hsa-miR-520e-001119	20.283
hsa-miR-15a-000389	15.823
hsa-let-7c-000379	10.384
hsa-miR-15b-000390	7.283
hsa-miR-149-002255	5.183
hsa-miR-301-000528	5.124
hsa-let-7f-2#-002418	5.027
hsa-miR-106b-000442	4.284
hsa-miR-195-000494	4.129
hsa-miR-1255A-002805	4.028
hsa-miR-26a-2#-002115	3.183
hsa-miR-623-001555	3.121
hsa-miR-587-001540	3.023
hsa-miR-125b-000449	2.499
hsa-miR-122#-002130	2.348
hsa-miR-643-001594	2.333
hsa-miR-454#-001996	1.568

Table 3.10 Top 5 overlapping predicted miRNA:mRNA interactions: 24 h (n = 1) Table displays overlapping predicted mRNA:miRNA interactions between correlation analysis, MINE, GenMir++, TargetScan and microRNA.org for laminar (control) v oscillatory flow in HAECs at 10 dyne/cm^2 (MirTarVis+ v0.8.1.1).

miRNA	mRNA	
hsa-let-7g-002282	USP21	Ubiquitin Specific Peptidase 21
hsa-let-7a-000377	PAK1	Serine/threonine-protein kinase 1
hsa-let-7e-002406	NCOA1	Nuclear Receptor Co-activator 1
hsa-let-7c-000379	RNF20	Ring Finger Protein 20
hsa-let-7e-002406	NCOA3	Nuclear Receptor Co-activator 3

Table 3.11 Top 12 overlapping predicted miRNA:mRNA interactions: 48 h (n = 3) Table displays overlapping predicted mRNA:miRNA interactions between correlation analysis, GenMir++, TargetScan and microRNA.org for laminar (control) v oscillatory flow in endothelial cells, 48 h, 10 dyne/cm^2 (MirTarVis+ v0.8.1.1). Note that p-values are not provided, as these data comprise ranked, overlapping results

miRNA	mRNA	
hsa-let-7a-000377	AURKB	Aurora kinase B
hsa-let-7b-002619	AURKB	Aurora kinase B
hsa-let-7f-000382	PAK1	Serine/threonine-protein kinase 1
hsa-let-7f-000382	NCOA3	Nuclear Receptor Co-activator 3
hsa-let-7f-000382	DOT1L	Disruptor of telomeric silencing 1
hsa-let-7b-002619	PAK1	Serine/threonine-protein kinase 1
hsa-let-7b-002619	NCOA1	Nuclear Receptor Co-activator 1
hsa-let-7b-002619	DOT1L	Disruptor of telomeric silencing 1
hsa-let-7f-000382	USP21	Ubiquitin Specific Peptidase 21
hsa-let-7f-000382	NCOA1	Nuclear Receptor Co-activator 1
hsa-let-7b-002619	RNF20	Ring Finger Protein 20
hsa-let-7b-002619	NCOA3	Nuclear Receptor Co-activator 3

Table 3.12 Top 12 overlapping predicted miRNA:mRNA interactions: 72 h (n = 1). Table displays overlapping predicted mRNA:miRNA interactions between GenMir++, TargetScan and microRNA.org for laminar (control) v oscillatory flow in HAECs, 72 h, 10 dyne/cm^2 (MirTarVis+ v0.8.1.1).

miRNA	mRNA	
hsa-let-7b-002619	AURKB	Aurora kinase B
hsa-let-7f-000382	AURKB	Aurora kinase B
hsa-let-7f-000382	PAK1	Serine/threonine-protein kinase 1
hsa-let-7b-002619	PAK1	Serine/threonine-protein kinase 1
hsa-let-7f-000382	NCOA1	Nuclear Receptor Co-activator 1
hsa-let-7f-000382	DOT1L	Disruptor of telomeric silencing 1
hsa-let-7b-002619	NCOA1	Nuclear Receptor Coactivator 1
hsa-let-7b-002619	DOT1L	Disruptor of telomeric silencing 1
hsa-let-7g-002282	USP21	Ubiquitin Specific Peptidase 21
hsa-let-7f-000382	USP21	Ubiquitin Specific Peptidase 21
hsa-let-7c-000379	NCOA3	Nuclear Receptor Co-activator 3
hsa-let-7f-000382	NCOA3	Nuclear Receptor Co-activator 3
hsa-let-7b-002619	RNF20	Ring Finger Protein 20
hsa-let-7b-002619	NCOA3	Nuclear Receptor Co-activator 3

3.3 Discussion

The Ibidi® system is a state-of-the-art system for *in vitro* endothelial shearing and perfusion, typically using either HAECs or HUVECs (Belair *et al.*, 2015; Serbanovic-Canic *et al.*, 2017). It comprises a flatbed chamber, onto which HAECs were cultured in 2D. Comparable systems utilise 3D architecture to accomplish the same task, yielding their own advantages and disadvantages. (Bailey *et al.*, 2017; Sfriso *et al.*, 2017, 2018). The confocal microscopy images served as controls, ensuring that, using the Ibidi® system, cells had re-aligned appropriately in the direction of laminar media flow (but not oscillatory flow), thus serving as a positive indicator of shear stress-mediated changes to endothelium in agreement with literature (Kwon *et al.*, 2016; Sfriso *et al.*, 2018). Once cells were shown to respond to shear, appropriate experiments were then undertaken to further examine mechano-regulated epigenetic changes. Polarisation of HAECs is a critical factor involved in endothelial barrier maintenance required for continued vascular health (Poirier *et al.*, 2011). Polarisation involves alteration of the thick, circumferential ring of actin bundles organised around cell boundaries (Yonemura *et al.*, 1995; Zamansky *et al.*, 1991). In this respect, the studies of Hahn and Schwartz (2009) have previously revealed that endothelial cells respond to mechano-transduction with a characteristic inflammatory curve illustrated in Figure 3.8:

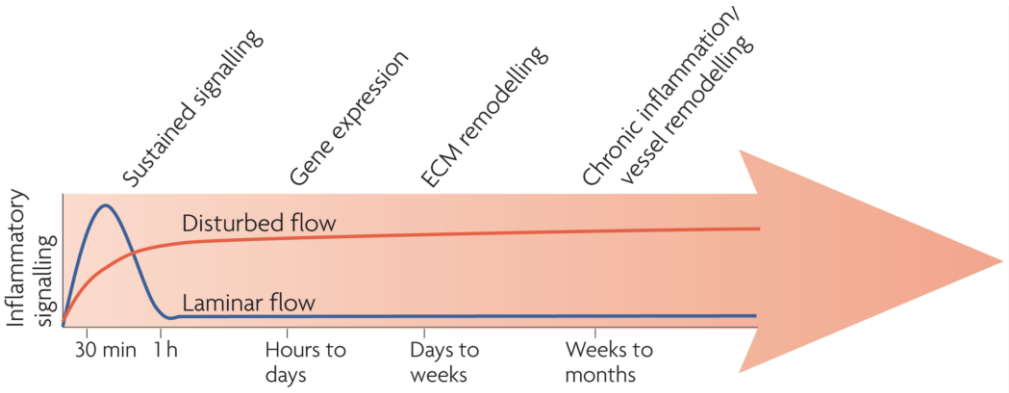

Figure 3.8 Time course of endothelial activation
Disturbed (oscillatory) flow leads to a cascade of changes in the initial stages of shear, over time giving rise to a chronic inflammatory phenotype that invariably leads to injurious vessel re-modelling associated with atherosclerotic plaque formation (Hahn and Schwartz, 2009).

These authors clearly showed that HAECs, in response to both laminar and oscillatory flow patterns, yield an inflammatory response in the initial few hours, after which, a clear difference emerges between the two states. Laminar flow conditions result in greatly reduced inflammatory signalling, while disturbed oscillatory flow continues to cause inflammation. Gene expression changes occur within a period of hours to days, within the time-frame of this experiment. This is in agreement with Iyer *et al* (2012), who suggest a distinct timeline where mechanical activation is followed by actin re-organisation and chromatin re-assembly, and subsequent translocation of transcription co-factors from cytoplasm to nucleus. Kwon *et al* (2016) demonstrated endothelial polarisation *in vivo* within 4.5 h using zebrafish models, but did not investigate the inflammatory response.

The physical difference in our HAECs between the two flow patterns was clear: oscillatory flow was a disturbed type that, while unhealthy in the vascular compartment (Green *et al.*, 2018), was nevertheless a stimulatory one. Over the three timepoints (24, 48 and 72 h), cells in the experimental (oscillatory) condition responded as anticipated. Endothelial nitric oxide (eNOS) production declined, and F-actin staining revealed a random pattern of cellular alignment. Nitric oxide (NO) induces dilation of blood vessels in response to laminar shear stress and is a necessary factor for continued health of the vascular system (Chen *et al.*, 2008). Inhibition of eNOS causes reduced NO production, ultimately leading to endothelial dysfunction (Rippe *et al.*, 2012). Both laminar and oscillatory conditions initially expressed low levels of eNOS in comparison to a static control (itself a relatively unhealthy state for cells) at 24 h. Moreover, HAECs exposed to oscillatory shear stress continued to express low levels of eNOS and to exhibit an inflammatory profile up to 72 h.

Laminar flow served as a healthy cell control in this experiment, with elevated levels of eNOS anticipated (Moore *et al.*, 2010). As expected, laminar flow pattern elicit the desired non-inflammatory profile after 24 h – somewhat longer perhaps than that reported by Hahn and Schwartz (2009). The first 24 h appeared to result in HAECs acquiring a quiescent profile. Quiescent cells remain withdrawn from the cell cycle and fail to proliferate until exposure to particular conditions, such as growth factors or hormones. Essentially, they remain in the G_0 phase of the cell cycle. Vasculature is naturally predisposed to particular flow types depending on its anatomical location (long straight sections being predisposed to laminar shear stress and bifurcations to

disturbed/oscillatory flow). However, the persistent laminar flow of 10 dynes/cm^2 for the duration of this experiment was perhaps a factor that served to induce this quiescence.

Further experimental procedures revealed a number of genes that exhibited expressional fold changes worthy of note. In order to best consider these data and their implications, the various mRNA, miRNA, and their reported interactions in particular will be discussed sequentially in the following section according to timepoint.

3.3.1 The effect of oscillatory shear (OSS) on mRNA/miRNA expression at 24 h

Of the eighty-four genes analysed on the epigenetic enzymes array, thirty-seven were up-regulated while only two demonstrated down-regulation at 24 h. Interestingly, comparatively few of the eighty-four chromatin modification genes were stimulated at the same point in time. The most important/relevant of these genes to the hypotheses and aims of this thesis are placed into context below.

Protein arginine methyltransferase 6 (PRMT6) expression change was among the highest (5-fold) of those epigenetic enzymes altered by 10 dyne/cm^2 OSS at 24 h. The PRMT family are responsible for generating NOS inhibitors by the proteolysis of methylated proteins (Lo Sardo *et al.*, 2013), and notably, PRMT7 was also up-regulated 2.6-fold. NO, as previously discussed, plays important roles within the cardiovascular system. However, literature does not propose any link with atherosclerotic development beyond this. PHR21B demonstrated similarly high expression change (5.37-fold) among those chromatin modifiers examined. Interestingly, a relationship between PHF21B and endothelium has been reported in literature, with knockdown of the known epigenome regulator, Enhancer of Zeste Homolog 2 (EZH2), shown to up-regulate PHF21B expression (Dreger *et al.*, 2012).

A perhaps more relevant gene was P21 activated kinase-1 (PAK1). PAK1 is an important regulator of actin, and a member of the highly conserved serine/threonine protein kinase family (Wang *et al.*, 2018). Hence, its 3.17-fold up-regulation at 24 h was of particular interest. Moreover, PAK1 was shown to be up-regulated in the oscillatory condition across timepoints, further suggesting its importance within the

adaptive mechanisms being investigated. PAK1 is associated with cytoskeletal re-organisation [localised to focal complexes and regulation of actin de-polymerisation (Li *et al.*, 2008)]. Therefore, such up-regulated activity is unsurprising, given the experimental setup. Nevertheless, PAK1 up-regulation effectively acted as a control, verifying the effects of shear stress in the model system and the sensitivity of the arrays as a means of detection. Importantly, PAK1 conveys signals through an inter-molecular auto-phosphorylation-induced conformational modification. It does so without transfer of a phosphate group to any immediate downstream effectors. Ke *et al.* (2013) propose that this signal transduction cascade is achieved via the scaffolding network itself. Together with the observable physical haemodynamic response of HAECs to oscillatory shear stress discussed previously, this adds weight to the hypothesis of epigenetic regulation of endothelium.

PAK1 interactions with up-regulated let-7 miRNA were suggested across the various timepoints of this experimental setup. A wide range of let-7 miRNA have now been predicted and/or experimentally validated in numerous species, including human (Su *et al.*, 2012). Isoforms of these highly-conserved miRNA act by complimentary pairing to protein-coding mRNA, hence directing their post-transcriptional fate (H. Lee *et al.*, 2016). Recent literature has shown that let-7 miRNA generate a protective effect by regulating inflammation in diabetes-associated atherosclerosis (Brennan *et al.*, 2017). Given the role that diabetes plays in accelerating atherosclerosis, the up-regulation of numerous let-7 miRNA at 24 h is striking. Moreover, a number of such miRNA:mRNA overlapping interactions involving let-7 miRNA proposed by miRTarVis+ remained consistent over the three timepoints, suggesting a level of stability in cellular response to oscillatory shear stress and hence presenting a number of likely candidates for further investigation.

Another up-regulated (2.56-fold) gene of interest is Disruptor of Telomere silencing 1-Like (DOT1L). DOT1L is a histone methyltransferase [targeting histone 3, lysine 79 (H3K79)] implicated in a number of biological processes, including CVD. It achieves this by suppressing Wnt signalling through inhibition of sirtuin-1 (SIRT1), an important regulator of gene transcription (Monteagudo *et al.*, 2017).

Of those genes down-regulated in response to OSS, the methyltransferase, SETD6, has been shown to be a negative regulator of the oxidative stress response (Chen *et*

al., 2016). Hence its down-regulation (-4.77-fold) at 24 h is of particular interest, especially given that none of the miRNA assayed were found to exhibit any association. Its regulation must therefore be achieved by a separate mechanism. The curtailment of SETD6 has been demonstrated to cause elevated intracellular Nuclear Factor-Like 2 (NRF2) transcription factor levels. NRF2, in turn, induces expression of a number of cytoprotective genes that protect from inflammation and oxidative stress (Wasik *et al.*, 2017; Bricambert *et al.*, 2018). Interestingly, NRF2 has been shown to exhibit both pro- and anti-atherogenic effects in experimental animal models (Mimura and Itoh, 2015). Nuclear factor κB (NF-κB) is another important mediator of inducible transcription. This pleiotropic signalling pathway controls key physiological and pathological states, including inflammation (Chang *et al.*, 2011). Its involvement with SETD6, therefore, renders SETD6 a target of interest.

Overall, at 24 h *in vitro*, experimental data revealed relatively few up-/down-regulated genes, and add further weight to the theory that both laminar and oscillatory model conditions were inflammatory. Certainly, little indication of chromatin re-modelling was evident. Nevertheless, epigenetic enzyme expression was notably present, indicating the beginnings of a cellular response to oscillatory flow that was subsequently detected at the ensuing 48 h timepoint.

3.3.2 The effect of OSS on mRNA/miRNA expression at 48 h

Of the three timepoints assessed, the 48 h timepoint yielded the largest number of genes with altered expression levels, with many of the same genes discussed at the 24 h timepoint recurring. While each of the initial timepoint experiments (24-72 h) were carried out only once (Figures 3.3 and 3.4), the 48 h timepoint was deemed sufficiently interesting to warrant further investigation. Hence, this timepoint was repeated n = 3, with subsequent bioinformatical analyses gaining statistical weight as a consequence. Accordingly, only the n = 3 data will be discussed for this timepoint. Replicates did reveal some variation between samples, highlighting the inherent variability of gene arrays as a method of analysis (Jovanovic *et al.*, 2001). Nevertheless, averaged values confirmed a number of genes with a consistent expression pattern, despite fluctuations in fold change. P-values >0.05 were excluded.

Bromodomain-containing protein 7 (BRD7) demonstrated the largest increased expression (18.86 fold) in the oscillatory model. While relatively little about this protein family's relationship with atherosclerotic development is understood, studies have revealed an association with atherogenesis (Yan *et al.*, 2018). BRD7 protein is predominantly located in the nucleus, playing an important role in transcriptional regulation by binding to acetylated histone via its bromodomain. Recent contradictory *in vivo* studies have shown that BRD7 is involved in early acute inflammation by inhibiting the NF-κB signalling pathway, thereby suggesting an anti-inflammatory role (Zhao *et al.*, 2017). As BRD7 was not predicted to interact with any of the pool of up-regulated miRNA present on array cards A or B, it suggests a lack of regulatory oversight via this mechanism. Its up-regulation in response to OSS nevertheless presents it as a possible gene of interest for further study.

The histone demethylase Plant Homeodomain Finger 2 (PHF2) was the second-most up-regulated gene (8.57-fold) due to OSS at 48 h. The role of PHF2 in inflammatory pathways is well documented in literature (Bricambert *et al.*, 2018). Liu *et al.* (2017) speculate that PHF2, in association with the transcription co-activator, ARID5B, are together situated at a pivotal gene regulatory axis, responsible for epigenetic control of immune and metabolic homeostasis. This is achieved via methylation of a particular CpG within an ARID5B enhancer region, and inversely correlates with ARID5B expression. Moreover, the authors report that knock-down of ARID5B lead to a reduction in atherosclerosis-related inflammatory and lipid metabolism pathway-related genes, and inhibited cell migration and phagocytosis. As with SETD6, discussed previously, PHF2 has been shown in literature to activate the transcription factor, NRF2 (Bricambert *et al.*, 2018). Together with its up-regulation in the oscillatory shear stress model at 48 h, these data strongly implicate PHF2 as an epigenetically-regulated pro-atherosclerotic gene of interest (Liu *et al.*, 2017).

Notably, a number of miRNA were listed as having possible interactions with multiple different mRNA. For example, the online databases used in the bioinformatic analyses have shown hsa-let-7f-000382 to have interactions with both PAK1 and Nuclear Receptor Co-Activator 3 (NCOA3). This was a result of the GenMir++ script analysis, which considers predicted miRNA regulators, the mRNA target and the profiles of all other predicted miRNAs for the same target. While unsurprising given their nature as

transcriptional regulators, it does serve to narrow the field of targets for future investigation considerably.

As at 24 h, DOT1L demonstrated up-regulation at 48 h. However, unlike the 24 h timepoint, MirTarVis+ algorithms suggested likely interactions with the let-7 miRNA, hsa-let-7f-000382 and hsa-let-7b-002619. As discussed previously, the let-7 miRNA family are associated with an anti-inflammatory protective effect. Their up-regulation at 48 h therefore suggests a timeline where DOT1L up-regulation occurs by 24 h and persists through to the 48 h timepoint. By 48 h, the let-7 miRNA, hsa-let-7f-000382 and hsa-let-7b-002619, are themselves up-regulated as regulatory agents in response. Notably, DOT1L was not observed in list of up-regulated mRNA at 72 h. This by itself makes a compelling argument for added investigation of the other timepoints, as the n = 1 analyses have no statistical validity. Regardless, the data at 48 h are statistically robust, rendering the combined targets of extreme interest, and certainly worthy of further examination by themselves.

3.3.3 The effect of OSS on mRNA/miRNA expression at 72 h

Oscillatory flow at the 72 h timepoint was expected to yield an elevated inflammatory gene expression response in accordance with literature (Green *et al.*, 2018). Interestingly however, a decrease in overall differential gene expression across both mRNA arrays occurred. The 72 h timepoint may in fact represent an unhealthy state in both model conditions due to the "closed" nature of the Ibidi® perfusion system, which allowed a build-up of inflammatory cytokines over time and caused a feedback loop. Recirculation of chemokines, cytokines, etc. permits cell-cell communication within the system, and is consistent with the operation of a number of other microfluidic systems (Sfriso *et al.*, 2018). It is notable that Green *et al* (2018) utilised an orbital shaker plate for generation of their 72 h timepoint. The "closed system" explanation nevertheless conflicts with eNOS data obtained from the same model system, which showed a significant reduction in eNOS expression in the oscillatory condition at 72 h. The reason for this is unexplained at present and may represent an artefact of the model system.

3.4 Summary

This study demonstrated that HAECs did exhibit an epigenetic response to oscillatory shear stress in a time-dependent manner. However, while robust comparisons between laminar and oscillatory flow patterns could be drawn, the Ibidi® perfusion system was inadequate for prolonged (>48 h) experimental procedures. Results revealed that HAEC response to oscillatory shear stress was most pronounced at 48 h, at which point, changes in expression of a number of epigenetically relevant genes were noted. These include a number of overlapping predicted mRNA:miRNA interactions of interest, including suggestion of a possible timeline for miRNA regulation of DOT1L. While gene arrays and bioinformatical software analyses, such as those used in this chapter, provide useful, contextual identification of targets, verification of their efficacy and involvement in such mechanisms must nevertheless be validated using additional means. This is particularly true for software analyses where algorithms and databases are constantly updated/refined/improved over time. A select number of those genes identified at the 48 h timepoint using the MirVarTis+ method that combined experimental data with software analyses represent suitable candidates for such an approach, and will now be investigated in Chapter Four.

Chapter Four

HAEC response to magnesium in the presence of pro-inflammatory oscillatory shear stress

4.1 Introduction

Magnesium (Mg) is a micro-nutrient, critically involved in membrane function, muscle contraction, protein assembly and DNA replication. It is also an essential co-factor in many enzymatic reactions. Mg supplementation is becoming increasingly utilised in maintaining physiological health, particularly that of the cardiovascular system (Maier, 2012). It plays a critical role in modulating vascular smooth muscle tone, endothelial cell function, and myocardial excitability and is thus central to the pathogenesis of several cardiovascular disorders such as hypertension, atherosclerosis, coronary artery disease, congestive heart failure, and cardiac arrhythmias. Epigenetic processes may influence health and ageing in a number of ways. Nutritional magnesium supplementation may act beneficially through epigenetic mechanisms, as well as traditional cellular and molecular pathways. In this respect, mechanical forces, such as the OSS-inducing epigenetic processes investigated in Chapter Three, may commonly be directed to specific ion channels. Such Mg channels can open rapidly and amplify the signal by permitting entry of large numbers of ions (Gillespie and Walker, 2001). **This lends credence to the hypothesis that Mg may represent an important regulatory/therapeutic element in the development of the type of vascular inflammation already observed in the previous chapter**. The work outlined in this chapter has concentrated on the potential anti-inflammatory and cyto-protective effects of Oriel Mineral Complex (OMC), as a therapeutic follow-up to work outlined in Chapter Three.

OMC is derived from seawater. Seawater comprises numerous different materials, including dissolved minerals from the earth's crust and those released from water-dwelling organisms. Mg is ubiquitous in such water. Water solubility presents a significant challenge in formulating such supplements, as it occurs naturally as a crystalline structure. Therefore, extraction of Mg from seawater, using seawater itself as a diluent medium, circumvents this problem. In this respect, we investigated the hypothesis that the ionic form of Mg, which predominates in OMC, would elicit a greater effect on vascular cell functions than other comparable forms of Mg.

In contrast to the slow mechanism of Mg^{2+} transport in other cell types, HAEC membranes are highly permeable (Zhang *et al.*, 1997). Mg^{2+} transport disruption may predispose individuals to development of CVD (Houston, 2011), hence the possible

involvement of Mg^{2+} ion supplements in anti-inflammatory processes was investigated. TRPM6/7 channel proteins are involved in Mg^{2+} absorption via paracellular-passive and transcellular-active pathways (Schuchardt and Hahn, 2017). While molecular mechanisms controlling Mg levels in the body are not well understood, TRPM7 (transient receptor potential cation channel, subfamily M, member 7) has been identified as a key regulator of whole-body Mg homeostasis, and associated with Mg deficiency in vascular endothelial cells (Baldoli *et al.*, 2013). TRPM7 and its closely related magnesium receptor, transient receptor potential melastatin 6 (TRPM6) are unique in that these extraordinary proteins comprise two distinct functional moieties: an ion channel segment and a α-type serine/threonine kinase domain. The TRPM 6/7 channel pair are also capable of influencing each other's biological activity (Schmitz *et al.*, 2005). Other transporters of interest include Mg transporter 1 (MagT1), demonstrated in literature to show high selectivity for Mg and a possible involvement in cellular functions beyond Mg homeostasis (Wolf and Trapani, 2011), and the Cyclin M (CNNM) family of transporters.

The daily recommended Mg dose has been approximated at ≥ 300 mg/day or 6mg/kg bodyweight for either sex (Jahnen-Dechent and Ketteler, 2012). Hypomagnesemia is present in 48% of the US population (Rosanoff *et al*., 2012), with a prevalence of approximately 10% among hospital patients (Swaminathan, 2003) and contributes to accelerated ageing, inflammation and chronic illness (Zhang *et al*., 2017). This is manifested through increased C-reactive protein and cytokine exaggeration, increased nuclear factor kB (NF-kB) expression and platelet dysfunction, which can lead to thrombosis. Thus, magnesium appears to play a vital function in cardiovascular stability and health, but an optimal dose and formulation has yet to be defined.

4.1.1 Study aims

Chapter Three established the pro-inflammatory effect of oscillatory shear stress on HAECs and identified a number of putative epigenetic genes and miRNA involved. In this chapter, 6 of those epigenetic genes (3 epigenetic enzymes and 3 chromatin modification factors) will be further investigated within the context of assessing the putative beneficial effects of magnesium (particularly OMC). In particular, the genetic and functional characteristics of HAECs exposed to inflammatory conditions

imparted specifically through oscillatory shear stress will be assessed (see Figure 4.1). As such, the overall aims of this chapter include:

- To investigate the optimal extracellular concentration of OMC and compare different Mg forms ($MgCl_2$ and Mg aspartate) on HAEC adhesion.
- To investigate the anti-inflammatory effect of a range of different forms of Mg (OMC, $MgCl_2$ and Mg aspartate) on HAECs exposed to oscillatory shear stress.
- To investigate the gene expression of a range of Mg receptors to the presence of Mg at 10mM using qRT-PCR.
- To investigate the effect of 10mM Mg (OMC, $MgCl_2$ and Mg aspartate) on a range of putative epigenetic targets (identified in Chapter Three) using qRT-PCR.

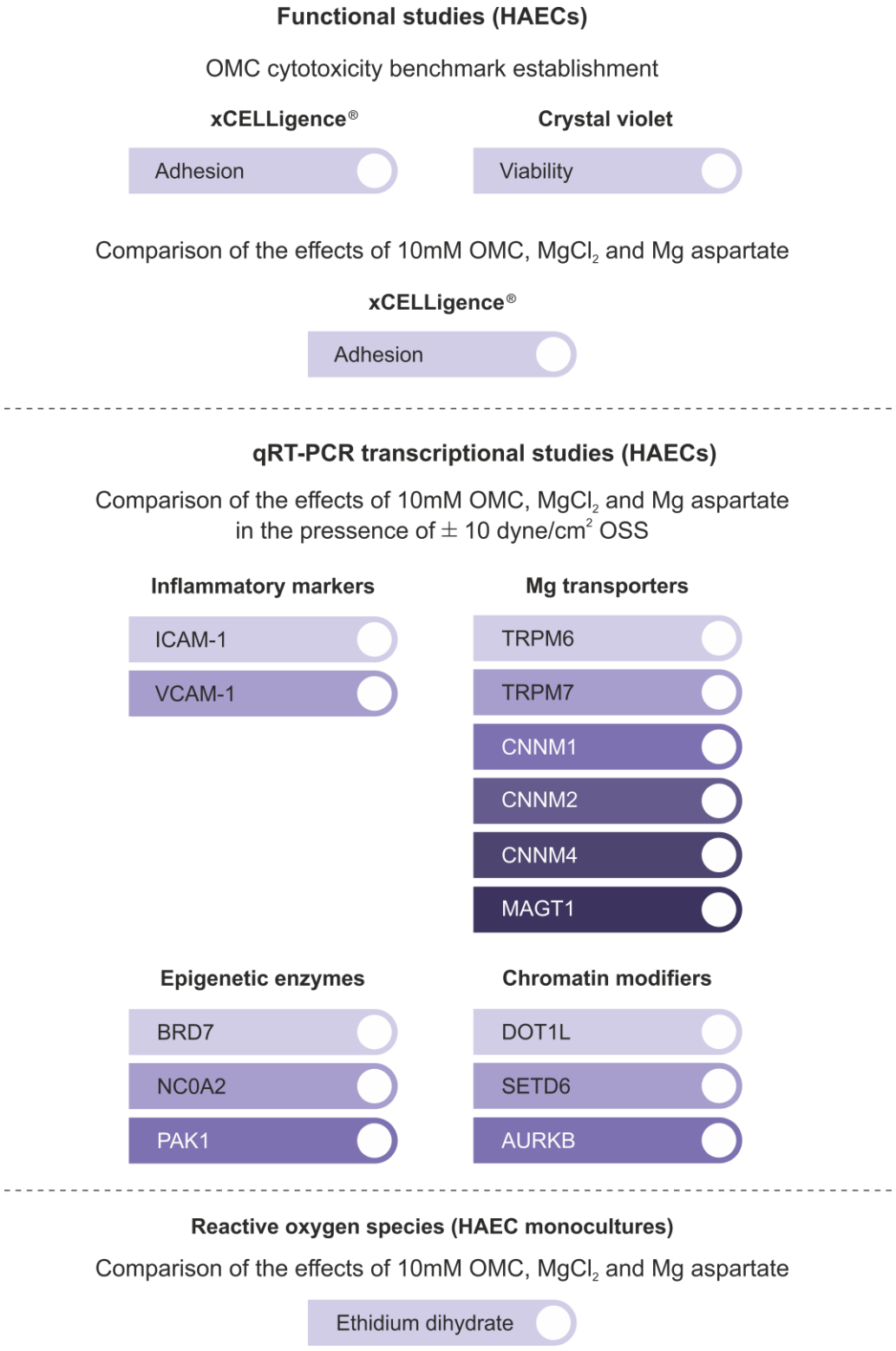

Figure 4.1 Diagram outlining the experimental approach taken in Chapter Four

4.2 Results

4.2.1 Cytotoxicity of OMC to HAECs

HAECs were seeded onto xCELLigence® E-plates® at a concentration of $3x10^4$ cells/well. Cells were then exposed to varying extracellular concentrations of OMC Mg for 24 h using the xCELLigence® real-time electrical impedance system to ascertain the optimum dosage at which HAECs exhibited improved adhesion profiles (Figure 4.2A). Cytotoxic concentrations could therefore be eliminated from future studies, and the optimum concentration for experimental purposes identified.

The system generated arbitrary impedance "Cell Index, (CI)" values based on cellular adherence in real time over 24 h, thereby generating a unique adhesion "profile" for cells incubated at each OMC concentration. 10mM OMC yielded the most efficient overall profile, with other concentrations yielding similar, albeit slightly less efficient adhesion profiles over the same time period. As CI values correlate with the extent of cell attachment, adhesion efficiency is defined as greater CI values over the initial period of attachment (initial few hours) in addition to higher CI values for any given timepoint thereafter.

10mM resulted in a CI value of 2.2 after 2 hours, whereas 5mM had a CI of 1.7 at the same timepoint. This trend continued for the duration of the experiment (10 h), at which time the 10mM concentration resulted in a CI of 3.8 compared to the 5mM equivalent of 2.6. Wells with no cells and wells with cells in Mg-free media served as experimental controls. These exhibited minimal CI values.

Analysis of slope data (Figure 4.2B) revealed the rate of adhesion/proliferation as a function of time between 1.75 h and 10 h (following initial settling of cells that would otherwise skew results). This represents a different measure of cell dynamics than the overall adhesion profile shown in Figure 4.2A. Data show that 10mM OMC yielded the significantly highest rate of adhesion/proliferation ($P \leq 0.001$) overall in comparison to the 0mM control. 10mM OMC also yielded a significantly ($P \leq 0.05$) higher rate of adhesion/proliferation than either 5mM or 20mM, the nearest concentrations tested.

4.2.2 Crystal violet viability study on HAECs exposed to varying concentrations of OMC Mg

HAECs were exposed to varying concentrations of OMC for timepoints of 0, 6, 12, 18 and 24 h in 96-well plates, before staining with crystal violet in order to ascertain cell viability.

Results indicated that 5 - 20mM OMC yielded higher levels of adhesion/viability of HAECs than those of higher concentrations (40mM and above) (Figure 4.3).

4.2.3 HAEC adhesion response to 10mM magnesium

HAECs were seeded onto xCELLigence® E-plates® at a concentration of $3x10^4$ cells/well. Cells were then exposed to a uniform concentration of 10mM Mg for 24 h from a variety of common sources (Mg aspartate, $MgCl_2$), in addition to OMC, and adhesion monitored using the xCELLigence® electrical impedance system. (Figure 4.4).

While all three Mg sources demonstrated a similar adhesion profile pattern, $MgCl_2$ resulted in the most efficient, with the greatest CI values overall. After only 1 hour, $MgCl_2$ had a CI value of 4.2. In contrast, OMC exposure resulted in a CI value of 2.8 at the same interval, making it the second-most efficient profile at that timepoint. This pattern continued for the duration of the exposure period. Wells with no cells and wells with cells in Mg-free media served as experimental controls. These exhibited minimal CI values.

Slope analysis of the interval following 1.75 h shows that all Mg types produced adhesion rates that were not significantly different from the Mg-free control. HAECs demonstrated significantly greater adhesion rates in response to $MgCl_2$ compared to OMC (see Figure 4.4B).

4.2.4 Down-regulation of inflammatory marker genes, ICAM-1 and VCAM-1, when exposed to 10mM Mg in a pro-inflammatory model

The anti-inflammatory effects of Mg on HAECs in the pro-inflammatory OSS model were ascertained by investigating expression of known HAEC inflammatory markers, ICAM-1 and V-CAM-1.

HAECs were exposed to oscillatory flow (±10 dyne/cm^2) for 48 h, whilst in the presence of 10mM magnesium (OMC, Mg aspartate or $MgCl_2$) prior to whole cell mRNA harvesting. Samples were subsequently analysed by qRT-PCR using primers specific for inflammatory marker genes, ICAM-1 and VCAM-1.

All three magnesium preparations significantly ($P \leq 0.05$) and comparably reduced expression of ICAM-1 under inflammatory oscillatory shear conditions. (Figure 4.5A). A similar observation was made with respect to VCAM-1, although the effect of OCM did not reach statistical significance. (Figure 4.5B).

4.2.5 HAEC Magnesium receptor response to 10mM magnesium after 48 h exposure to oscillatory shear stress

Magnesium transport receptors in HAECs were investigated in order to further elucidate the mechanism by which Mg uptake/absorption occurred, while under the influence of a known inflammatory stimulus, OSS.

HAECs were exposed to oscillatory flow (±10 dyne/cm^2) for 48 h, while in the presence of 10mM magnesium (OMC, Mg aspartate and $MgCl_2$) prior to whole cell mRNA harvesting. Samples were subsequently analysed by qRT-PCR using primers specific for a range of Mg receptors: TRPM6, TRPM7, CNNM1, CNNM2 and CNNM4, and MagT1. HAECs in Mg-free media were used as experimental controls in all instances.

Results showed contrasting effects of Mg to the inflammatory stimulus. TRPM7 exhibited significant ($P \leq 0.05$) down-regulation in response to 10mM Mg exposure (Figure 4.6A), while TRPM6 resulted in up-regulation due to the same stimulus (Figure 4.6B). CNNM1 resulted in statistically significant ($P \leq 0.05$) up-regulation due to Mg exposure (Figure 4.6C), while CNNM2 exhibited no significant difference

compared to controls (Figure 4.6D) and CNNM4 exhibited significant ($P \leq 0.05$) down-regulation in response to the same stimuli (Figure 4.6E). MagT1 exhibited no significant difference compared to controls (Figure 4.6F).

In all instances, there was no significant ($P \leq 0.05$) difference between the effects of the varying Mg sources.

4.2.6 HAEC epigenetic-associated gene response to 10mM magnesium after 48 h exposure to oscillatory shear stress

Data in Chapter Three demonstrated a clear epigenetic response to OSS in HAECs at 48 h, with subsequent analysis revealing a number of genes of interest. Of these, 6 were selected for further investigation. The expression of these genes in response to 10mM extracellular Mg was investigated.

Mg-starved HAECs were exposed to oscillatory flow (±10 dyne/cm^2) for 48 h, while in the presence of 10mM magnesium (OMC, Mg aspartate and $MgCl_2$) prior to whole cell mRNA harvesting. Samples were subsequently analysed by qRT-PCR using primers specific for each epigenetic-associated gene: AURKB, DOT1L and SETD6 (epigenetic enzymes) and BRD7, PAK1 and NCOA3 (chromatin modification factors). HAECs in Mg-free media were used as experimental controls in all instances.

Figures 4.7C and F show that NCOA3 and AURKB demonstrated no significant change in expression. Figures 4.7B, D and E show that DOTL1, SETD6 and PAK1 data demonstrated significant ($P \leq 0.05$) up-regulation. Only BRD7 expression was significantly down-regulated. Of each of these genes, no significant difference was observed between Mg sources, except for PAK1 expression, which although up-regulated in all instances, was not significantly up-regulated by exposure to OMC.

4.2.7 10mM Mg elicits no effect on ROS production in HAECs exposed to TNF-α for 12 h

HAECs were exposed to 0, 10 and 100 ng/mL TNF-α for 12 h, while in the presence of 10mM magnesium (OMC, Mg aspartate and $MgCl_2$). Samples were subsequently analysed by flow cytometry using DHE staining.

Figure 4.8 shows that while TNF-α did induce a dose-dependent inflammatory response in HAECs, no significant difference was observed between Mg types or the Mg-free control following exposure to either 0, 10 or 100 ng/mL TNF-α.

Figures:

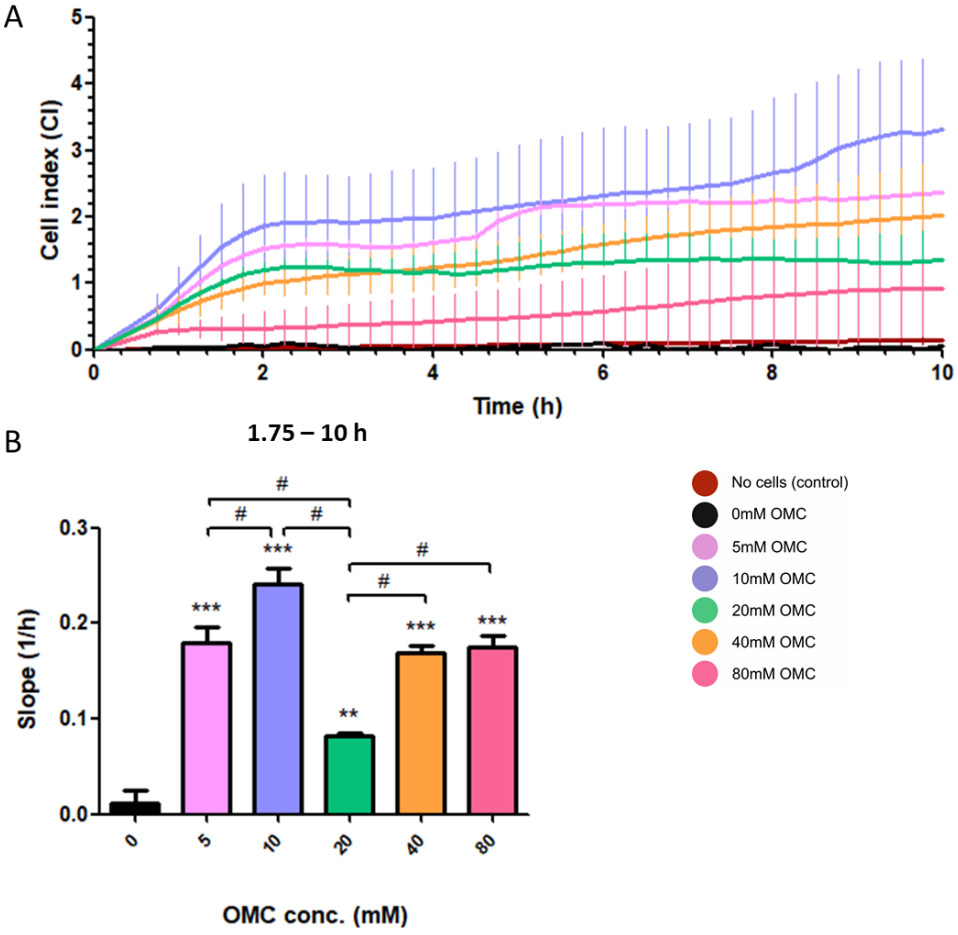

Figure 4.2 xCELLigence® adhesion profile of HAECs treated with varying concentrations of OMC Mg for 24 h
(A) Adhesion profile of HAECs treated with varying concentrations of OMC Mg for 24 h (first 10 h shown only, after which, CI values stabilised). Results are averaged from three independent experiments (n = 3 ± SD). (B) Rate of adhesion/proliferation of HAECs between 1.75 h and 10 h. Rate was determined by calculating the slope of the line between determined timepoints. Results are averaged from three independent experiments (n = 3 ± SD); ***P≤0.001 0mM OMC, **P≤0.025 0mM OMC. #P≤0.05.

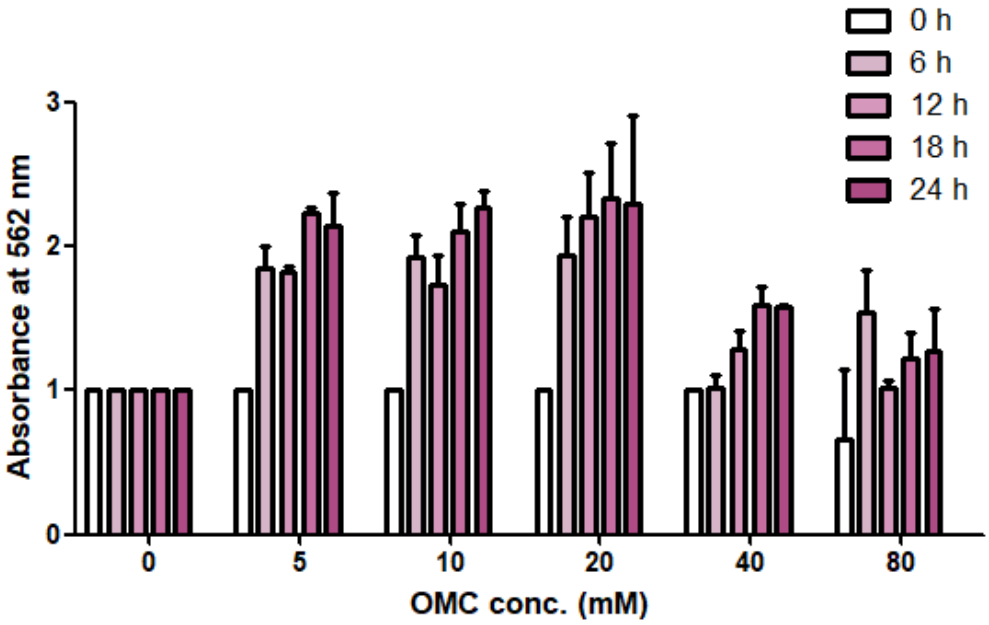

Figure 4.3 Crystal violet adhesion data for HAECs treated with varying concentrations of Mg (OMC only) for 24 h.
Static, quiescent, Mg-starved HAECs were exposed to varying concentrations of OMC for timepoints of 0, 6, 12, 18 and 24 h in 96-well plates, before staining with crystal violet in order to ascertain cell viability as a function of time and Mg concentration. Results are averaged from three independent experiments (n = 3) ± SD, the 0mM concentration is normalised to 1.0.

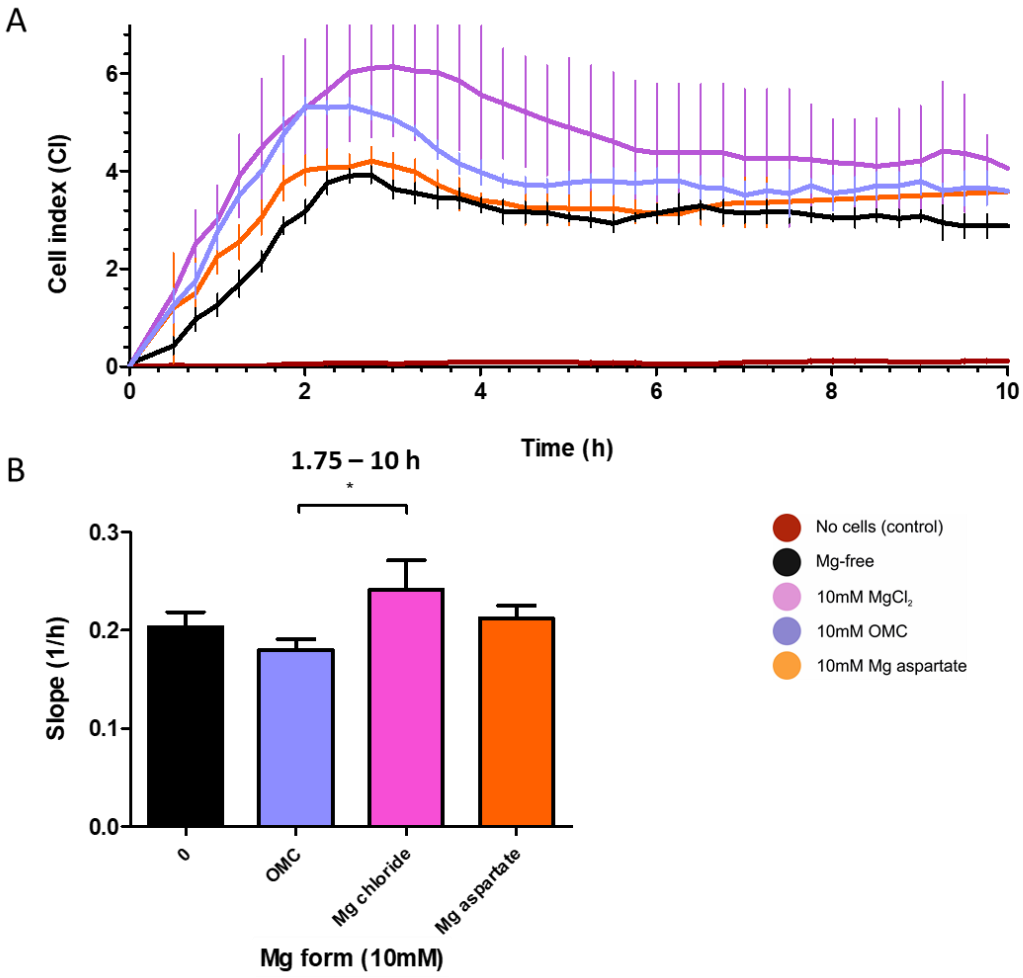

Figure 4.4 xCELLigence® adhesion profile of HAECs treated with different Mg sources (10mM) for 24 h. (first 10 h shown only)

xCELLigence® adhesion profile of HAECs treated with different Mg sources (10mM) for 24 h. (first 10 h shown only)

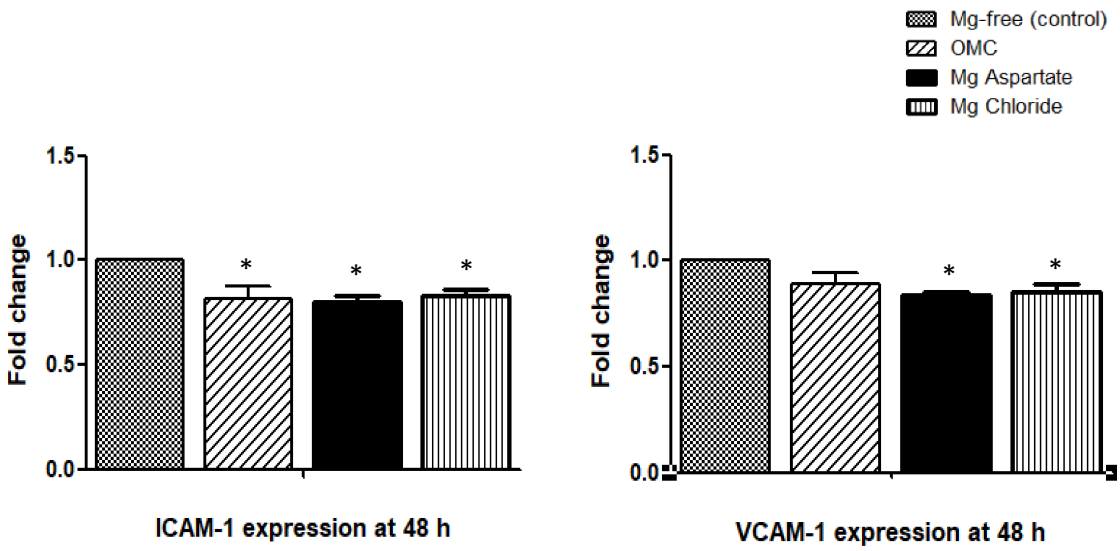

Figure 4.5 Downregulation of inflammatory marker genes, ICAM-1 and VCAM-1, exposed to 10mM Mg in a pro-inflammatory OSS model

HAECs were exposed to oscillatory flow (±10 dyne/cm^2) for 48 h, in the presence and absence of 10mM magnesium (OMC, Mg aspartate and $MgCl_2$) prior to whole cell mRNA harvesting. Samples were subsequently analysed by qRT-PCR using primers specific for inflammatory marker genes: (A) ICAM-1; (B) VCAM-1. Results are averaged from three independent experiments (n = 3) ± SD. *P≤0.05 vs untreated control.

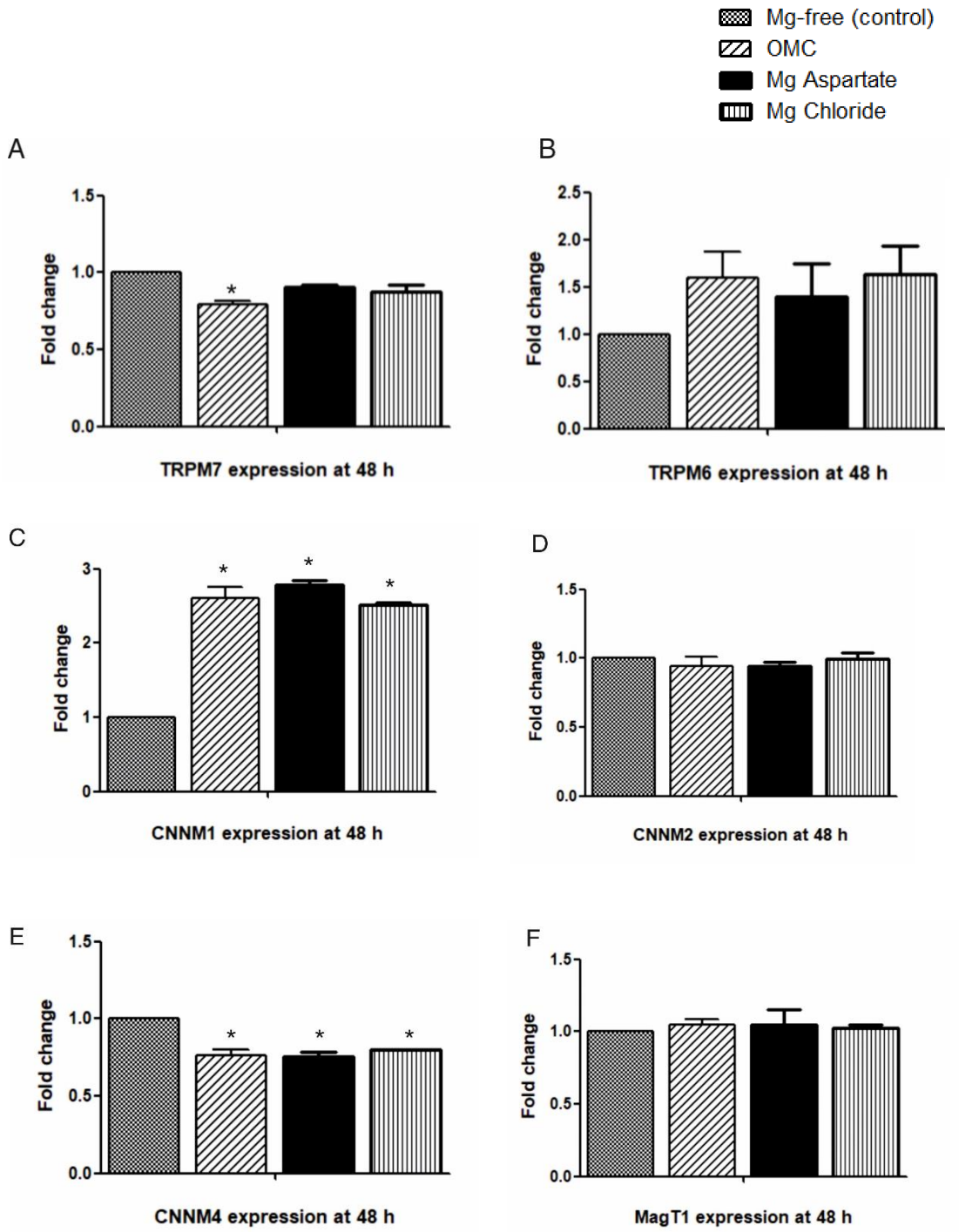

Figure 4.6 HAEC magnesium receptor response to 10mM magnesium in the presence of oscillatory shear stress after 48 h

HAECs were exposed to oscillatory flow (±10 dyne/cm^2) for 48 h, while in the presence of 10mM magnesium (OMC, Mg aspartate and $MgCl_2$) prior to whole cell mRNA harvesting. Samples were subsequently analysed by qRT-PCR using primers specific for each Mg receptor: (A) TRPM7 (B) TRPM6 (C) CNNM1 (D) CNNM2 (E) CNNM4 (F) MagT1. Results are averaged from three independent experiments (n = 3) ± SD. *P≤0.05 vs untreated control.

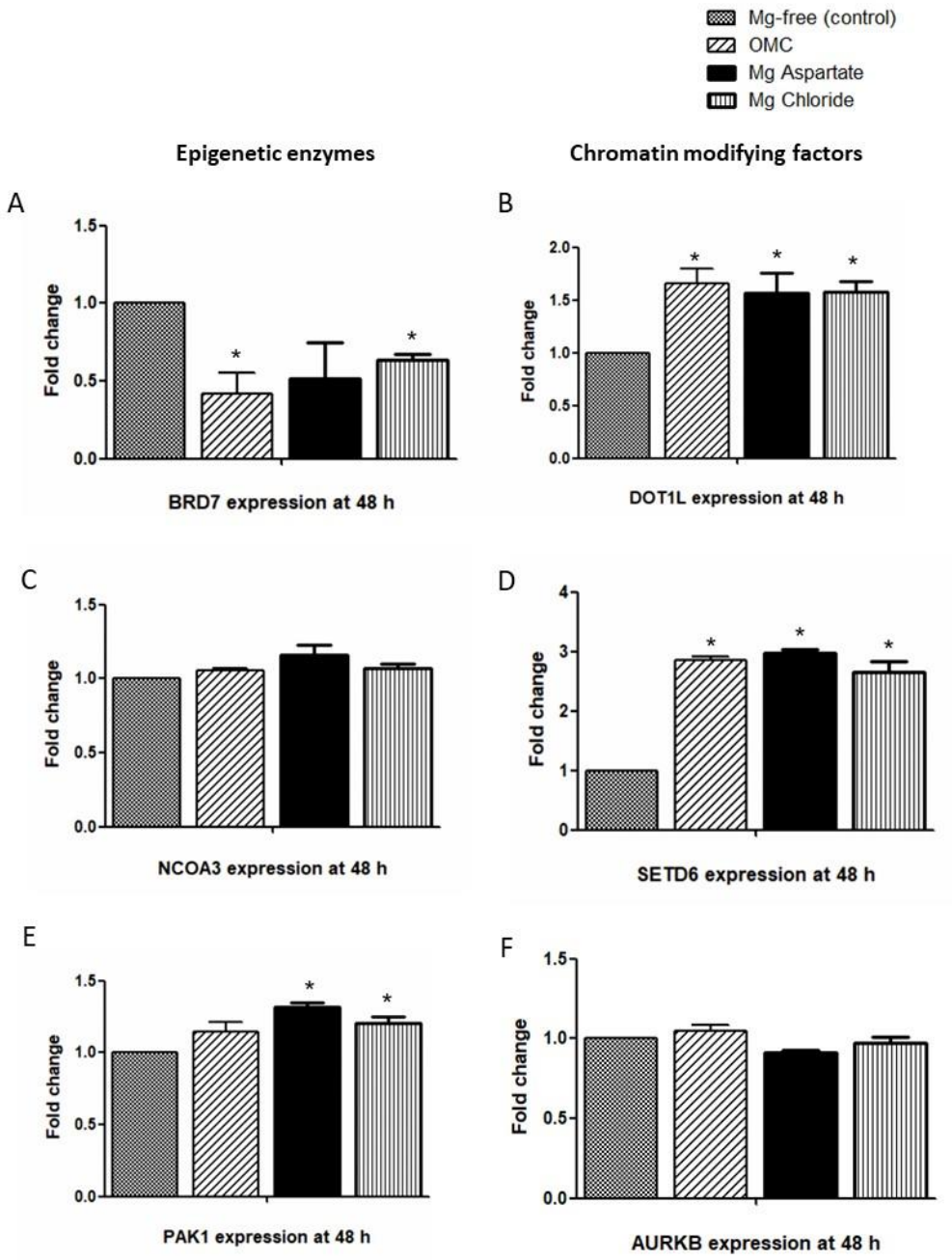

Figure 4.7 Effect of 10mM Mg on a range of putative gene targets (identified in Results Chapter Three) in the presence of oscillatory shear stress after 48 h
HAECs were exposed to oscillatory flow (±10 dyne/cm^2) for 48 h, while in the presence of 10mM magnesium (OMC, Mg aspartate and $MgCl_2$) prior to whole cell mRNA harvesting. Samples were subsequently analysed by qRT-PCR using primers specific for each gene: (A) BRD7 (B) DOT1L (C) NCOA3 (D) SETD6 (E) PAK1 (F) AURKB. Results are averaged from three independent experiments (n = 3) ± SD. *P≤0.05 vs untreated control.

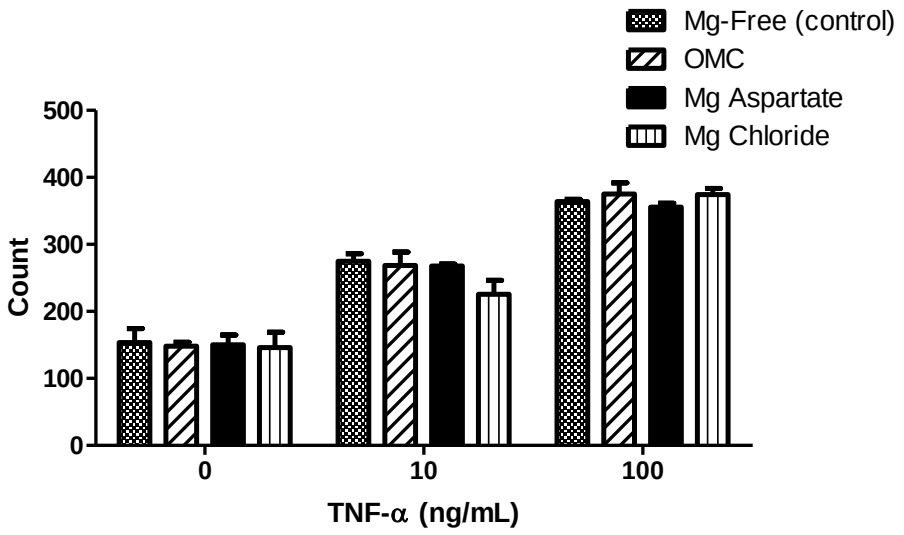

Figure 4.8 Effect of 10mM Mg on ROS production in HAECs exposed to TNF-α HAECs were exposed to 0, 10 and 100 ng/mL TNF-α for 12 h, while in the presence of 10mM magnesium (OMC, Mg aspartate and $MgCl_2$). Samples were subsequently analysed by flow cytometry using DHE staining. Results are averaged from three independent experiments (n = 3) ± SD.

4.3 Discussion

4.3.1 HAEC Adhesion response to Mg

The adaptive capabilities of vascular endothelium have previously been discussed at length. It is nevertheless important to stress that endothelial function has been significantly correlated to Mg levels in literature. Indeed, supplementation with Mg has been shown to increase endothelial function, in association with an exercise programme in patients with coronary artery disease and in diabetic individuals (Maier, 2012; S. Lee *et al.*, 2016). As such, the regulatory properties of Mg on cell adhesion were assessed.

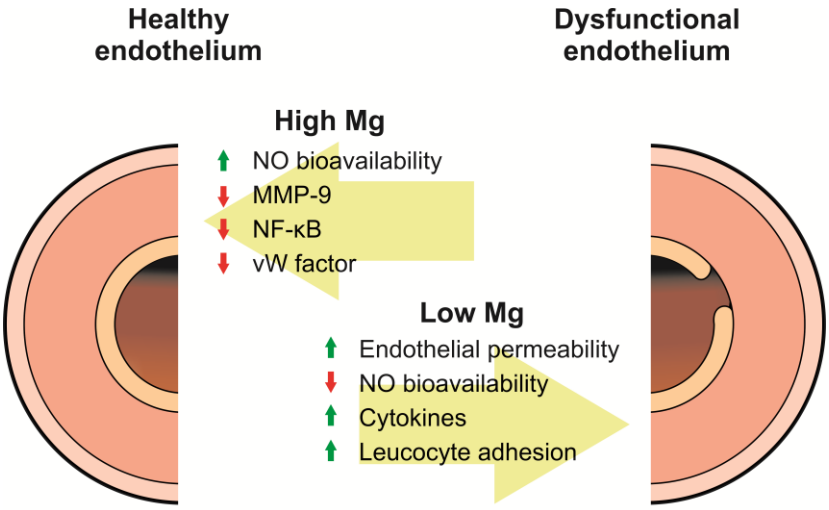

Figure 4.9 Magnesium contribution to endothelial dysfunction
(Adapted from Maier, 2012)

Although it has been stated that the physio-chemical properties of Mg, not its relative abundance, are what actually determine its effects (Wolf and Cittadini, 2003), dose remains a key factor governing the quantity absorbed, as Figure 4.9 illustrates. In healthy individuals, Mg serum concentration is closely maintained within a narrow physiological range (0.65–1.05 mM/L) (Jahnen-Dechent and Ketteler, 2012). In principle, relative Mg uptake is higher in dietary testing when ingested in multiple low doses throughout the day in contrast to a single, large dose (Schuchardt and Hahn, 2017). Such division was not possible within the setup of these experiments. Nevertheless, a strong correlation between dosage and adhesion profile of HAECs was observed. 10mM Mg (in the form of OMC) was shown to promote good cellular adhesion in HAECs, with a notable improvement after only one hour in comparison to other concentrations (Figure 4.1), as denoted by an increase in electrical impedance values. The 5mM concentration, while reduced, still yielded a positive profile. This was the lowest concentration tested, with 0mM used as a control. Here, the adhesion profile was greatly reduced, as anticipated. Low extracellular Mg levels have previously been found to result in retarded EC proliferation, while promoting the adoption of a senescent/pro-atherosclerotic phenotype (Maier, 2012). Intracellular Mg levels occur naturally at relatively high levels (Cowan, 1995). While the mechanical environment is an important regulator of endothelial cell adhesion, so too is the chemical environment, affecting integrin-matrix binding, adhesion strength, as well as influencing cell migration (Reinhart-King, 2008).

The semi-quantitative data of the xCELLigence® adhesion experiment showed good tolerance within the 20 - 40mM Mg range, in agreement with this and with Drynda *et al*. (2010) in SMCs. However, the apparent preferential response of HAECs to the 10mM concentration may be due in part to a delay in cells acquiring the intracellular levels at lower concentration doses, and may not be interpreted as a readout of long-term HAEC Mg requirement. Indeed, literature shows that increasing extracellular Mg^{2+} in SMCs may result in increased free Mg^{2+} intracellularly, but only after a period of 6 days (Touyz and Yao, 2003). Data for HAECs, published by Zhang *et al*. (1997), however, did show a more rapid uptake in this cell type. Nevertheless, the results of the adhesion experiment were relevant to the 48 h time period under investigation. The data presented in this chapter demonstrate a concentration-dependent response similar to that observed by Ma *et al*. (2016) in SMCs. Certainly adhesion data in these experiments draws some striking comparisons to the data reported in that study, with agreement between both data sets that 10mM promoted optimal adhesion.

In SMCs, Mg has been shown to increase DNA/protein synthesis, mediated by extracellular signal-regulated kinase (ERK)1/2-dependent signalling pathways (Touyz and Yao, 2003). While induction of cell cycle activation was also reported, substitution of nutrient medium for basal medium prior to the HAEC adhesion experiment resulted in senescence, and hence elimination of differences in cell cycle as a source of variability. Ergo, a similar Mg-induced mechanism may well be in operation in HAECs, inducing increased adhesion and cell spreading. HAECs, as adherent cells, are dependent on anchorage as a stimulus. The form of adherence to substrate is known to determine the mechanical balance of such cells (Teichmann *et al.*, 2012). While initial adhesion is passive, later stages involve active processes (actin polymerisation and mysosin contraction) that are essential for polarised cells to spread (McGrath, 2007). Data from the xCELLigence® experiments were obtained using a static culture of quiescent cells, hence up-regulation of adhesive pathways observed were not in receipt of external stimulus or enticement to polarise. Consequently, given the large number of ways in which Mg may affect enzymatic activity, it is therefore possible that such adhesion is mediated by metabolic processes involving ATP.

Analysis of corresponding slope data showed that HAECs responded to the presence of Mg broadly equally, within the context that all conditions demonstrated

significantly greater ($P \leq 0.001$) proliferation rates than the Mg-free control, and indicative that Mg is required for such cellular activity, as anticipated. Importantly however, 10mM OMC itself demonstrated a significantly greater ($P \leq 0.05$) rate of proliferation than either 5 or 20mM, the nearest concentrations to 10mM tested. Interestingly, 20mM OMC demonstrated the lowest rate among all those tested, with the exception of the Mg-free control. These data present an anomalous result, as concentrations on either side resulted in greater levels of proliferation. 20mM demonstrated a profile with standard deviations no greater than comparator concentrations, and relatively stable CI values beyond the 2 h point.

The crystal violet adhesion/viability assay essentially acted as a comparator for the xCELLigence® adhesion experiment against which, results could be validated. Both data sets were in broad agreement, lending confidence in the use of 10mM (the median concentration suggested by the crystal violet data, and the singular concentration suggested by the xCELLigence® data) as the benchmark concentration, against which, other forms of Mg should be compared. Literature cites numerous studies on the topic of Mg bioavailability (Firoz and Graber, 2001; Coudray *et al.*, 2005), and while there is some disagreement among researchers (due in part to a lack of standardised testing), a limited consensus that greater bioavailability of salts such as magnesium chloride and magnesium aspartate (Firoz and Graber, 2001; Ranade and Somberg, 2001) therefore led to their choice in these studies as worthy comparators against OMC. This choice was also based on the precedent of using Mg compounds as therapeutics in literature (Rochelson *et al.*, 2007).

Figure 4.3A clearly shows that Mg treatment (OMC, Mg aspartate and $MgCl_2$) yielded an increase in HAEC adhesion in comparison to controls (Mg-free media), as they each produced similarly positive adhesion profiles in HAECs. This supports the literature (Newhouse and Finstad, 2000) which state that Mg is an important co-factor in general, regardless of specific chemical structure when initially administered. The raised Mg-free profile in comparison to Figure 4.1A illustrates the necessity of the included controls on each E-plate® and a reminder of the variability of each experimental setup using this technique. Nevertheless, as a result of the included controls, notable differences were observed between each Mg source. $MgCl_2$ demonstrated the highest initial impedance values. This is an important timescale, as it eliminates the potential for cell proliferation to obscure results. Notably, OMC

yielded a similar, but less efficient profile, while Mg aspartate produced the lowest profile of the three sources tested. These data strongly suggest that Mg, as the largest principal component in OMC (appendix A) is responsible for the effects observed.

Analysis of adhesion rates for these experiments provided less valuable information in this case. During the 1.75 – 10 h interval, no statistically significant difference was observed between those HAECs treated with Mg and those which were cultured in Mg-free medium. While cells did exhibit different adhesion profiles, illustrated by increased CI values, the rates at which cells proliferated thereafter was statistically insignificant.

4.3.2 HAEC response to 10mM Mg in a simulated inflammatory environment

Chapter Three demonstrated that vascular inflammation can be triggered by controlling the biomechanical environment using the Ibidi® perfusion system to model inflammatory OSS. As such, the natural next step involving Mg was to investigate whether it could be used to reduce inflammation in this model. This was approached from a genetic perspective, initially investigating the effect of magnesium transporters in the system before expanding to determine the effect of Mg on a number of epigenetic genes identified in the previous chapter.

Figure 4.5 showed a significant ($P \leq 0.05$) down-regulation of both ICAM-1 and VCAM-1 genes in response to 10mM Mg treatment in the pro-inflammatory model. Both genes are known endothelial inflammatory markers, hence any significant reduction in their expression signals an anti-inflammatory effect. Moreover, these data serve to indicate that any effect observed in other genes under the same conditions are likely also anti-inflammatory. Low serum Mg^{2+} levels have been shown in literature to stimulate over-expression of VCAM-1 on the surface of ECs (Belin and He, 2007). High VCAM-1 (and ICAM-1) levels, in turn, assist leukocyte migration and may therefore be termed pro-atherosclerotic (Dragoni *et al.*, 2017). However, the observed reduction in VCAM-1 expression may not be solely attributed to restoration of acceptable intra-cellular Mg values.

4.3.3 Effect of 10mM Mg on HAEC magnesium receptors

Magnesium may influence the epigenetic processes discussed in this thesis in a number of ways. With optimal OMC Mg levels established, investigation continued by examining endothelial cell Mg transporter molecules and their individual response to 10mM Mg in the established model of damaging OSS.

Down-regulation of TRPM7 (Figure 4.6A) and the increased adherence of HAECs exposed to all sources of Mg fits broadly in line with data by Zeng *et al*. (2015), where TRPM7 silencing was found to promote cell adhesion, migration, wound healing, and tube formation in HUVECs. The authors speculated that this was due to increased phosphorylation of ERK and subsequent downstream increase in cell contractility and motility. This also ties with observed data in the xCELLigence® adhesion experiments, discussed previously, and literature discussing the likely involvement of Mg in the pathway. However, it should be noted that gene expression data were generated in a model mimicking oscillatory flow, a proven pro-inflammatory stimulus, against which, anti-inflammatory mechanisms could operate. In contrast, all adhesion data were generated in static models. Therefore, no direct accreditation to genetic data may be made. Paradoxically, a previous study reported that dysregulation of TRPM7 was associated with endothelial dysfunction in inherited hypomagnesemia (Paravicini *et al.*, 2009), though genetic mutations in the TRPM family not accounted for in that study have been found to elicit similar results (Chan *et al.*, 2015). Clearly TRPM7 may play an important role in regulating vascular competence, with specific levels of Mg critical to its operation. The 10mM concentration used in these experiments may represent a compromise between the competing reports.

TRPM6 is a close homologue to TRPM7 and the pair are capable of influencing each other's biological activity (Schmitz *et al.*, 2005; Zierler *et al.*, 2017). While Figure 4.6B did show up-regulation of TRPM6 in comparison to the Mg-free control, no statistical significance was observed. It is possible that exposure to Mg affected TRPM6 expression, perhaps through TRPM7 interaction, but not to significant levels. The additional 2.3mM Ca^{2+} present in OMC when normalised to 10mM was not controlled for, but this did not appear to impact expression levels compared to uniform Mg types.

The CNNM family serve to purge Mg^{2+} from cells, maintaining intra-cellular levels within acceptable parameters; with dysfunction responsible for inherited hypomagnesemia (Funato and Miki, 2018). In relation to inflammation, most publications report changes in CNNM2 expression. For example, Vishnolia *et al* (2018) report that CNNM2 knockdown is responsible for higher blood flow, increased arterial pulse and linear velocity. Based on literature, and given the experimental setup, this gene was anticipated to demonstrate some involvement. Surprisingly, experimental data show that CNNM2 did not exhibit any significant change (Figure 4.6D). Instead, both CNNM1 and CNNM4 exhibited opposing responses to the oscillatory stimulus; a response that evidently indicates some function related to vascular inflammation. CNNM4 was significantly down-regulated (Figure 4.6E). In contrast, CNNM1 showed significant up-regulation; this clear increase in expression is in stark contrast to other genes examined in this study. However, the role of CNNM1 with respect to vasculature is so far undocumented in literature. It is feasible that this could be evidence of a pathway through which Mg affects regulation of other genes within the parameters of these experiments, particularly due to its pronounced increase with respect to other genes examined. On the other hand, this may simply represent a snapshot of Mg transport response to influx of treatment, acting in concert with its homologues.

The high Mg selectivity possessed by MagT1 led to the expectation that it may exhibit some response to the stimuli. No significant response was observed, however. When taken together with inflammatory marker data that did exhibit changes in expression, it suggests that MagT1 is not involved in the reduction of inflammation in this model system. Together, these data demonstrate that 10mM Mg treatment of HAECs in an experimental setup that mimics a pro-atherosclerotic, pro-inflammatory system does stimulate up-regulation of a number of Mg receptor genes (TRPM7, CNNM1 and CNNM3). While such activity may be expected, the exclusion of Mg receptors MagT1, TRPM6 and CNNM2 demonstrates the involvement of more selective pathways through which the inferred anti-inflammatory effects occur.

4.3.4 HAEC Epigenetic gene response to 10mM Mg in a pro-inflammatory vascular endothelial model

The 6 epigenetic genes (3 epigenetic enzymes and 3 modification factors) chosen for investigation in this chapter were selected from the list of prospective targets generated by MirTarVis+ analysis in Chapter Three, and examined at the 48 h timepoint identified as the most dynamic in terms of gene expression change. While previously discussed in terms of inflammation and atherogenesis, the epigenetic genes discussed in this chapter will be examined from the point of view of their interaction with Mg.

4.3.4.1 Effect of 10mM Mg on epigenetic enzymes (SETD6, AURKB and DOT1L) in a pro-inflammatory vascular endothelial model

Magnesium influences enzyme activity by (i) binding to ligands such as ATP in ATP-requiring enzymes, (ii) binding to the active site of the enzyme, (iii) causing a conformational change during the catalytic process, (iv) promoting the aggregation of multi-enzyme complexes or (v) a mixture of the above mechanisms. (Swaminathan, 2003). Given the extent to which Mg may impact on enzymatic activity, it is no surprise that Mg treatment affected many of the epigenetic enzymes under investigation in this chapter.

The methyltransferase, SET domain containing 6 (SETD6), has been shown to be involved in the Wnt signalling pathway, as well as a negative regulator of the oxidative stress response (Chen *et al*. 2016). SETD6 achieves this by mono-methylating the RelA subunit of NF-κB (Chang *et al.*, 2011). Rochelson *et al*., (2007) demonstrated the use of Mg sulphate to similarly reduce inflammation through the NF-κB pathway. The significant up-regulation of SETD6 across all three Mg comparators is therefore of extreme interest. NF-κB has strong links with hypomagnesemia, with low levels shown to result in development of a pro-atherogenic phenotype (Ferre *et al.*, 2010). While this has not been attributed to SETD6 involvement in literature, data in this chapter show that Mg treatment clearly induces an epigenetically-controlled anti-inflammatory response through the action of this methyltransferase.

In order to determine if 10mM Mg could indeed attenuate oxidative stress in this manner, static HAEC monocultures were exposed to various concentrations of the

inflammatory cytokine, TNF-α, in order to induce an inflammatory response. Data clearly indicate that co-treatment with Mg for 12 h did not elicit any observable response in the reduction of ROS. While this represents a conclusive result, it does not, however, rule out the possibility that Mg could elicit its anti-inflammatory effect through SETD6 by other means.

Another of the epigenetic enzymes identified in the previous chapter was AURKB, a serine/threonine-protein kinase. The fact that 10mM Mg treatment did not result in any significant change in gene expression in this gene suggests that although it may play a role in HAEC inflammatory response to OSS, this role is unaffected by Mg.

DOT1L was shown to be up-regulated in response to 10 dyne/cm^2 OSS in Chapter Three. Treatment with 10mM Mg resulted in significantly-increased ($P \leq 0.05$) expression of DOT1L following 48 h exposure to an OSS environment. This confirmed DOT1L as an epigenetic enzyme of interest, with methyltransferase activity again occurring in response to that stimulus in repeated experiments. Moreover, it infers that this activity was elevated by Mg treatment. While its role in embryonic development is well explored, no literature has been found that surveyed the Mg aspect of DOT1L function. Nevertheless, Figure 4.7B showed a clear link between Mg treatment at 10mM and up-regulation of the methyltransferase gene. DOT1L is an angiogenic promoter through the vascular endothelial growth factor (VEGF) signalling pathway (Wong *et al.*, 2015). There is evidence to show VEGF/Mg interaction; Hong *et al*., (2006) describe a mechanism where VEGF releases intracellular Mg from intracellular stores, but no data on extracellular uptake. Deficiency of DOT1L has been shown to inhibit cell proliferation (Kim *et al.*, 2012). Ergo, the response observed in these data may be representative of proliferating HAECs compensating for the pro-inflammatory environment. It is therefore likely that up-regulation of DOT1L is an undesirable effect of Mg treatment.

4.3.4.2 Effect of 10mM Mg on epigenetic modification factors (PAK1, NCOA3 & BRD7) in a pro-inflammatory vascular endothelial model

Progression towards an inflammatory phenotype occurs via numerous pathways, including activation of NF-κB, a mechanism known to be influenced by Mg (Maier, 2012). Bromodomain-containing protein 7 (BRD7) functions as both co-activator and

as co-repressor, and is speculated to play a role in chromatin re-modelling (Kaeser *et al.*, 2008). BRD7 is a transcriptional co-repressor that down-regulates expression of target genes, achieved by binding to target promoters, leading to increased histone H3 acetylation at 'Lys-9' (H3K9ac). Literature describes in detail BRD7 interaction with tumour suppressors, p53 and p300, and recruitment to target gene promoters, influencing acetylation of histones and p53, as well as affecting promoter activity. BRD7 has been postulated to serve as a p53 co-factor (Drost *et al.*, 2010). P53 has a direct link with atherosclerosis, where it has been shown to regulate growth arrest, cell senescence and apoptosis of VSMCs in murine models (Mercer and Bennett, 2006). With specific regard to endothelial dysfunction, p53 has been shown to lead to inflammatory gene expression and impairment of endothelium-dependent vasodilatation (Kumar *et al.*, 2011). Hence, the observed down-regulation of BRD7 demonstrates a clear anti-inflammatory pathway.

As with AURKB, discussed previously, NCOA3, a sensitive nuclear receptor, did not result in any significant change in gene expression, suggesting that although it may play a role in HAEC inflammatory response to oscillatory shear stress, this role is unaffected by Mg.

In contrast, PAK1 expression was demonstrated to be significantly up-regulated ($P \leq 0.05$) after 48 h, due to $MgCl_2$ and Mg aspartate exposure (but not OMC exposure), clearly demonstrating a response in line with the type of primary and secondary adhesion ligand anchorage-reliant mechanisms required in a turbulent flow environment and confirmation of the array data previously obtained for this gene. While this has already been examined in Chapter Three, its increased up-regulation in response to Mg treatment prompts further discussion. PAK1 over-expression and activation may be a key co-ordinator of aberrant cell survival, with relevance to atherogenesis, as has been shown in some cancer studies (Li *et al.*, 2008). Figure 4.8 (below) shows that the PAK1 protein interacts with numerous others. In this case, up-regulation may occur through its interaction with Rac1 [via its CRIB domain, followed by auto-phosphorylation on T423 in its kinase domain (Li *et al.*, 2008)]. The super-family have been shown to regulate many aspects of intra-cellular cytoskeletal dynamics, including actin, microtubule and microfilament organisation, and are controlled by their guanine nucleotide binding states in cells (Zhang *et al.*, 2000; Tan *et al.*, 2008; Ng *et al.*, 2010).

Mg has been reported to affect actin polymerisation by altering steps associated with actin attachment and detachment. This is proposed to be due to Mg^{2+} exchange in the active site, although it remains unclear how it impacts attachment. Swenson *et al*., (2014) further state that changes in Mg or ADP concentrations shift the MgADP:ADP ratio resulting in an impact on myosin motor activity that is limited by the ADP release rate constant (e.g. contractile speed and/or intracellular transport). This again suggests a metabolic pathway/effect, and may compliment the enzymatic activity discussed previously.

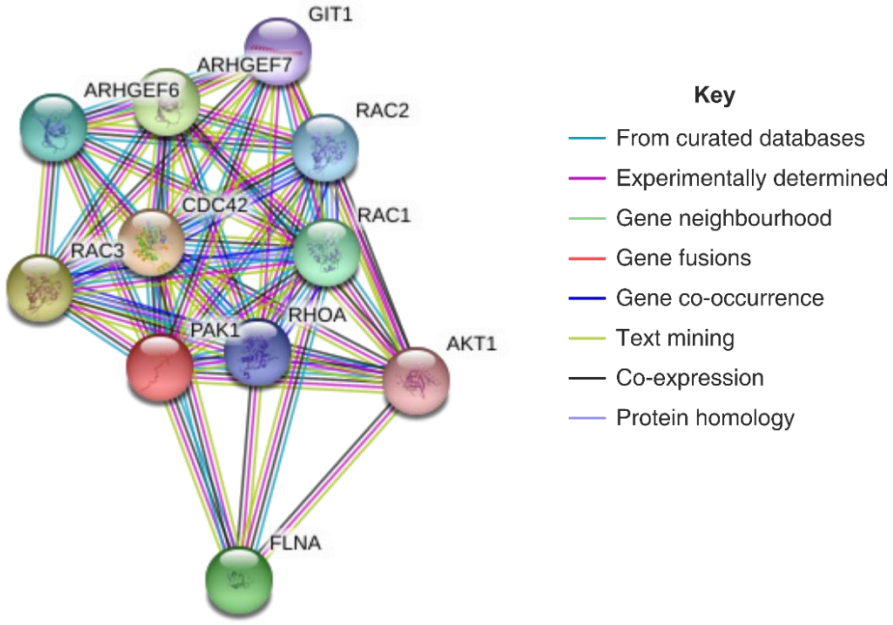

Figure 4.10 Node diagram illustrating PAK1 interactions with other proteins, including members of the Rac and Rho family
(STRING database, v11.0)

While increased numbers of PAK1 mRNA transcripts may be a reflection of the cell's activity within the inflammatory environment, raised Mg levels may serve to positively reinforce this gene activity further. Although the gene was shown to exhibit increased expression due to all sources of Mg, the fact that OMC did not induce significant change may be of some relevance. Of those examined in this study, this was the only gene to be affected differently by OMC. Here, structural differences in Mg types and their relative bioavailability within the monoculture environment may play a role: OMC is proposed to contain free ionised Mg, among other constituents

listed in Appendix A. The fact that it exists as a mixture would call into question its relative chemical stability; another reason to use Mg compounds as comparators. Nevertheless, free ionised Mg comprises only 0.5 – 5% total cellular Mg. The remaining fraction is bound to anionic compounds, including ATP, ADP, citrate, proteins, RNA and DNA, or is sequestered within mitochondria and endoplasmic reticulum (Swaminathan, 2003). In addition, the fact that such differences were not detected in other genes, raises the possibility of the action of other trace elements within OMC specifically on this pathway.

Epigenetic modifications play an important role in regulating gene expression in a number of inflammatory and anti-inflammatory processes within the vascular system. Data examined in this chapter show that a number of these epigenetically-driven processes are affected by the application of Mg, within the context of a pro-inflammatory model. A number of these processes may therefore be interpreted as anti-inflammatory. Their consequent interaction with the miRNA identified in Chapter Three, may further elucidate this role.

4.4 Summary

Mg bioavailability varies depending on dosage, preparation and the presence of enhancing/inhibiting factors (Schuchardt and Hahn, 2017). The complex nature of OMC therefore obfuscates the results observed in this chapter. Nevertheless, the fact that xCELLigence® data and gene expression results are largely consistent across the different Mg forms strongly points to Mg as the principle active substance in seawater-derived OMC, as opposed to the numerous other trace elements contained within the mineral complex.

In this regard, observed anti-inflammatory effects and adhesion data, coupled with those data on epigenetic genes, together point to Mg as a playing an important role in epigenetically-regulated CVD, so far unexplored in literature. Data demonstrate that 10mM Mg treatment of HAECs in an experimental setup that mimics a pro-atherosclerotic, pro-inflammatory system does stimulate up-regulation of a number of Mg receptor genes (TRPM7, CNNM1 and CNNM3). While such activity may be expected, the exclusion of Mg receptors MagT1, TRPM6 and CNNM2 demonstrates the involvement of more selective pathways through which the inferred anti-

inflammatory effects occur. The links between Mg-controlled TRPM7 up-regulation, its involvement in the ERK/MAPK pathway and HAEC adhesion data represent a credible mechanism, through which, endothelial dysfunction may operate. At minimum, it presents a scenario for further investigation.

More work is required to elucidate the effects of DOT1L and other epigenetic genes. Mg may exhibit an inferred effect on chromatin re-modelling through PAK1, and other epigenetic regulators, and it is reasonable to conclude that further investigation would allow for a clearer interpretation, particularly in association with miRNA data from Chapter Three.

It is obvious that the effect of magnesium treatment as it has been explored in these experiments may result in effects, some of which, may be undesirable/unintended. It is clear that raised Mg levels have complex effects on HAECs – Observed anti-inflammatory effects and adhesion data, coupled with indications that metabolic mechanisms may underpin these effects suggest that Mg may present possible agent through which wound healing and angiogenesis may occur. These effects in a larger, more complex system will be explored in Chapter Five.

Chapter Five

The effect of 10mM magnesium treatment on an *in vitro* multicellular skin burn model

5.1 Introduction

Chapter Four examined the effects of 10mM Mg treatment on a model of vascular injury, imparted specifically through OSS. It was clear that raised Mg levels resulted in complex effects on HAECs. Observed anti-inflammatory effects and adhesion data, coupled with indications that metabolic mechanisms may underpin these effects, suggested that Mg may present a possible agent through which wound healing and angiogenesis may occur. To this end, this chapter will explore these effects using a skin burn model: an alternative, but equally relevant model of injury that incorporates the vascular cell component. As a result, multiple cell types will be investigated in order to ascertain their response to Mg treatment in both monoculture and co-culture environments. These will comprise Normal Human Dermal Fibroblast cells (NHDFCs) and Human Adult Dermal Keratinocyte cells (HAKCs), and their influence on vasculature function will be investigated through transcriptional changes.

It has long been known that Mg levels at the site of dermal wounds are elevated in comparison to serum levels (Grzesiak and Pierschbacher, 1995). The skin's primary function is to protect the body from exogenous environmental influences. It is comprised of two major layers – the epidermis and dermis, with each further divided into morphologically-distinct sub-layers. The stratum corneum (corneocytes surrounded by lipid regions) acts as the main barrier, and comprises the outermost layer of epidermis. Keratinocyte cells originate in the stratum basale and transition up through the layers of the epidermis. Blood vessels are located immediately below this in the dermis. Hence, for the absorption of trans-dermal Mg under normal circumstances, it must first permeate the stratum corneum. Once this is achieved, Mg may then be transported in circulation.

Experiments in this chapter will focus on wound healing, the complex cellular and biochemical process without which, the restoration of structurally damaged tissue would not be possible. Burn injuries may penetrate dermal sub-layers and result in an inflammatory response that involves underlying blood vessels. Burn damage causes the death of skin cells, leading to loss of body fluids followed by dehydration, electrolyte imbalance, and renal and circulatory failure (Shpichka *et al.*, 2019). Wound healing comprises a dynamic set of interactions between numerous cell types, ECM, mediators and cytokines. Skin cells migrate from the wound margin into the

wound to restore skin integrity. This is primarily achieved by fibroblasts, with support from keratinocytes.

In first-aid treatments, dressings are typically used to facilitate repair/regeneration of damaged tissue. These form a physical barrier between the damage site and external environment. Hydrogels are an example of active dressings that have been used as therapeutic delivery mechanisms for cutaneous wound healing and burn treatment. A partnership with a hydrogel manufacturer led to the inclusion of OMC as a possible therapeutic agent for investigation. While the concentration of OMC was undisclosed, the experimental design presented an opportunity to gain further insight into the performance of OMC. **As such, the hypothesis that Mg may be of benefit as an anti-inflammatory/therapeutic agent in a multicellular model of inflammation/injury was investigated.** To this end, an *in vitro* skin burn model will be developed, through which, an OMC-infused hydrogel therapeutic will be tested for possible anti-inflammatory/stimulatory gene expression. Skin cell monocultures (NHDFCs and HAKCs) will be assessed in conjunction with HAECs in order to ascertain the functional effect of Mg on migration/wound healing and angiogenesis (specifically tube formation). As both adhesion and migration share common mechanisms, 10mM OMC Mg was chosen as a satisfactory concentration to continue these investigations.

Study aims

In this chapter, the possible anti-inflammatory/stimulatory effects of Mg on induced thermal burns on an *in vitro* 3D skin model were investigated (see Figure 5.1). Hence, the overall aims of this chapter include:

- To develop an *in vitro* skin burn model, through which, an OMC-infused hydrogel therapeutic will be tested for wound healing gene expression using qRT-PCR arrays.
- To assess an OMC-infused hydrogel therapeutic for fibrotic gene expression using qRT-PCR arrays on the *in vitro* skin burn model.

- To investigate the effects of 10mM Mg (OMC, $MgCl_2$ and Mg aspartate) on cell migration in cell types representative of dermal tissue (NHDFCs, HAKCs and HAECs).
- To assess the effect of 10mM Mg (OMC, $MgCl_2$ and Mg aspartate) on HAEC tube formation.

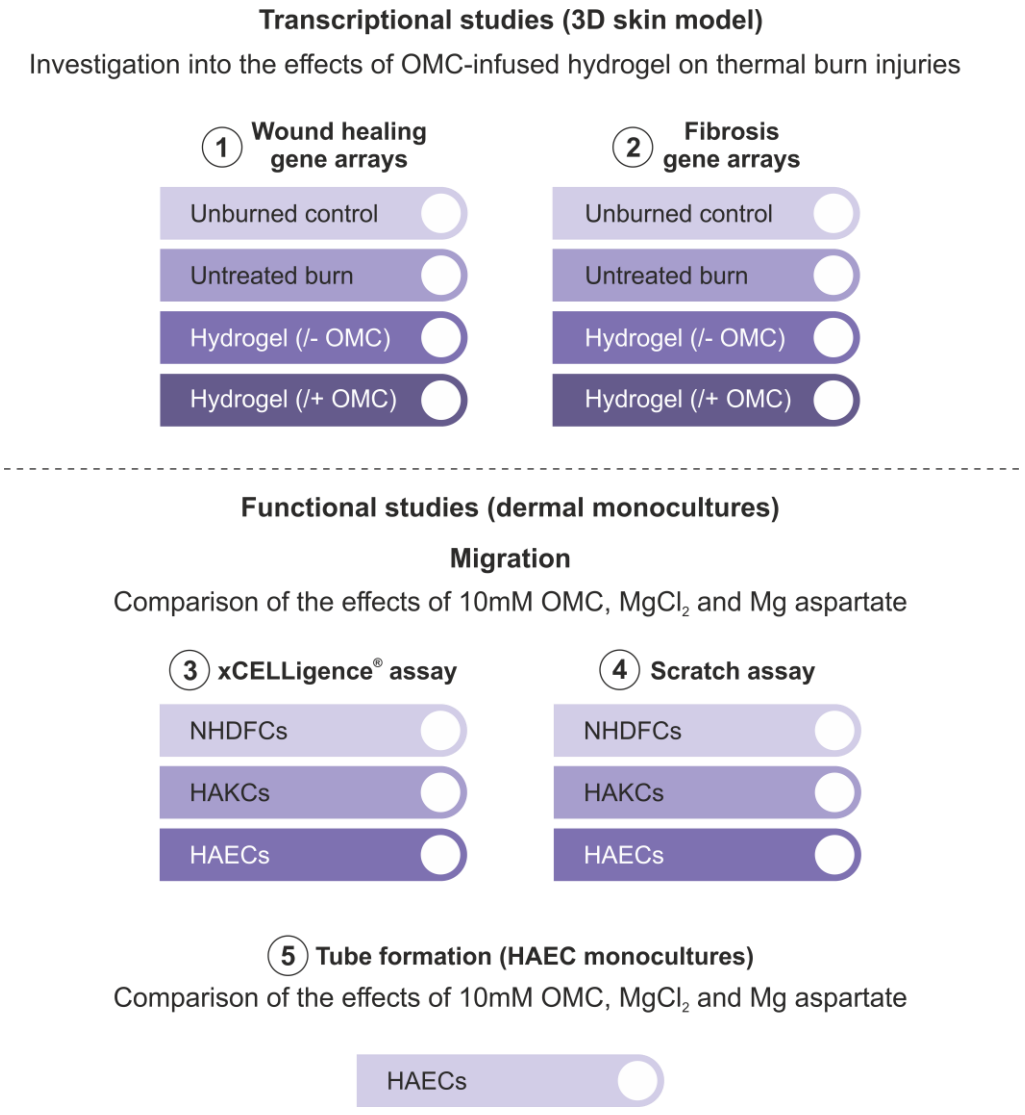

Figure 5.1 Diagram outlining the experimental approach taken in this chapter

5.2 Results

Three-dimensional cell culture models (LabSkin™) were purchased from Innovenn Ltd, UK. These consisted of dermal fibroblast and keratinocyte cells suspended within a fibrin matrix. *In vitro* burn insults were applied to 3D models using a modified animal model protocol by Cai *et al.*, (2014) using custom-milled 3.66g brass weights heated to 100°C. Immediately following the burn insult, weights were removed and the appropriate treatment was topically applied. Each treatment consisted of custom-fitted 2.5 cm gauze disks soaked in the appropriate treatment (hydrogel /- OMC, or hydrogel /+ OMC), and compared to non-treated and healthy controls. Models were returned to the incubator for 24 h, after which time, they were sampled for subsequent analysis.

RNA from 3 mm Labskin™ sample biopsies was subsequently harvested using the TRIzol® isolation method as described in section 2.2.4.2. Genetic material was investigated using RT^2 arrays (Qiagen) containing primers for wound-healing genes (see Appendix A for complete gene list).

Results for each condition are as follows:

5.2.1 The Effect of Control (unburned) v Burn (untreated) on wound healing mRNA expression in 3D skin model, 24 h post-burn (n = 3)

Figure 5.2A shows that in total, 21 genes were up-regulated (2.02 to 25.47-fold) in response to the 10 second burn insult, while 11 genes were down-regulated (2.11 to 18.99-fold) in response to the same stimulus within a >2-fold limit (see Table 5.1).

The top 3 up-regulated genes were IL6 (25.47-fold), CSF5 (23.21-fold) and CXCL5 (16.91-fold). Up-regulated genes included a number of inflammatory markers and MMPs. In contrast, the majority of down-regulated genes related to collagen/ECM-producing genes (COL3A1, COL5A3) and integrins (ITGA2, ITGB6, ITGA6 and ITGA3).

5.2.2 The Effect of Control (untreated burn) v Burn (hydrogel /- OMC) on wound healing mRNA expression in 3D skin model, 24 h post-burn (n = 3)

In total, 14 genes demonstrated up-regulation within a >2-fold limit, whilst 9 genes were down-regulated in response to hydrogel (/- OMC) treatment compared to an untreated burn control (see Figure 5.2B). Up-regulated genes included a number of inflammatory cytokines (TNF, IL6) in addition to collagen-producing gene COL5A1 and Integrin ITGB3. Down-regulated genes included a number of MMPs and integrins ITGB6 and ITGA6 (see Table 5.2).

5.2.3 The Effect of Control (untreated burn) v Burn (hydrogel /+ OMC) on wound healing mRNA expression in 3D skin model, 24 h post-burn (n = 3)

Figure 5.2C shows that in total, 17 genes were up-regulated within a >2-fold limit in response to hydrogel (/+ OMC) treatment in comparison to an untreated burn control. Table 5.3 shows that these included the anti-inflammatory cytokine, IL10, a number of ECM-producing genes (COL5A3, COL4A1, COL1A1, COL3A1, COL5A1) in addition to inflammatory marker, IL2. 10 genes were down-regulated, consisting of integrins, MMPs and the pro-angiogenic gene, VEGFA.

5.2.4 The Effect of Control (hydrogel /- OMC) v Burn (hydrogel /+ OMC) on wound healing mRNA expression in 3D skin model: 24 h post-burn (n = 3)

Figure 5.2D shows that when comparing hydrogel (/+ OMC) to hydrogel (/- OMC) as a treatment on the same 10-second burn insult, 11 genes were up-regulated in response to the inclusion of OMC. COLA1, COL4A1, COL3A1 and the pro-angiogeneic ANGPT1 gene were significantly up-regulated. Table 5.4 shows 10 genes were down-regulated, including VEGFA and a number of inflammatory markers (TNF, IL1B, IL6).

Genetic material was also investigated using RT^2 arrays (Qiagen) containing primers for fibrosis-associated genes (see Appendix A for complete gene list). Results for each condition are as follows:

5.2.5 The Effect of Control (unburned) v Burn (untreated) on fibrotic mRNA expression in 3D skin model, 24 h post-burn (n = 3)

Figure 5.3A indicates that in total, 19 genes were found to be up-regulated within the >2-fold transcriptional change limit when comparing the untreated burn to the unburned control. These included a number of markers of inflammation (IL3RA2, IL4, TNF) and MMPS (MMP1, MMP3, MMP8) 8 down-regulated genes were observed, and included COL3A1, integrins ITGA2, ITGA2 and ITGB6, as well as PDGFA (see Table 5.5).

5.2.6 The Effect of Control (untreated burn) v Burn (hydrogel /- OMC) on wound healing mRNA expression in 3D skin model, 24 h post-burn (n = 3)

10 genes within the >2-fold limit were up-regulated in response to hydrogel (/- OMC) treatment when compared to the untreated control (see Figure 5.3B). These included TNF, MMP1 and MMP13 and well as TGFB3. 8 genes were down-regulated, which included MMPs and interleukins (see Table 5.6).

5.2.7 The Effect of Control (untreated burn) v Burn (hydrogel /+ OMC) on wound healing mRNA expression in 3D skin model, 24 h post-burn (n = 3)

In response to hydrogel (/+ OMC) treatment, 12 genes exhibited up-regulation within the >2-fold limit in comparison to the untreated control (see Figure 5.3C). These included ITGB3, COL3A1, ENG and PDGFA. In response to the same stimulus, 10 genes demonstrated down-regulation. These included a number of integrins, interleukins and VEGFA (see Table 5.7).

5.2.8 The Effect of Control (hydrogel /- OMC) v Burn (hydrogel /+ OMC) on wound healing mRNA expression in 3D skin model: 24 h post-burn (n = 3)

When comparing hydrogel (/+ OMC) to hydrogel (/- OMC) as a treatment on the same 10-second burn insult, Figure 5.3D indicates that 5 genes were up-regulated (ITGB6,

CXCR4, IL10, COL3A1 and CCR2). 9 genes were down-regulated in response to the same stimulus, and included a number of interleukins, MMP13 and TNF (see Table 5.8).

While gene array data permitted an over-arching view of processes likely to occur in human skin as a result of treatment that included OMC, monoculture experiments facilitated an in-depth view of functional processes within that model related to specific cell types. Hence, dermal cells (NHDFCs, HAKCs and HAECs) were examined individually for their migratory response to 10mM Mg. To this end, two complimentary assays were employed: the electrical impedance-based xCELLigence® migration protocol, and the more traditional scratch assay. The xCELLigence® approach encompassed a 3D element that more closely resembled the *in vivo* paradigm. In contrast, the scratch assay inflicted physical damage to cells and striped ECM from the monolayer. Combining data from both allowed a clearer picture of the effect of Mg treatment to emerge. Following this, Mg was further examined for its potential pro-angiogenic properties in HAECs.

5.2.9 The effect of 10mM Mg on HAEC migration

Serum and Mg-starved HAECs were seeded onto xCELLigence® CIM-plates® at a concentration of $3x10^4$ cells/well with full-serum media used as a chemoattractant in the bottom of each well. Cells were then exposed to a uniform concentration of 10mM Mg for 24 h in a variety of common forms (Mg aspartate, $MgCl_2$), in addition to the OMC form, and migration monitored using the xCELLigence® electrical impedance system. (Figure 5.4A).

All three Mg forms clearly diverged from the profile generated by the Mg-free control for the full duration of the experiment. $MgCl_2$ generated the most efficient migration profile (greater CI values for any given timepoint) than either OMC or Mg aspartate.

Slope data is used to describe the steepness or changing rate of a curve within a given timeframe. Such data strip away the more complex profile, and enable a clearer view of how cells perform as a result of each stimulus at specific points during the assay, in this case, 45 min. – 4 h. This early timeframe discounts initial setup, which may result

in inaccurate readings, and gives insight into the migratory response of cells during the first few hours of the assay.

Figure 5.4B revealed that $MgCl_2$, OMC and Mg aspartate all performed significantly ($P \leq 0.05$) better than the Mg-free control.

5.2.10 The effect of 10mM Mg on wound closure in HAECs

Confluent monolayers of HAECs were individually scratched with sterile 200 μL pipette tips using firm, even pressure. Cells were washed with warm PBS, removing damaged cells and debris, before adding the treated medium (10mM OMC, $MgCl_2$ or Mg aspartate). A Leica DM500 microscope with ICC50 camera module was used to capture 40X images at 6 h regular intervals during wound closure, with Image J software (National Institutes for Health, USA) software and the MRI Wound Healing Tool.ijm macro plugin subsequently used to quantify the rate by measuring tube length. Measurements were reported in pixels, and results quantified as percentage of the initial wound area remaining at each timepoint.

As healthy cells migrate from the scratch margin to bridge the gap and heal the wound, the initial area decreases in size. Figure 5.5A shows that 10mM Mg treatment resulted in relatively linear decreases in wound area over 24 h. At the 24 h timepoint, $MgCl_2$ had reduced the wound area to approximately 40%, while OMC and Mg aspartate reduced wound area to approximately 50 and 70% respectively. Figure 5.5B shows representative images of these at 0 and 24 h timepoints.

5.2.11 The effect of 10mM Mg on NHDFC migration

Serum and Mg-starved NHDFCs were seeded onto xCELLigence® CIM-plates® at a concentration of $3x10^4$ cells/well with serum used as a chemoattractant in the bottom of each well. Cells were then exposed to a uniform concentration of 10mM Mg for 24 h in a variety of common forms (Mg aspartate, $MgCl_2$), in addition to the OMC form, and migration monitored using the xCELLigence® electrical impedance system.

Differences between Mg types were not apparent until after the initial 2 h, after which, 10mM $MgCl_2$ treatment in NHDFCs demonstrated the greatest level of migration

efficiency (higher CI values for any given timepoint). Error bars in Figure 5.6A show a clear difference between $MgCl_2$ and OMC/Mg aspartate, and this trend continued beyond the 15 h shown.

Figure 5.6A shows that OMC and Mg aspartate treatment at the same 10mM concentration exhibited very similar migration profiles up until the 7 h timepoint, at which point they diverged. Mg aspartate treatment resulted in a migratory plateau in NHDFCs, while OMC continued to result in NHDFC migration.

Slope data (Figure 5.6B) reflected the rate at which cells migrated during the first few hours of the assay, discounting initial setup time. Mg treatment at 10mM resulted in significantly greater ($P \leq 0.05$) levels of migration than the Mg-free control. Slope data showed no statistically significant difference between Mg forms.

5.2.12 The effect of 10mM Mg on wound closure in NHDFCs

Confluent monolayers of NHDFCs were individually scratched with sterile 200 μL pipette tips using firm, even pressure. Cells were washed with warm PBS, removing damaged cells and debris, before adding the treated medium (10mM OMC, $MgCl_2$ or Mg aspartate). A Leica DM500 microscope with ICC50 camera module was used to capture 40X images at 6 h regular intervals during wound closure, with Image J software (National Institutes for Health, USA) and the MRI Wound Healing Tool.ijm macro plugin subsequently used to quantify the rate by measuring wound area. Measurements were reported in pixels, and results quantified as percentage of the initial wound area at each timepoint.

Figure 5.7A shows that 10mM Mg aspartate treatment performed less effectively at the 12 and 18 h timepoints than other Mg forms tested. However, by 24 h, 10mM $MgCl_2$, OMC and Mg aspartate all resulted in approximately 40% wound closure. These results are reflected in Figure 5.7B, which shows representative images of each condition at timepoints 0 and 24 h.

5.2.13 The effect of 10mM Mg on HAKC migration

Serum and Mg-starved HAKCs were seeded onto xCELLigence® CIM-plates® at a concentration of $5x10^4$ cells/well with full-serum media used as a chemoattractant in the bottom of each well. Cells were then exposed to a uniform concentration of 10mM Mg for 24 h in a variety of common forms (Mg aspartate, $MgCl_2$), in addition to OMC, and migration monitored using the xCELLigence® electrical impedance system.

Figure 5.8A shows a steady increase in CI value for each of the Mg treatment conditions as cells migrated through the 8 μm pores of the polyethylene terephthalate (PET) membrane towards the serum chemoattractant in the bottom chamber of each well. $MgCl_2$ treatment resulted in the greatest overall migration efficiency (defined as greater CI values for any given timepoint). Lower efficiencies were observed for OMC and Mg aspartate respectively in comparison to the Mg-free control. Of these two Mg forms, OMC treatment resulted in greater CI values until the 13 h timepoint, at which point their profiles overlapped, and remained so until the experiment was completed.

Slope data (Figure 5.8B) showed that $MgCl_2$ and OMC exhibited statistically significantly different ($P \leq 0.05$) migration rates than the Mg-free control during their initial response to Mg.

5.2.14 The effect of 10mM Mg on wound closure in HAKCs

Confluent monolayers of HAKCs were individually scratched with sterile 200 μL pipette tips using firm, even pressure. Cells were washed with warm PBS, removing damaged cells and debris, before adding the treated medium (10mM OMC, $MgCl_2$ or Mg aspartate). A Leica DM500 microscope with ICC50 camera module was used to capture 40X images at 6 h regular intervals during wound closure, with Image J software (National Institutes for Health, USA) and the MRI Wound Healing Tool.ijm macro plugin subsequently used to quantify the rate by measuring wound area. Measurements were reported in pixels, and results quantified as percentage of the initial wound area at each timepoint.

Figure 5.9A shows that10mM Mg aspartate treatment resulted in the greatest reduction in wound area in HAKCs after 24 h, where wound size was reduced by approximately 50% of its initial area. OMC effects were comparable to that of Mg aspartate for the

initial 18 h., but less effective by the 24 h timepoint. $MgCl_2$ was notably less effective on HAKCs overall, with wound area matching that of the Mg-free control, which reduced wound area by only 38% after 24 h. Figure 5.9B shows representative images of these at 0 and 24 h timepoints.

5.2.15 The effect of 10mM Mg on tube formation in HAECs

The tube formation assay is a tool for angiogenesis quantification. It is based on the principle that cells differentiate morphologically within 24 h, where cells initially adhere to the matrix, then migrate toward each other, align and form tubes/capillary-like structures.

MaxGel™ ECM was used to form a basement membrane-like surface in each 4 mm well. A 50 μL $2x10^5$ cells/mL HAEC suspension was subsequently used to seed on top of this. Cells were observed and imaged in 6-h intervals. A Leica DM500 microscope with ICC50 camera module was used to capture 100X images at 4 h regular intervals during this process, with Image J (National Institutes for Health, USA) software and the MRI Wound Healing Tool.ijm macro plugin subsequently used to quantify the rate by measuring tube length. Measurements were reported in pixels and converted to % wound closure of initial area.

Figure 5.10A shows that $MgCl_2$ treatment demonstrated significantly greater ($P \leq 0.05$) levels of tube formation in comparison to either OMC or Mg aspartate in HAECs. This trend was the same at both 12 and 24 h timepoints. The Mg-free control produced no measurable tubes/capillary-like structures. Figure 5.10B shows representative images of these at 0 and 24 h timepoints.

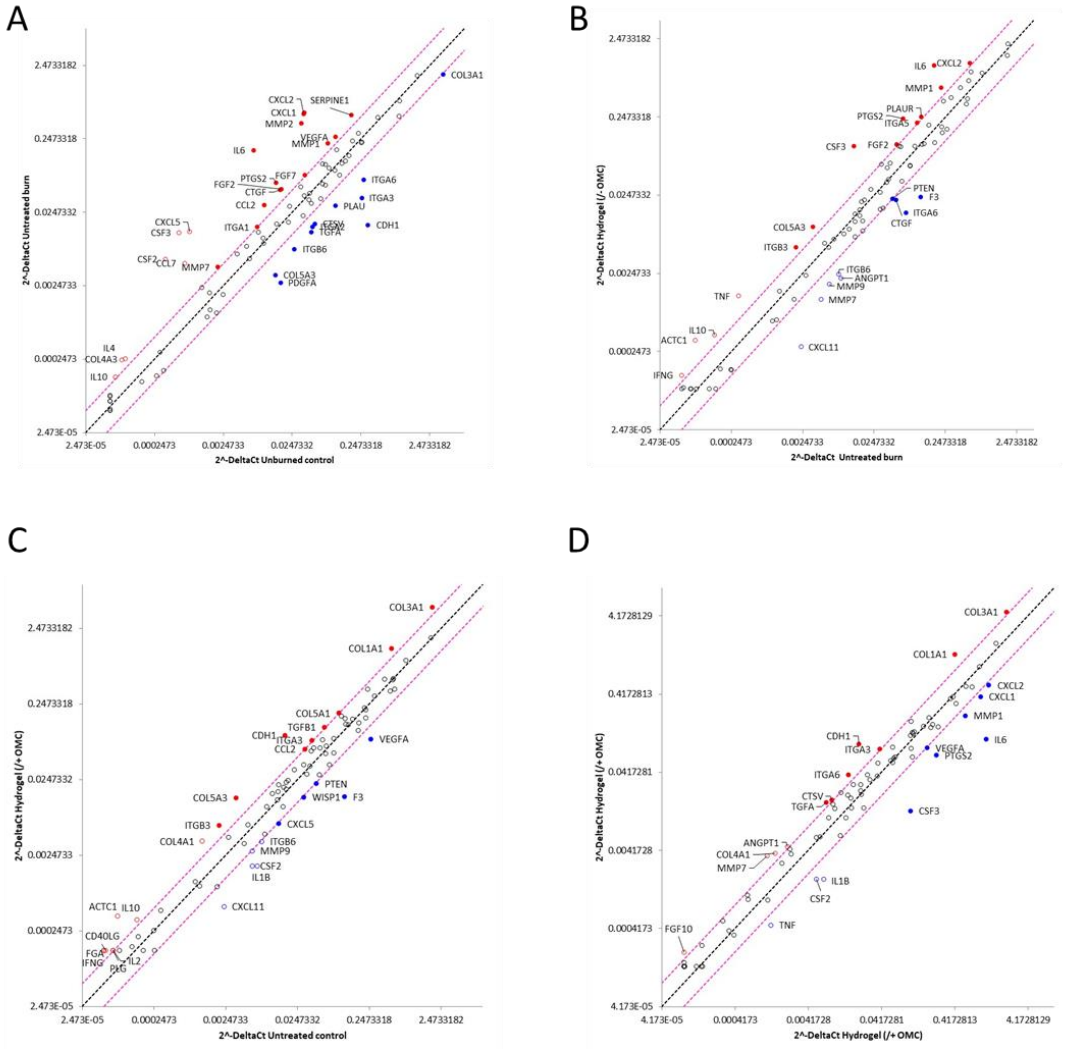

Figure 5.2 Effect of hydrogel (/± OMC) v burn on wound healing mRNA expression 24 h post-burn

(A) Untreated burn v unburned control. (B) Hydrogel (/- OMC) v untreated burn. (C) Hydrogel (/+ OMC) v untreated burn. (D) Hydrogel (/+ OMC) v hydrogel (/= OMC). Scatter plot represents normalised gene expression for all genes present on the array. The central line indicates unchanged gene expression. Dotted lines indicate selected fold regulation threshold. Data points beyond these represent genes that meet the selected 2-fold regulation threshold. Appropriate corrections were made using proprietary Qiagen RT2 analysis software. CT cut-off was set at 35. CT values for endogenous control genes were geometrically averaged and used in ΔΔCT calculations. (n = 3 for each array).

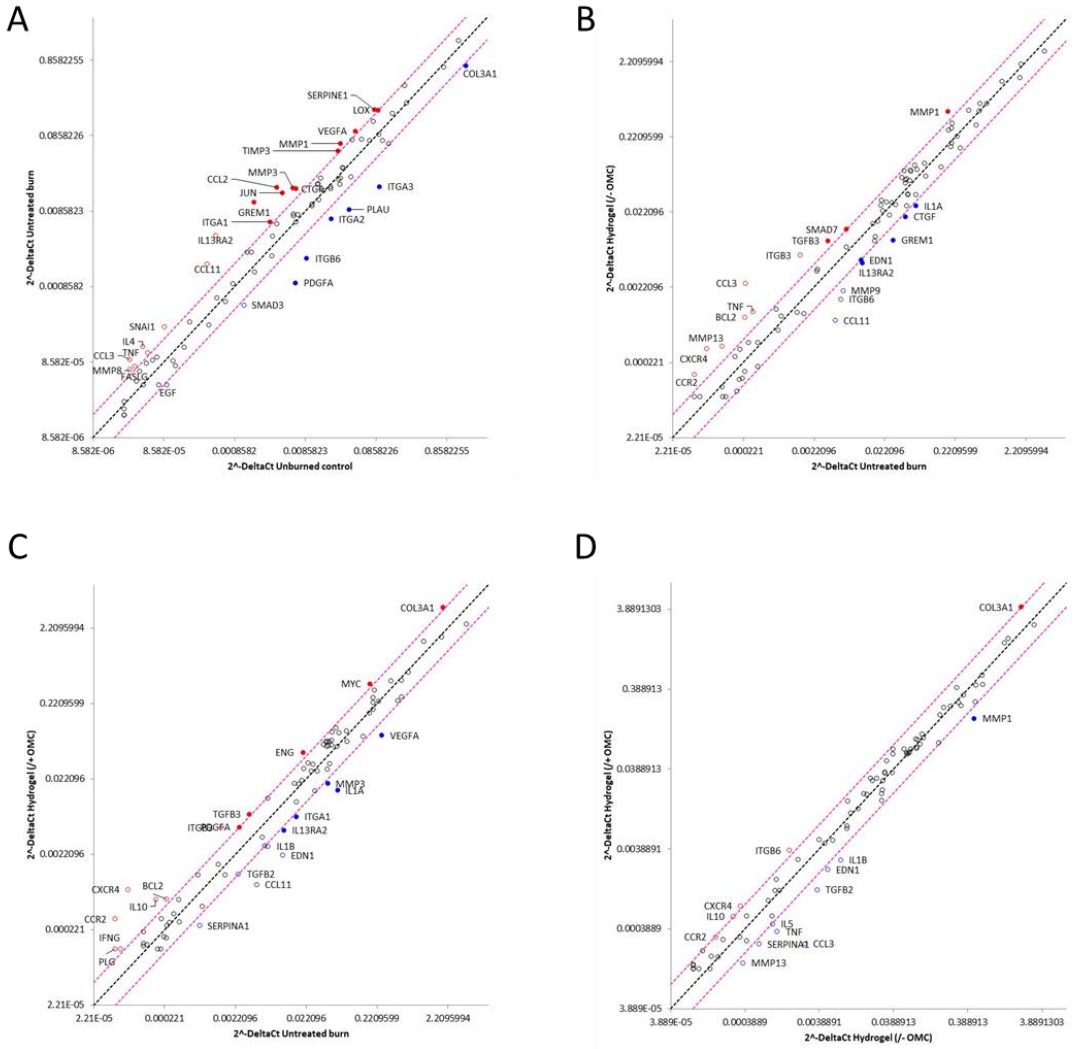

Figure 5.3 Effect of hydrogel (/± OMC) v burn on fibrosis mRNA expression 24 h post-burn

(A) Untreated burn v unburned control. (B) Hydrogel (/- OMC) v untreated burn. (C) Hydrogel (/+ OMC) v untreated burn. (D) Hydrogel (/+ OMC) v hydrogel (/= OMC). Scatter plot represents normalised gene expression for all genes present on the array. The central line indicates unchanged gene expression. Dotted lines indicate selected fold regulation threshold. Data points beyond these represent genes that meet the selected 2-fold regulation threshold. Appropriate corrections were made using proprietary Qiagen RT2 analysis software. CT cut-off was set at 35. CT values for endogenous control genes were geometrically averaged and used in ΔΔCT calculations. (n = 3 for each array).

Tables 5.1 – 5.8

Table 5.1 The Effect of Control (unburned) v Burn (untreated) on wound healing mRNA expression in a 3D skin model, 24 h post-burn (n = 3)
Note that data shown are limited to fold changes of 2 or above. All displayed data demonstrated a statistical significance of $P \leq 0.005$.

Gene	Fold change
IL6	25.47
CSF3	23.21
CXCL5	16.91
CSF2	16.17
CXCL1	15.21
CXCL2	14.73
MMP2	12.01
CCL7	7.36
PTGS2	4.38
CCL2	3.22
CTGF	2.99
IL4	2.98
FGF2	2.96
SERPINE1	2.89
COL4A3	2.71
MMP1	2.61
VEGFA	2.46
MMP7	2.18
IL10	2.13
FGF7	2.10
ITGA1	2.02
COL3A1	-2.11
CTSV	-3.04
ITGA2	-3.14
ITGB6	-3.40
PLAU	-3.49
TGFA	-3.53
ITGA6	-3.96
COL5A3	-4.10
PDGFA	-6.16
ITGA3	-6.52
CDH1	-18.99

Table 5.2 The Effect of Control (untreated burn) v Burn (hydrogel /- OMC) on wound healing mRNA expression in 3D skin model, 24 h post-burn (n = 3)
Note that data shown are limited to fold changes of 2 or above. All displayed data demonstrated a statistical significance of $P \leq 0.005$.

Gene	Fold Change
CSF3	8.01
IL6	6.51
ACTC1	4.51
TNF	4.12
PTGS2	3.74
IL10	2.82
COL5A3	2.80
MMP1	2.73
ITGB3	2.69
IFNG	2.49
CXCL2	2.26
PLAUR	2.16
FGF2	2.16
ITGA5	2.08
PTEN	-2.04
CTGF	-2.30
MMP9	-3.22
ITGB6	-3.25
MMP7	-3.88
ANGPT1	-3.97
ITGA6	-4.64
F3	-4.73
CXCL11	-8.23

Table 5.3 The Effect of Control (untreated burn) v Burn (hydrogel /+ OMC) on wound healing mRNA expression in 3D skin model, 24 h post-burn (n = 3)
Note that data shown are limited to fold changes of 2 or above. All displayed data demonstrated a statistical significance of $P \leq 0.005$.

Gene	Fold change
CDH1	5.76
ACTC1	5.13
COL5A3	4.12
COL4A1	3.26
ITGB3	3.09
FGA	2.76
IFNG	2.76
COL1A1	2.66
CD40LG	2.59
COL3A1	2.54
IL10	2.43
ITGA3	2.11
TGFB1	2.10
PLG	2.05
IL2	2.04
COL5A1	2.03
CCL2	2.00
MMP9	-2.05
WISP1	-2.07
PTEN	-2.07
CXCL5	-2.08
ITGB6	-2.09
VEGFA	-3.07
CSF2	-3.20
IL1B	-3.75
CXCL11	-4.51
F3	-7.63

Table 5.4 The Effect of Control (hydrogel /- OMC) v Burn (hydrogel /+ OMC) on wound healing mRNA expression in 3D skin model: 24 h post-burn (n = 3)
Note that data shown are limited to fold changes of 2 or above. All displayed data demonstrated a statistical significance of P ≤005.

Gene	Fold change
CDH1	4.64
COL1A1	3.21
MMP7	3.09
ITGA6	2.61
COL4A1	2.60
FGF10	2.50
TGFA	2.33
COL3A1	2.22
ANGPT1	2.16
CTSV	2.13
ITGA3	2.10
VEGFA	-2.04
CXCL2	-2.25
CXCL1	-2.43
MMP1	-2.65
TNF	-2.78
CSF2	-2.99
PTGS2	-3.42
IL1B	-3.78
CSF3	-7.76
IL6	-10.21

Table 5.5 Healthy (unburned) control v burn (no treatment) on fibrosis mRNA expression in 3D skin model, 24 h post-burn (n = 3)

Note that data shown are limited to fold changes of 2 or above. All displayed data demonstrated a statistical significance of $P \leq 0.005$.

Gene	Fold change
IL13RA2	8.88
GREM1	7.03
CCL2	5.21
CCL11	4.91
JUN	3.72
CCL3	3.27
IL4	3.18
MMP3	3.04
SNAI1	2.92
CTGF	2.68
MMP1	2.48
MMP8	2.45
SERPINE1	2.34
VEGFA	2.29
FASLG	2.29
ITGA1	2.29
TNF	2.27
TIMP3	2.18
LOX	2.04
COL3A1	-2.17
EGF	-2.18
SMAD3	-2.36
ITGA2	-2.91
PLAU	-3.94
ITGB6	-4.40
ITGA3	-5.26
PDGFA	-6.39

Table 5.6 Effect of untreated burn (control) v hydrogel (-OMC) on fibrosis mRNA expression in 3D skin model, 24 h post-burn (n = 3)
Note that data shown are limited to fold changes of 2 or above. All displayed data demonstrated a statistical significance of $P \leq 0.005$.

Gene	Fold Regulation
CCL3	10.50
CXCR4	5.06
ITGB3	4.22
BCL2	3.83
TNF	3.55
CCR2	3.49
MMP13	3.29
MMP1	2.75
TGFB3	2.69
SMAD7	2.05
EDN1	-2.03
IL1A	-2.28
CTGF	-2.29
IL13RA2	-2.30
MMP9	-2.85
GREM1	-3.11
ITGB6	-3.40
CCL11	-5.53

Table 5.7 Effect of hydrogel-OMC (control) v hydrogel+OMC on fibrosis mRNA expression in 3D skin model: 24 h post-burn (n = 3)
Note that data shown are limited to fold changes of 2 or above. All displayed data demonstrated a statistical significance of $P \leq 0.005$.

Gene	Fold change
CXCR4	11.36
CCR2	6.99
ITGB3	3.60
IL10	3.35
PLG	2.80
ENG	2.49
BCL2	2.42
IFNG	2.33
MYC	2.31
COL3A1	2.21
TGFB3	2.20
PDGFA	2.05
TGFB2	-2.01
IL1B	-2.25
ITGA1	-2.26
IL13RA2	-2.30
MMP3	-2.33
SERPINA1	-2.73
VEGFA	-3.06
IL1A	-3.90
EDN1	-4.78
CCL11	-5.06

Table 5.8 Effect of hydrogel-OMC (control) v hydrogel+OMC on fibrosis mRNA expression in 3D skin model: 24 h post-burn (n = 3)
Note that data shown are limited to fold changes of 2 or above. All displayed data demonstrated a statistical significance of $P \leq 0.005$.

Gene	Fold change
ITGB6	2.43
CXCR4	2.24
IL10	2.11
COL3A1	2.02
CCR2	2.00
IL5	-2.04
EDN1	-2.36
SERPINA1	-2.39
MMP13	-2.52
IL1B	-2.67
MMP1	-2.86
TNF	-2.94
TGFB2	-3.03
CCL3	-9.86

Figures 5.4 – 5.10

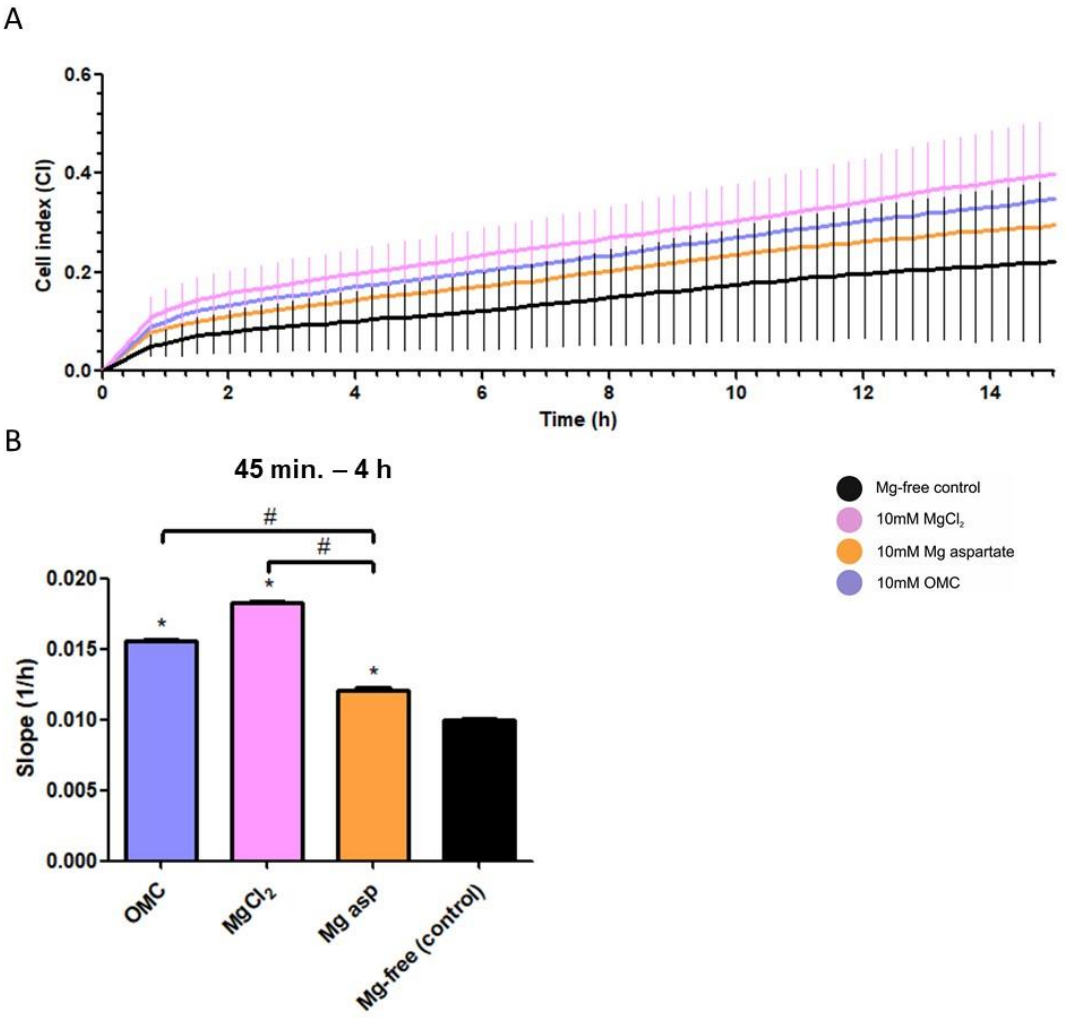

Figure 5.4 xCELLigence® migration profile of HAECs treated with different Mg forms (10mM) for 24 h (first 15 h shown only)

(A) Static quiescent, Mg-starved HAECs were exposed to 10mM Mg in a variety of common forms (Mg aspartate, $MgCl_2$) in addition to OMC using the xCELLigence® electrical impedance system. Results are averaged from three independent experiments (n = 3) ± SD. (B) Rate of migration of HAECs between 45 min. and 4 h. Rate was determined by calculating the slope of the line between determined timepoints. Results are averaged from three independent experiments (n = 3 ± SD). *P≤0.05 vs Mg-free control. # P≤0.05.

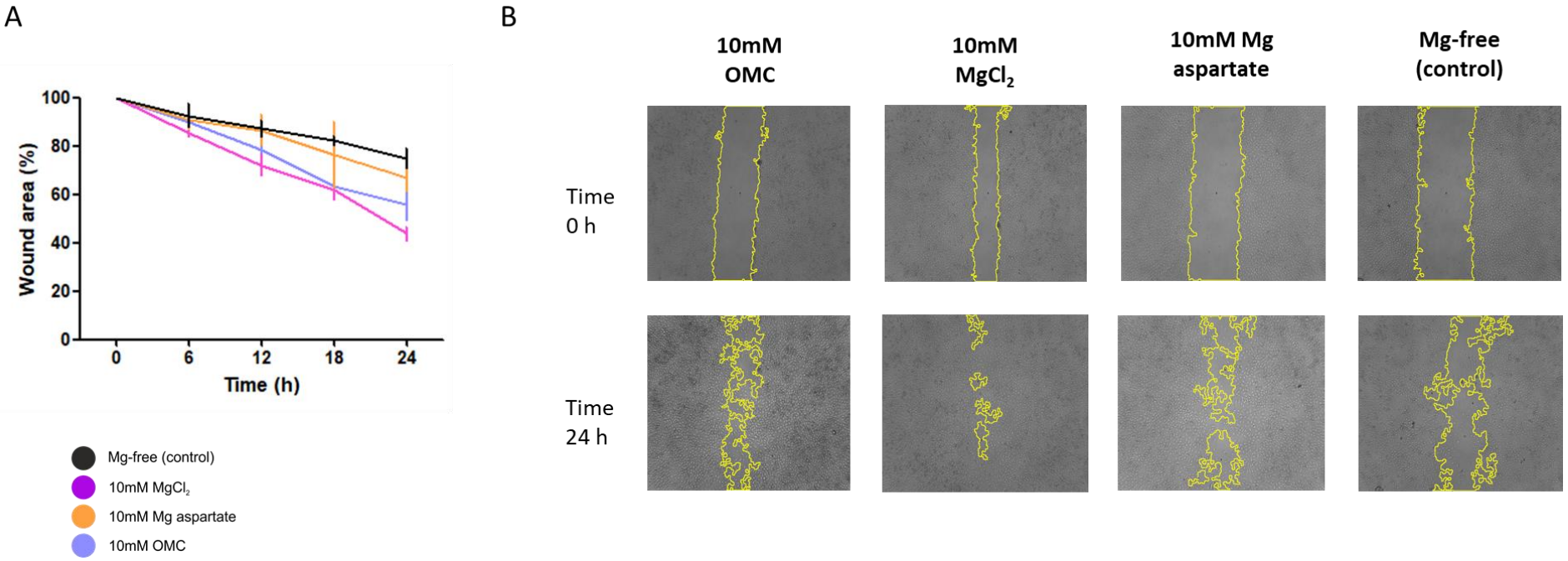

Figure 5.5 Effect of 10mM Mg on wound healing in HAECs
(A) Scratch repair rate in HAECs over 24 h (n = 3) (B) Representative images of wound healing in HAECs at time = 0 h and time = 24 h.

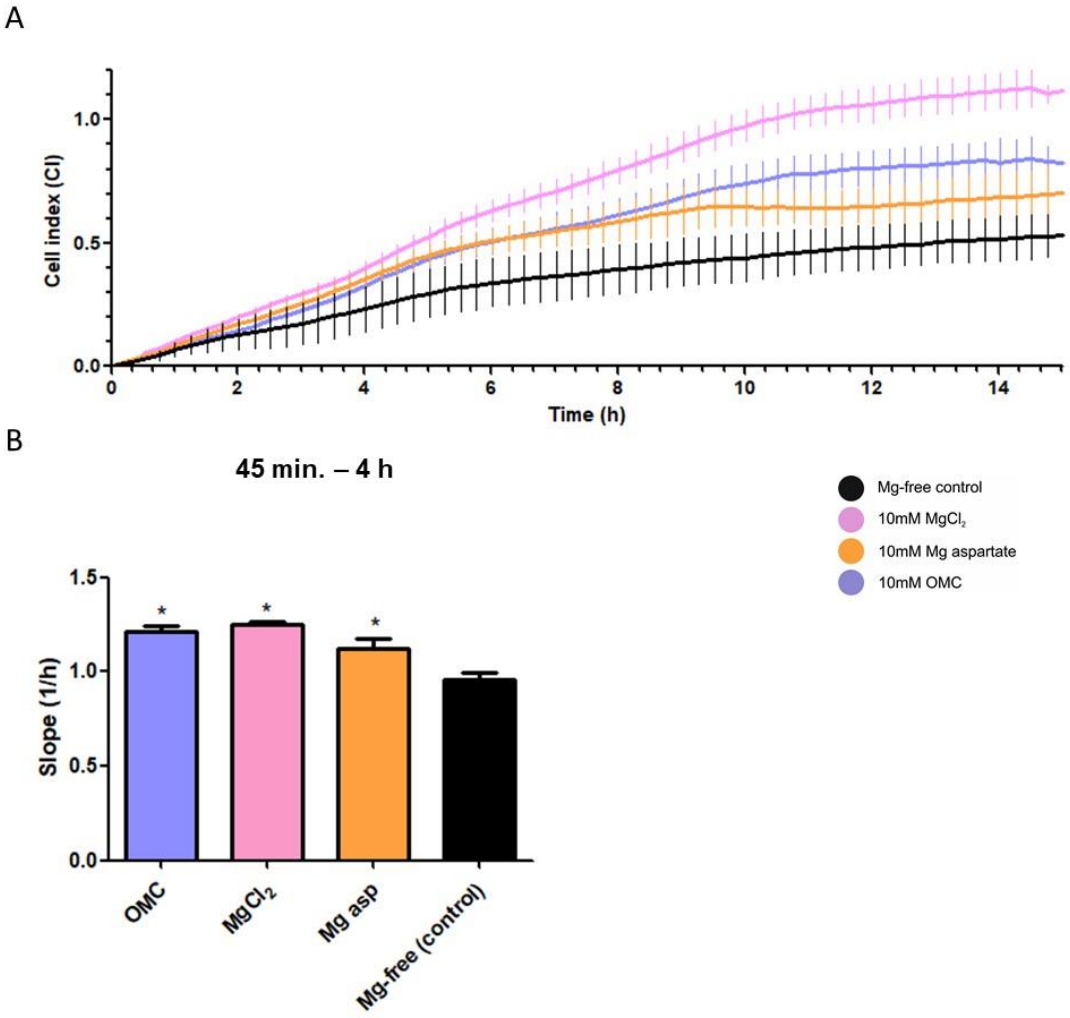

Figure 5.6 xCELLigence® migration profile of NHDFCs treated with different Mg forms (10mM) for 24 h (first 15 h shown only).

(A) Static quiescent, Mg-starved NHDFCs were exposed to 10mM Mg in a variety of common forms (Mg aspartate, $MgCl_2$) in addition to OMC using the xCELLigence® electrical impedance system. Results are averaged from three independent experiments (n = 3) ± SD. (B) Rate of migration of NHDFCs between 45 min. and 4 h. Rate was determined by calculating the slope of the line between determined timepoints. Results are averaged from three independent experiments (n = 3 ± SD). *P≤0.05 vs Mg-free control.

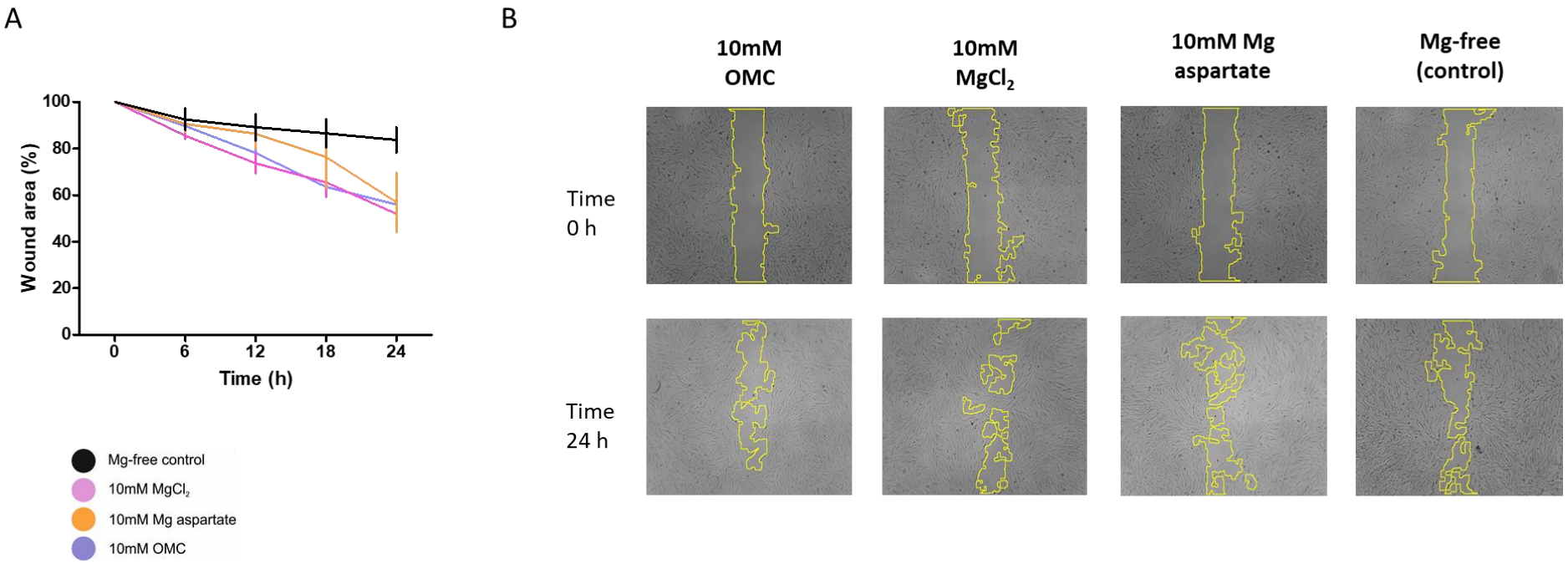

Figure 5.7 Effect of 10mM Mg on wound healing in NHDFCs

(A) Scratch repair rate in NHDFCs over 24 h (n = 3) (B) Representative images of wound healing in NHDFCs at time = 0 h and time = 24 h.

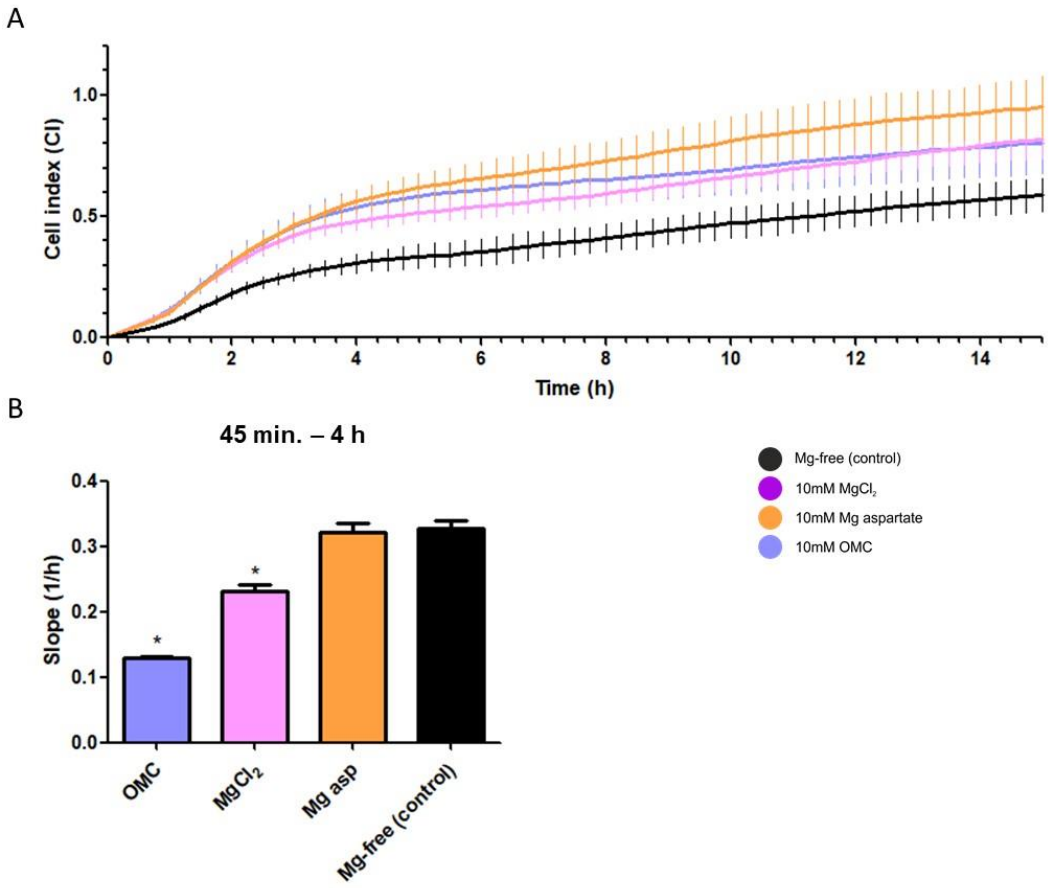

Figure 5.8 xCELLigence® migration profile of HAKCs treated with different Mg forms (10mM) for 24 h (first 15 h shown only)

(A) Static quiescent, Mg-starved HAKCs were exposed to 10mM Mg in a variety of common forms (Mg aspartate, $MgCl_2$) in addition to OMC using the xCELLigence® electrical impedance system. Results are averaged from three independent experiments (n = 3) ± SD. (B) Rate of migration of HAKCs between 45 min. and 4 h. Rate was determined by calculating the slope of the line between determined timepoints. Results are averaged from three independent experiments (n = 3 ± SD). *P≤0.05 vs Mg-free control.

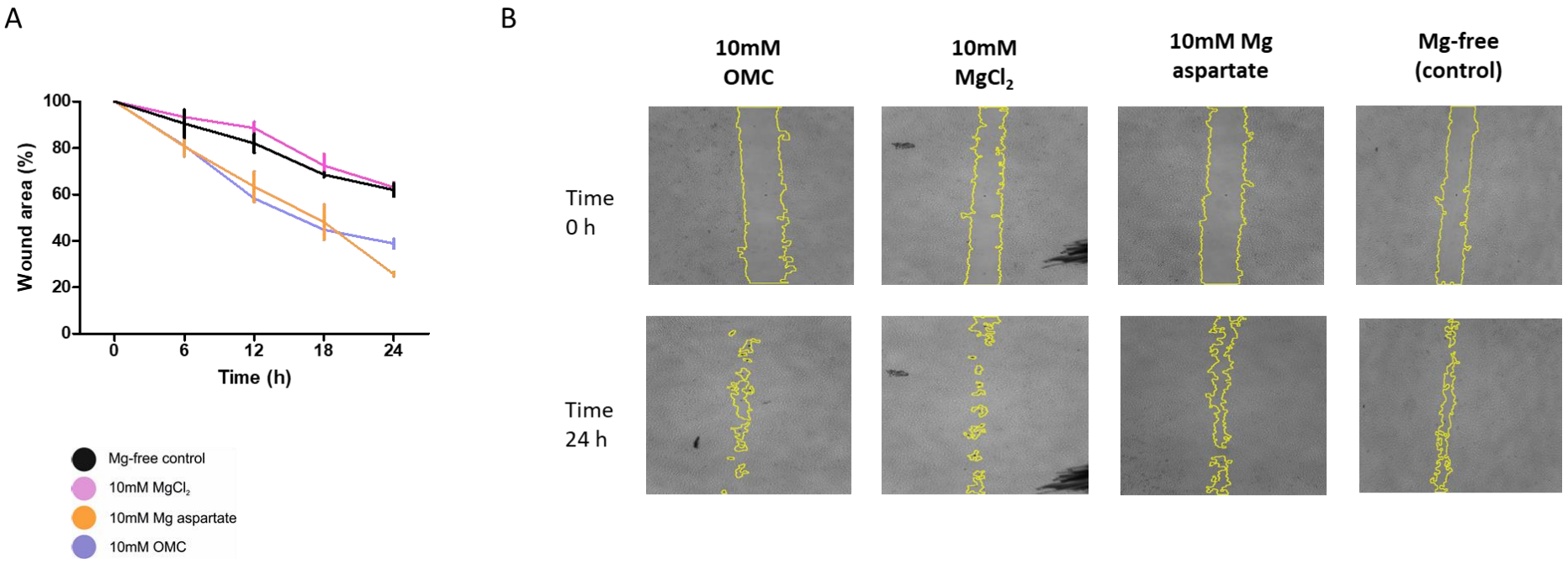

Figure 5.9 Effect of 10mM Mg on wound healing in HAKCs
(A) Scratch repair rate in HAECs over 24 h (n = 3) (B) Representative images of wound healing in HAECs at time = 0 h and time = 24 h

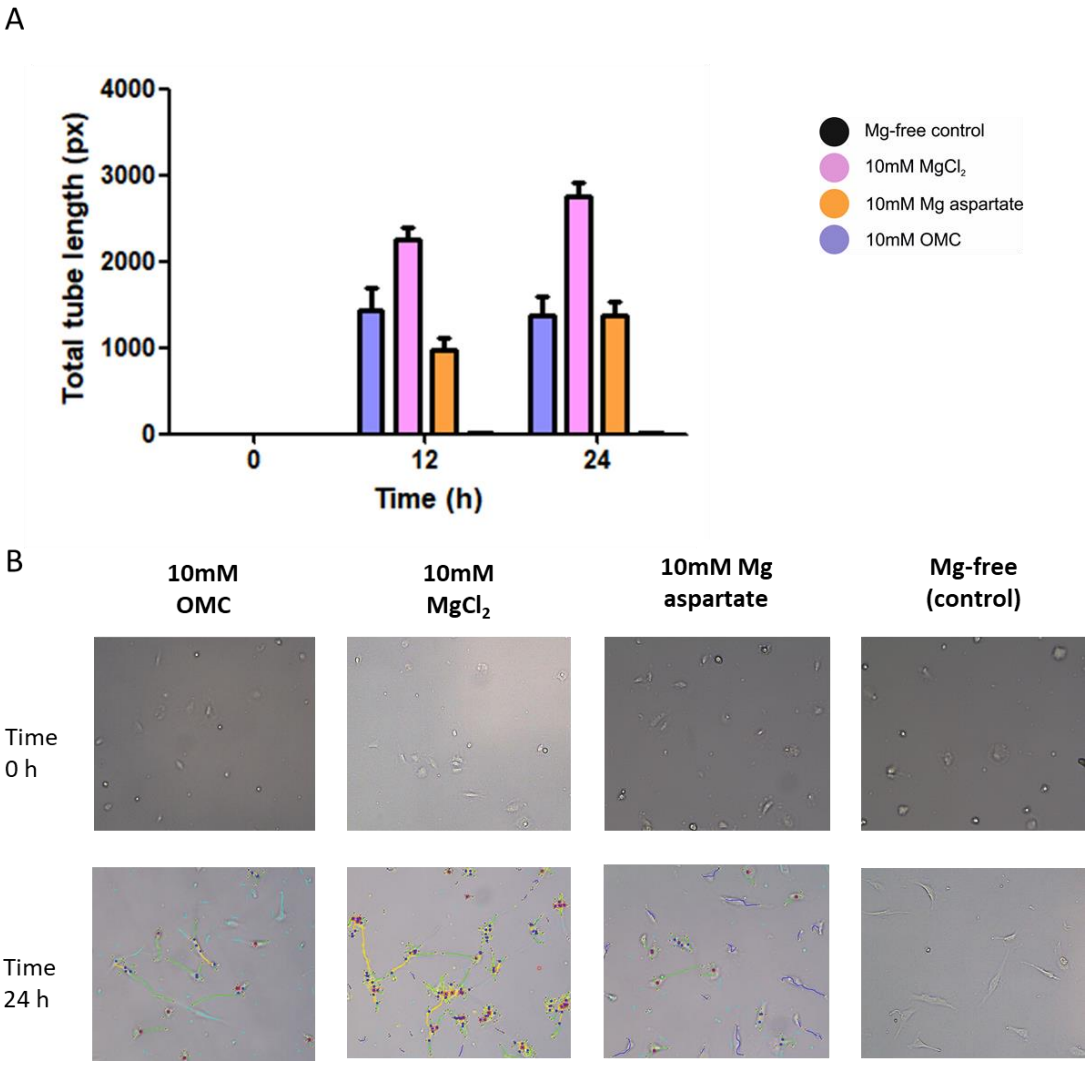

Figure 5.10 Effect of 10mM Mg on HAEC tube formation/sprouting
(A) Static quiescent, Mg-starved HAECs were exposed to 10mM Mg in a variety of common forms (Mg aspartate, $MgCl_2$) in addition to OMC on MaxGel™ ECM. Results are averaged from three independent experiments (n = 3) ± SD. (B) Representative images of tube formation/sprouting in HAECs at time = 0 h and time = 24 h. Coloured lines indicate sprout/tube outline detection and signify length.

5.3 Discussion

The anti-inflammatory effects of Mg supplementation on an *in vitro* 3D dermal burn model were examined using Qiagen RT^2 profiler gene array platforms. Examination of this model at a genetic level facilitated an over-arching view of the processes likely to occur *in vivo*. The 3D co-culture injury model enabled cellular cross-talk affecting transcriptional regulation of genes involved in wound healing and development of scar tissue (fibrosis). Wound healing/fibrosis are processes in which cell behaviour is orchestrated by a higher level of tissue control than 2D monolayer assays are able to capture (Safferling *et al.*, 2013). Hence beyond this, functional studies (migration and tube formation) were performed in monoculture environments in order to clarify observed effects at a functional level. As such, this discussion will progress in the order outlined in Figure 5.1.

The wound healing array contained genes important for each of the three phases of wound healing, including ECM re-modelling factors, inflammatory cytokines and chemokines, as well as growth factors and major signalling molecules. The *in vitro* 3D model consisted of a co-culture of dermal fibroblasts and keratinocytes. Though limited, the 3D model did yield some insight into the complex interactions occurring within skin tissue in response to hydrogel (/+ OMC) treatment. Due to manufacturing and other constraints, it was not possible to compare hydrogels that incorporated $MgCl_2$ or Mg aspartate. Nevertheless, these data further elucidate the effects of OMC as set out in the objectives of this thesis.

5.3.1 The effect of hydrogel (/+ OMC) on wound healing gene expression 24 h post-burn

In comparison to the healthy (unburned) control, expression of a number of genes of interest underwent significant changes. Specifically, the untreated burn induced up-regulation of a number of inflammatory markers as well as down-regulation of ECM-producing genes. Taken together, these data are characteristic of those anticipated from a burn injury. They indicate that the model responded appropriately to the induced injury, and validate its use as a model of thermal burn injury.

Treatment with hydrogel (/- OMC) lead to a different cohort of up/down-regulated genes in comparison to the untreated burn. ECM-producing genes that had been down-regulated in response to burn without treatment were largely restored to normal levels when treated with hydrogel. This was also the case for platelet-derived growth factor (PDGF) expression, and suggests some increase in inter-cellular cross-talk. Subcutaneous temperature will continue to rise even after the heat source has been removed *in vivo*. Hence rapid cooling of the burn/dissipation of heat is recommended in order to minimise the extent and depth of the wound (Shrivastava and Goel, 2010). Coats *et al.*, (2002) previously verified the cooling properties of the specific hydrogel (/- OMC) used in these experiments, thereby helping to explain the observed effects. Nevertheless, expression of genes such as IL10 and MMP1 remained at similar levels to the untreated control, while additional inflammatory markers such as TNF were up-regulated.

Transcriptional changes as a result of treatment with hydrogel (/+ OMC) show a continuation of the trends observed in the untreated burn and hydrogel (/- OMC) conditions. Here, up-regulation of ECM-producing and integrin-related genes was demonstrated. Of particular note was Angiopoietin-1 (ANG1), up-regulated 2.16-fold. ANGPT1 is a specific growth factor that acts to facilitate stable and functional vasculature through the Tie2 and Tie1 receptors (Cho *et al.*, 2006). Of further relevance, was the fact that E-cadherin (CDH1) was up-regulated 5.76-fold. In the untreated burn model, it was down-regulated 18.99-fold. In addition, inflammatory cytokines (IL1B, CXCL5) were down-regulated, while the anti-inflammatory cytokine, IL10, was up regulated 2.43-fold. These observations may be attributed to the inclusion of OMC. These data suggest that the incorporation of OMC in the hydrogel stimulated the expression of beneficial wound healing genes *in vitro*. There were, however, some genes that demonstrated contrary results. VEGFA was down-regulated 3.07-fold. Negative regulation of this gene by hydrogel (/+ OMC) is likely detrimental to the wound healing process as it is an important angiogenesis and vasculogenesis factor, in addition to promoting endothelial cell proliferation, migration, and induction of blood vessel permeabilisation.

Directly comparing gene expression as a result of hydrogel treatment with and without OMC acted as a control, negating the cooling effects of the hydrogel, and enabled a clear look at the effects of the therapeutic in relative isolation. E-cadherin (CDH1)

and COL1A1, for example, were up-regulated as demonstrated in the comparison between hydrogel (/+ OMC) and the untreated burn. Similarly, VEGFA exhibited down-regulation, further suggesting that OMC is a negative regulator of this gene. This is not an unexpected result, as the negative relationship between VEGFA and elevated Mg, the principal component in OMC, is established in literature (Xu, *et al.*, 2019) though the authors propose no firm mechanism as to its cause. Hong *et al.*, (2006) previously suggested that VEGFA serves to increase Mg from intra-cellular Mg^{2+} stores through the tyrosine kinase/PI3K/PLCγ-dependent signalling pathways in HUVECs. The 3D model was not Mg-starved like other experimental conditions in this thesis, and instead was cultured in normal culture medium in order to accurately mimic the type of first-aid treatment likely to be received under typical, yet controlled, conditions. As such, it is possible that cell response to additional Mg negated the requirement to draw from intra-cellular stores, hence down-regulating VEGFA expression. This process has not been confirmed in dermal cells, but does present a possible explanation for the trends observed.

The comparison between hydrogel (/+ OMC) and the untreated control revealed that transforming growth factor alpha (TGFA) and fibroblast growth factor-10 (FGF10) were up-regulated 2.33 and 2.50-fold respectively. TGFA has been shown both *in vivo* and *in vitro* to accelerate events associated with cell migration and epidermal wound repair (Cheng *et al.*, 2008). It is particularly present in the wound margin (Wenczak, *et al.*, 1992), the area sampled in these experiments. Prostaglandin-endoperoxide synthase 2 (PTGS2), which was down-regulated 3.42-fold, is involved in the conversion of arachidonic acid to prostaglandin H2, an important precursor of prostacyclin, expressed in inflammation. Along with down-regulation of other inflammatory markers, TNF and IL6, these signify a possible beneficial effect attributed to the inclusion of OMC.

Overall, these *in vitro* data suggest that treatment of a dermal burn injury with hydrogel (/- OMC) results in restoration of down-regulated ECM-producing genes to normal levels. Further, incorporation of OMC in the hydrogel stimulated wound healing through the expression of a number of EMC-producing genes and integrins, while attenuating expression of inflammatory cytokines. These were observed in addition to those naturally expressed as a result of burn injury. Additional unpublished experiments carried out in the laboratory demonstrated that incorporation of OMC

with the hydrogel retained the cooling effects previously observed by Coats *et al.*, (2002) in hydrogel (/- OMC). Nevertheless, while some beneficial effects are observed, they are tempered by the complex interplay between genes and between cell types that makes interpretation difficult to determine. As inflammation marks the second stage of wound healing, it is certainly promising that only some of the inflammatory markers assayed experienced a shift in transcriptional levels, leaving others free to engage in pathways necessary for complete restoration of the wound site.

5.3.2 The effect of hydrogel (/+ OMC) on fibrosis gene expression 24 h post-burn

As a condition arising from abnormal fibroblast activation leading to excessive accumulation of ECM, fibrosis occurs after deep dermal burn injury with prolonged inflammation. Scarring and its accompanying aesthetic and functional sequelae still pose major challenges. Mg treatment has demonstrated a capacity to reduce inflammation. It was therefore of interest to investigate whether hydrogel (/+ OMC) had the potential to prevent/reduce scarring. As with the initial wound healing, this was pursued from a genetic perspective.

Treatment with hydrogel (/- OMC) resulted in mixed results, with a reduction in the number of up-regulated genes in comparison to the untreated control. TNF expression was up-regulated 3.55-fold, along with CCL3, another inflammatory cytokine. Gremlin1, which had demonstrated a 7.03-fold increase in expression in the untreated burn model, was down-regulated 3.11-fold. Down-regulation of Gremlin1, a gene associated with angiogenesis (Chen *et al.*, 2013), may be perceived as a negative consequence of hydrogel (/- OMC) treatment.

In contrast, treatment with hydrogel (/+ OMC) showed up-regulation of anti-inflammatory IL10 (3.35-fold). IL10 plays a role in fetal regeneration, and over-expression has recently been shown to deliver scarless healing in post-natal tissue (King *et al.*, 2014). IL10 has been shown to regulate collagen type 1 and MMP expression *in vitro* (Reitamo *et al.*, 1994), rendering this a result worthy of further investigation. Additionally, endoglin (ENG) expression was elevated 2.49-fold in the hydrogel (/+ OMC) condition. The transmembrane glycoprotein is a type III co-receptor for the TGFβ receptors (Pericacho *et al.*, 2013), of which TGFβ3 was also up-regulated 2.20-fold. It is expressed in vascular endothelial and smooth muscle

cells, where it plays an important role in vessel wall homeostasis. It is known to be elevated in the endothelial cells of neovascularised tissues and hence may be referred to as pro-angiogenic. Here, it was clearly expressed by either fibroblast or keratinocyte cells, but it again suggests cross-communication within the model. Studies have correlated elevated levels of ENG with $MgSO_4$ treatment in microvascular endothelial cells, though the concentration was not stated (Korish, 2012). CCR2 (up-regulated 6.99-fold) plays a critical role in the establishment of a regulated inflammatory response in wound healing, driving macrophage recruitment.

A number of genes common to both wound healing and fibrosis panels displayed similar expression patterns under the same conditions, as in the case of the hydrogel (± OMC) comparison. These included TNF, COL1A1 and CCR2 genes. The fibrosis panel showed that the chemokine receptor, CXCR4, was up-regulated 2.24-fold, but transcriptional levels were markedly decreased than those observed in hydrogel (/+ OMC) and untreated control comparison. This suggests that the cooling effect exerted by the gel results in gene expression that is somewhat attenuated by the addition of OMC.

ENG expression was increased 1.59-fold, below the threshold for inclusion in the table, but still demonstrating an increase with hydrogel (/+ OMC) treatment. While COL3A1 expression remained at elevated levels, TNF was down-regulated 2.94-fold. Similarly, TGFβ2, a known inhibitor of cell migration, was down-regulated 3.03-fold. MMP1 and 13 were down-regulated 2.86 and 2.52-fold respectively. Transcriptional change observed in these genes may be attributed to the inclusion of OMC in the hydrogel, and their relationship with Mg in particular.

Overall, a very similar pattern of gene expression was observed between wound healing and fibrosis arrays. Analysis does show evidence of suppression of some markers of inflammation. The increased expression of IL10 in response to hydrogel (/+ OMC) treatment perhaps represents the most potentially positive benefit in terms of preventing formation of scar tissue. As fibrosis results from long term inflammation in fibroblasts, further analysis at extended timepoints is required to ascertain any effect. However, this would be in the absence of continued treatment, as hydrogel (/+ OMC) is a topical first-aid treatment.

5.3.2 Examination of the functional response of dermal cells to 10mM Mg treatment

In vitro analysis of cell migration is a useful approach to quantify alterations in cell migratory capacity in response to Mg treatment. Such analyses in a dermal model are important because cells release various peptide growth factors that stimulate migration into the wound site, and cause proliferation in order to reconstitute the damaged tissue. This type of interaction is exemplified in dermal fibroblast cells, but is also observed in keratinocyte and endothelial cells.

Two complimentary approaches were used: the electrical impedance-based xCELLigence® migration protocol, and the more traditional scratch assay. The xCELLigence® approach required cells to migrate through the 8 μm pores of a polyethylene terephthalate (PET) membrane towards a chemoattractant (serum) in the bottom chamber of each well. Thus, this model encompassed a 3D element that more closely resembled the *in vivo* paradigm. In contrast, the scratch technique required cells to migrate across the flat plane formed by the scratch. The creation of the scratch, however, inflicted physical damage to cells and striped ECM from the monolayer. It was hence more representative of the type of *in vitro* cellular response to an actual wound. While many of the trends observed in the xCELLigence® migration assays were mirrored in the scratch assays, some notable differences were observed. Combining data from both allowed a clearer picture of the effect of Mg treatment to emerge.

HAEC adhesion was discussed in Chapter Four within the context of Mg in a turbulent OSS environment. In this chapter, HAECs were again analysed within the context of 10mM Mg treatment using similar techniques, but from a migratory perspective. As both adhesion and migration share common mechanisms, 10mM Mg was chosen as a satisfactory concentration to continue these investigations. Lapidos *et al.*, (2001) demonstrated that Mg^{2+} could induce both chemokinetic and chemotactic migration in HUVECs, peaking at 0.1 and 10 mM, respectively. In the xCELLigence® assays carried out for this chapter, 10mM Mg was present in both upper and lower chambers, ruling out any chemotactic response to Mg. Instead, these experiments focused on examining Mg as an aid to migration.

Examination of xCELLigence® data revealed that 10mM Mg treatment lead to improved HAEC migration in comparison to the Mg-free control. Banai *et al.*, (1990) evaluated migration of bovine adrenal cortex capillary endothelial cells using six different $MgSO_4$ concentrations in various culture conditions. Their findings correlate strongly with data presented in this chapter, where they reported that very low magnesium concentrations inhibited cell proliferation. Hydrogel gene expression data, discussed previously, showed increased levels of IL6 in the (/- OMC) and untreated conditions. Bernardini *et al.*, (2005) correlated low extra-cellular Mg levels and increased levels of IL6 in 1G11 (lung endothelial) cells with inhibited impeded cell migration. (Bernardini *et al.*, 2005) further reported dose-dependent increases in migration when Mg levels were increased beyond the normal serum concentration, up to 2.4mM. Similarly, Maier *et al.*, (2004), recorded dose-dependent increases in migration up to 5mM. Such concentrations within a certain range may serve to increase intrinsic ATPase activity (Lamalice, *et al.*, 2007). Mg demonstrates the ability to form chelates with important intracellular anionic-ligands, particularly Adenosine triphosphate (ATP) (Swaminathan, 2003). Indeed, free ionised Mg constitutes only 0.5 - 5% of total cellular magnesium; the remainder is bound to anionic compounds such as ATP, ADP, citrate, proteins, RNA and DNA or is sequestered within mitochondria and endoplasmic reticulum (Swaminathan, 2003). Such activity could boost assembly of actin filaments during cellular filopodia and lamellipodia extension. This would in many respects explain the observations in the data presented in this chapter. In lower Mg conditions, metabolomic pathways that result in decreased high-energy phosphates, as well as protein/carbohydrate synthesis may negatively impact cell migration.

Endothelial cell adhesion and migration are fundamental mechanisms linked to a number of physiological processes, including vascular development and angiogenesis. Moreover, these processes are linked with many proteins arising from intra-cellular communication demonstrated to be transcriptionally up-regulated in the 3D model, such as angiopoietin-1. Further examination of xCELLigence® HAEC data showed that $MgCl_2$ generated the most efficient migration profile (greater CI values for any given timepoint) than either OMC or Mg aspartate. This is in agreement with the scratch data, which show a similar trend. $MgCl_2$ treatment resulted in wound closure

of 60% by 24 h. In a similar migration experiment conducted by Zhao *et al.*, (2015), 10 - 20mM $MgCl_2$ treatment also resulted in increased HAEC migration.

In vivo, fibroblast cells are responsible for synthesis of collagens, glycosaminoglycans, and other critical glycoproteins of the ECM. As such, fibroblast cells are completely surrounded by ECM (Rhee, 2009). Like HAECs, fibroblasts utilise specific cytoskeletal proteins to adapt to their environment (Trepat *et al.*, 2012). xCELLigence® data showed that treatment with 10mM Mg produced NHDFC migration profiles with clear differences between treatment types, with $MgCl_2$ treatment demonstrating the greatest level of migration efficiency (higher CI values for any given timepoint).

Slope data analysis (rate of migration as a function of time) for Mg aspartate treatment in the same dataset showed no statistically significant difference between Mg forms in the initial few hours. However, the full profile revealed a migratory plateau for Mg aspartate, while OMC continued to result in NHDFC migration. Notably, scratch assay data for Mg aspartate treatment did result in lower wound closure rates at the 12 and 18 h timepoints, but overall, data showed a similar endpoint (~40% reduction in wound area at 24 h) for all Mg treatments.

Literature points to Mg treatment having a beneficial effect on fibroblast migration. A recent investigation by Amberg *et al.*, (2018) details an experiment that examined migration of fibroblasts directly on Mg surfaces. They reported increased migration on Mg in comparison to plastic surfaces. As a result of their experimental setup, Mg concentrations (75mM) were far beyond those trialled in this thesis. Moreover, the authors used immunohistology to demonstrate that increased extra-cellular $MgCl_2$ levels (75mM) lead to increased focal adhesions in fibroblasts.

Keratinocyte cells originate in the stratum basale and transition up through the layers of the epidermis under normal conditions. They become more active during wound healing, when they migrate as flat monolayer sheets, and are an example of collective cell migration (Grada *et al.*, 2017). E-cadherin, shown to increase expression in response to hydrogel (/+ OMC) treatment, is a critical regulator of this process (Hwang *et al.*, 2012), indicating that HAKC migration was indeed stimulated in the 3D model. Elevated extracellular Mg, but not Ca, has been shown to stimulate proliferation of new-born murine keratinocytes and to extend the confluent phase of

epidermal cell growth beyond 10 days (Tennenbaum, *et al.,* 1990). These are in broad agreement with HAKC xCELLigence® migration data analysis that showed a migratory response to the inclusion of 10mM Mg in culture medium. Further analysis showed that Mg aspartate treatment resulted in the greatest overall migration efficiency (defined as greater CI values for any given timepoint). Impaired efficiencies were observed for OMC and $MgCl_2$ respectively in comparison to the Mg-free control. Wound closure data revealed a somewhat different result. 10mM Mg aspartate treatment resulted in the greatest reduction in wound area in 24h, in agreement with xCELLigence® data. However, $MgCl_2$, which had shown a comparable migration profile with OMC in the xCELLigence® data, demonstrated relatively poor performance in the wound healing assay on par with that of the Mg-free control. Literature does not offer any insight into this. However, the two assays performed were designed to be complimentary; not necessarily repeating the same set of conditions. The results observed may be due to metabolic processes related to Mg ATP binding. Notably, adhesion data were not obtained for fibroblast or keratinocyte cells. Such data may yield further insight, particularly the apparent preference that HAKCs demonstrated for Mg aspartate in these assays.

In order to facilitate regeneration of normal tissue in damaged areas, neo-vascularisation and collagen synthesis followed by re-epithelialisation are important processes of note (Day, 2005; Sasaki, *et al.,* 2017). Migration and proliferation are crucial steps in the highly complex and co-ordinated series of events that lead up to angiogenesis, where sprouts invade the newly ECM-rich wound and organise into a microvascular network throughout the granulation tissue. The process requires the activation of several signalling pathways converging on cytoskeletal re-modelling (Lamalice, *et al.,* 2007). Moreover, these processes are influenced by extra-cellular signals from the local microenvironment.

Data show that $MgCl_2$ treatment demonstrated significantly greater ($P \leq 0.05$) levels of tube formation in comparison to either OMC or Mg aspartate in HAECs. This is consistent with migration data, discussed previously. Importantly, this trend was the same at both the 12 and 24 h timepoints, suggesting a linear and stable effect over time. Of further importance was the fact that the Mg-free control produced no measurable tubes/structures. (It should be noted that some very small sprouts were apparent in the images, but not detectable by the software used to analyse these data).

There is some evidence in literature to suggest that angiogenic growth factors, such as FGF10, shown to be transcriptionally upregulated in response to hydrogel (/+ OMC) treatment, may result in activation of TRPM channels (Zeng *et al.*, 2015), previously investigated in Chapter Four. Previous discussion has outlined how literature presents conflicting information concerning the effects of TRPM7. The fact that its gene expression was unchanged by 10mM $MgCl_2$ and Mg aspartate treatment in Chapter Four while 10mM OMC resulted in a significant ($P \leq 0.05$) down-regulation suggests that TRPM7 does not play an important role in angiogenesis. It also suggests that OMC either is less bioavailable to cells via the TRPM7 channel, or satisfies Mg requirement with lowered channel expression occurring as a result. Certainly, the fact that OMC is outpaced by $MgCl_2$ in the tube formation experiment confirms cell preference for this form of Mg. It may also be possible that some interaction between TRPM6 and 7 occurred. Nevertheless, the data in this chapter coupled with Mg receptor data in the previous chapter strongly supports the hypothesis that Mg and the TRPM receptors are possible modulators of the angiogenic phenotype of microvascular endothelial cells proposed by Baldoli and Maier, (2012).

The extremely limited tube formation observed in the Mg-free control is in agreement with Maier *et al.*, (2007), who reported an impairment of the angiogenic balance "switch" as an effect of extremely low extra-cellular Mg in murine models. Although this study concerned tumour formation, it nonetheless remains a valid comparator due to the angiogenic processes at work, and one of the only reports in literature concerning the effects of TRPM, Mg and angiogenesis in animal models. More recent *in vitro* research has demonstrated up-regulation of the pro-inflammatory cytokine, IL-1α, in low-Mg cultured cells. It has been found to be a potent mediator of endothelial activation and inducer of angiogenic markers in endothelial cells (Salmeron *et al.*, 2016). Gene array data showed that this was down-regulated in response to hydrogel (/± OMC), suggesting that its expression was attenuated by the gel itself, and limited the potential effect of Mg. It is unclear if pro-angiogenic VEGFA expression was negatively affected in the same way that dermal fibroblasts and keratinocytes were in the 3D model when exposed to OMC. This presents an interesting candidate gene for further investigation.

It should be noted that endothelial cells are highly heterogenous, and as such, the responses of HAECs reported in this chapter are not absolutely reflective of the

behaviour of microvasculature. In addition, while the 3D skin model was a complex dermal co-culture, it did not integrate the vascular component, hence the multifaceted interplay between vascular and dermal cell types was not able to be ascertained.

Discussion has so far been limited to Mg supplementation as a beneficial agent. The experimental conditions used in this thesis exceed normal serum concentrations. Literature has also shown a wide range of Mg concentrations used in a variety of experimental setups, many of which also exceed this level. Hypermagnesemia and Mg toxicity are rare, but may occur as a consequence of conditions such as diabetes mellitus and sepsis (Van Laecke, 2018), particularly if dietary supplementation is continued. Due to its relatively minor electrophysiological and hemodynamic effects, intravenous Mg may be safely given in conditions of hypomagnesmia (Keren *et al.*, 1988).

5.4 Summary

The first section of this chapter examined transcriptional change in a 3D skin burn model as a result of the application of a hydrogel (/+ OMC). In terms of wound healing, hydrogel (/+ OMC) treatment at the provided concentration demonstrated a capacity to stimulate expression of a number of wound healing genes, while simultaneously suppressing expression of particular inflammatory markers. These data mark the initiation of the healing process in the first 24 h post-burn, and a reduction in inflammation may offer some relief from pain. Transcriptional change is not necessarily reflective of protein levels, however, with numerous processes including post-transcriptional modifications and other regulatory factors that affect translation and impact on functional effects.

In relation to fibrosis, context is required for gene expression analysis. As a first-aid measure, hydrogel (/+ OMC) is designed for emergency/short term application. Analysis at 24 h does give some indication of the likely effect at a transcriptional level, with suppression of inflammatory markers evident. However, longer timescale experiments examining the effect of the emergency/short term topical application of hydrogel (/+ OMC) are required. Again, protein levels must be ascertained in order to develop a true picture of the effects inferred from these data. In both cases, the absence of a known concentration of OMC in the hydrogel undoubtedly impedes

interpretation, and may only be considered in broad terms in relation to other concentrations examined and those presented in literature. It may even benefit from further optimisation.

The second part of this chapter concerned the comparative performance on the functional effects of OMC, $MgCl_2$ and Mg aspartate in a dermal model. While no mechanistic assays were performed, functional data provides clear evidence that elevated Mg levels may positively influence cell migration, growth, and facilitate regeneration of damaged dermal tissue. Possible mechanisms of action for further investigation may nevertheless be drawn from observed data and comparable literature. Both 2D and 3D cell culture models have their own intrinsic benefits and disadvantages. Although the complex nature of dermal wound healing lends itself to study using 3D models, 2D monoculture assays are nevertheless useful in ascertaining particular aspects of the process otherwise obscured in the co-culture. For example, gene expression data, while useful, could not be assigned to any particular cell type.

OMC treatment has shown possible beneficial properties in a complex model of wound healing that incorporates the cardiovascular compartment, albeit in an indirect non-contact way. These trends are indicative of cytokine activity that demonstrate anti-inflammatory properties that may extend beyond the models examined so far. These effects as a therapeutic application in systemic circulation will be examined in Chapter Six.

Chapter Six

An examination of the functional effects of OMC as part of a dietary supplement in a randomised controlled intervention in middle-aged women

6.1 Introduction

Given the weight of evidence showing the potential anti-inflammatory effects of Mg (the principal component of OMC) in model systems in previous chapters, **this chapter will investigate the potential beneficial effects of Mg supplementation in systemic circulation.** This was achieved through a human intervention carried out within the School of Health & Human Performance, DCU, in conjunction with Neal's Yard Remedies, UK. The company incorporated an undisclosed concentration of OMC into a functional food supplement drink; consisting of two functional health supplements (1) OMC and (2) *Boswellia serrata* (BS) extract. The purpose of this study was to examine the potential anti-oxidative and anti-inflammatory effects of these two natural products in addition to platelet activity in a cohort of 45-65 year old healthy females.

Platelets, as one of the primary focuses of this chapter, may act as sensitive markers of overall vascular health. Platelets are tiny fragments of larger cells (megakaryocyte stem cells), which circulate within the blood stream. Blood is essentially composed of two principle components: plasma and cells. Plasma is the liquid component of blood, comprising a mixture of water (90-92%), sugars, fats, gases, hormones and proteins (eg. albumin, immunoglobulins, etc.). Other nutrients, vitamins and electrolytes are also contained within plasma. Hematopoietic stem cells are capable of giving rise to all other blood cells (erythrocytes, white blood cells, and platelets) (Bryder *et al.*, 2006). The main function of platelets is to aid in primary haemostasis - blood clotting. They complete this by adhering to an injured vessel wall and then to each other to form a small clot. Recently, platelets have been implicated in the aetiology of many physiological conditions, including skin health (Elghblawi, 2018). Platelet activity may vary amongst individuals of varying health status/fitness/age. While platelets were originally associated with haemostasis, more recent research has linked them with disease processes, such as inflammation, innate immunity, CVD and tumour metastasis. Platelets exist in vast numbers in circulating human blood, on average one trillion are present at any one time in circulation. They resemble a discoid shape, approximately 2-4 μm in diameter, with a volume of approximately about 7 μm^3 (McFadyen and Kaplan, 2015). Platelets are capable of communication with

each other and other cell types via a range of bioactive substances secreted from their intracellular granules (Golebiewska and Poole, 2015).

Functional platelet disorders may involve any aspect of platelet physiology, with many different effects or outcomes. These include platelet number (thrombocytosis or thrombocytopenia); changes in platelet production/destruction; altered adhesion to sites of vascular injury and/or influence on hemostasis and wound healing; and altered activation or receptor functions, shape change, spreading and release reactions, pro-coagulant and anti-fibrinolytic activity (Lassila, 2016). For the purposes of this chapter, the term "platelet function" is broken down into two broad functional activities: platelet adhesion and platelet aggregation. Platelet aggregation is influenced by the mechanical shear environment within the vascular system, discussed previously. Such physical agonists, in addition to chemical agonists, such as adenosine diphosphate and serotonin, may trigger platelet activation (Nobili *et al.*, 2008).

Literature is supportive of the beneficial effects of both Mg and *Boswellia serrata* on cardiovascular health. In terms of Mg, literature reports induced release of vasodilators, NO and prostacyclin from endothelium due to increased Mg supplementation (Watson *et al.*, 1986). Ravn *et al.*, (1996) showed that administration of 0.5 – 1.0mM $MgSO_4$ resulted in a dose-dependent inhibition of platelet aggregation in healthy volunteers. An animal study showed Mg supplementation negated blood pressure rise in DOCA hypertensive rats. Moreover, the authors associated these findings with inhibition of platelet calcium uptake and decreased intracellular free calcium concentration (Kh *et al.*, 2000). *Boswellia serrata* (BS) is a plant that produces Indian frankincense. The plant is native to much of India and the Punjab region that extends into Pakistan. Boswellic acids (BA), in particular, constitute a group of unique pentacyclic triterpene acids with multiple pharmacological activities that confer anti-inflammatory properties (Siemoneit *et al.*, 2017). This intervention represents a novel investigation into the effects of these combined therapeutics, and any health information gained may be of relevance to the health and well-being market - promoting compression of morbidity.

6.1.2 Study design

Briefly, 16 healthy females (51.6 ± 4.1 years; Table 6.1)) participated in the study. One participant was pre-menopausal, 6 participants were peri-menopausal, and 7 participants were post-menopausal. The intervention was conducted in a randomised, single-blind manner. Following determination of physical parameters (height, weight) and baseline blood draw, participants were randomised into two separate groups, as outlined in Table 6.2, to either the treatment (OMC+BA) supplement or a glycerine placebo solution along with comprehensive instructions on supplement dosage for the 28-day period.

Table 6.1 Anthropometric measurements for the OMC+BA supplement human intervention.

	N	Range	Minimum	Maximum	Mean	Std. deviation
Age (years)	16	14	45	59	51.63	4.064
Height (m)	16	0.57	1.31	1.88	1.66	0.12
Weight (Kg)	16	65.40	55.00	120.40	71.23	17.22
BMI ($Kg \cdot m^{-2}$)	16	24.14	19.87	44.01	26.29	6.80

Table 6.2 Anthropometric measurements for the OMC+BA supplement human intervention as separate groups. 16 female participants were randomised into placebo and treatment groups prior to initiation of the 28-day intervention.

	Placebo group			Treatment group		
	N	Mean	Std. deviation	N	Mean	Std. deviation
Age (years)	8	54.29	3.30	8	49.25	3.34
Height (m)	8	1.65	0.05	8	1.65	0.17
Weight (Kg)	8	71.39	22.5	8	68.29	10.95
BMI ($Kg \cdot m^{-2}$)	8	26.33	8.37	8	25.40	5.60

All participants provided informed consent in compliance with the Helsinki Declaration. The experimental protocol was approved by the DCU ethics committee (DCUREC/2016/221). All participants were asked to adhere to the same pre-testing protocol in order to participate: no strenuous exercise 24 h pre-testing, no consumption of alcohol 48 h prior and not taking any prescription medications. Prior to testing all participants completed a survey to ensure suitability for testing and signed consent forms (see Appendix B).

Various biological parameters (platelet function, inflammatory biomarker profiling and oxidative stress in the blood) were assessed before and after the 28-day supplementation intervention (Figure 6.1). The platelet function test, and BMI fall under the physiological measurement. Biomarker studies were used examine cardiovascular and inflammatory health. Blood was drawn immediately prior to, and after, the 28-day supplementation period (treatment v placebo control) and functional analysis was carried out using the Impact-R system as detailed in Chapter Two. Results were expressed as the percentage of the well surface covered by platelet aggregates representing adhesion and the average size of the aggregates representing platelet aggregation. A one-way analysis of co-variance (ANCOVA) was used to compare post-intervention values differed between placebo and treatment groups, while controlling for differences observed at baseline. This was achieved by the generation of estimated marginal means, statistically eliminating the effect of "pre"-intervention effects. Levene's test and normality checks were carried out and the assumptions met. Post hoc tests (Bonferonni) were used to determine the significance of observed differences.

Effect size (the dimensionless measure of the magnitude of the difference in outcome between groups) inform clinicians about the magnitude of treatment effects (McGough and Faraone, 2009). Partial Eta^2 (η^2) values were used to determine effect size for each of the parameters in this chapter, and are comparable with Cohen's guidelines (Richardson, 2011):

<0.2 trivial

>0.2 <0.5 small

>0.5 <0.8 moderate

>0.8 large

The F-test of significance was used to test each main and interaction effect. F was calculated as between-groups variance divided by within-groups variance. If the resultant p-value was ≤0.05, then significant relationships existed.

Whilst not ideal due to the incorporation of dual therapeutic supplements, the intervention afforded further opportunity to study the effects of OMC, this time in human systemic circulation.

6.1.3 Study aims

Platelets have the ability to affect overall health in humans in both a positive and negative manner. Functional foods have been associated with platelet function and health, hence this study aimed to examine the effect of a functional drink supplement on platelet function/health, its protective capacity on thrombosis, and its overall effect on systemic inflammation and Reactive Oxygen Species (ROS).

Hence, the overall aims of this chapter include:

- To assess platelet function (adhesion and aggregation) in participants as a result of consumption of the supplement over a 28-day period.
- To assess protein biomarker signature from platelet-poor plasma samples of participants as a result of consumption of the supplement over a 28-day period using a panel of inflammatory markers (Olink, Sweden).
- To assess the effect on ROS in plasma from participants as a result of consumption of the supplement over a 28-day period.

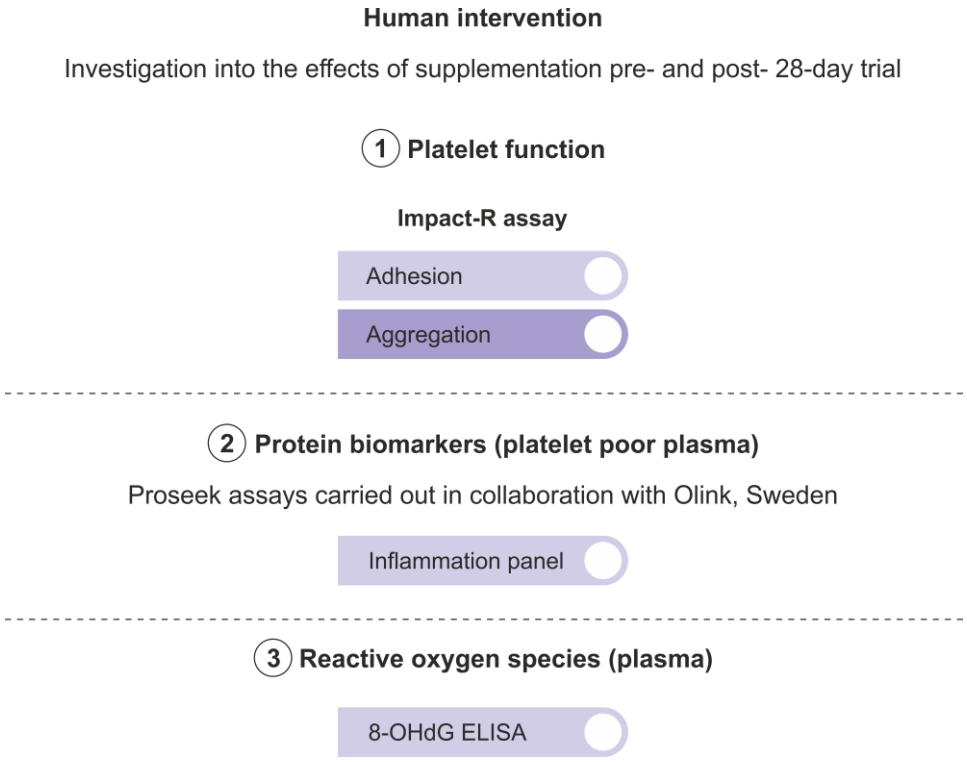

Figure 6.1 Diagram outlining the experimental approach taken in this chapter

6.2 Results

6.2.1 The effect of OMC + *Boswellia serrata* supplementation on platelet function in a randomised population of 16 healthy women (45-65 years)

Blood was drawn immediately prior to, and after, the 28-day supplementation period (treatment v placebo control) and functional analysis was carried out using the Impact-R system. Adhesion was defined as the percentage of the observable well surface covered by platelets. Aggregation was defined as the area (μm^2) of aggregated platelets on the observable well surface. Both placebo and treatment groups presented notably higher surface coverage and aggregate size at baseline than typical levels (7.5% and 25 μm^2 respectively).

6.2.1.1 Platelet adhesion

A significant difference was observed between placebo and treatment groups (estimated marginal means: 76.5 vs 71.3% POST PLACEBO vs. POST

TREATMENT respectively; P=0.001) in terms of change in platelet adhesion as a function of PRE values for platelet adhesion [F=141337 P=0.001. The effect size (partial η^2) was 0.56 interpreted as a moderate effect (see Figure 6.2).

6.2.1.2 Platelet aggregation

A significant difference was observed between placebo and treatment groups (estimated marginal means: 130.792 vs 94.458 μm, POST PLACEBO vs. POST TREATMENT respectively; P=0.05) in terms of change in platelet aggregation as a function of PRE values for platelet aggregation [F=1731.293, P=0.000]. The effect size (partial η^2) was 0.47, interpreted as a small effect (see Figure 6.2).

6.2.2 The effect of OMC + *Boswellia serrata* supplementation on protein biomarker concentrations in a randomised population of 16 healthy women (45-65 years)

Blood samples were drawn pre and post 28-day intervention and centrifuged to produce platelet-poor plasma (PPP). Protein biomarker expression of PPP was assessed using the Proseek® Inflammatory protein biomarker panel (Olink, Sweden). This allowed simultaneous evaluation of the expression levels of 96 protein biomarkers in each sample. Olink Proseek® results are typically expressed as normalised protein expression (NPX) on a log2 scale. Therefore, a normalised increase of 1 equals a two-fold increase in protein concentration. However, for the purposes of these analyses, NPX values were converted into linear scale: 2^{NPX} = linear NPX and assessed using SPSS v 24.0.

The expression profiles of these proteins were analysed pre- and post-intervention. Of the 32 samples analysed (16 pre- and 16 post-), 76 out of 92 proteins were detected. Due to technical issues identified with the BDNF assay, no data were reported for this particular analyte in any samples. One participant sample did not pass the quality control check and was therefore excluded from further analysis. Concentrations of 3 proteins differed significantly between pre- and post- conditions when analysed using a one-way ANCOVA (see Figure 6.2).

TGF-α

There was a significant difference between the placebo and treatment groups (estimated marginal means: 13.79 vs 9.94 NPX POST PLACEBO vs. POST TREATMENT respectively; P=0.026) in terms of change in TGF-α concentrations as a function of PRE concentrations for TGF-α [F=13.726, P=0.003]. The effect size (partial η^2) was 0.53, interpreted as a moderate effect for the decrease in TGF-a in the treatment group (see Figure 6.3).

Axin-1

There was a significant difference between the placebo and treatment groups (estimated marginal means: 3.47 vs 7.03 NPX POST PLACEBO vs. POST TREATMENT respectively; P=0.045) in terms of change in Axin-1 concentrations as a function of PRE concentrations for Axin-1 [F=4.979, P=0.844]. The effect size (partial η^2) was 0.29, interpreted as a small effect for the increase in Axin-1 in the treatment group (see Figure 6.3).

STAMPB

There was a significant difference between the placebo and treatment groups (estimated marginal means: 9.07 vs 14.96 NPX POST PLACEBO vs. POST TREATMENT respectively; P=0.042) in terms of change in STAMBP as a function of PRE concentrations for STAMBP [F=5.207 data, P=0.812]. The effect size (partial η^2) was 0.30, interpreted as a moderate effect for the increase in STAMPB in the treatment group (see Figure 6.3).

6.2.3 The effect of OMC + *Boswellia serrata* supplementation on ROS levels in a randomised population of 16 healthy women (45-65 years)

8-hydroxydeoxyguanosine (8-OHdG), an oxidised nucleoside of DNA resulting from a hydroxyl radical attack on guanine, is the most frequently detected and studied DNA lesion (Wu *et al.,* 2004). It is well accepted that these free radical-induced oxidative lesions are potential biomarkers of oxidative DNA damage.

In the experiments carried out in this chapter, 8-OHdG was used as a biomarker of oxidative DNA damage caused by ROS. An enzyme-linked immunosorbent assay

(ELISA) was used for quantification of water-soluble 8-Hydroxydeoxyguanosine (8-OHdG) in plasma samples using an ELISA kit (Cloud Clone, USA). The kit utilised a competitive inhibition enzyme immunoassay technique. Samples were measured in triplicate against an internal standard curve read at ƛ450 nm.

There was no significant difference between the placebo and treatment groups (estimated marginal means: 213.38 vs 201.06 POST PLACEBO vs. POST TREATMENT respectively; P=0.711) in terms of change in 8-OHdG concentrations as a function of PRE concentrations for 8-OHdG [F=8.440, P=0.102]. The effect size (partial η^2) was 0.01, interpreted as a trivial effect (see Table 6.4 and Figure 6.4).

Figures 6.2 – 6.4:

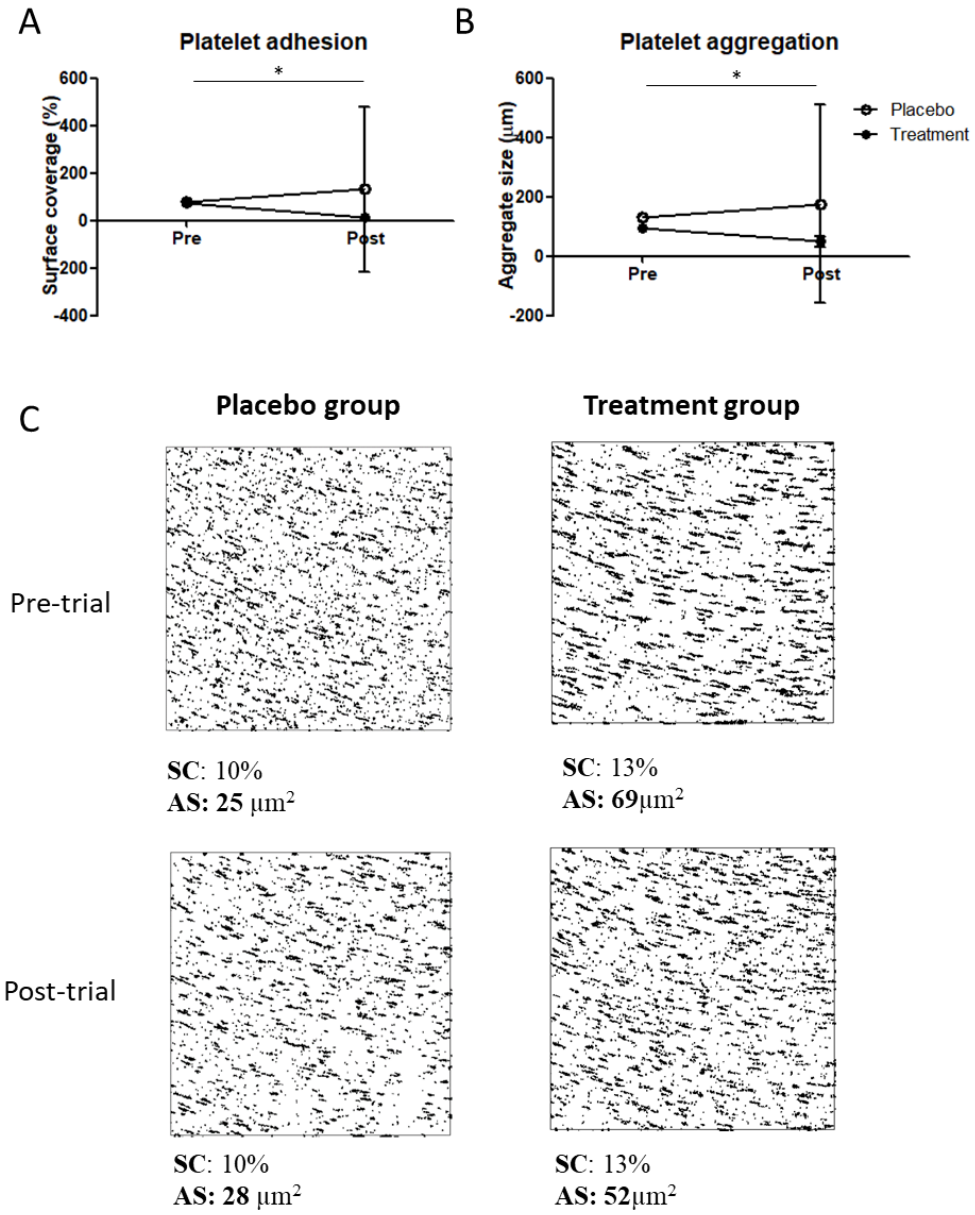

Figure 6.2 Platelet adhesion and aggregation as markers of overall health in placebo and treatment groups post- 28-day intervention. (A) Plot represents platelet adhesion measured as surface coverage using the Impact-R cone and plate analyser in placebo and treatment groups post-intervention with estimated marginal means calculated by ANCOVA. (B) Plot represents platelet aggregation measured as aggregate size using the Impact-R cone and plate analyser in placebo and treatment groups post-intervention with estimated marginal means calculated by ANCOVA. (C) Representative images of *ex vivo* Impact-R platelet adhesion (surface coverage) and aggregation (aggregate size). * P≤0.05

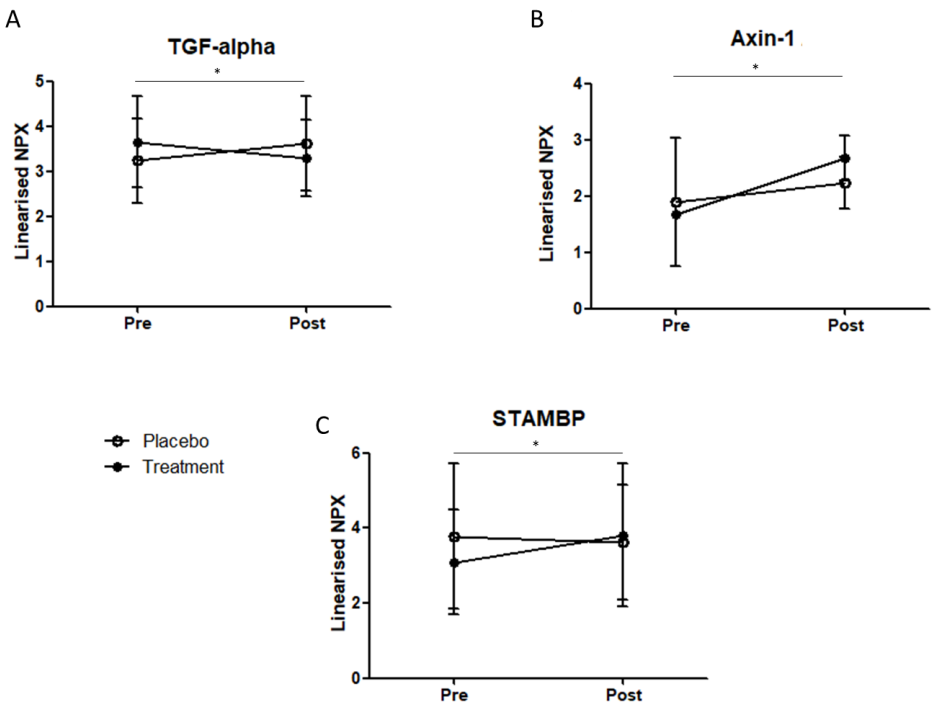

Figure 6.3 Plot representations of significantly changed protein concentrations between placebo and treatment groups post-intervention. Plots represent protein concentrations measured by Proseek® (Olink, Sweden) in placebo and treatment groups pre- and post-intervention (A) TGF-α significantly (P≤0.05) increased in the placebo group post-intervention (B) Axin-1 significantly (P≤0.05) increased in the treatment group post-intervention (C) STAMBP significantly (P≤0.05) increased in the treatment group post-intervention. * P≤0.05

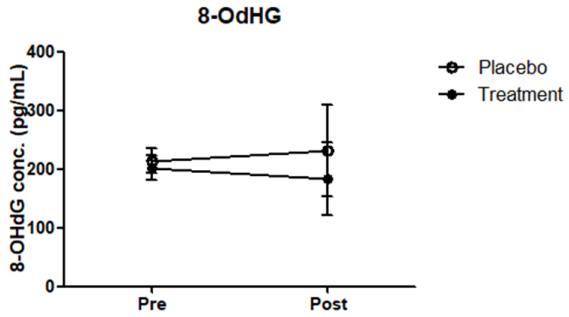

Figure 6.4 Measurement of 8-hydroxy-2'-deoxyguanosine (8-OHdG) as a biomarker for oxidative stress in placebo and treatment groups post-intervention. Plot represents 8-OHdG concentrations measured by ELISA in placebo and treatment groups post-intervention with estimated marginal means calculated by ANCOVA.

6.3 Discussion

Platelet function is an important index in the understanding of hemostasis and thrombosis and may also yield important information relating to overall health. This study employed a human intervention to explore the differences in platelet function as a result of supplementation over a 28-day period. The main findings support the use of OMC and BA as a beneficial dietary supplement, with notable changes in platelet function observed as a result of the intervention. *Ex vivo* measurement of platelet adhesion was significantly different between treatment and placebo groups post-intervention. Statistical analysis revealed a 2.5% increase in adhesion in the raw data for the placebo group, while the treatment group underwent a 2.7% increase. Analysis by ANCOVA accounted for differences at baseline, and revealed that this difference was statistically significant ($P \leq 0.05$) between groups. An effect size estimate provides an interpretable value on the direction and magnitude of an effect of an intervention. At 0.560, this was interpreted as a moderate effect. Nevertheless, the data strongly suggest that supplementation at the prescribed dose results in reduced platelet adhesion over a 28-day period. It is notable that platelets demonstrated greater than average adhesion response in both groups prior to beginning the intervention. This is likely an age-related occurrence, where platelet activity is increased with age (particularly middle-age), in line with data published by Jones (2016) and driven by changes in hematopoietic tissue, blood composition and vascular health. Daily supplementation with OMC and BS brought the treatment group to within "normal" parameters. Platelet adhesion concerns a collaborative effort of various platelet receptors, fundamentally leading to platelet activation and aggregation. Similarly, platelet aggregation was shown to decrease significantly ($P=0.05$) post-intervention.

Due to the inclusion of dual therapeutics in the supplement (i.e. OMC and BS), observed effects on platelet function may not be solely attributed to either Mg or BAs. However, reported effects in literature may help to illuminate this. Dong *et al.*, (2008) demonstrated that $MgSO_4$ up-regulates ultra-large von Willebrand factor (vWF) proteolysis under shear stress conditions. They hypothesised that high $MgSO_4$ reduces vWF binding to collagen. vWF was a critical component of the Impact-R platelet assay, forming the active surface upon which platelets could activate and adhere. At areas of high shear rates (>1000s-1) such as small arteries or atherosclerotic vessels, interaction between vWF and platelet receptor GPIbα is required to reduce the velocity

of fast moving platelets, enabling the formation of additional bonds and definitive arrest of platelets (Ruggeri, 2007). It is possible that this mechanism was compromised by the inclusion of OMC, leading to reduced levels of adhesion. Platelet activity may also be attenuated as a result of the antagonistic relationship between Mg^{2+} and Ca^{2+}, which plays a crucial role in platelet activation (Hwang, *et al.*,1992; Sheu *et al.*, 2002). In contrast, a sub-group of BAs, characterised by an 11-keto group, raises intracellular Ca^{2+} concentrations and causes moderate aggregation of human platelets (Siemoneit *et al.*, 2017). With specific regard to aggregation, BAs induce release of arachidonic acid and the synthesis of 12-H(P)ETE in human platelets by unique Ca^{2+}-independent routes (Poeckel *et al.*, 2006; Siemoneit *et al.*, 2017) leading to aggregation.

Diet may also impact platelet function. It is possible that participants' diet, particularly 24 h prior to assaying, may have influenced the results. Thus, the lack of dietary control in the present study represents an important limitation to the study design. Better dietary control will be necessary in order to clarify results of any future experiments. Nevertheless, data from these experiments indicates that the supplement, taken at the dose prescribed and examined under the conditions set out, induces a moderately beneficial effect on platelet function in comparison with the placebo control; in effect, attenuating both adhesion and aggregation when measured *ex vivo* using the assays described.

The effect of the supplement on platelet poor-plasma (PPP) -based protein biomarkers was examined in collaboration with Olink, Sweden. The Proseek® multiplex assay is a sensitive and specific assay developed for biomarker screening which enabled the screening of 96 protein biomarkers related to inflammation. Of these, only 3 of the 72 detected proteins demonstrated significant change between groups in response to supplementation when baseline differences between groups were accounted for. The inflammatory markers measured were an indicator of sub-clinical health and not a disease diagnostic or prognostic. Instead, these act as a measure of cardiovascular competence and overall physiological health in response to the supplement intervention.

The significant ($P \leq 0.05$) increase in the treatment group of Axis inhibition protein 1 (Axin-1), a negative regulator of the Wnt/β-catenin pathway is of particular relevance

for platelet function. Specifically, the Wnt3a ligand has been shown to inhibit platelet adhesion, activation, dense granule secretion, and aggregation. Axin-1 acts by binding to β-catenin and glycogen synthase kinase-3 (GSK-3) to promote β-catenin phosphorylation and subsequent degradation (Li *et al.*, 2012). This behaviour aligns with reduced platelet activity, discussed previously, and may represent the mechanism through which this effect is achieved. Interestingly, Montes de Oca *et al.*, (2014) reported that elevated Mg concentrations served to inhibit phosphate-induced activation of Wnt/β-catenin signalling pathway in vascular smooth muscle cells. More recently, Hung *et al.*, (2019) has reported activation of the canonical pathway in bone marrow stromal cells with 10mM Mg. While these are different cell lines to the present study, these data indicate that Mg has potent effects on key pathways.

Transforming growth factor alpha (TGF-α) was also significantly increased ($P \leq 0.05$) post-intervention. Statistical analysis showed that the largest change (27.9% decrease) occurred in the placebo group, while TGF-α in the treatment group increased by only 3.67%. A moderate effect size (0.534) was determined for this protein. As changes were observed in both groups, interpretation of the cause is difficult to determine. However, the decline observed in the placebo group may indicate a maintenance effect elicited by the supplement.

TGF-α has been shown both *in vivo* and *in vitro* to accelerate events associated with cell migration and epidermal wound repair (Cheng *et al.*, 2008). Notably, TGF-α was transcriptionally down-regulated in untreated skin burn in Chapter Five, but demonstrated increased transcriptional levels with the application of hydrogel (/+ OMC). No literature relating to the effects of BAs on this protein was available.

Concentrations of the deubiquitinase enzyme, STAM-binding protein (STAMBP) were significantly different post-intervention between treatment and placebo groups. No associations with either Mg or BAs are reported in literature, to the best of my knowledge. However, imbibement of the supplement at the stated dosage for the duration of the intervention period clearly resulted in increased concentrations of the protein. STAMBP plays a key role in cell surface receptor-mediated endocytosis and sorting, with its expression associated with accumulation of ubiquitin-conjugated protein aggregates (McDonell *et al.*, 2013). It is unclear how this relates to

cardiovascular health, but may represent a possible novel target for future experiments.

Different biological responses to oxidative species depend on the ROS and on the tissue-specific sensitivity to oxidative damage. In systemic circulation, platelet function is finely regulated by a balance between the vasculature's redox environment and the oxidative processes that occur within it (Murphy *et al.,* 2014). Data throughout this thesis points to Mg, including OMC, eliciting a capacity to attenuate ROS. Indeed, Mg was previously assayed for such a capacity in Chapter Four, using DHE staining in HAECs. The assay conducted in this chapter, however, represented a very different paradigm. Here, detection of oxidised guanine residues in plasma samples was indicative of oxidative damage throughout the entire body, affecting multiple different cell types. Moreover, it deals with the incorporation of dual therapeutics. Therefore, while this discussion maintains a cardiovascular focus, this parameter largely relates to total health. Measurement of 8-OHdG plasma concentrations pre and post-intervention revealed that the treatment group showed no significant ($P \leq 0.05$) change in 8-OHdG concentrations compared to the placebo group. These data suggest that consumption of the supplement mixture does not result in reduced 8-OHdG concentrations in women aged between 45 and 65. 8-OHdG concentrations have been shown to increase with age (Hamilton *et al.,* 2001). Although they may be produced from apoptosis, they primarily arise from the repair of oxidative damage to methylated guanine. As a result, 8-OHdG may be interpreted as a measure of the type of epigenetic modifications discussed in previous chapters. Specifically, their presence may represent re-writing/erasing of epigenetic marks. This permits an alternative perspective on the data, but one in which consumption of the supplement again exerted no effect.

Measured increases in 8-OHdG arising from oxidative damage to DNA has been attributed to smoking and lack of physical activity. (Cao *et al.,* 2016). In the intervention detailed in this chapter, low participant numbers did not permit meaningful statistical analyses relating age, BMI, smoking or alcohol intake to the functional indices measured. At only 16 participants, resultant statistical power to determine data distribution and significant change between groups was reduced as a consequence. This was evident in the large effect sizes demonstrated. Certainly, a more extensive intervention with larger participant numbers would confer added

statistical weight to any findings. Other limitations include dietary control, as discussed above, and the fact that the daily intake of the supplement was not independently verified. In totality, these data are preliminary but promising for future work.

6.4 Summary

Data in this chapter show that the supplement, taken for 28 days at the directed dose, resulted in significantly ($P \leq 0.05$) reduced platelet adhesion and platelet aggregation. All participants in this intervention were reportedly healthy females, with normal ability to react to vascular injury. However, over-accumulation of platelets at sites of atherosclerotic plaque rupture is one of the key pathogenic events triggering arterial thrombus formation. This may lead to acute myocardial infarction or ischemic stroke in unhealthy individuals. As such, it is possible that the observed reduction in adhesion due to the supplement intervention may serve to reduce aggregation in larger populations and hence reduce thrombotic tendencies.

Inflammatory biomarker analysis in PPP revealed very little change overall at the conclusion of the intervention. Of the 96 proteins assayed, the levels of 3 proteins (TGF-α, AXIN-1 and STAMBP) were significantly altered post-intervention. The largest change occurred in the placebo group for TGF-α, which may suggest an attenuative effect exhibited by the supplement. Although both therapeutic substances, OMC and BS, previously reported anti-inflammatory properties in previous experiments and in literature respectively, little of these appeared to translate into tangible effects *in vivo* at the dose prescribed in this intervention.

While levels of 8-OHdG varied in individual participants, no significant difference between groups was determined. Hence, no change in ROS levels was achieved by consumption of the supplement, in agreement with prior ROS experiments outlined in this thesis. As such, doubt is cast over the potential anti-oxidative properties of OMC.

The work carried out in this chapter represented an initial foray into the effects of OMC in human participants. Nevertheless, a number of limitations are highlighted. The effects of Mg and *Boswellia serrata* are indistinguishable from each other due to the nature of the supplement mixture, and it is unknown if the observed effects are

separate, antagonistic or synergistic. Further investigation into the separate effects of each of the two components is required. Knowledge of their concentrations may allow optimisation of the functional effects observed.

Chapter Seven

Overall summary

7.1 Final discussion

This thesis set out to explore the juncture between vascular inflammation, epigenetics and magnesium supplementation. The efficacy of Mg as a therapeutic agent to combat inflammatory response/atherogenesis was investigated, with particular emphasis given to OMC. This was ascertained through the development of increasingly complex models of vascular injury, in which a number of key genes and mechanisms involved in epigenetically-regulated vascular ageing were identified. Further investigations were carried out on the wound healing and pro-angiogenic potential of Mg, to the point where OMC was trialled on a small number of participants as a potential therapeutic supplement. In completing these objectives, a comprehensive picture of the role of Mg as a potential anti-inflammatory agent was drawn.

Initial work was carried out to identify key parameters, along which, the main goals of this thesis could be progressed. Analysis of the effects of OSS on HAECs revealed a time-dependent epigenetic response. The 48 h timepoint was identified as the most active, whereby changes in expression of a greater number of epigenetically relevant genes were noted. These included a number of overlapping predicted mRNA:miRNA interactions of interest. As such, the 48 h timepoint was used for subsequent investigations with Mg. Additional timepoints may have provided further information, but time and cost considerations prevented their inclusion beyond the initial investigation. Determination of the efficacy of OMC was another key part of this thesis. OMC treatment was found to be most effective in HAECs at 10mM. As such, all other experiments were carried out using this concentration, except in cases where the concentration was unknown due to manufacturing partnerships. Together, these initial parameters set the stage for deeper investigation.

7.2 The efficacy of OMC as an anti-inflammatory agent

The data presented in these chapters creates a more informed picture of the efficacy of Mg as an anti-inflammatory therapeutic. Inferences drawn suggest that Mg (in any of the forms assayed) plays an important role in epigenetically-regulated CVD, thus far unexplored in literature. Data demonstrate that 10mM Mg treatment of HAECs in an experimental setup that mimics a pro-atherosclerotic/pro-inflammatory system stimulates up-regulation of a number of Mg receptor genes (TRPM7, CNNM1 and

CNNM3). While such activity may be expected, the exclusion of other Mg receptors demonstrated the involvement of more selective pathways through which the inferred anti-inflammatory effects occurred.

With particular regard to OMC, it was found to elicit a beneficial anti-inflammatory effect in line with comparator forms. Interestingly, in most cases, OMC was out-performed by $MgCl_2$. Literature cites numerous studies using $MgCl_2$ and its effects are widely acknowledged. OMC is stated to exist in an ionic form, which was expected to result in increased bioavailability manifested as increased cell adhesion and migration. Data acquired in these experiments did not support this. The dissociation of more standardised compound Mg forms in media appeared to elicit an equal or greater effect than "ionic" OMC. The reactive nature of ions may induce the formation of more stable compounds within OMC over time, rendering its bioavailability on par with other forms. Indeed, background sweeps using the xCELLigence® did not signal any noticeable decrease in electrical impedance due to the increased presence of electrolytes in the medium.

Due to the fact that OMC existed as a complex mixture of minerals, effects observed in this thesis involving OMC may not be solely attributable to Mg or any other individual component within the mix. Nevertheless, as the primary constituent in OMC, Mg served as the most appropriate element to compare against. This was confirmed by largely consistent data that strongly pointed to Mg as the principle active substance in seawater-derived OMC, as opposed to the numerous other trace elements contained within the mineral complex. Nevertheless, the presence of these other minerals, particularly calcium, may have influenced the results attained, particularly so in cases where no Mg comparator was used. Mg is a natural calcium antagonist, and calcium-magnesium ratio is a critical factor that influences cell migration. In the experiments carried out for this thesis, calcium levels were not controlled for. As a mineral complex, OMC contained approximately 0.003mM Ca^{2+}, when normalised to 10mM Mg. Such small levels were unlikely to contribute to the effects observed, and calcium levels in all experiments were essentially that of the cell culture medium.

While no overall consensus was found, selection of appropriate comparators was based on bioavailability reported in literature. This was limited to two ($MgCl_2$ and Mg aspartate) due to the increasing experimental complexity of each additional

comparator. Comparison with other Mg supplements was not possible due to their complex composition, which included addition of sugars and other packing ingredients, as well as differing concentrations overall.

7.3 Summary

- In a pro-inflammatory, pro-atherosclerotic experimental model of vascular injury, HAECs exhibited an epigenetic response in a time-dependent manner.
- Response to OSS was most distinct at 48 h, at which point, changes in expression of a number of epigenetically relevant genes were noted.
- These include a number of overlapping predicted mRNA:miRNA interactions of interest, including suggestion of a possible timeline for miRNA regulation of DOT1L.
- Investigation of OMC against appropriate Mg comparators strongly pointed to Mg as the principle active substance in seawater-derived OMC, as opposed to the numerous other trace elements contained within the mineral complex.
- Data demonstrated that 10mM Mg treatment of HAECs in an experimental setup that mimics a pro-atherosclerotic, pro-inflammatory system stimulated up-regulation of a number of Mg receptor genes (TRPM7, CNNM1 and CNNM3).
- Exclusion of Mg receptors MagT1, TRPM6 and CNNM2 demonstrated the involvement of more select pathways through which inferred anti-inflammatory effects occur.
- In an *in vitro* model of wound healing that incorporated the cardiovascular compartment, hydrogel (/+ OMC) treatment at the provided concentration demonstrated a capacity to stimulate expression of a number of wound healing genes, while simultaneously suppressing transcriptional expression of particular inflammatory markers at 24 h.
- Functional data showed clear evidence that magnesium constitutes an important molecular constituent in this process, leading to increased cell migration and growth response, and facilitating regeneration of damaged dermal tissue. As such, the inclusion of magnesium as a therapeutic aid in the stabilisation of burn injuries is a warranted addition.

- A human trial to assess the beneficial effects of a magnesium-based supplement mixture on vascular competence indicated that magnesium elicits beneficial effects on platelets and the vascular compartment through reduced platelet adhesion and aggregation.

7.4 Limitations and future work

As with any research study, a number of limitations were present. In this section, these limitations will be discussed, and additional experiments outlined chapter by chapter.

7.4.1 Chapter Three and Four limitations and future work

Single replicate array data used in both of these chapters is not sufficient to validate trends observed in preliminary analysis. Moreover, gene expression data alone is not sufficient to discern mechanisms of action. These data did, however, facilitate the identification of a number of target genes and mechanisms that should be followed up in future work. In addition, a number of miRNA of interest were identified in this study, but not subject to more rigorous investigation. To this end, a number of experiments are recommended:

A. Methylome profiling of HAECs exposed to 10 dyne/cm^2 laminar and oscillatory flow conditions

Analysis of the enormous scale of epigenetic modification and the resultant complex patterns of methylation in the genome (methylome) were limited to only those concerned with epigenetic enzymes and modification factors, as per the objectives set out. However, these were limited to those commercially available in an array format for standard qRT-PCR. Advances in microarray and next-generation sequencing technologies permit the construction of genomic maps of DNA methylation at even single-cell resolution, are available commercially. Hence, although beyond the scope of this thesis, it may provide clearer insight into the mechanisms discussed, as well as identifying other target mRNA/miRNA not included in the analyses performed.

B. Western blot analysis on select proteins of interest to verify translational alteration by miRNA

Gene expression data alone is not sufficient to discern the mechanisms of action. While certain genes may be up- or down-regulated, mechanisms within the cell may ensure the destruction or translation of their respective proteins regardless. This is particularly important with respect to miRNA and its mode of action. The experimental data presented in Chapters Three and Four should be followed up by Western blot assay to assess the translational reality. In particular, data for genes such as TRPM7 and DOT1L would benefit from an additional mechanistic analysis.

C. siRNA silencing of select target genes

The addition of small interfering RNA (siRNA) to cells is a technique used to significantly decrease (but not eliminate) the expression of a selected gene in that cell to the point that it is effectively functioning without it. This is commonly referred to as "silencing" of the gene in question, and allows down-stream examination of the effects of that gene in its virtual absence.

Silencing of select genetic targets identified in these chapters would allow further elucidation of their action/effect, particularly Mg transporters and the exact mechanism through which OMC is working in comparison to other forms.

Chapter Five limitations and future work

Wound healing and fibrosis gene array data presented in Chapter Five were not supported by any other genetic assay. Such arrays can potentially yield false positives, hence the requirement to confirm results by other means. As such, the following experiments are recommended:

A. Validation of wound healing and fibrosis gene array data by individual qRT-PCR assay.

Individual investigation of some genes in previous chapters revealed differences in expression levels when analysed in isolation. Hence, confirmation of the expression levels observed in the array data would lend greater confidence to the findings.

B. Western blot analysis on select proteins of interest to verify translational alteration by miRNA

As in Chapters Three and Four, the experimental data presented in Chapter Five should be followed up by Western blot assay to assess the translational effects at a protein level.

C. siRNA silencing of select target genes

As in Chapters Three and Four, the experimental array data would be bolstered by an additional, more mechanistic, approach. Gene silencing of select targets, such as the potential anti-inflammatory and collagen-producing genes identified, would enable such a functional analysis.

Chapter Six limitations and future work

The clinical study carried out in Chapter Six was extremely limited at only 16 participants, and yielded poor statistical power as evidenced by the small effect sizes. In addition, the presence of *Boswellia serrata* was confounding factor in determining the effects of OMC. As such, the following approach is recommended:

A. Repeat of the human trial using greater participant numbers and employing a supplement without *Boswellia serrata*

Greater participant numbers would facilitate increased statistical power in subsequent analyses.

The effects of OMC and *Boswellia serrata* are indistinguishable from each other due to the nature of supplement mixture, and it is unknown if the observed effects are separate, antagonistic or synergistic. Removal of *Boswellia serrata* from the

supplement mixture would enable a clearer understanding of the effect directly attributable to OMC.

Bibliography

Abd, E., Yousef, S. A., Pastore, M. N., Telaprolu, K., Mohammed, Y. H., Namjoshi, S., Grice, J. E. and Roberts, M. S. (2016) Skin models for the testing of transdermal drugs, *Clin. Pharmacol.* Dove Medical Press, **8**, pp. 163–176.

Adamian, A. A., Dobysh, S. V, Kilimchuk, L. E., Shandurenko, I. N. and Chekmareva, I. A. (2004) Development of new biologically active dressings and methodology of their use., *Khirurgiia (Sofiia).* Russia (Federation), (12), pp. 10–14.

Aird, W. C. (2007a) Phenotypic heterogeneity of the endothelium: I. Structure, function, and mechanisms, *Circ. Res.* 2007/02/03, **100**(2), pp. 158–173.

Aird, W. C. (2007b) Vascular bed-specific thrombosis, *J. Thromb. Haemost.* 2007/08/01, **5 Suppl 1**, pp. 283–291.

Alexander, J. S. and Elrod, J. W. (2002) Extracellular matrix, junctional integrity and matrix metalloproteinase interactions in endothelial permeability regulation, *J. Anat.* 2002/08/07, **200**(6), pp. 561–574.

Alkagiet, S. and Tziomalos, K. (2017) Vascular calcification: the role of microRNAs., *Biomol. Concepts*. Germany, **8**(2), pp. 119–123.

Allison, K. (2002) The UK pre-hospital management of burn patients: current practice and the need for a standard approach., *Burns*. Netherlands, **28**(2), pp. 135–142.

Almousa, L. A., Salter, A. M. and Langley-Evans, S. C. (2018) Magnesium deficiency heightens lipopolysaccharide-induced inflammation and enhances monocyte adhesion in human umbilical vein endothelial cells., *Magnes. Res.* England, **31**(2), pp. 39–48.

Altura, B. M., Shah, N. C., Shah, G. J., Zhang, A., Li, W., Zheng, T., Perez-Albela, J. L. and Altura, B. T. (2014) Short-term Mg deficiency upregulates protein kinase C isoforms in cardiovascular tissues and cells; relation to NF-kB, cytokines, ceramide salvage sphingolipid pathway and PKC-zeta: hypothesis and review., *Int. J. Clin. Exp. Med.*, **7**(1), pp. 1–21.

Amberg, R., Elad, A., Rothamel, D., Fienitz, T., Szakacs, G., Heilmann, S. and Witte, F. (2018) Design of a migration assay for human gingival fibroblasts on biodegradable magnesium surfaces., *Acta Biomater*. England, **79**, pp. 158–167.

Andrews, C. J., Kempf, M., Kimble, R. and Cuttle, L. (2016) Development of a Consistent and Reproducible Porcine Scald Burn Model, *PLoS One*. Public Library of Science, **11**(9), pp. e0162888–e0162888.

Arciniegas, E., Ponce, L., Hartt, Y., Graterol, A. and Carlini, R. G. (2000) Intimal thickening involves transdifferentiation of embryonic endothelial cells., *Anat. Rec.* United States, **258**(1), pp. 47–57.

Baccarelli, A. A. and Byun, H.-M. (2015) Platelet mitochondrial DNA methylation: a potential new marker of cardiovascular disease., *Clin. Epigenetics*. Germany, **7**, p. 44.

Bailey, K. A., Haj, F. G., Simon, S. I. and Passerini, A. G. (2017) Atherosusceptible Shear Stress Activates Endoplasmic Reticulum Stress to Promote Endothelial Inflammation, *Sci. Rep.*, **7**(1), p. 8196.

Baldoli, E., Castiglioni, S. and Maier, J. A. (2013) Regulation and function of TRPM7 in human endothelial cells: TRPM7 as a potential novel regulator of endothelial function, *PLoS One*. 2013/03/28, **8**(3), p. e59891.

Baldoli, E. and Maier, J. A. M. (2012) Silencing TRPM7 mimics the effects of magnesium deficiency in human microvascular endothelial cells., *Angiogenesis*. Germany, **15**(1), pp. 47–57.

Banai, S., Haggroth, L., Epstein, S. E. and Casscells, W. (1990) Influence of extracellular magnesium on capillary endothelial cell proliferation and migration., *Circ. Res.* United States, **67**(3), pp. 645–650.

Barres, R., Osler, M. E., Yan, J., Rune, A., Fritz, T., Caidahl, K., Krook, A. and Zierath, J. R. (2009) Non-CpG methylation of the PGC-1alpha promoter through DNMT3B controls mitochondrial density., *Cell Metab.* United States, **10**(3), pp. 189–198.

Bazzoni, G. and Dejana, E. (2004) Endothelial cell-to-cell junctions: molecular organization and role in vascular homeostasis, *Physiol Rev*. 2004/07/23, **84**(3), pp. 869–901.

Belair, D. G., Whisler, J. A., Valdez, J., Velazquez, J., Molenda, J. A., Vickerman, V., Lewis, R., Daigh, C., Hansen, T. D., Mann, D. A., Thomson, J. A., Griffith, L.

G., Kamm, R. D., Schwartz, M. P. and Murphy, W. L. (2015) Human vascular tissue models formed from human induced pluripotent stem cell derived endothelial cells., *Stem Cell Rev.* United States, **11**(3), pp. 511–525.

Belin, R. J. and He, K. (2007) Magnesium physiology and pathogenic mechanisms that contribute to the development of the metabolic syndrome., *Magnes. Res.* England, **20**(2), pp. 107–129.

Benda, N. M. M., Seeger, J. P. H., van Lier, D. P. T., Bellersen, L., van Dijk, A. P. J., Hopman, M. T. E. and Thijssen, D. H. J. (2015) Heart failure patients demonstrate impaired changes in brachial artery blood flow and shear rate pattern during moderate-intensity cycle exercise, *Exp. Physiol.* John Wiley & Sons, Ltd (10.1111), **100**(4), pp. 463–474.

Berger, M. M., Rothen, C., Cavadini, C. and Chiolero, R. L. (1997) Exudative mineral losses after serious burns: a clue to the alterations of magnesium and phosphate metabolism., *Am. J. Clin. Nutr.* United States, **65**(5), pp. 1473–1481.

Berger, S. L., Kouzarides, T., Shiekhattar, R. and Shilatifard, A. (2009) An operational definition of epigenetics, *Gene. Dev.* 2009/04/03, **23**(7), pp. 781–783.

Bernardini, D., Nasulewic, A., Mazur, A. and Maier, J. A. M. (2005) Magnesium and microvascular endothelial cells: a role in inflammation and angiogenesis., *Front. Biosci.* United States, **10**, pp. 1177–1182.

Bonaterra, G. A., Zugel, S., Thogersen, J., Walter, S. A., Haberkorn, U., Strelau, J. and Kinscherf, R. (2012) Growth differentiation factor-15 deficiency inhibits atherosclerosis progression by regulating interleukin-6-dependent inflammatory response to vascular injury, *J. Am. Hear. Assoc.* 2013/01/15, **1**(6), p. e002550.

Borissoff, J. I., Joosen, I. A., Versteylen, M. O., Brill, A., Fuchs, T. A., Savchenko, A. S., Gallant, M., Martinod, K., Ten Cate, H., Hofstra, L., Crijns, H. J., Wagner, D. D. and Kietselaer, B. L. J. H. (2013) Elevated levels of circulating DNA and chromatin are independently associated with severe coronary atherosclerosis and a prothrombotic state., *Arterioscler. Thromb. Vasc. Biol.* United States, **33**(8), pp. 2032–2040.

Boulanger, C. M., Amabile, N., Guerin, A. P., Pannier, B., Leroyer, A. S., Mallat, C.

N., Tedgui, A. and London, G. M. (2007) In vivo shear stress determines circulating levels of endothelial microparticles in end-stage renal disease, *Hypertension*. 2007/02/21, **49**(4), pp. 902–908.

Braye, F., Hautier, A., Bouez, C. and Damour, O. (2005) [Skin substitutes reconstructed in the laboratory: application in burn treatment]., *Pathol. Biol. (Paris).* France, **53**(10), pp. 613–617.

Brennan, E., Wang, B., McClelland, A., Mohan, M., Marai, M., Beuscart, O., Derouiche, S., Gray, S., Pickering, R., Tikellis, C., de Gaetano, M., Barry, M., Belton, O., Ali-Shah, S. T., Guiry, P., Jandeleit-Dahm, K. A. M., Cooper, M. E., Godson, C. and Kantharidis, P. (2017) Protective Effect of let-7 miRNA Family in Regulating Inflammation in Diabetes-Associated Atherosclerosis., *Diabetes*. United States, **66**(8), pp. 2266–2277.

Bricambert, J., Alves-Guerra, M.-C., Esteves, P., Prip-Buus, C., Bertrand-Michel, J., Guillou, H., Chang, C. J., Vander Wal, M. N., Canonne-Hergaux, F., Mathurin, P., Raverdy, V., Pattou, F., Girard, J., Postic, C. and Dentin, R. (2018) The histone demethylase Phf2 acts as a molecular checkpoint to prevent NAFLD progression during obesity., *Nat. Commun.* England, **9**(1), p. 2092.

Brindle, P., Beswick, A., Fahey, T. and Ebrahim, S. (2006) Accuracy and impact of risk assessment in the primary prevention of cardiovascular disease: a systematic review, *Heart*. 2006/04/20, **92**(12), pp. 1752–1759.

Bryder, D., Rossi, D. J. and Weissman, I. L. (2006) Hematopoietic stem cells: the paradigmatic tissue-specific stem cell, *Am. J. Pathol.* American Society for Investigative Pathology, **169**(2), pp. 338–346.

Burggren, W. (2016) Epigenetic Inheritance and Its Role in Evolutionary Biology: Re-Evaluation and New Perspectives., *Biology (Basel).* Switzerland, **5**(2).

Cai, E. Z., Ang, C. H., Raju, A., Tan, K. B., Hing, E. C. H., Loo, Y., Wong, Y. C., Lee, H., Lim, J., Moochhala, S. M., Hauser, C. A. and Lim, T. C. (2014) Creation of consistent burn wounds: a rat model., *Arch. Plast. Surg.*, **41**(4), pp. 317–324.

Cao, C., Lai, T., Li, M., Zhou, H., Lv, D., Deng, Z., Ying, S., Chen, Z., Li, W. and Shen, H. (2016) Smoking-promoted oxidative DNA damage response is highly

correlated to lung carcinogenesis, *Oncotarget*. Impact Journals LLC, **7**(14), pp. 18919–18926.

Carr, M. J., Li, Y., Rezakhanlou, A. M. and Ghahary, A. (2017) Keratinocyte-Releasable Factors Stimulate the Expression of Granulocyte Colony-Stimulating Factor in Human Dermal Fibroblasts., *J. Cell. Biochem.* United States, **118**(2), pp. 308–317.

Celermajer, D. S., Sorensen, K. E., Spiegelhalter, D. J., Georgakopoulos, D., Robinson, J. and Deanfield, J. E. (1994) Aging is associated with endothelial dysfunction in healthy men years before the age-related decline in women., *J. Am. Coll. Cardiol.* United States, **24**(2), pp. 471–476.

Chan, K. H. K., Chacko, S. A., Song, Y., Cho, M., Eaton, C. B., Wu, W.-C. H. and Liu, S. (2015) Genetic variations in magnesium-related ion channels may affect diabetes risk among African American and Hispanic American women., *J. Nutr.*, **145**(3), pp. 418–424.

Chang, Y., Levy, D., Horton, J. R., Peng, J., Zhang, X., Gozani, O. and Cheng, X. (2011) Structural basis of SETD6-mediated regulation of the NF-kB network via methyl-lysine signaling, *Nucleic Acids Res.* 2011/04/22. Oxford University Press, **39**(15), pp. 6380–6389.

Chatzizisis, Y. S., Coskun, A. U., Jonas, M., Edelman, E. R., Feldman, C. L. and Stone, P. H. (2007) Role of endothelial shear stress in the natural history of coronary atherosclerosis and vascular remodeling: molecular, cellular, and vascular behavior, *J. Am. Coll. Cardiol.* 2007/06/30, **49**(25), pp. 2379–2393.

Chen, A., Feldman, M., Vershinin, Z. and Levy, D. (2016) SETD6 is a negative regulator of oxidative stress response., *Biochim. Biophys. Acta*. Netherlands, **1859**(2), pp. 420–427.

Chen, K.-C., Wang, Y.-S., Hu, C.-Y., Chang, W.-C., Liao, Y.-C., Dai, C.-Y. and Juo, S.-H. H. (2011) OxLDL up-regulates microRNA-29b, leading to epigenetic modifications of MMP-2/MMP-9 genes: a novel mechanism for cardiovascular diseases., *FASEB J.* United States, **25**(5), pp. 1718–1728.

Chen, Ming-Huang, Yeh, Y.-C., Shyr, Y.-M., Jan, Y.-H., Chao, Y., Li, C.-P., Wang,

S.-E., Tzeng, C.-H., Chang, P. M.-H., Liu, C.-Y., Chen, Ming-Han, Hsiao, M. and Huang, C.-Y. F. (2013) Expression of gremlin 1 correlates with increased angiogenesis and progression-free survival in patients with pancreatic neuroendocrine tumors., *J. Gastroenterol.* Japan, **48**(1), pp. 101–108.

Chen, T., Huang, Z., Wang, L., Wang, Y., Wu, F., Meng, S. and Wang, C. (2009) MicroRNA-125a-5p partly regulates the inflammatory response, lipid uptake, and ORP9 expression in oxLDL-stimulated monocyte/macrophages, *Cardiovasc. Res.* 2009/04/21, **83**(1), pp. 131–139.

Chen, W., Bacanamwo, M. and Harrison, D. G. (2008) Activation of p300 Histone Acetyltransferase Activity Is an Early Endothelial Response to Laminar Shear Stress and Is Essential for Stimulation of Endothelial Nitric-oxide Synthase mRNA Transcription, *J. Biol. Chem.* American Society for Biochemistry and Molecular Biology, **283**(24), pp. 16293–16298.

Cheng, C.-F., Fan, J., Fedesco, M., Guan, S., Li, Y., Bandyopadhyay, B., Bright, A. M., Yerushalmi, D., Liang, M., Chen, M., Han, Y.-P., Woodley, D. T. and Li, W. (2008) Transforming growth factor alpha (TGFalpha)-stimulated secretion of HSP90alpha: using the receptor LRP-1/CD91 to promote human skin cell migration against a TGFbeta-rich environment during wound healing., *Mol. Cell. Biol.* United States, **28**(10), pp. 3344–3358.

Cho, C.-H., Sung, H.-K., Kim, K.-T., Cheon, H. G., Oh, G. T., Hong, H. J., Yoo, O.-J. and Koh, G. Y. (2006) COMP-angiopoietin-1 promotes wound healing through enhanced angiogenesis, lymphangiogenesis, and blood flow in a diabetic mouse model., *Proc. Natl. Acad. Sci. U.S.A.* United States, **103**(13), pp. 4946–4951.

Chollangi, T., Clabault, H., Thibeault, A.-A. H., Yong, H. E. J., Narula, S., Menkhorst, E., Sanderson, J. T., Vaillancourt, C. and Murthi, P. (2018) An Electrical Impedance-Based Assay to Examine Functions of Various Placental Cell Types In Vitro, in Murthi, P. and Vaillancourt, C. (eds) *Preeclampsia Methods Protoc.* New York, NY: Springer New York, pp. 267–276.

Chomczynski, P. and Sacchi, N. (1987) Single-step method of RNA isolation by acid guanidinium thiocyanate-phenol-chloroform extraction, *Anal. Biochem.* 1987/04/01, **162**(1), pp. 156–159.

Chomczynski, P. and Sacchi, N. (2006) The single-step method of RNA isolation by acid guanidinium thiocyanate-phenol-chloroform extraction: twenty-something years on., *Nat. Protoc.* England, **1**(2), pp. 581–585.

Chubanov, V., Mittermeier, L. and Gudermann, T. (2018) Role of kinase-coupled TRP channels in mineral homeostasis., *Pharmacol. Ther.* England, **184**, pp. 159–176.

Coats, T. J., Edwards, C., Newton, R. and Staun, E. (2002) The effect of gel burns dressings on skin temperature., *Emerg. Med. J.* England, **19**(3), pp. 224–225.

Conway, D. and Schwartz, M. A. (2012) Lessons from the endothelial junctional mechanosensory complex, *F1000 Biol. Rep.* 2012/01/13, **4**, p. 1.

Coudray, C., Rambeau, M., Feillet-Coudray, C., Gueux, E., Tressol, J. C., Mazur, A. and Rayssiguier, Y. (2005) Study of magnesium bioavailability from ten organic and inorganic Mg salts in Mg-depleted rats using a stable isotope approach., *Magnes. Res.* England, **18**(4), pp. 215–223.

Cummins, P. M., von Offenberg Sweeney, N., Killeen, M. T., Birney, Y. A., Redmond, E. M. and Cahill, P. A. (2007) Cyclic strain-mediated matrix metalloproteinase regulation within the vascular endothelium: a force to be reckoned with., *Am. J. Physiol. Heart Circ. Physiol.* United States, **292**(1), pp. H28-42.

Day, R. M. (2005) Bioactive glass stimulates the secretion of angiogenic growth factors and angiogenesis in vitro., *Tissue Eng.* United States, **11**(5–6), pp. 768–777.

Dhaliwal, K. and Lopez, N. (2018) Hydrogel dressings and their application in burn wound care., *Br. J. Community Nurs.* England, **23**(Sup9), pp. S24–S27.

Dong, J., Cruz, M. A., Aboulfatova, K., Martin, C., Choi, H., Bergeron, A. L., Martini, S. R., Kroll, M. H. and Kent, T. A. (2008) Magnesium maintains endothelial integrity, up-regulates proteolysis of ultra-large von Willebrand factor, and reduces platelet aggregation under flow conditions., *Thromb. Haemost.* Germany, **99**(3), pp. 586–593.

Dragoni, S., Hudson, N., Kenny, B.-A., Burgoyne, T., McKenzie, J. A., Gill, Y., Blaber, R., Futter, C. E., Adamson, P., Greenwood, J. and Turowski, P. (2017) Endothelial MAPKs Direct ICAM-1 Signaling to Divergent Inflammatory

Functions., *J. Immunol.*, **198**(10), pp. 4074–4085.

Dreger, H., Ludwig, A., Weller, A., Stangl, V., Baumann, G., Meiners, S. and Stangl, K. (2012) Epigenetic regulation of cell adhesion and communication by enhancer of zeste homolog 2 in human endothelial cells., *Hypertension*. United States, **60**(5), pp. 1176–1183.

Drost, J., Mantovani, F., Tocco, F., Elkon, R., Comel, A., Holstege, H., Kerkhoven, R., Jonkers, J., Voorhoeve, P. M., Agami, R. and Del Sal, G. (2010) BRD7 is a candidate tumour suppressor gene required for p53 function., *Nat. Cell Biol.* England, **12**(4), pp. 380–389.

Duffy, E., Guzman, K. De, Wallace, R., Murphy, R. and Morrin, A. (2017) Non-Invasive Assessment of Skin Barrier Properties: Investigating Emerging Tools for In Vitro and In Vivo Applications, *Cosmetics*, **4**(4).

Dvashi, Z., Sar Shalom, H., Shohat, M., Ben-Meir, D., Ferber, S., Satchi-Fainaro, R., Ashery-Padan, R., Rosner, M., Solomon, A. S. and Lavi, S. (2014) Protein phosphatase magnesium dependent 1A governs the wound healing-inflammation-angiogenesis cross talk on injury., *Am. J. Pathol.* United States, **184**(11), pp. 2936–2950.

Ebert, M. S. and Sharp, P. A. (2012) Roles for microRNAs in conferring robustness to biological processes, *Cell*. 2012/05/01, **149**(3), pp. 515–524.

Elghblawi, E. (2018) Platelet-rich plasma, the ultimate secret for youthful skin elixir and hair growth triggering., *J. Cosmet. Dermatol.* England, **17**(3), pp. 423–430.

Falk, E., Shah, P. K. and Fuster, V. (1995) Coronary plaque disruption, *Circulation*. 1995/08/01, **92**(3), pp. 657–671.

Fang, Z. and Rajewsky, N. (2011) The impact of miRNA target sites in coding sequences and in 3'UTRs, *PLoS One*. 2011/03/30, **6**(3), p. e18067.

Faouzi, M., Kilch, T., Horgen, F. D., Fleig, A. and Penner, R. (2017) The TRPM7 channel kinase regulates store-operated calcium entry, *J. Physiol.*, **595**(10), pp. 3165–3180.

Feng, S., Jacobsen, S. E. and Reik, W. (2010) Epigenetic reprogramming in plant and animal development., *Science*. United States, **330**(6004), pp. 622–627.

Feoktistova, M., Geserick, P. and Leverkus, M. (2016) Crystal Violet Assay for Determining Viability of Cultured Cells., *Cold Spring Harb. Protoc.* United States, **2016**(4), p. pdb.prot087379.

Ferre, S., Baldoli, E., Leidi, M. and Maier, J. A. M. (2010) Magnesium deficiency promotes a pro-atherogenic phenotype in cultured human endothelial cells via activation of NFkB., *Biochim. Biophys. Acta*. Netherlands, **1802**(11), pp. 952–958.

Firoz, M. and Graber, M. (2001) Bioavailability of US commercial magnesium preparations., *Magnes. Res.* England, **14**(4), pp. 257–262.

Fontes, J. D., Yamamoto, J. F., Larson, M. G., Wang, N., Dallmeier, D., Rienstra, M., Schnabel, R. B., Vasan, R. S., Keaney Jr., J. F. and Benjamin, E. J. (2013) Clinical correlates of change in inflammatory biomarkers: The Framingham Heart Study, *Atherosclerosis*. 2013/03/16.

Franklin, S. S., Lopez, V. A., Wong, N. D., Mitchell, G. F., Larson, M. G., Vasan, R. S. and Levy, D. (2009) Single versus combined blood pressure components and risk for cardiovascular disease: the Framingham Heart Study., *Circulation*. United States, **119**(2), pp. 243–250.

Freshney, R. (2016) *Culture of Animal Cells: A Manual of Basic Technique and Specialized Applications*. 7th ed. New York: Wiley-Blackwell.

Fukagawa, T., Nogami, M., Yoshikawa, M., Ikeno, M., Okazaki, T., Takami, Y., Nakayama, T. and Oshimura, M. (2004) Dicer is essential for formation of the heterochromatin structure in vertebrate cells., *Nat. Cell Biol.* England, **6**(8), pp. 784–791.

Funato, Y. and Miki, H. (2018) Molecular function and biological importance of CNNM family Mg2+ transporters., *J. Biochem.* England.

Galkina, E. and Ley, K. (2007) Leukocyte influx in atherosclerosis, *Curr. Drug Targets*. 2008/01/29, **8**(12), pp. 1239–1248.

Ghaffari, A., Kilani, R. T. and Ghahary, A. (2009) Keratinocyte-conditioned media regulate collagen expression in dermal fibroblasts., *J. Invest. Dermatol.* United States, **129**(2), pp. 340–347.

Ghinea, N., Leabu, M., Hasu, M., Muresan, V., Colceag, J. and Simionescu, N.

(1987) Prelesional events in atherogenesis. Changes induced by hypercholesterolemia in the cell surface chemistry of arterial endothelium and blood monocytes, in rabbit, *J. Submicrosc. Cytol. Pathol.* 1987/04/01, **19**(2), pp. 209–227.

Gillespie, P. G. and Walker, R. G. (2001) Molecular basis of mechanosensory transduction., *Nature*. England, **413**(6852), pp. 194–202.

Gimbrone Jr., M. A., Topper, J. N., Nagel, T., Anderson, K. R. and Garcia-Cardena, G. (2000) Endothelial dysfunction, hemodynamic forces, and atherogenesis, *Ann. N. Y. Acad. Sci.* 2000/06/24, **902**, pp. 230–240.

Glik, J., Labus, W., Kitala, D., Mikus-Zagorska, K., Roberts, C. D., Nowak, M., Kasperczyk, A. and Kawecki, M. (2018) A 2000 patient retrospective assessment of a new strategy for burn wound management in view of infection prevention and treatment., *Int. Wound J.* England, **15**(3), pp. 344–349.

Golebiewska, E. M. and Poole, A. W. (2015) Platelet secretion: From haemostasis to wound healing and beyond., *Blood Rev.* England, **29**(3), pp. 153–162.

Gonzalez-Gay, M. A., Gonzalez-Juanatey, C. and Martin, J. (2005) Rheumatoid arthritis: a disease associated with accelerated atherogenesis, *Semin. Arthritis Rheum.* 2005/08/09, **35**(1), pp. 8–17.

Goodwin, N. S., Spinks, A. and Wasiak, J. (2016) The efficacy of hydrogel dressings as a first aid measure for burn wound management in the pre-hospital setting: a systematic review of the literature., *Int. Wound J.* England, **13**(4), pp. 519–525.

Grada, A., Otero-Vinas, M., Prieto-Castrillo, F., Obagi, Z. and Falanga, V. (2017) Research Techniques Made Simple: Analysis of Collective Cell Migration Using the Wound Healing Assay., *J. Invest. Dermatol.* United States, **137**(2), pp. e11–e16.

Gradinaru, D., Borsa, C., Ionescu, C. and Prada, G. I. (2015) Oxidized LDL and NO synthesis--Biomarkers of endothelial dysfunction and ageing., *Mech. Ageing Dev.* Ireland, **151**, pp. 101–113.

GRAHAM, L. A., CAESAR, J. J. and BURGEN, A. S. (1960) Gastrointestinal absorption and excretion of Mg 28 in man., *Metabolism.* United States, **9**, pp. 646–659.

Green, J. P., Souilhol, C., Xanthis, I., Martinez-Campesino, L., Bowden, N. P.,

Evans, P. C. and Wilson, H. L. (2018) Atheroprone flow activates inflammation via endothelial ATP-dependent P2X7-p38 signalling, *Cardiovasc. Res.*, **114**(2), pp. 324–335. Available at: http://dx.doi.org/10.1093/cvr/cvx213.

Grzesiak, J. J. and Pierschbacher, M. D. (1995) Shifts in the concentrations of magnesium and calcium in early porcine and rat wound fluids activate the cell migratory response, *J. Clin. Invest.*, **95**(1), pp. 227–233.

Gurven, M., Jaeggi, A. V, Kaplan, H. and Cummings, D. (2013) Physical activity and modernization among Bolivian Amerindians., *PLoS One*. United States, **8**(1), p. e55679.

Hahn, C. and Schwartz, M. A. (2009) Mechanotransduction in vascular physiology and atherogenesis., *Nat. Rev. Mol. Cell Biol.* England, **10**(1), pp. 53–62.

Hamilton, M. L., Van Remmen, H., Drake, J. A., Yang, H., Guo, Z. M., Kewitt, K., Walter, C. A. and Richardson, A. (2001) Does oxidative damage to DNA increase with age?, *Proc. Natl. Acad. Sci. U.S.A.* 2001/08/21. The National Academy of Sciences, **98**(18), pp. 10469–10474.

Hannum, G., Guinney, J., Zhao, L., Zhang, L., Hughes, G., Sadda, S., Klotzle, B., Bibikova, M., Fan, J.-B., Gao, Y., Deconde, R., Chen, M., Rajapakse, I., Friend, S., Ideker, T. and Zhang, K. (2013) Genome-wide methylation profiles reveal quantitative views of human aging rates., *Mol. Cell*. United States, **49**(2), pp. 359–367.

Harris, T. A., Yamakuchi, M., Ferlito, M., Mendell, J. T. and Lowenstein, C. J. (2008) MicroRNA-126 regulates endothelial expression of vascular cell adhesion molecule 1, *Proc. Natl. Acad. Sci. U.S.A.* 2008/01/30, **105**(5), pp. 1516–1521.

Hashimoto, K., Otero, M., Imagawa, K., de Andrés, M. C., Coico, J. M., Roach, H. I., Oreffo, R. O. C., Marcu, K. B. and Goldring, M. B. (2013) Regulated transcription of human matrix metalloproteinase 13 (MMP13) and interleukin-1β (IL1B) genes in chondrocytes depends on methylation of specific proximal promoter CpG sites, *J. Biol. Chem.* 2013/02/15. American Society for Biochemistry and Molecular Biology, **288**(14), pp. 10061–10072.

Hernesniemi, J. A., Seppala, I., Lyytikainen, L. P., Mononen, N., Oksala, N., Hutri-

Kahonen, N., Juonala, M., Taittonen, L., Smith, E. N., Schork, N. J., Chen, W., Srinivasan, S. R., Berenson, G. S., Murray, S. S., Laitinen, T., Jula, A., Kettunen, J., Ripatti, S., Laaksonen, R., *et al.* (2012) Genetic profiling using genome-wide significant coronary artery disease risk variants does not improve the prediction of subclinical atherosclerosis: the Cardiovascular Risk in Young Finns Study, the Bogalusa Heart Study and the Health 2000 Survey--a meta, *PLoS One*. 2012/02/02, **7**(1), p. e28931.

Heyn, H., Moran, S., Hernando-Herraez, I., Sayols, S., Gomez, A., Sandoval, J., Monk, D., Hata, K., Marques-Bonet, T., Wang, L. and Esteller, M. (2013) DNA methylation contributes to natural human variation., *Genome Res.* United States, **23**(9), pp. 1363–1372.

Hoffend, N. C., Magner, W. J. and Tomasi, T. B. (2017) The epigenetic regulation of Dicer and microRNA biogenesis by Panobinostat., *Epigenetics*. United States, **12**(2), pp. 105–112.

Hong, B.-Z., Kang, H.-S., So, J.-N., Kim, H.-N., Park, S.-A., Kim, S.-J., Kim, K.-R. and Kwak, Y.-G. (2006) Vascular endothelial growth factor increases the intracellular magnesium., *Biochem. Biophys. Res. Commun.* United States, **347**(2), pp. 496–501.

Horvath, S. (2013) DNA methylation age of human tissues and cell types., *Genome Biol.* England, **14**(10), p. R115.

Horvath, S. and Ritz, B. R. (2015) Increased epigenetic age and granulocyte counts in the blood of Parkinson's disease patients., *Aging (Albany. NY).* United States, **7**(12), pp. 1130–1142.

Houseman, E. A., Accomando, W. P., Koestler, D. C., Christensen, B. C., Marsit, C. J., Nelson, H. H., Wiencke, J. K. and Kelsey, K. T. (2012) DNA methylation arrays as surrogate measures of cell mixture distribution., *BMC Bioinformatics*. England, **13**, p. 86.

Hove, J. R., Koster, R. W., Forouhar, A. S., Acevedo-Bolton, G., Fraser, S. E. and Gharib, M. (2003) Intracardiac fluid forces are an essential epigenetic factor for embryonic cardiogenesis, *Nature*. 2003/01/10, **421**(6919), pp. 172–177.

Huang, W., Wang, Y., Huang, Z., Wang, X., Chen, L., Zhang, Y. and Zhang, L. (2018) On-Demand Dissolvable Self-Healing Hydrogel Based on Carboxymethyl Chitosan and Cellulose Nanocrystal for Deep Partial Thickness Burn Wound Healing., *ACS Appl. Mater. Inter.* United States.

Hung, C.-C., Chaya, A., Liu, K., Verdelis, K. and Sfeir, C. (2019) The role of magnesium ions in bone regeneration involves the canonical Wnt signaling pathway., *Acta Biomater.* England.

Hwang, D. L., Yen, C. F. and Nadler, J. L. (1992) Effect of extracellular magnesium on platelet activation and intracellular calcium mobilization., *Am. J. Hypertens.* United States, **5**(10), pp. 700–706.

Hwang, S., Zimmerman, N. P., Agle, K. A., Turner, J. R., Kumar, S. N. and Dwinell, M. B. (2012) E-cadherin is critical for collective sheet migration and is regulated by the chemokine CXCL12 protein during restitution, *J. Biol. Chem.* 2012/05/01. American Society for Biochemistry and Molecular Biology, **287**(26), pp. 22227–22240.

Inoue, A., Jiang, L., Lu, F., Suzuki, T. and Zhang, Y. (2017) Maternal H3K27me3 controls DNA methylation-independent imprinting., *Nature*. England, **547**(7664), pp. 419–424.

Iruela-Arispe, M. L. and Dvorak, H. F. (1997) Angiogenesis: a dynamic balance of stimulators and inhibitors., *Thromb. Haemost.* Germany, **78**(1), pp. 672–677.

Ivanov, M., Baranova, A., Butler, T., Spellman, P. and Mileyko, V. (2015) Non-random fragmentation patterns in circulating cell-free DNA reflect epigenetic regulation., *BMC Genomics*. England, **16 Suppl 13**, p. S1.

Iyer, K. V., Pulford, S., Mogilner, A. and Shivashankar, G. V (2012) Mechanical Activation of Cells Induces Chromatin Remodeling Preceding MKL Nuclear Transport, *Biophys. J.* The Biophysical Society, **103**(7), pp. 1416–1428.

Jahnen-Dechent, W. and Ketteler, M. (2012) Magnesium basics., *Clin. Kidney J.* England, **5**(Suppl 1), pp. i3–i14.

Jamaluddin, M. S., Weakley, S. M., Zhang, L., Kougias, P., Lin, P. H., Yao, Q. and Chen, C. (2011) miRNAs: roles and clinical applications in vascular disease, *Expert*

Rev Mol Diagn. 2010/12/22, **11**(1), pp. 79–89.

Jiang, X., Yang, F., Tan, H., Liao, D., Bryan, R. M. J., Randhawa, J. K., Rumbaut, R. E., Durante, W., Schafer, A. I., Yang, X. and Wang, H. (2005) Hyperhomocystinemia impairs endothelial function and eNOS activity via PKC activation., *Arterioscler. Thromb. Vasc. Biol.* United States, **25**(12), pp. 2515–2521.

Jiang, Y.-Z., Manduchi, E., Stoeckert, C. J. J. and Davies, P. F. (2015) Arterial endothelial methylome: differential DNA methylation in athero-susceptible disturbed flow regions in vivo., *BMC Genomics*. England, **16**, p. 506.

Jin, J., Wu, L.-J., Jun, J., Cheng, X., Xu, H., Andrews, N. C. and Clapham, D. E. (2012) The channel kinase, TRPM7, is required for early embryonic development., *Proc. Natl. Acad. Sci. U.S.A.* United States, **109**(5), pp. E225-33.

Jones, C. I. (2016) Platelet function and ageing, *Mamm. Genome*. 2016/04/11. Springer US, **27**(7–8), pp. 358–366.

Jovanovic, B. D., Huang, S., Liu, Y., Naguib, K. N. and Bergan, R. C. (2001) A simple analysis of gene expression and variability in gene arrays based on repeated observations., *Pharmacogenomics J.* New Zealand, **1**(2), pp. 145–152.

Juvvuna, P. K., Khandelia, P., Lee, L. M. and Makeyev, E. V (2012) Argonaute identity defines the length of mature mammalian microRNAs, *Nucleic Acids Res.* 2012/04/17, **40**(14), pp. 6808–6820.

Jylhava, J., Pedersen, N. L. and Hagg, S. (2017) Biological Age Predictors., *EBioMedicine*. Netherlands, **21**, pp. 29–36.

Kadoglou, N. P., Moustardas, P., Kapelouzou, A., Katsimpoulas, M., Giagini, A., Dede, E., Kostomitsopoulos, N., Karayannacos, P. E., Kostakis, A. and Liapis, C. D. (2013) The anti-inflammatory effects of exercise training promote atherosclerotic plaque stabilization in apolipoprotein E knockout mice with diabetic atherosclerosis, *Eur J Histochem*. 2013/04/04, **57**(1), p. e3.

Kaeser, M. D., Aslanian, A., Dong, M.-Q., Yates, J. R. 3rd and Emerson, B. M. (2008) BRD7, a novel PBAF-specific SWI/SNF subunit, is required for target gene activation and repression in embryonic stem cells., *J. Biol. Chem.* United States, **283**(47), pp. 32254–32263.

Kaitsuka, T., Katagiri, C., Beesetty, P., Nakamura, K., Hourani, S., Tomizawa, K., Kozak, J. A. and Matsushita, M. (2014) Inactivation of TRPM7 kinase activity does not impair its channel function in mice, *Sci. Rep.* Nature Publishing Group, **4**, p. 5718.

Kananen, L., Marttila, S., Nevalainen, T., Jylhava, J., Mononen, N., Kahonen, M., Raitakari, O. T., Lehtimaki, T. and Hurme, M. (2016) Aging-associated DNA methylation changes in middle-aged individuals: the Young Finns study., *BMC Genomics*. England, **17**, p. 103.

Kass, L., Rosanoff, A., Tanner, A., Sullivan, K., McAuley, W. and Plesset, M. (2017) Effect of transdermal magnesium cream on serum and urinary magnesium levels in humans: A pilot study., *PLoS One*. United States, **12**(4), p. e0174817.

Ke, N., Wang, X., Xu, X. and Abassi, Y. A. (2011) The xCELLigence system for real-time and label-free monitoring of cell viability., *Methods Mol. Biol.* United States, **740**, pp. 33–43.

Keihani, S., Hosseinpanah, F., Barzin, M., Serahati, S., Doustmohamadian, S. and Azizi, F. (2015) Abdominal obesity phenotypes and risk of cardiovascular disease in a decade of follow-up: the Tehran Lipid and Glucose Study., *Atherosclerosis*. Ireland, **238**(2), pp. 256–263.

Keren, A., Dorian, P., Davy, J. M. and Opie, L. H. (1988) Effects of magnesium on ischemic and reperfusion arrhythmias in the rat heart and electrophysiologic effects of hypermagnesemia in the anesthetized dog., *Cardiovasc. drugs Ther.* United States, **2**(5), pp. 637–645.

Kh, R., Khullar, M., Kashyap, M., Pandhi, P. and Uppal, R. (2000) Effect of oral magnesium supplementation on blood pressure, platelet aggregation and calcium handling in deoxycorticosterone acetate induced hypertension in rats., *J. Hypertens.* England, **18**(7), pp. 919–926.

Kim, W., Kim, R., Park, G., Park, J.-W. and Kim, J.-E. (2012) Deficiency of H3K79 histone methyltransferase Dot1-like protein (DOT1L) inhibits cell proliferation., *J. Biol. Chem.*, **287**(8), pp. 5588–5599.

King, A., Balaji, S., Le, L. D., Crombleholme, T. M. and Keswani, S. G. (2014)

Regenerative Wound Healing: The Role of Interleukin-10, *Adv. wound care*. Mary Ann Liebert, Inc., **3**(4), pp. 315–323.

Klein, G. L., Nicolai, M., Langman, C. B., Cuneo, B. F., Sailer, D. E. and Herndon, D. N. (1997) Dysregulation of calcium homeostasis after severe burn injury in children: possible role of magnesium depletion., *J. Pediatr.* United States, **131**(2), pp. 246–251.

Klein, G. L. (2011) Burns: where has all the calcium (and vitamin D) gone?, *Adv. Nutr.* American Society for Nutrition, **2**(6), pp. 457–462.

Klein, G. L. and Herndon, D. N. (1998) Magnesium deficit in major burns: role in hypoparathyroidism and end-organ parathyroid hormone resistance., *Magnes. Res.* England, **11**(2), pp. 103–109.

Korish, A. A. (2012) Magnesium sulfate therapy of preeclampsia: an old tool with new mechanism of action and prospect in management and prophylaxis., *Hypertens. Res.* England, **35**(10), pp. 1005–1011.

Krapivinsky, G., Krapivinsky, L., Manasian, Y. and Clapham, D. E. (2014) The TRPM7 chanzyme is cleaved to release a chromatin-modifying kinase., *Cell*. United States, **157**(5), pp. 1061–1072.

Kruth, H. S. (2001) Macrophage foam cells and atherosclerosis, *Front Biosci.* 2001/03/07, **6**, pp. D429-55.

Kumar, A., Kim, C.-S., Hoffman, T. A., Naqvi, A., Dericco, J., Jung, S.-B., Lin, Z., Jain, M. K. and Irani, K. (2011) p53 impairs endothelial function by transcriptionally repressing Kruppel-Like Factor 2., *Arterioscler. Thromb. Vasc. Biol.* United States, **31**(1), pp. 133–141.

Kwon, H.-B., Wang, S., Helker, C. S. M., Rasouli, S. J., Maischein, H.-M., Offermanns, S., Herzog, W. and Stainier, D. Y. R. (2016) In vivo modulation of endothelial polarization by Apelin receptor signalling, *Nat. Commun.* The Author(s), **7**, p. 11805. Available at: http://dx.doi.org/10.1038/ncomms11805.

Van Laecke, S. (2018) Hypomagnesemia and hypermagnesemia., *Acta Clin. Belg.* England, pp. 1–7.

Lamalice, L., Le Boeuf, F. and Huot, J. (2007) Endothelial cell migration during

angiogenesis., *Circ. Res.* United States, **100**(6), pp. 782–794.

Lapidos, K. A., Woodhouse, E. C., Kohn, E. C. and Masiero, L. (2001) Mg(++)-induced endothelial cell migration: substratum selectivity and receptor-involvement., *Angiogenesis*. Germany, **4**(1), pp. 21–28.

Lassila, R. (2016) Platelet Function Tests in Bleeding Disorders., *Semin. Thromb. Hemost.* United States, **42**(3), pp. 185–190.

Lee, H., Han, S., Kwon, C. S. and Lee, D. (2016) Biogenesis and regulation of the let-7 miRNAs and their functional implications, *Protein Cell*. 2015/09/23. Higher Education Press, **7**(2), pp. 100–113.

Lee, S., Ryu, J. H., Kim, S. J., Ryu, D. R., Kang, D. H. and Choi, K. B. (2016) The Relationship between Magnesium and Endothelial Function in End-Stage Renal Disease Patients on Hemodialysis, *Yonsei Med. J.* 2016/08/30. Yonsei University College of Medicine, **57**(6), pp. 1446–1453.

Lehoux, S. and Tedgui, A. (2003) Cellular mechanics and gene expression in blood vessels, *J. Biomech.* 2003/04/16, **36**(5), pp. 631–643.

Lepers, R., Stapley, P. J. and Cattagni, T. (2016) Centenarian athletes: Examples of ultimate human performance?, *Age Ageing*. England, **45**(5), pp. 732–736.

Li, Q., Mullins, S. R., Sloane, B. F. and Mattingly, R. R. (2008) p21-Activated kinase 1 coordinates aberrant cell survival and pericellular proteolysis in a three-dimensional culture model for premalignant progression of human breast cancer, *Neoplasia*. Neoplasia Press Inc., **10**(4), pp. 314–329. Available at: https://www.ncbi.nlm.nih.gov/pubmed/18392133.

Li, V. S. W., Ng, S. S., Boersema, P. J., Low, T. Y., Karthaus, W. R., Gerlach, J. P., Mohammed, S., Heck, A. J. R., Maurice, M. M., Mahmoudi, T. and Clevers, H. (2012) Wnt signaling through inhibition of beta-catenin degradation in an intact Axin1 complex., *Cell*. United States, **149**(6), pp. 1245–1256.

Liang, C.-C., Park, A. Y. and Guan, J.-L. (2007) In vitro scratch assay: a convenient and inexpensive method for analysis of cell migration in vitro, *Nat. Protoc.* Nature Publishing Group, **2**, p. 329. Available at: https://doi.org/10.1038/nprot.2007.30.

Liang, G., Chan, M. F., Tomigahara, Y., Tsai, Y. C., Gonzales, F. A., Li, E., Laird,

P. W. and Jones, P. A. (2002) Cooperativity between DNA methyltransferases in the maintenance methylation of repetitive elements., *Mol. Cell. Biol.* United States, **22**(2), pp. 480–491.

Van Lint, P. and Libert, C. (2007) Chemokine and cytokine processing by matrix metalloproteinases and its effect on leukocyte migration and inflammation., *J. Leukoc. Biol.* United States, **82**(6), pp. 1375–1381.

Liu, Y., Reynolds, L. M., Ding, J., Hou, Li, Lohman, K., Young, T., Cui, W., Huang, Z., Grenier, C., Wan, M., Stunnenberg, H. G., Siscovick, D., Hou, Lifang, Psaty, B. M., Rich, S. S., Rotter, J. I., Kaufman, J. D., Burke, G. L., Murphy, S., *et al.* (2017) Blood monocyte transcriptome and epigenome analyses reveal loci associated with human atherosclerosis, *Nat. Commun.*, **8**(1), p. 393.

Lu, D. and Kassab, G. S. (2011) Role of shear stress and stretch in vascular mechanobiology., *J. R. Soc. Interface*, **8**(63), pp. 1379–1385.

Lund, G., Andersson, L., Lauria, M., Lindholm, M., Fraga, M. F., Villar-Garea, A., Ballestar, E., Esteller, M. and Zaina, S. (2004) DNA methylation polymorphisms precede any histological sign of atherosclerosis in mice lacking apolipoprotein E., *J. Biol. Chem.* United States, **279**(28), pp. 29147–29154.

Lusis, A. J. (2000) Atherosclerosis, *Nature*. 2000/09/23, **407**(6801), pp. 233–241.

Ma, J., Folsom, A. R., Melnick, S. L., Eckfeldt, J. H., Sharrett, A. R., Nabulsi, A. A., Hutchinson, R. G. and Metcalf, P. A. (1995) Associations of serum and dietary magnesium with cardiovascular disease, hypertension, diabetes, insulin, and carotid arterial wall thickness: the ARIC study. Atherosclerosis Risk in Communities Study., *J. Clin. Epidemiol.* United States, **48**(7), pp. 927–940.

Macfarlane, L. A. and Murphy, P. R. (2010) MicroRNA: Biogenesis, Function and Role in Cancer, *Curr. Genomics*. 2011/05/03, **11**(7), pp. 537–561.

Mack, J. J., Mosqueiro, T. S., Archer, B. J., Jones, W. M., Sunshine, H., Faas, G. C., Briot, A., Aragón, R. L., Su, T., Romay, M. C., McDonald, A. I., Kuo, C.-H., Lizama, C. O., Lane, T. F., Zovein, A. C., Fang, Y., Tarling, E. J., de Aguiar Vallim, T. Q., Navab, M., *et al.* (2017) NOTCH1 is a mechanosensor in adult arteries, *Nat. Commun.*, **8**(1), p. 1620.

Madaghiele, M., Demitri, C., Sannino, A. and Ambrosio, L. (2014) Polymeric hydrogels for burn wound care: Advanced skin wound dressings and regenerative templates., *Burn. trauma*. England, **2**(4), pp. 153–161.

Maier, J. A. (2012) Endothelial cells and magnesium: implications in atherosclerosis, *Clin. Sci.* 2012/01/18, **122**(9), pp. 397–407.

Maier, J. A. M., Bernardini, D., Rayssiguier, Y. and Mazur, A. (2004) High concentrations of magnesium modulate vascular endothelial cell behaviour in vitro., *Biochim. Biophys. Acta*. Netherlands, **1689**(1), pp. 6–12.

Maier, J. A. M., Nasulewicz-Goldeman, A., Simonacci, M., Boninsegna, A., Mazur, A. and Wolf, F. I. (2007) Insights into the mechanisms involved in magnesium-dependent inhibition of primary tumor growth., *Nutr. Cancer*. United States, **59**(2), pp. 192–198.

Malek, A. M., Izumo, S. and Alper, S. L. (1999) Modulation by pathophysiological stimuli of the shear stress-induced up-regulation of endothelial nitric oxide synthase expression in endothelial cells., *Neurosurgery*. United States, **45**(2), pp. 334–335.

Marieb, E. N. (2006) *Human Anatomy and Physiology*. 7th edn. Pearson Prentice Hall.

Marioni, R. E., Shah, S., McRae, A. F., Chen, B. H., Colicino, E., Harris, S. E., Gibson, J., Henders, A. K., Redmond, P., Cox, S. R., Pattie, A., Corley, J., Murphy, L., Martin, N. G., Montgomery, G. W., Feinberg, A. P., Fallin, M. D., Multhaup, M. L., Jaffe, A. E., *et al.* (2015) DNA methylation age of blood predicts all-cause mortality in later life, *Genome Biol.* 2015/01/31, **16**, p. 25.

Mazlyzam, A. L., Aminuddin, B. S., Fuzina, N. H., Norhayati, M. M., Fauziah, O., Isa, M. R., Saim, L. and Ruszymah, B. H. I. (2007) Reconstruction of living bilayer human skin equivalent utilizing human fibrin as a scaffold., *Burns*. Netherlands, **33**(3), pp. 355–363.

McDonell, L. M., Mirzaa, G. M., Alcantara, D., Schwartzentruber, J., Carter, M. T., Lee, L. J., Clericuzio, C. L., Graham, J. M. J., Morris-Rosendahl, D. J., Polster, T., Acsadi, G., Townshend, S., Williams, S., Halbert, A., Isidor, B., David, A., Smyser, C. D., Paciorkowski, A. R., Willing, M., *et al.* (2013) Mutations in STAMBP,

encoding a deubiquitinating enzyme, cause microcephaly-capillary malformation syndrome., *Nat. Genet.* United States, **45**(5), pp. 556–562.

McFadyen, J. D. and Kaplan, Z. S. (2015) Platelets are not just for clots., *Transfus. Med. Rev.* United States, **29**(2), pp. 110–119.

McGough, J. J. and Faraone, S. V (2009) Estimating the size of treatment effects: moving beyond p values, *Psychiatry (Edgmont).* Matrix Medical Communications, **6**(10), pp. 21–29. Available at: https://www.ncbi.nlm.nih.gov/pubmed/20011465.

McGrath, J. L. (2007) Cell spreading: the power to simplify., *Curr. Biol.* England, **17**(10), pp. R357-8.

Meems, L. M. G., Mahmud, H., Buikema, H., Tost, J., Michel, S., Takens, J., Verkaik-Schakel, R. N., Vreeswijk-Baudoin, I., Mateo-Leach, I. V, van der Harst, P., Plosch, T. and de Boer, R. A. (2016) Parental vitamin D deficiency during pregnancy is associated with increased blood pressure in offspring via Panx1 hypermethylation., *Am. J. Physiol. Heart Circ. Physiol.* United States, **311**(6), pp. H1459–H1469.

Menghini, R., Casagrande, V., Cardellini, M., Martelli, E., Terrinoni, A., Amati, F., Vasa-Nicotera, M., Ippoliti, A., Novelli, G., Melino, G., Lauro, R. and Federici, M. (2009) MicroRNA 217 modulates endothelial cell senescence via silent information regulator 1., *Circulation*. United States, **120**(15), pp. 1524–1532.

Mercer, J. and Bennett, M. (2006) The role of p53 in atherosclerosis., *Cell Cycle*. United States, **5**(17), pp. 1907–1909.

Mi, T., Dong, Y., Santhanam, U. and Huang, N. (2018) Niacinamide and 12-hydroxystearic acid prevented benzo(a)pyrene and squalene peroxides induced hyperpigmentation in skin equivalent., *Exp. Dermatol.* Denmark.

Mimura, J. and Itoh, K. (2015) Role of Nrf2 in the pathogenesis of atherosclerosis., *Free Radic. Biol. Med.* United States, **88**(Pt B), pp. 221–232.

Mitchell, C. A., Donaldson, M., Francese, S. and Clench, M. R. (2016) MALDI MSI analysis of lipid changes in living skin equivalents in response to emollient creams containing palmitoylethanolamide., *Methods*. United States, **104**, pp. 93–100.

Mohiuddin, M., Pan, H. A., Hung, Y. C. and Huang, G. S. (2012) Control of growth

and inflammatory response of macrophages and foam cells with nanotopography, *Nanoscale Res. Lett.* 2012/07/18, **7**(1), p. 394.

Monedero, J., Lyons, E. J. and O'Gorman, D. J. (2015) Interactive video game cycling leads to higher energy expenditure and is more enjoyable than conventional exercise in adults., *PLoS One*. United States, **10**(3), p. e0118470.

Monteagudo, S., Cornelis, F. M. F., Aznar-Lopez, C., Yibmantasiri, P., Guns, L.-A., Carmeliet, P., Cailotto, F. and Lories, R. J. (2017) DOT1L safeguards cartilage homeostasis and protects against osteoarthritis, *Nat. Commun.* Nature Publishing Group, **8**, p. 15889.

Montero, D., Pierce, G. L., Stehouwer, C. D. A., Padilla, J. and Thijssen, D. H. J. (2015) The impact of age on vascular smooth muscle function in humans., *J. Hypertens.*, **33**(3), pp. 445–53; discussion 453.

Montes de Oca, A., Guerrero, F., Martinez-Moreno, J. M., Madueno, J. A., Herencia, C., Peralta, A., Almaden, Y., Lopez, I., Aguilera-Tejero, E., Gundlach, K., Buchel, J., Peter, M. E., Passlick-Deetjen, J., Rodriguez, M. and Munoz-Castaneda, J. R. (2014) Magnesium inhibits Wnt/beta-catenin activity and reverses the osteogenic transformation of vascular smooth muscle cells., *PLoS One*. United States, **9**(2), p. e89525.

Moore, J. P., Weber, M. and Searles, C. D. (2010) Laminar Shear Stress Modulates Phosphorylation and Localization of RNA Polymerase II on the Endothelial Nitric Oxide Synthase Gene, *Arterioscler. Thromb. Vasc. Biol.*, pp. 561–567.

Morais, E. S., Silva, N. H. C. S., Sintra, T. E., Santos, S. A. O., Neves, B. M., Almeida, I. F., Costa, P. C., Correia-Sa, I., Ventura, S. P. M., Silvestre, A. J. D., Freire, M. G. and Freire, C. S. R. (2019) Anti-inflammatory and antioxidant nanostructured cellulose membranes loaded with phenolic-based ionic liquids for cutaneous application., *Carbohydr. Polym.* England, **206**, pp. 187–197.

Munhoz, A. C., Riva, P., Simões, D., Curi, R. and Carpinelli, A. R. (2016) Control of Insulin Secretion by Production of Reactive Oxygen Species: Study Performed in Pancreatic Islets from Fed and 48-Hour Fasted Wistar Rats, *PLoS One*. Public Library of Science, **11**(6), pp. e0158166–e0158166.

Murphy, D. D., Reddy, E. C., Moran, N. and O'Neill, S. (2014) Regulation of platelet activity in a changing redox environment., *Antioxid. Redox Signal.* United States, **20**(13), pp. 2074–2089.

Muslin, A. J. (2010) Phenotypic high-throughput screening in atherosclerosis research: focus on macrophages, *J. Cardiovasc. Transl. Res.* 2010/07/14, **3**(5), pp. 448–453.

Nakou, E. S., Liberopoulos, E. N., Milionis, H. J. and Elisaf, M. S. (2008) The role of C-reactive protein in atherosclerotic cardiovascular disease: an overview, *Curr. Vasc. Pharmacol.* 2008/10/16, **6**(4), pp. 258–270.

Nevalainen, T., Kananen, L., Marttila, S., Jylhävä, J., Mononen, N., Kähönen, M., Raitakari, O. T., Hervonen, A., Jylhä, M., Lehtimäki, T. and Hurme, M. (2017) Obesity accelerates epigenetic aging in middle-aged but not in elderly individuals, *Clin. Epigenetics*. BioMed Central, **9**, p. 20.

Newhouse, I. J. and Finstad, E. W. (2000) The effects of magnesium supplementation on exercise performance., *Clin. J. Sport Med.* United States, **10**(3), pp. 195–200.

Ng, Y.-W., Raghunathan, D., Chan, P. M., Baskaran, Y., Smith, D. J., Lee, C.-H., Verma, C. and Manser, E. (2010) Why an A-loop phospho-mimetic fails to activate PAK1: understanding an inaccessible kinase state by molecular dynamics simulations., *Structure*. United States, **18**(7), pp. 879–890.

Nobili, M., Sheriff, J., Morbiducci, U., Redaelli, A. and Bluestein, D. (2008) Platelet activation due to hemodynamic shear stresses: damage accumulation model and comparison to in vitro measurements, *ASAIO J.*, **54**(1), pp. 64–72.

North, B. J. and Sinclair, D. A. (2012) The intersection between aging and cardiovascular disease., *Circ. Res.* United States, **110**(8), pp. 1097–1108.

Paravicini, T. M., Yogi, A., Mazur, A. and Touyz, R. M. (2009) Dysregulation of vascular TRPM7 and annexin-1 is associated with endothelial dysfunction in inherited hypomagnesemia., *Hypertension*. United States, **53**(2), pp. 423–429.

Park, K.-S. and Park, D.-H. (2018) The effect of Korean red ginseng on full-thickness skin wound healing in rats, *J. Ginseng Res.*

Pepper, M. S., Spray, D. C., Chanson, M., Montesano, R., Orci, L. and Meda, P. (1989) Junctional communication is induced in migrating capillary endothelial cells, *J. Cell Biol.* 1989/12/01, **109**(6 Pt 1), pp. 3027–3038.

Pericacho, M., Velasco, S., Prieto, M., Llano, E., López-Novoa, J. M. and Rodríguez-Barbero, A. (2013) Endoglin haploinsufficiency promotes fibroblast accumulation during wound healing through Akt activation, *PLoS One*. Public Library of Science, **8**(1), pp. e54687–e54687.

Pfaffeneder, T., Hackner, B., Truss, M., Munzel, M., Muller, M., Deiml, C. A., Hagemeier, C. and Carell, T. (2011) The discovery of 5-formylcytosine in embryonic stem cell DNA., *Angew. Chem. Int. Ed. Engl.* Germany, **50**(31), pp. 7008–7012.

Plichta, J. K., Droho, S., Curtis, B. J., Patel, P., Gamelli, R. L. and Radek, K. A. (2014) Local burn injury impairs epithelial permeability and antimicrobial peptide barrier function in distal unburned skin, *Crit. Care Med.*, **42**(6), pp. e420–e431.

Poeckel, D., Tausch, L., Kather, N., Jauch, J. and Werz, O. (2006) Boswellic acids stimulate arachidonic acid release and 12-lipoxygenase activity in human platelets independent of Ca2+ and differentially interact with platelet-type 12-lipoxygenase., *Mol. Pharmacol.* United States, **70**(3), pp. 1071–1078.

Poirier, C., Gorshkov, B. A., Zemskova, M. A., Bogatcheva, N. V and Verin, A. D. (2011) TIMAP protects endothelial barrier from LPS-induced vascular leakage and is down-regulated by LPS, *Respir. Physiol. Neurobiol.* 2011/09/13, **179**(2–3), pp. 334–337.

Rae, L., Fidler, P. and Gibran, N. (2016) The Physiologic Basis of Burn Shock and the Need for Aggressive Fluid Resuscitation., *Crit. Care Clin.* United States, **32**(4), pp. 491–505.

Rahier, J.-F., Druez, A., Faugeras, L., Martinet, J.-P., Gehenot, M., Josseaux, E., Herzog, M., Micallef, J., George, F., Delos, M., De Ronde, T., Badaoui, A. and D'Hondt, L. (2017) Circulating nucleosomes as new blood-based biomarkers for detection of colorectal cancer., *Clin. Epigenetics*. Germany, **9**, p. 53.

Ranade, V. V and Somberg, J. C. (2001) Bioavailability and pharmacokinetics of

magnesium after administration of magnesium salts to humans., *Am. J. Ther.* United States, **8**(5), pp. 345–357.

Ravn, H. B., Kristensen, S. D., Vissinger, H. and Husted, S. E. (1996) Magnesium inhibits human platelets., *Blood Coagul. Fibrinolysis*. England, **7**(2), pp. 241–244.

Reinhart-King, C. A. (2008) Endothelial cell adhesion and migration., *Methods Enzymol.* United States, **443**, pp. 45–64.

Reitamo, S., Remitz, A., Tamai, K. and Uitto, J. (1994) Interleukin-10 modulates type I collagen and matrix metalloprotease gene expression in cultured human skin fibroblasts., *J. Clin. Invest.* United States, **94**(6), pp. 2489–2492.

Rhee, S. (2009) Fibroblasts in three dimensional matrices: cell migration and matrix remodeling., *Exp. Mol. Med.* United States, **41**(12), pp. 858–865.

Ribeiro, W. N., Yamada, A. T. and Benvenuti, L. A. (2014) Case 4/2014--A 66-year-old man with acute myocardial infarction and death in asystole after primary coronary angioplasty., *Arq. Bras. Cardiol.*, **103**(3), pp. e31-6.

Richardson, J. T. E. (2011) Eta squared and partial eta squared as measures of effect size in educational research, *Educ. Res. Rev.*, **6**(2), pp. 135–147.

Ridker, P. M., Danielson, E., Rifai, N. and Glynn, R. J. (2006) Valsartan, blood pressure reduction, and C-reactive protein: primary report of the Val-MARC trial, *Hypertension*. 2006/05/23, **48**(1), pp. 73–79.

Ridker, P. M., Everett, B. M., Thuren, T., MacFadyen, J. G., Chang, W. H., Ballantyne, C., Fonseca, F., Nicolau, J., Koenig, W., Anker, S. D., Kastelein, J. J. P., Cornel, J. H., Pais, P., Pella, D., Genest, J., Cifkova, R., Lorenzatti, A., Forster, T., Kobalava, Z., *et al.* (2017) Antiinflammatory Therapy with Canakinumab for Atherosclerotic Disease., *N. Engl. J. Med.* United States, **377**(12), pp. 1119–1131.

Ridker, P. M., MacFadyen, J. G., Thuren, T., Everett, B. M., Libby, P. and Glynn, R. J. (2017) Effect of interleukin-1beta inhibition with canakinumab on incident lung cancer in patients with atherosclerosis: exploratory results from a randomised, double-blind, placebo-controlled trial., *Lancet*. England, **390**(10105), pp. 1833–1842.

Rippe, C., Blimline, M., Magerko, K. A., Lawson, B. R., LaRocca, T., Donato, A. J.

and Seals, D. R. (2012) MicroRNA Changes in Human Arterial Endothelial Cells with Senescence: Relation to Apoptosis, eNOS and Inflammation, *Exp. Gerontol.*, **47**(1), pp. 45–51.

Rochelson, B., Dowling, O., Schwartz, N. and Metz, C. N. (2007) Magnesium sulfate suppresses inflammatory responses by human umbilical vein endothelial cells (HuVECs) through the NFkappaB pathway., *J. Reprod. Immunol.* Ireland, **73**(2), pp. 101–107.

Ruggeri, Z. M. (2007) The role of von Willebrand factor in thrombus formation., *Thromb. Res.* United States, **120 Suppl 1**, pp. S5-9.

Rundhaug, J. E. (2005) Matrix metalloproteinases and angiogenesis., *J. Cell. Mol. Med.* England, **9**(2), pp. 267–285.

Ryazanova, L. V, Rondon, L. J., Zierler, S., Hu, Z., Galli, J., Yamaguchi, T. P., Mazur, A., Fleig, A. and Ryazanov, A. G. (2010) TRPM7 is essential for Mg(2+) homeostasis in mammals., *Nat. Commun.* England, **1**, p. 109.

Ryazanova, L. V, Hu, Z., Suzuki, S., Chubanov, V., Fleig, A. and Ryazanov, A. G. (2014) Elucidating the role of the TRPM7 alpha-kinase: TRPM7 kinase inactivation leads to magnesium deprivation resistance phenotype in mice., *Sci. Rep.* England, **4**, p. 7599.

Safferling, K., Sütterlin, T., Westphal, K., Ernst, C., Breuhahn, K., James, M., Jäger, D., Halama, N. and Grabe, N. (2013) Wound healing revised: a novel reepithelialization mechanism revealed by in vitro and in silico models, *J. Cell Biol.* The Rockefeller University Press, **203**(4), pp. 691–709.

Sah, R., Mesirca, P., Mason, X., Gibson, W., Bates-Withers, C., Van den Boogert, M., Chaudhuri, D., Pu, W. T., Mangoni, M. E. and Clapham, D. E. (2013) Timing of myocardial trpm7 deletion during cardiogenesis variably disrupts adult ventricular function, conduction, and repolarization., *Circulation*. United States, **128**(2), pp. 101–114.

Sahni, J., Tamura, R., Sweet, I. R. and Scharenberg, A. M. (2010) TRPM7 regulates quiescent/proliferative metabolic transitions in lymphocytes., *Cell Cycle*. United States, **9**(17), pp. 3565–3574.

Salmeron, K., Aihara, T., Redondo-Castro, E., Pinteaux, E. and Bix, G. (2016) IL-1alpha induces angiogenesis in brain endothelial cells in vitro: implications for brain angiogenesis after acute injury., *J. Neurochem.* England, **136**(3), pp. 573–580.

Lo Sardo, A., Altamura, S., Pegoraro, S., Maurizio, E., Sgarra, R. and Manfioletti, G. (2013) Identification and characterization of new molecular partners for the protein arginine methyltransferase 6 (PRMT6), *PLoS One*. Public Library of Science, **8**(1), pp. e53750–e53750.

Sasaki, Y., Sathi, G. A. and Yamamoto, O. (2017) Wound healing effect of bioactive ion released from Mg-smectite., *Mater. Sci. Eng. C. Mater. Biol. Appl.* Netherlands, **77**, pp. 52–57.

Savoia, C., Battistoni, A., Calvez, V., Cesario, V., Montefusco, G. and Filippini, A. (2017) Microvascular Alterations in Hypertension and Vascular Aging., *Curr. Hypertens. Rev.* United Arab Emirates, **13**(1), pp. 16–23.

Schiff, B. A. (2009) CHAPTER 3 - Wound Healing, in Eisele, D. W. and Smith, R. V. B. T.-C. in H. and N. S. (Second E. (eds). Philadelphia: Mosby, pp. 39–45.

Schmitz, C., Dorovkov, M. V, Zhao, X., Davenport, B. J., Ryazanov, A. G. and Perraud, A.-L. (2005) The channel kinases TRPM6 and TRPM7 are functionally nonredundant., *J. Biol. Chem.* United States, **280**(45), pp. 37763–37771.

Schuchardt, J. P. and Hahn, A. (2017) Intestinal Absorption and Factors Influencing Bioavailability of Magnesium-An Update, *Curr. Nutr. Food Sci.* 2017/11/. Bentham Science Publishers, **13**(4), pp. 260–278.

Serbanovic-Canic, J., de Luca, A., Warboys, C., Ferreira, P. F., Luong, L. A., Hsiao, S., Gauci, I., Mahmoud, M., Feng, S., Souilhol, C., Bowden, N., Ashton, J.-P., Walczak, H., Firmin, D., Krams, R., Mason, J. C., Haskard, D. O., Sherwin, S., Ridger, V., *et al.* (2017) Zebrafish Model for Functional Screening of Flow-Responsive Genes., *Arterioscler. Thromb. Vasc. Biol.* United States, **37**(1), pp. 130–143.

Serebryannyy, L. A., Cruz, C. M. and de Lanerolle, P. (2016) A Role for Nuclear Actin in HDAC 1 and 2 Regulation., *Sci. Rep.* England, **6**, p. 28460.

Sfriso, R., Bongoni, A., Banz, Y., Klymiuk, N., Wolf, E. and Rieben, R. (2017)

Assessment of the Anticoagulant and Anti-inflammatory Properties of Endothelial Cells Using 3D Cell Culture and Non-anticoagulated Whole Blood., *J. Vis. Exp.* United States, (127).

Sfriso, R., Zhang, S., Bichsel, C. A., Steck, O., Despont, A., Guenat, O. T. and Rieben, R. (2018) 3D artificial round section micro-vessels to investigate endothelial cells under physiological flow conditions., *Sci. Rep.* England, **8**(1), p. 5898.

Sheu, J.-R., Hsiao, G., Shen, M.-Y., Fong, T.-H., Chen, Y.-W., Lin, C.-H. and Chou, D.-S. (2002) Mechanisms involved in the antiplatelet activity of magnesium in human platelets., *Br. J. Haematol.* England, **119**(4), pp. 1033–1041.

Shpichka, A., Butnaru, D., Bezrukov, E. A., Sukhanov, R. B., Atala, A., Burdukovskii, V., Zhang, Y. and Timashev, P. (2019) Skin tissue regeneration for burn injury, *Stem Cell Res. Ther.* BioMed Central, **10**(1), p. 94.

Shrimanker, I. and Bhattarai, S. (2019) Electrolytes, in. Treasure Island (FL).

Shrivastava, P. and Goel, A. (2010) Pre-hospital care in burn injury, *Indian J. Plast. Surg.* Medknow Publication, **43**(Suppl), pp. S15–S22.

Siemoneit, U., Tausch, L., Poeckel, D., Paul, M., Northoff, H., Koeberle, A., Jauch, J. and Werz, O. (2017) Defined Structure-Activity Relationships of Boswellic Acids Determine Modulation of Ca2+ Mobilization and Aggregation of Human Platelets by Boswellia serrata Extracts., *Planta Med.* Germany, **83**(12–13), pp. 1020–1027.

Slaviero, L., Avruscio, G., Vindigni, V. and Tocco-Tussardi, I. (2018) Antiseptics for burns: a review of the evidence., *Ann. Burns Fire Disasters*. Italy, **31**(3), pp. 198–203.

Song, Y., Ridker, P. M., Manson, J. E., Cook, N. R., Buring, J. E. and Liu, S. (2005) Magnesium intake, C-reactive protein, and the prevalence of metabolic syndrome in middle-aged and older U.S. women., *Diabetes Care*. United States, **28**(6), pp. 1438–1444.

Soriano-Tarraga, C., Mola-Caminal, M., Giralt-Steinhauer, E., Ois, A., Rodriguez-Campello, A., Cuadrado-Godia, E., Gomez-Gonzalez, A., Vivanco-Hidalgo, R. M., Fernandez-Cadenas, I., Cullell, N., Roquer, J. and Jimenez-Conde, J. (2017) Biological age is better than chronological as predictor of 3-month outcome in

ischemic stroke., *Neurology*. United States, **89**(8), pp. 830–836.

de Sousa, F. D., Vasconselos, P. D., da Silva, A. F. B., Mota, E. F., da Rocha Tome, A., Mendes, F. R. da S., Gomes, A. M. M., Abraham, D. J., Shiwen, X., Owen, J. S., Lourenzoni, M. R., Campos, A. R., Moreira, R. de A. and Monteiro-Moreira, A. C. de O. (2019) Hydrogel and membrane scaffold formulations of Frutalin (breadfruit lectin) within a polysaccharide galactomannan matrix have potential for wound healing., *Int. J. Biol. Macromol.* Netherlands, **121**, pp. 429–442.

Spitalnik, P. (no date) *No Title*, *Histol. Lab Man.* Available at: https://histologylab.ctl.columbia.edu/lab09/the-aorta/ (Accessed: 5 July 2019).

Strawn, W. B., Gallagher, P., Dean, R. H., Ganten, D. and Ferrario, C. M. (1997) Endothelial injury in transgenic (mRen-2)27 hypertensive rats, *Am. J. Hypertens.* 1997/01/01, **10**(1), pp. 51–57.

Strohacker, K., Breslin, W. L., Carpenter, K. C., Davidson, T. R., Agha, N. H. and McFarlin, B. K. (2012) Moderate-intensity, premeal cycling blunts postprandial increases in monocyte cell surface CD18 and CD11a and endothelial microparticles following a high-fat meal in young adults, *Appl. Physiol. Nutr. Metab.* 2012/04/24, **37**(3), pp. 530–539.

Su, J.-L., Chen, P.-S., Johansson, G. and Kuo, M.-L. (2012) Function and regulation of let-7 family microRNAs., *MicroRNA*. United Arab Emirates, **1**(1), pp. 34–39.

Su, L.-T., Liu, W., Chen, H.-C., Gonzalez-Pagan, O., Habas, R. and Runnels, L. W. (2011) TRPM7 regulates polarized cell movements., *Biochem. J.* England, **434**(3), pp. 513–521.

Sumpio, B. E., Riley, J. T. and Dardik, A. (2002) Cells in focus: endothelial cell, *Int. J. Biochem. Cell Biol.* 2002/10/16, **34**(12), pp. 1508–1512.

Swaminathan, R. (2003) Magnesium metabolism and its disorders, *Clin. Biochem. Rev.* The Australian Association of Clinical Biochemists, **24**(2), pp. 47–66. Available at: https://www.ncbi.nlm.nih.gov/pubmed/18568054.

Swenson, A. M., Trivedi, D. V, Rauscher, A. A., Wang, Y., Takagi, Y., Palmer, B. M., Málnási-Csizmadia, A., Debold, E. P. and Yengo, C. M. (2014) Magnesium modulates actin binding and ADP release in myosin motors, *J. Biol. Chem.*

2014/07/08. American Society for Biochemistry and Molecular Biology, **289**(34), pp. 23977–23991.

Tan, W., Palmby, T. R., Gavard, J., Amornphimoltham, P., Zheng, Y. and Gutkind, J. S. (2008) An essential role for Rac1 in endothelial cell function and vascular development., *FASEB J.* United States, **22**(6), pp. 1829–1838.

Tarantini, S., Giles, C. B., Wren, J. D., Ashpole, N. M., Valcarcel-Ares, M. N., Wei, J. Y., Sonntag, W. E., Ungvari, Z. and Csiszar, A. (2016) IGF-1 deficiency in a critical period early in life influences the vascular aging phenotype in mice by altering miRNA-mediated post-transcriptional gene regulation: implications for the developmental origins of health and disease hypothesis., *Age (Dordr).* Netherlands, **38**(4), pp. 239–258.

Teichmann, J., Morgenstern, A., Seebach, J., Schnittler, H.-J., Werner, C. and Pompe, T. (2012) The control of endothelial cell adhesion and migration by shear stress and matrix-substrate anchorage., *Biomaterials*. Netherlands, **33**(7), pp. 1959–1969.

Tennenbaum, T., Yuspa, S. H. and Kapitulnik, J. (1990) Magnesium and phosphate enrichment of culture medium stimulates the proliferation of epidermal cells from newborn and adult mice., *J. Cell. Physiol.* United States, **143**(3), pp. 431–438.

Tiwari, V. K. (2012) Burn wound: How it differs from other wounds?, *Indian J. Plast. Surg.*, **45**(2), pp. 364–373.

Toh, K. C., Ramdas, N. M. and Shivashankar, G. V (2015) Actin cytoskeleton differentially alters the dynamics of lamin A, HP1alpha and H2B core histone proteins to remodel chromatin condensation state in living cells., *Integr. Biol. (Camb).* England, **7**(10), pp. 1309–1317.

Touyz, R. M. and Yao, G. (2003) Modulation of vascular smooth muscle cell growth by magnesium-role of mitogen-activated protein kinases., *J. Cell. Physiol.* United States, **197**(3), pp. 326–335.

Townsend, J. C., Steinberg, D. H., Nielsen, C. D., Todoran, T. M., Patel, C. P., Leonardi, R. A., Wolf, B. J., Brilakis, E. S., Shunk, K. A., Goldstein, J. A., Kern, M. J. and Powers, E. R. (2013) Comparison of Lipid Deposition at Coronary

Bifurcations Versus at Nonbifurcation Portions of Coronary Arteries as Determined by Near-Infrared Spectroscopy, *Am. J. Cardiol.* 2013/05/07.

Trepat, X., Chen, Z. and Jacobson, K. (2012) Cell migration, *Compr. Physiol.*, **2**(4), pp. 2369–2392.

Uehiro, N., Sato, F., Pu, F., Tanaka, S., Kawashima, M., Kawaguchi, K., Sugimoto, M., Saji, S. and Toi, M. (2016) Circulating cell-free DNA-based epigenetic assay can detect early breast cancer., *Breast Cancer Res.* England, **18**(1), p. 129.

VanderLaan, P. A., Reardon, C. A. and Getz, G. S. (2004) Site specificity of atherosclerosis: site-selective responses to atherosclerotic modulators, *Arter. Thromb Vasc Biol*. 2003/11/08, **24**(1), pp. 12–22.

Venturelli, M., Schena, F. and Richardson, R. S. (2012) The role of exercise capacity in the health and longevity of centenarians., *Maturitas*. Ireland, **73**(2), pp. 115–120.

Volokh, O. I., Derkacheva, N. I., Studitsky, V. M. and Sokolova, O. S. (2016) [Structural studies of chromatin remodeling factors]., *Mol. Biol. (Mosk).* Russia (Federation), **50**(6), pp. 922–934.

Wang, Y., Wang, S., Lei, M., Boyett, M., Tsui, H., Liu, W. and Wang, X. (2018) The p21-activated kinase 1 (Pak1) signalling pathway in cardiac disease: from mechanistic study to therapeutic exploration., *Br. J. Pharmacol.* England, **175**(8), pp. 1362–1374.

Wasik, U., Milkiewicz, M., Kempinska-Podhorodecka, A. and Milkiewicz, P. (2017) Protection against oxidative stress mediated by the Nrf2/Keap1 axis is impaired in Primary Biliary Cholangitis, *Sci. Rep.* Nature Publishing Group, **7**, p. 44769.

Waterland, R. A. (2008) Epigenetic epidemiology of obesity: application of epigenomic technology., *Nutr. Rev.* United States, **66 Suppl 1**, pp. S21-3.

Watson, K. V, Moldow, C. F., Ogburn, P. L. and Jacob, H. S. (1986) Magnesium sulfate: rationale for its use in preeclampsia., *Proc. Natl. Acad. Sci. U.S.A.* United States, **83**(4), pp. 1075–1078.

Weidner, C. I., Lin, Q., Koch, C. M., Eisele, L., Beier, F., Ziegler, P., Bauerschlag, D. O., Jockel, K.-H., Erbel, R., Muhleisen, T. W., Zenke, M., Brummendorf, T. H. and Wagner, W. (2014) Aging of blood can be tracked by DNA methylation changes

at just three CpG sites., *Genome Biol.* England, **15**(2), p. R24.

Wenczak, B. A., Lynch, J. B. and Nanney, L. B. (1992) Epidermal growth factor receptor distribution in burn wounds. Implications for growth factor-mediated repair, *J. Clin. Invest.*, **90**(6), pp. 2392–2401.

van der Wijst, M. G. P., van Tilburg, A. Y., Ruiters, M. H. J. and Rots, M. G. (2017) Experimental mitochondria-targeted DNA methylation identifies GpC methylation, not CpG methylation, as potential regulator of mitochondrial gene expression., *Sci. Rep.* England, **7**(1), p. 177.

Wiles, M. E., Wagner, T. L. and Weglicki, W. B. (1997) Effect of acute magnesium deficiency (MgD) on aortic endothelial cell (EC) oxidant production., *Life Sci.* Netherlands, **60**(3), pp. 221–236.

Wolf, F. I. and Cittadini, A. (2003) Chemistry and biochemistry of magnesium., *Mol. Aspects Med.* England, **24**(1–3), pp. 3–9.

Wolf, F. I. and Trapani, V. (2011) MagT1: a highly specific magnesium channel with important roles beyond cellular magnesium homeostasis., *Magnes. Res.* England, **24**(3), pp. S86-91.

Wolf, S. M., Lawrenz, F. P., Nelson, C. A., Kahn, J. P., Cho, M. K., Clayton, E. W., Fletcher, J. G., Georgieff, M. K., Hammerschmidt, D., Hudson, K., Illes, J., Kapur, V., Keane, M. A., Koenig, B. A., Leroy, B. S., McFarland, E. G., Paradise, J., Parker, L. S., Terry, S. F., *et al.* (2008) Managing incidental findings in human subjects research: analysis and recommendations., *J. Law. Med. Ethics*. United States, **36**(2), pp. 211,219-248.

Wong, M., Polly, P. and Liu, T. (2015) The histone methyltransferase DOT1L: regulatory functions and a cancer therapy target., *Am. J. Cancer Res.*, **5**(9), pp. 2823–2837.

Wu, L. L., Chiou, C. C., Chang, P. Y. and Wu, J. T. (2004) Urinary 8-OHdG: a marker of oxidative stress to DNA and a risk factor for cancer, atherosclerosis and diabetics., *Clin. Chim. Acta.* Netherlands, **339**(1–2), pp. 1–9.

Wu, S. C. and Zhang, Y. (2010) Active DNA demethylation: many roads lead to Rome., *Nat. Rev. Mol. Cell Biol.* England, **11**(9), pp. 607–620.

Xia, M.-F., Bian, H., Liu, H., Wu, H.-J., Zhang, Z.-G., Lu, Z.-Q. and Gao, X. (2017) Hypokalemia, hypomagnesemia, hypocalciuria, and recurrent tetany: Gitelman syndrome in a Chinese pedigree and literature review, *Clin. case reports*. John Wiley and Sons Inc., **5**(5), pp. 578–586.

Xu, L., Willumeit-Romer, R. and Luthringer-Feyerabend, B. J. C. (2019) Effect of magnesium-degradation products and hypoxia on the angiogenesis of human umbilical vein endothelial cells., *Acta Biomater.* England.

Xu, Q. (2006) The impact of progenitor cells in atherosclerosis., *Nat. Clin. Pract. Cardiovasc. Med.* England, **3**(2), pp. 94–101.

Yan, A., Yue, T., Li, L., Li, W., Li, Q. and Li, J. (2018) Bromodomain-containing protein 7 deficiency augments atherosclerotic lesions in ApoE(-/-) mice., *Biochem. Biophys. Res. Commun.* United States, **495**(3), pp. 2202–2208.

Yan, T.-T., Li, Q., Zhang, X.-H., Wu, W.-K., Sun, J., Li, L., Zhang, Q. and Tan, H.-M. (2010) Homocysteine impaired endothelial function through compromised vascular endothelial growth factor/Akt/endothelial nitric oxide synthase signalling., *Clin. Exp. Pharmacol. Physiol.* Australia, **37**(11), pp. 1071–1077.

Yang, X., Wei, J., He, Y., Jing, T., Li, Y., Xiao, Y., Wang, B., Wang, W., Zhang, J. and Lin, R. (2017) SIRT1 inhibition promotes atherosclerosis through impaired autophagy., *Oncotarget*. United States, **8**(31), pp. 51447–51461.

Yin, Y., Morgunova, E., Jolma, A., Kaasinen, E., Sahu, B., Khund-Sayeed, S., Das, P. K., Kivioja, T., Dave, K., Zhong, F., Nitta, K. R., Taipale, M., Popov, A., Ginno, P. A., Domcke, S., Yan, J., Schubeler, D., Vinson, C. and Taipale, J. (2017) Impact of cytosine methylation on DNA binding specificities of human transcription factors., *Science*. United States, **356**(6337).

Yuan, T., Jiao, Y., de Jong, S., Ophoff, R. A., Beck, S. and Teschendorff, A. E. (2015) An integrative multi-scale analysis of the dynamic DNA methylation landscape in aging., *PLoS Genet.*, **11**(2), p. e1004996.

Yuan, Y., Li, P. and Ye, J. (2012) Lipid homeostasis and the formation of macrophage-derived foam cells in atherosclerosis, *Protein Cell*. 2012/03/27, **3**(3), pp. 173–181.

Zeng, Z., Inoue, K., Sun, H., Leng, T., Feng, X., Zhu, L. and Xiong, Z.-G. (2015) TRPM7 regulates vascular endothelial cell adhesion and tube formation., *Am. J. Physiol. Cell Physiol.* United States, **308**(4), pp. C308-18.

Zhang, A., Altura, B. T. and Altura, B. M. (1997) Elevation of extracellular magnesium rapidly raises intracellular free Mg2+ in human aortic endothelial cells: is extracellular Mg2+ a regulatory cation?, *Front. Biosci.* United States, **2**, pp. a13-7.

Zhang, B., Zhang, Y., Wang, Z. and Zheng, Y. (2000) The role of Mg2+ cofactor in the guanine nucleotide exchange and GTP hydrolysis reactions of Rho family GTP-binding proteins., *J. Biol. Chem.* United States, **275**(33), pp. 25299–25307.

Zhao, J., Chen, L., Shu, B., Tang, J., Zhang, L., Xie, J., Liu, X., Xu, Y. and Qi, S. (2015) Granulocyte/macrophage colony-stimulating factor attenuates endothelial hyperpermeability after thermal injury., *Am. J. Transl. Res.* United States, **7**(3), pp. 474–488.

Zhao, N. and Zhu, D. (2015) Endothelial responses of magnesium and other alloying elements in magnesium-based stent materials, *Metallomics*. 2014/11/03, **7**(1), pp. 118–128.

Zhao, R., Liu, Y., Wang, H., Yang, J., Niu, W., Fan, S., Xiong, W., Ma, J., Li, X., Phillips, J. B., Tan, M., Qiu, Y., Li, G. and Zhou, M. (2017) BRD7 plays an anti-inflammatory role during early acute inflammation by inhibiting activation of the NF-κB signaling pathway, *Cell. Mol. Immunol.* 2016/07/04. Nature Publishing Group, **14**(10), pp. 830–841.

Zierler, S., Hampe, S. and Nadolni, W. (2017) TRPM channels as potential therapeutic targets against pro-inflammatory diseases., *Cell Calcium*. Netherlands, **67**, pp. 105–115.

Zomer, A., Vendrig, T., Hopmans, E. S., van Eijndhoven, M., Middeldorp, J. M. and Pegtel, D. M. (2010) Exosomes: Fit to deliver small RNA, *Commun. Integr. Biol.* 2010/11/09, **3**(5), pp. 447–450.

Appendices

These appendices are composed of supplementary material for each of the results chapters. Data include material such as certificates of analyses, questionnaires and supporting material related to the human trial. Appendix A contains information related to Chapter Four and Five, and Appendix B contains information related to Chapter Six.

List of Contents

Appendix A

Table A1 Oriel (OMC) certificate of analysis, Questor Centre, Queens University, Belfast

Table A2 RT^2 Profiler Epigenetic chromatin modification enzymes array (Qiagen) gene list

Table A3 RT^2 Profiler Epigenetic chromatin re-modelling array (Qiagen) gene list

Table A4 RT^2 Profiler Wound-healing array (Qiagen) gene list

Table A5 RT^2 Profiler Fibrosis array (Qiagen) gene list

Table A6 miRNA TLDA Card A v 2.0

Table A7 miRNA TLDA Card B v 3.0

Table A8 Proseek® inflammation panel (Olink, Sweden) protein biomarker list

Appendix B

Table B1 ANCOVA statistical analyses for each parameter in the OMC+BA supplement human intervention (Chapter Six)

Ethical approval granted by DCU Research Ethics Committee

Application to Dublin City University Research Ethics Committee for human intervention

Figure B1 Human Trial Recruitment poster with tear-off contact details

Human intervention questionnaire

Informed consent form for human intervention

Safety data sheets

Appendix A

Table A1 Oriel (OMC) certificate of analysis, Questor Centre, Queens University, Belfast

Ingredient Name	**Oriel Magnesium & Mineral Extract/Oriel Marine Extract/Deep Sea Mineral Extract**				
Manufacturer's Name	Oriel Marine Extracts (A trading name of The Oriel Sea Salt Co. Ltd)				
Manufacturer Location	Port Oriel, Clogherhead, Drogheda, County Louth, A92V97C Ireland				
Manufacture Date	Mar-17				
Batch Number	ME1003				
Shelf Life (concentrate)	48 months				
Appearance	Slightly viscous, free flowing liquid				
Colour	Clear with slightly yellow tint when in larger volume				
Appearance	Feels slightly oily. Is Non adherent. No foreign material visible				
Taste & Odor	Intense Mineral salt taste. No noticeable odor.				
Density	38% (+/- 15%)				
pH	7.4 (+/- 15%)				
Viscosity	4.61 mPa.s (25° C @ 50rpm) **(+ / -** 15%)				
Certificate of Analysis					
Mineral Name	**Mineral Symbol**	**Analysis Type**	**Result**	**Unit of Measure**	**Molarity**
Magnesium	Mg	ICP-OES	74305	mg/l	3.06
Potassium	K	ICP-OES	28456	mg/l	0.73
Sodium	Na	ICP-OES	12087	mg/l	0.53
Boron	B	ICP-OES	250	mg/l	0.020
Calcium	Ca	ICP-OES	37.2	mg/l	0.001
Copper	Cu	ICP-OES	2.18	mg/l	0
Nickel	Ni	ICP-OES	1.34	mg/l	0
Silicon	Si	ICP-OES	0.95	mg/l	0
Zinc	Zn	ICP-OES	0.15	mg/l	0
Aluminium	Al	ICP-OES	<0.05	mg/l	0
Arsenic	As	ICP-OES	<0.05	mg/l	0
Barium	Ba	ICP-OES	<0.05	mg/l	0
Cadmium	Cd	ICP-OES	<0.05	mg/l	0
Cobalt	Co	ICP-OES	<0.05	mg/l	0
Chromium	Cr	ICP-OES	<0.05	mg/l	0
Iron	Fe	ICP-OES	<0.05	mg/l	0
Mercury	Hg	ICP-OES	<0.05	mg/l	0
Manganese	Mn	ICP-OES	<0.05	mg/l	0
Lead	Pb	ICP-OES	<0.05	mg/l	0
Antimony	Sb	ICP-OES	<0.05	mg/l	0
Selenium	Se	ICP-OES	<0.05	mg/l	0
Tin	Sn	ICP-OES	<0.05	mg/l	0
Strontium	Sr	ICP-OES	<0.05	mg/l	0
Titanium	Ti	ICP-OES	<0.05	mg/l	0
Vanadium	V	ICP-OES	<0.05	mg/l	0
We hereby state that the raw materials used in in the above named products are not Genetically Modified and do not contain any Genetically Modified Organisms. No GMO products, ingredients or potential sources are used or present in our manufacturing or processing facility or process.					
Analysis Completed By	**Name**	The Questor Centor, Queens University, Belfast			
	Sample ID	Marine Mineral Extract			
	Questor ID	17 10 57			
	Contact	Julie-Anne Hanna			
	Email	j.a.hanna@qub.ac.uk			
	Phone	00 44 28 9097 4675			
Document Prepared by	**Name**	Brian Fitzpatrick			
	Email	brianf@orielseasalt.com			
	Phone	00 353 87 2329199			

RT^2 Profiler array (Qiagen) Gene lists and OLINK Proseek® (Olink, Sweden) protein biomarker lists

Table A2 RT^2 Profiler Epigenetic chromatin modification enzymes array (Qiagen) gene list

UniGene	Symbol	Description
Hs.491060	ASH1L	Ash1 (absent, small, or homeotic)-like (Drosophila)
Hs.592510	ATF2	Activating transcription factor 2
Hs.250822	AURKA	Aurora kinase A
Hs.442658	AURKB	Aurora kinase B
Hs.98338	AURKC	Aurora kinase C
Hs.371416	CARM1	Coactivator-associated arginine methyltransferase 1
Hs.269092	CDYL	Chromodomain protein, Y-like
Hs.701991	CIITA	Class II, major histocompatibility complex, transactivator
Hs.728790	CSRP2BP	CSRP2 binding protein
Hs.202672	DNMT1	DNA (cytosine-5-)-methyltransferase 1
Hs.515840	DNMT3A	DNA (cytosine-5-)-methyltransferase 3 alpha
Hs.643024	DNMT3B	DNA (cytosine-5-)-methyltransferase 3 beta
Hs.713641	DOT1L	DOT1-like, histone H3 methyltransferase (S. cerevisiae)
Hs.409210	DZIP3	DAZ interacting protein 3, zinc finger
Hs.709218	EHMT2	Euchromatic histone-lysine N-methyltransferase 2
Hs.464733	ESCO1	Establishment of cohesion 1 homolog 1 (S. cerevisiae)
Hs.99480	ESCO2	Establishment of cohesion 1 homolog 2 (S. cerevisiae)
Hs.632532	HAT1	Histone acetyltransferase 1
Hs.88556	HDAC1	Histone deacetylase 1
Hs.26593	HDAC10	Histone deacetylase 10
Hs.404802	HDAC11	Histone deacetylase 11
Hs.3352	HDAC2	Histone deacetylase 2
Hs.519632	HDAC3	Histone deacetylase 3
Hs.20516	HDAC4	Histone deacetylase 4
Hs.438782	HDAC5	Histone deacetylase 5
Hs.6764	HDAC6	Histone deacetylase 6
Hs.200063	HDAC7	Histone deacetylase 7
Hs.310536	HDAC8	Histone deacetylase 8
Hs.196054	HDAC9	Histone deacetylase 9
Hs.463045	KAT2A	K(lysine) acetyltransferase 2A
Hs.533055	KAT2B	K(lysine) acetyltransferase 2B
Hs.528299	KAT5	K(lysine) acetyltransferase 5
Hs.491577	KAT6A	K(lysine) acetyltransferase 6A
Hs.35758	KAT6B	K(lysine) acetyltransferase 6B
Hs.21907	KAT7	K(lysine) acetyltransferase 7
Hs.533803	KAT8	K(lysine) acetyltransferase 8
Hs.591518	KDM1A	Lysine (K)-specific demethylase 1A
Hs.155983	KDM4A	Lysine (K)-specific demethylase 4A
Hs.709425	KDM4C	Lysine (K)-specific demethylase 4C
Hs.443650	KDM5B	Lysine (K)-specific demethylase 5B
Hs.631768	KDM5C	Lysine (K)-specific demethylase 5C
Hs.223678	KDM6B	Lysine (K)-specific demethylase 6B
Hs.25674	MBD2	Methyl-CpG binding domain protein 2
Hs.258855	MLL	Myeloid/lymphoid or mixed-lineage leukemia (trithorax homolog, Drosophila)
Hs.647120	MLL3	Myeloid/lymphoid or mixed-lineage leukemia 3
Hs.592262	MLL5	Myeloid/lymphoid or mixed-lineage leukemia 5 (trithorax homolog, Drosophila)
Hs.709264	MYSM1	Myb-like, SWIRM and MPN domains 1
Hs.596314	NCOA1	Nuclear receptor coactivator 1
Hs.592142	NCOA3	Nuclear receptor coactivator 3
Hs.368971	NCOA6	Nuclear receptor coactivator 6
Hs.197071	NEK6	NIMA (never in mitosis gene a)-related kinase 6
Hs.106861	NSD1	Nuclear receptor binding SET domain protein 1
Hs.435714	PAK1	P21 protein (Cdc42/Rac)-activated kinase 1
Hs.20521	PRMT1	Protein arginine methyltransferase 1
Hs.154163	PRMT2	Protein arginine methyltransferase 2
Hs.152337	PRMT3	Protein arginine methyltransferase 3
Hs.367854	PRMT5	Protein arginine methyltransferase 5
Hs.26006	PRMT6	Protein arginine methyltransferase 6
Hs.712584	PRMT7	Protein arginine methyltransferase 7
Hs.504530	PRMT8	Protein arginine methyltransferase 8

Hs.591490	RNF2	Ring finger protein 2
Hs.729085	RNF20	Ring finger protein 20
Hs.445387	RPS6KA3	Ribosomal protein S6 kinase, 90kDa, polypeptide 3
Hs.510225	RPS6KA5	Ribosomal protein S6 kinase, 90kDa, polypeptide 5
Hs.297483	SETD1A	SET domain containing 1A
Hs.507122	SETD1B	SET domain containing 1B
Hs.517941	SETD2	SET domain containing 2
Hs.510407	SETD3	SET domain containing 3
Hs.606200	SETD4	SET domain containing 4
Hs.288164	SETD5	SET domain containing 5
Hs.592060	SETD6	ET domain containing 6
Hs.480792	SETD7	SET domain containing (lysine methyltransferase) 7
Hs.572262	SETD8	SET domain containing (lysine methyltransferase) 8
Hs.643565	SETDB1	SET domain, bifurcated 1
Hs.631789	SETDB2	SET domain, bifurcated 2
Hs.567571	SMYD3	SET and MYND domain containing 3
Hs.522639	SUV39H1	Suppressor of variegation 3-9 homolog 1 (Drosophila)
Hs.632120	SUV420H1	Suppressor of variegation 4-20 homolog 1 (Drosophila)
Hs.379466	UBE2A	Ubiquitin-conjugating enzyme E2A
Hs.730071	UBE2B	Ubiquitin-conjugating enzyme E2B
Hs.99819	USP16	Ubiquitin specific peptidase 16
Hs.8015	USP21	Ubiquitin specific peptidase 21
Hs.462492	USP22	Ubiquitin specific peptidase 22
Hs.113876	WHSC1	Wolf-Hirschhorn syndrome candidate 1
Hs.520640	ACTB	Actin, beta
Hs.534255	B2M	Beta-2-microglobulin
Hs.592355	GAPDH	Glyceraldehyde-3-phosphate dehydrogenase
Hs.412707	HPRT1	Hypoxanthine phosphoribosyltransferase 1
Hs.546285	RPLP0	Ribosomal protein, large, P0
N/A	HGDC	Human Genomic DNA Contamination
N/A	RTC	Reverse Transcription Control
N/A	RTC	Reverse Transcription Control
N/A	RTC	Reverse Transcription Control
N/A	PPC	Positive PCR Control
N/A	PPC	Positive PCR Control
N/A	PPC	Positive PCR Control

Table A3 RT^2 Profiler Epigenetic chromatin re-modelling array (Qiagen) gene list

UniGene	Symbol	Description
Hs.468972	ARID1A	AT rich interactive domain 1A (SWI-like)
Hs.374043	ASXL1	Additional sex combs like 1 (Drosophila)
Hs.509140	BAZ1A	Bromodomain adjacent to zinc finger domain, 1A
Hs.728963	BAZ1B	Bromodomain adjacent to zinc finger domain, 1B
Hs.314263	BAZ2A	Bromodomain adjacent to zinc finger domain, 2A
Hs.470369	BAZ2B	Bromodomain adjacent to zinc finger domain, 2B
Hs.380403	BMI1	Polycomb ring finger oncogene
Hs.444200	BPTF	Bromodomain PHD finger transcription factor
Hs.127950	BRD1	Bromodomain containing 1
Hs.75243	BRD2	Bromodomain containing 2
Hs.522472	BRD3	Bromodomain containing 3
Hs.187763	BRD4	Bromodomain containing 4
Hs.437894	BRD7	Bromodomain containing 7
Hs.519337	BRD8	Bromodomain containing 8
Hs.482520	BRDT	Bromodomain, testis-specific
Hs.1004	BRPF1	Bromodomain and PHD finger containing, 1
Hs.520096	BRPF3	Bromodomain and PHD finger containing, 3
Hs.654740	BRWD1	Bromodomain and WD repeat domain containing 1
Hs.170667	BRWD3	Bromodomain and WD repeat domain containing 3
Hs.77254	CBX1	Chromobox homolog 1
Hs.381189	CBX3	Chromobox homolog 3
Hs.714363	CBX4	Chromobox homolog 4
Hs.349283	CBX5	Chromobox homolog 5
Hs.592201	CBX6	Chromobox homolog 6
Hs.356416	CBX7	Chromobox homolog 7
Hs.387258	CBX8	Chromobox homolog 8

Hs.269092	CDYL	Chromodomain protein, Y-like
Hs.373908	CDYL2	Chromodomain protein, Y-like 2
Hs.643465	CHD1	Chromodomain helicase DNA binding protein 1
Hs.220864	CHD2	Chromodomain helicase DNA binding protein 2
Hs.25601	CHD3	Chromodomain helicase DNA binding protein 3
Hs.162233	CHD4	Chromodomain helicase DNA binding protein 4
Hs.522898	CHD5	Chromodomain helicase DNA binding protein 5
Hs.371979	CHD6	Chromodomain helicase DNA binding protein 6
Hs.20395	CHD7	Chromodomain helicase DNA binding protein 7
Hs.530698	CHD8	Chromodomain helicase DNA binding protein 8
Hs.59159	CHD9	Chromodomain helicase DNA binding protein 9
Hs.208597	CTBP1	C-terminal binding protein 1
Hs.501345	CTBP2	C-terminal binding protein 2
Hs.368367	CTCF	CCCTC-binding factor (zinc finger protein)
Hs.503510	EED	Embryonic ectoderm development
Hs.444082	EZH2	Enhancer of zeste homolog 2 (Drosophila)
Hs.504091	HINFP	Histone H4 transcription factor
Hs.46700	ING1	Inhibitor of growth family, member 1
Hs.107153	ING2	Inhibitor of growth family, member 2
Hs.489811	ING3	Inhibitor of growth family, member 3
Hs.524210	ING4	Inhibitor of growth family, member 4
Hs.645460	ING5	Inhibitor of growth family, member 5
Hs.292949	INO80	INO80 homolog (S. cerevisiae)
Hs.405610	MBD1	Methyl-CpG binding domain protein 1
Hs.25674	MBD2	Methyl-CpG binding domain protein 2
Hs.178728	MBD3	Methyl-CpG binding domain protein 3
Hs.35947	MBD4	Methyl-CpG binding domain protein 4
Hs.200716	MECP2	Methyl CpG binding protein 2 (Rett syndrome)
Hs.525629	MTA1	Metastasis associated 1
Hs.173043	MTA2	Metastasis associated 1 family, member 2
Hs.159223	NAB2	NGFI-A binding protein 2 (EGR1 binding protein 2)
Hs.106861	NSD1	Nuclear receptor binding SET domain protein 1
Hs.189920	PBRM1	Polybromo 1
Hs.316750	PCGF1	Polycomb group ring finger 1
Hs.371617	PCGF2	Polycomb group ring finger 2
Hs.144309	PCGF3	Polycomb group ring finger 3
Hs.500512	PCGF5	Polycomb group ring finger 5
Hs.335808	PCGF6	Polycomb group ring finger 6
Hs.305985	PHC1	Polyhomeotic homolog 1 (Drosophila)
Hs.524271	PHC2	Polyhomeotic homolog 2 (Drosophila)
Hs.166204	PHF1	PHD finger protein 1
Hs.516079	PHF13	PHD finger protein 13
Hs.211441	PHF2	PHD finger protein 2
Hs.502458	PHF21A	PHD finger protein 21A
Hs.254097	PHF21B	PHD finger protein 21B
Hs.348921	PHF3	PHD finger protein 3
Hs.474980	PHF5A	PHD finger protein 5A
Hs.356501	PHF6	PHD finger protein 6
Hs.372719	PHF7	PHD finger protein 7
Hs.631989	RING1	Ring finger protein 1
Hs.591490	RNF2	Ring finger protein 2
Hs.298990	SMARCA2	SWI/SNF related, matrix associated, actin dependent regulator of chromatin, subfamily a, member 2
Hs.327527	SMARCA4	SWI/SNF related, matrix associated, actin dependent regulator of chromatin, subfamily a, member 4
Hs.558463	SPEN	Spen homolog, transcriptional regulator (Drosophila)
Hs.462732	SUZ12	Suppressor of zeste 12 homolog (Drosophila)
Hs.440382	TRIM27	Tripartite motif containing 27
Hs.144447	WDR11	WD repeat domain 11
Hs.446240	ZMYND8	Zinc finger, MYND-type containing 8
Hs.520640	ACTB	Actin, beta
Hs.534255	B2M	Beta-2-microglobulin
Hs.592355	GAPDH	Glyceraldehyde-3-phosphate dehydrogenase
Hs.412707	HPRT1	Hypoxanthine phosphoribosyltransferase 1
Hs.546285	RPLP0	Ribosomal protein, large, P0
N/A	HGDC	Human Genomic DNA Contamination
N/A	RTC	Reverse Transcription Control
N/A	RTC	Reverse Transcription Control
N/A	RTC	Reverse Transcription Control
N/A	PPC	Positive PCR Control
N/A	PPC	Positive PCR Control

N/A	PPC	Positive PCR Control

Table A4 RT^2 Profiler Wound-healing array (Qiagen) gene list

UniGene	Symbol	Description
Hs.500483	ACTA2	Actin, alpha 2, smooth muscle, aorta
Hs.118127	ACTC1	Actin, alpha, cardiac muscle 1
Hs.369675	ANGPT1	Angiopoietin 1
Hs.303649	CCL2	Chemokine (C-C motif) ligand 2
Hs.251526	CCL7	Chemokine (C-C motif) ligand 7
Hs.592244	CD40LG	CD40 ligand
Hs.461086	CDH1	Cadherin 1, type 1, E-cadherin (epithelial)
Hs.409662	COL14A1	Collagen, type XIV, alpha 1
Hs.172928	COL1A1	Collagen, type I, alpha 1
Hs.489142	COL1A2	Collagen, type I, alpha 2
Hs.443625	COL3A1	Collagen, type III, alpha 1
Hs.17441	COL4A1	Collagen, type IV, alpha 1
Hs.570065	COL4A3	Collagen, type IV, alpha 3 (Goodpasture antigen)
Hs.210283	COL5A1	Collagen, type V, alpha 1
Hs.445827	COL5A2	Collagen, type V, alpha 2
Hs.235368	COL5A3	Collagen, type V, alpha 3
Hs.1349	CSF2	Colony stimulating factor 2 (granulocyte-macrophage)
Hs.2233	CSF3	Colony stimulating factor 3 (granulocyte)
Hs.591346	CTGF	Connective tissue growth factor
Hs.476018	CTNNB1	Catenin (cadherin-associated protein), beta 1, 88kDa
Hs.421724	CTSG	Cathepsin G
Hs.632466	CTSK	Cathepsin K
Hs.660866	CTSL2	Cathepsin L2
Hs.789	CXCL1	Chemokine (C-X-C motif) ligand 1 (melanoma growth stimulating activity, alpha)
Hs.632592	CXCL11	Chemokine (C-X-C motif) ligand 11
Hs.590921	CXCL2	Chemokine (C-X-C motif) ligand 2
Hs.89714	CXCL5	Chemokine (C-X-C motif) ligand 5
Hs.419815	EGF	Epidermal growth factor
Hs.488293	EGFR	Epidermal growth factor receptor
Hs.335513	F13A1	C06 Hs.335513 NM_000129 F13A1 Coagulation factor XIII, A1 polypeptide
Hs.62192	F3	Coagulation factor III (thromboplastin, tissue factor)
Hs.351593	FGA	Fibrinogen alpha chain
Hs.664499	FGF10	Fibroblast growth factor 10
Hs.284244	FGF2	Fibroblast growth factor 2 (basic)
Hs.567268	FGF7	Fibroblast growth factor 7
Hs.799	HBEGF	Heparin-binding EGF-like growth factor
Hs.396530	HGF	Hepatocyte growth factor (hepapoietin A; scatter factor)
Hs.856	IFNG	Interferon, gamma
Hs.160562	IGF1	Insulin-like growth factor 1 (somatomedin C)
Hs.193717	IL10	IL10 Interleukin 10
Hs.126256	IL1B	Interleukin 1, beta
Hs.89679	IL2	Interleukin 2
Hs.73917	IL4	Interleukin 4
Hs.654458	IL6	Interleukin 6 (interferon, beta 2)
Hs.532082	IL6ST	Interleukin 6 signal transducer (gp130, oncostatin M receptor)
Hs.644352	ITGA1	Integrin, alpha 1
Hs.482077	ITGA2	Integrin, alpha 2 (CD49B, alpha 2 subunit of VLA-2 receptor)
Hs.265829	ITGA3	Integrin, alpha 3 (antigen CD49C, alpha 3 subunit of VLA-3 receptor)
Hs.694732	ITGA4	Integrin, alpha 4 (antigen CD49D, alpha 4 subunit of VLA-4 receptor)
Hs.505654	ITGA5	Integrin, alpha 5 (fibronectin receptor, alpha polypeptide)
Hs.133397	ITGA6	Integrin, alpha 6
Hs.436873	ITGAV	Integrin, alpha V (vitronectin receptor, alpha polypeptide, antigen CD51)
Hs.643813	ITGB1	Integrin, beta 1 (fibronectin receptor, beta polypeptide, antigen CD29 includes
Hs.218040	ITGB3	Integrin, beta 3 (platelet glycoprotein IIIa, antigen CD61)
Hs.536663	ITGB5	Integrin, beta 5
Hs.470399	ITGB6	Integrin, beta 6
Hs.431850	MAPK1	MAPK1 Mitogen-activated protein kinase 1
Hs.861	MAPK3	MAPK3 Mitogen-activated protein kinase 3
Hs.407995	MIF	Macrophage migration inhibitory factor (glycosylation-inhibiting factor)
Hs.83169	MMP1	Matrix metallopeptidase 1 (interstitial collagenase)
Hs.513617	MMP2	Matrix metallopeptidase 2 (gelatinase A, 72kDa gelatinase, 72kDa type IV collagenase)
Hs.2256	MMP7	Matrix metallopeptidase 7 (matrilysin, uterine)

Hs.297413	MMP9	Matrix metallopeptidase 9 (gelatinase B, 92kDa gelatinase, 92kDa type IV collagenase)
Hs.535898	PDGFA	Platelet-derived growth factor alpha polypeptide
Hs.491582	PLAT	Plasminogen activator, tissue
Hs.77274	PLAU	Plasminogen activator, urokinase
Hs.466871	PLAUR	Plasminogen activator, urokinase receptor
Hs.143436	PLG	Plasminogen
Hs.500466	PTEN	Phosphatase and tensin homolog
Hs.196384	PTGS2	Prostaglandin-endoperoxide synthase 2 (prostaglandin G/H synthase and cyclooxygenase)
Hs.413812	RAC1	Ras-related C3 botulinum toxin substrate 1 (rho family, small GTP binding protein Rac1)
Hs.247077	RHOA	Ras homolog gene family, member A
Hs.414795	SERPINE1	Serpin peptidase inhibitor, clade E (nexin, plasminogen activator inhibitor type 1), member 1
Hs.463059	STAT3	Signal transducer and activator of transcription 3 (acute-phase response factor)
Hs.503998	TAGLN	Transgelin
Hs.170009	TGFA	Transforming growth factor, alpha
Hs.645227	TGFB1	Transforming growth factor, beta 1
Hs.482390	TGFBR3	Transforming growth factor, beta receptor III
Hs.522632	TIMP1	TIMP metallopeptidase inhibitor 1
Hs.241570	TNF	TNF Tumor necrosis factor
Hs.73793	VEGFA	Vascular endothelial growth factor A
Hs.2257	VTN	Vitronectin
Hs.492974	WISP1	WNT1-inducible signalling pathway protein 1
Hs.696364	WNT5A	Wingless-type MMTV integration site family, member 5A
Hs.520640	ACTB	Actin, beta
Hs.534255	B2M	Beta-2-microglobulin
Hs.592355	GAPDH	Glyceraldehyde-3-phosphate dehydrogenase
Hs.412707	HPRT1	Hypoxanthine phosphoribosyltransferase 1
Hs.546285	RPLP0	Ribosomal protein, large, P0
N/A	HGDC	Human Genomic DNA Contamination
N/A	RTC	Reverse Transcription Control
N/A	RTC	Reverse Transcription Control
N/A	RTC	Reverse Transcription Control
N/A	PPC	Positive PCR Control
N/A	PPC	Positive PCR Control
N/A	PPC	Positive PCR Control

Table A5 RT^2 Profiler Fibrosis array (Qiagen) gene list

UniGene	Symbol	Description
Hs.500483	ACTA2	Actin, alpha 2, smooth muscle, aorta
Hs.19383	AGT	Angiotensinogen (serpin peptidase inhibitor, clade A, member 8)
Hs.525622	AKT1	V-akt murine thymoma viral oncogene homolog 1
Hs.150749	BCL2	B-cell CLL/lymphoma 2
Hs.473163	BMP7	Bone morphogenetic protein 7
Hs.74034	CAV1	Caveolin 1, caveolae protein, 22kDa
Hs.54460	CCL11	Chemokine (C-C motif) ligand 11
Hs.303649	CCL2	Chemokine (C-C motif) ligand 2
Hs.514107	CCL3	Chemokine (C-C motif) ligand 3
Hs.511794	CCR2	Chemokine (C-C motif) receptor 2
Hs.517106	CEBPB	CCAAT/enhancer binding protein (C/EBP), beta
Hs.489142	COL1A2	Collagen, type I, alpha 2
Hs.443625	COL3A1	COL3A1 Collagen, type III, alpha 1
Hs.591346	CTGF	Connective tissue growth factor
Hs.593413	CXCR4	Chemokine (C-X-C motif) receptor 4
Hs.728830	DCN	Decorin
Hs.511899	EDN1	Endothelin 1
Hs.419815	EGF	Epidermal growth factor
Hs.76753	ENG	Endoglin
Hs.2007	FASLG	Fas ligand (TNF superfamily, member 6)
Hs.40098	GREM1	Gremlin 1
Hs.396530	HGF	Hepatocyte growth factor (hepapoietin A; scatter factor)
Hs.856	IFNG	Interferon, gamma
Hs.193717	IL10	Interleukin 10
Hs.845	IL13	Interleukin 13
Hs.336046	IL13RA2	Interleukin 13 receptor, alpha 2
Hs.1722	IL1A	Interleukin 1, alpha
Hs.126256	IL1B	Interleukin 1, beta

Hs.73917	IL4	Interleukin 4
Hs.2247	IL5	Interleukin 5 (colony-stimulating factor, eosinophil)
Hs.5158	ILK	Integrin-linked kinase
Hs.632713	INHBE	Inhibin, beta E
Hs.644352	ITGA1	Integrin, alpha 1
Hs.482077	ITGA2	Integrin, alpha 2 (CD49B, alpha 2 subunit of VLA-2 receptor)
Hs.265829	ITGA3	Integrin, alpha 3 (antigen CD49C, alpha 3 subunit of VLA-3 receptor)
Hs.436873	ITGAV	Integrin, alpha V (vitronectin receptor, alpha polypeptide, antigen CD51)
Hs.643813	ITGB1	Integrin, beta 1 (fibronectin receptor, beta polypeptide, antigen CD29 includes MDF2, MSK12)
Hs.218040	ITGB3	Integrin, beta 3 (platelet glycoprotein IIIa, antigen CD61)
Hs.536663	ITGB5	Integrin, beta 5
Hs.470399	ITGB6	Integrin, beta 6
Hs.592171	ITGB8	Integrin, beta 8
Hs.714791	JUN	Jun proto-oncogene
Hs.102267	LOX	LOX Lysyl oxidase
Hs.713533	LTBP1	Latent transforming growth factor beta binding protein 1
Hs.83169	MMP1	Matrix metallopeptidase 1 (interstitial collagenase)
Hs.2936	MMP13	Matrix metallopeptidase 13 (collagenase 3)
Hs.2399	MMP14	Matrix metallopeptidase 14 (membrane-inserted)
Hs.513617	MMP2	Matrix metallopeptidase 2 (gelatinase A, 72kDa gelatinase, 72kDa type IV collagenase)
Hs.375129	MMP3	Matrix metallopeptidase 3 (stromelysin 1, progelatinase)
Hs.161839	MMP8	Matrix metallopeptidase 8 (neutrophil collagenase)
Hs.297413	MMP9	Matrix metallopeptidase 9 (gelatinase B, 92kDa gelatinase, 92kDa type IV collagenase)
Hs.202453	MYC	Myelocytomatosis viral oncogene homolog (avian)
Hs.654408	NFKB1	Nuclear factor of kappa light polypeptide gene enhancer in B-cells 1
Hs.535898	PDGFA	Platelet-derived growth factor alpha polypeptide
Hs.1976	PDGFB	Platelet-derived growth factor beta polypeptide
Hs.491582	PLAT	Plasminogen activator, tissue
Hs.77274	PLAU	Plasminogen activator, urokinase
Hs.143436	PLG	Plasminogen
Hs.525557	SERPINA1	Serpin peptidase inhibitor, clade A (alpha-1 antiproteinase, antitrypsin), member
Hs.414795	SERPINE1	Serpin peptidase inhibitor, clade E (nexin, plasminogen activator inhibitor type 1), member 1
Hs.596449	SERPINH1	Serpin peptidase inhibitor, clade H (heat shock protein 47), member 1, (collagen binding protein 1)
Hs.12253	SMAD2	SMAD family member 2
Hs.714621	SMAD3	SMAD family member 3
Hs.75862	SMAD4	SMAD family member 4
Hs.153863	SMAD6	SMAD family member 6
Hs.465087	SMAD7	SMAD family member 7
Hs.48029	SNAI1	Snail homolog 1 (Drosophila)
Hs.620754	SP1	Sp1 transcription factor
Hs.642990	STAT1	Signal transducer and activator of transcription 1, 91kDa
Hs.524518	STAT6	Signal transducer and activator of transcription 6, interleukin-4 induced
Hs.645227	TGFB1	Transforming growth factor, beta 1
Hs.133379	TGFB2	Transforming growth factor, beta 2
Hs.592317	TGFB3	Transforming growth factor, beta 3
Hs.494622	TGFBR1	Transforming growth factor, beta receptor 1
Hs.604277	TGFBR2	Transforming growth factor, beta receptor II (70/80kDa)
Hs.373550	TGIF1	TGFB-induced factor homeobox 1
Hs.164226	THBS1	Thrombospondin 1
Hs.371147	THBS2	Thrombospondin 2
Hs.522632	TIMP1	Metallopeptidase inhibitor 1
Hs.633514	TIMP2	Metallopeptidase inhibitor 2
Hs.644633	TIMP3	Metallopeptidase inhibitor 3
Hs.591665	TIMP4	Metallopeptidase inhibitor 4
Hs.241570	TNF	Tumor necrosis factor
Hs.73793	VEGFA	Vascular endothelial growth factor A
Hs.520640	ACTB	Actin, beta
Hs.534255	B2M	Beta-2-microglobulin
Hs.592355	GAPDH	Glyceraldehyde-3-phosphate dehydrogenase
Hs.412707	HPRT1	Hypoxanthine phosphoribosyltransferase 1
Hs.546285	RPLP0	Ribosomal protein, large, P0
N/A	HGDC	Human Genomic DNA Contamination
N/A	RTC	Reverse Transcription Control
N/A	RTC	Reverse Transcription Control
N/A	RTC	Reverse Transcription Control
N/A	PPC	Positive PCR Control
N/A	PPC	Positive PCR Control

N/A	PPC	Positive PCR Control

Table A6 miRNA TLDA Card A v 2.0

hsa-let-7a	hsa-miR-148a	mmu-miR-374-5p	hsa-miR-539
hsa-let-7c	hsa-miR-148b	hsa-miR-375	hsa-miR-541
hsa-let-7d	hsa-miR-149	hsa-miR-376a	hsa-miR-542-3p
hsa-let-7e	hsa-miR-150	hsa-miR-376b	hsa-miR-542-5p
hsa-let-7f	hsa-miR-152	hsa-miR-377	hsa-miR-544
hsa-let-7g	mmu-miR-153	mmu-miR-379	hsa-miR-545
hsa-miR-1	hsa-miR-154	hsa-miR-380-3p	hsa-miR-548a
hsa-miR-9	hsa-miR-181a	hsa-miR-381	hsa-miR-548a-5p
hsa-miR-10a	hsa-miR-181c	hsa-miR-382	hsa-miR-548b
hsa-miR-10b	hsa-miR-182	hsa-miR-383	hsa-miR-548b-5p
U6 snRNA	RNU48	hsa-miR-409-5p	hsa-miR-548c
U6 snRNA	hsa-miR-183	hsa-miR-410	hsa-miR-548c-5p
hsa-miR-15a	hsa-miR-184	hsa-miR-411	hsa-miR-548d
hsa-miR-15b	hsa-miR-185	hsa-miR-422a	hsa-miR-548d-5p
hsa-miR-16	hsa-miR-186	hsa-miR-423-5p	hsa-miR-551b
hsa-miR-17	mmu-miR-187	hsa-miR-424	hsa-miR-556-3p
hsa-miR-18a	hsa-miR-188-3p	hsa-miR-425-5p	hsa-miR-556-5p
hsa-miR-18b	hsa-miR-190	hsa-miR-429	hsa-miR-561
hsa-miR-19a	hsa-miR-191	hsa-miR-431	hsa-miR-570
hsa-miR-19b	hsa-miR-192	hsa-miR-433	hsa-miR-574-3p
hsa-miR-20a	hsa-miR-193a-3p	hsa-miR-449	hsa-miR-576-3p
hsa-miR-20b	hsa-miR-193a-5p	hsa-miR-449b	hsa-miR-576-5p
hsa-miR-21	hsa-miR-193b	hsa-miR-450a	hsa-miR-579
hsa-miR-22	hsa-miR-194	hsa-miR-450b-3p	hsa-miR-582-3p
hsa-miR-23a	hsa-miR-195	hsa-miR-450b-5p	hsa-miR-582-5p
hsa-miR-23b	hsa-miR-196b	mmu-miR-451	hsa-miR-589
hsa-miR-24	hsa-miR-197	hsa-miR-452	hsa-miR-590-5p
hsa-miR-25	hsa-miR-198	hsa-miR-453	hsa-miR-597
hsa-miR-26a	hsa-miR-199a	hsa-miR-454	hsa-miR-598
hsa-miR-26b	hsa-miR-199a-3p	hsa-miR-455-3p	mmu-miR-615
hsa-miR-27a	hsa-miR-199b	hsa-miR-455	hsa-miR-615-5p
hsa-miR-27b	hsa-miR-200a	hsa-miR-483-5p	hsa-miR-616
hsa-miR-28-3p	hsa-miR-200b	hsa-miR-484	hsa-miR-618
hsa-miR-28	hsa-miR-200c	hsa-miR-485-3p	hsa-miR-624
U6 snRNA	hsa-miR-202	hsa-miR-485-5p	hsa-miR-625
U6 snRNA	hsa-miR-203	hsa-miR-486-3p	hsa-miR-627
hsa-miR-29a	hsa-miR-204	hsa-miR-486	hsa-miR-628-5p
hsa-miR-29b	hsa-miR-205	hsa-miR-487a	hsa-miR-629
hsa-miR-29c	hsa-miR-208b	hsa-miR-487b	hsa-miR-636
hsa-miR-30b	hsa-miR-210	hsa-miR-488	hsa-miR-642
hsa-miR-30c	hsa-miR-214	hsa-miR-489	hsa-miR-651
hsa-miR-31	hsa-miR-215	hsa-miR-490	hsa-miR-652
hsa-miR-32	hsa-miR-216a	hsa-miR-491-3p	hsa-miR-653
hsa-miR-33b	hsa-miR-216b	mmu-miR-491	hsa-miR-654-3p
hsa-miR-34a	hsa-miR-217	hsa-miR-493	hsa-miR-654
hsa-miR-34c	hsa-miR-218	hsa-miR-494	hsa-miR-655
hsa-miR-92a	hsa-miR-219	mmu-miR-495	hsa-miR-660
mmu-miR-93	hsa-miR-221	mmu-miR-496	hsa-miR-671-3p
hsa-miR-95	hsa-miR-222	hsa-miR-499-3p	hsa-miR-672
mmu-miR-96	hsa-miR-223	mmu-miR-499	hsa-miR-674
hsa-miR-98	hsa-miR-224	hsa-miR-500	hsa-miR-708
hsa-miR-99a	hsa-miR-296-3p	hsa-miR-501-3p	hsa-miR-744
hsa-miR-99b	hsa-miR-296	hsa-miR-501	hsa-miR-758
hsa-miR-100	hsa-miR-299-3p	hsa-miR-502-3p	hsa-miR-871
hsa-miR-101	hsa-miR-299-5p	hsa-miR-502	hsa-miR-872
hsa-miR-103	hsa-miR-301	hsa-miR-503	hsa-miR-873
hsa-miR-105	hsa-miR-301b	hsa-miR-504	hsa-miR-874
hsa-miR-106a	hsa-miR-302a	hsa-miR-505	hsa-miR-875-3p
RNU44	ath-miR159a	hsa-miR-507	hsa-miR-876-3p
hsa-miR-106b	hsa-miR-302b	hsa-miR-508	hsa-miR-876-5p
hsa-miR-107	hsa-miR-302c	hsa-miR-508-5p	hsa-miR-885-3p
hsa-miR-122	hsa-miR-320	hsa-miR-509-5p	hsa-miR-885-5p
mmu-miR-124a	hsa-miR-323-3p	hsa-miR-510	hsa-miR-886-3p

hsa-miR-125a-3p	hsa-miR-324-3p	hsa-miR-512-3p	hsa-miR-886-5p
hsa-miR-125a-5p	hsa-miR-324-5p	hsa-miR-512-5p	hsa-miR-887
hsa-miR-125b	hsa-miR-326	hsa-miR-513-5p	hsa-miR-888
hsa-miR-126	hsa-miR-328	hsa-miR-515-3p	hsa-miR-889
hsa-miR-127	hsa-miR-329	hsa-miR-515-5p	hsa-miR-890
hsa-miR-127-5p	hsa-miR-330	hsa-miR-516a-5p	hsa-miR-891a
hsa-miR-128a	hsa-miR-330-5p	hsa-miR-516b	hsa-miR-891b
mmu-miR-129-3p	hsa-miR-331	hsa-miR-517a	hsa-miR-892a
hsa-miR-129	hsa-miR-331-5p	hsa-miR-517c	hsa-miR-147
hsa-miR-130a	hsa-miR-335	hsa-miR-518a-3p	hsa-miR-208
hsa-miR-130b	hsa-miR-337-5p	hsa-miR-518a-5p	hsa-miR-211
hsa-miR-132	hsa-miR-338-3p	hsa-miR-518b	hsa-miR-212
hsa-miR-133a	hsa-miR-339-3p	hsa-miR-518c	hsa-miR-219-1-3p
hsa-miR-133b	hsa-miR-339-5p	hsa-miR-518d	hsa-miR-219-2-3p
mmu-miR-134	hsa-miR-340	hsa-miR-518d-5p	hsa-miR-220
hsa-miR-135a	hsa-miR-155	hsa-miR-518e	hsa-miR-220b
hsa-miR-135b	hsa-let-7b	hsa-miR-518f	hsa-miR-220c
hsa-miR-136	hsa-miR-342-3p	hsa-miR-519a	hsa-miR-298
mmu-miR-137	hsa-miR-342-5p	hsa-miR-519d	hsa-miR-325
hsa-miR-138	hsa-miR-345	hsa-miR-519e	hsa-miR-346
hsa-miR-139-3p	hsa-miR-361	hsa-miR-520a	hsa-miR-376c
hsa-miR-139-5p	hsa-miR-362-3p	hsa-miR-520a#	hsa-miR-384
hsa-miR-140-3p	hsa-miR-362	hsa-miR-520d-5p	hsa-miR-412
mmu-miR-140	hsa-miR-363	hsa-miR-520g	hsa-miR-448
hsa-miR-141	hsa-miR-365	hsa-miR-521	hsa-miR-492
hsa-miR-142-3p	hsa-miR-367	hsa-miR-522	hsa-miR-506
hsa-miR-142-5p	hsa-miR-369-3p	hsa-miR-523	hsa-miR-509-3-5p
hsa-miR-143	hsa-miR-369-5p	hsa-miR-524-5p	hsa-miR-511
hsa-miR-145	hsa-miR-370	hsa-miR-525-3p	hsa-miR-517b
hsa-miR-146a	hsa-miR-371-3p	hsa-miR-525	hsa-miR-519c
hsa-miR-146b-3p	hsa-miR-372	hsa-miR-526b	hsa-miR-520b
hsa-miR-146b	hsa-miR-373	hsa-miR-532-3p	hsa-miR-520e
hsa-miR-147b	hsa-miR-374	hsa-miR-532	hsa-miR-520f

Table A7 miRNA TLDA Card B v 3.0

dme-miR-7	hsa-miR-644	hsa-miR-933	hsa-miR-620
hsa-miR-548I	hsa-miR-645	hsa-miR-934	hsa-miR-577
hsa-miR-30a-3p	hsa-miR-621	hsa-miR-935	hsa-miR-144
hsa-miR-30a-5p	hsa-miR-646	hsa-miR-936	hsa-miR-590-3P
hsa-miR-30d	hsa-miR-647	hsa-miR-937	hsa-miR-191#
hsa-miR-30e-3p	hsa-miR-648	hsa-miR-938	hsa-miR-665
hsa-miR-34b	hsa-miR-649	hsa-miR-939	hsa-miR-520D-3P
hsa-miR-126#	hsa-miR-650	hsa-miR-941	hsa-miR-1224-3P
hsa-miR-154#	hsa-miR-661	hsa-miR-335#	hsa-miR-1305
hsa-miR-182#	hsa-miR-662	hsa-miR-942	hsa-miR-513C
U6 snRNA	RNU48	hsa-miR-943	hsa-miR-513B
U6 snRNA	hsa-miR-571	hsa-miR-944	hsa-miR-1226#
hsa-miR-206	hsa-miR-572	hsa-miR-99b#	hsa-miR-1236
hsa-miR-213	hsa-miR-573	hsa-miR-124#	hsa-miR-1228#
hsa-miR-302c#	hsa-miR-575	hsa-miR-541#	hsa-miR-1225-3P
hsa-miR-302d	hsa-miR-578	hsa-miR-875-5p	hsa-miR-1233
hsa-miR-378	hsa-miR-580	hsa-miR-888#	hsa-miR-1227
hsa-miR-380-5p	hsa-miR-581	hsa-miR-892b	hsa-miR-1286
hsa-miR-1257	hsa-miR-583	hsa-miR-9#	hsa-miR-548M
hsa-miR-200a#	hsa-miR-584	hsa-miR-411#	hsa-miR-1179
hsa-miR-432	hsa-miR-585	hsa-miR-378	hsa-miR-1178
hsa-miR-432#	rno-miR-29c#	hsa-miR-151-3p	hsa-miR-1205
hsa-miR-497	hsa-miR-766	hsa-miR-340#	hsa-miR-1271
hsa-miR-500	hsa-miR-595	hsa-miR-190b	hsa-miR-1201
hsa-miR-1238	hsa-miR-668	hsa-miR-545#	hsa-miR-548J
hsa-miR-488	hsa-miR-767-5p	hsa-miR-183#	hsa-miR-1263
hsa-miR-517#	hsa-miR-767-3p	hsa-miR-192#	hsa-miR-1294
hsa-miR-516-3p	hsa-miR-454#	hsa-miR-200b#	hsa-miR-1269
hsa-miR-518c#	hsa-miR-769-5p	hsa-miR-200c#	hsa-miR-1265
hsa-miR-519e#	hsa-miR-770-5p	hsa-miR-155#	hsa-miR-1244
hsa-miR-520h	hsa-miR-769-3p	hsa-miR-10a#	hsa-miR-1303
hsa-miR-524	hsa-miR-802	hsa-miR-214#	hsa-miR-1259
mmu-let-7d#	hsa-miR-675	hsa-miR-218-2#	hsa-miR-548P

hsa-miR-363#	hsa-miR-505#	hsa-miR-129#	hsa-miR-1264
U6 snRNA	hsa-miR-218-1#	hsa-miR-22#	hsa-miR-1255B
U6 snRNA	hsa-miR-221#	hsa-miR-425#	hsa-miR-1282
rno-miR-7#	hsa-miR-222#	hsa-miR-30d#	hsa-miR-1255A
hsa-miR-656	hsa-miR-223#	hsa-let-7a#	hsa-miR-1270
hsa-miR-549	hsa-miR-136#	hsa-miR-424#	hsa-miR-1197
hsa-miR-657	hsa-miR-34b	hsa-miR-18b#	hsa-miR-1324
hsa-miR-658	hsa-miR-185#	hsa-miR-20b#	hsa-miR-548H
hsa-miR-659	hsa-miR-186#	hsa-miR-431#	hsa-miR-1254
hsa-miR-551a	hsa-miR-195#	hsa-miR-7-2#	hsa-miR-548K
hsa-miR-552	hsa-miR-30c-1#	hsa-miR-10b#	hsa-miR-1251
hsa-miR-553	hsa-miR-30c-2#	hsa-miR-34a#	hsa-miR-1285
hsa-miR-554	hsa-miR-32#	hsa-miR-181a-2#	hsa-miR-1245
hsa-miR-555	hsa-miR-31#	hsa-miR-744#	hsa-miR-1292
hsa-miR-557	hsa-miR-130b#	hsa-miR-452#	hsa-miR-1301
hsa-miR-558	hsa-miR-26a-2#	hsa-miR-409-3p	hsa-miR-1200
hsa-miR-559	hsa-miR-361-3p	hsa-miR-181c#	hsa-miR-1182
hsa-miR-562	hsa-let-7g#	hsa-miR-196a#	hsa-miR-1288
hsa-miR-563	hsa-miR-302b#	hsa-miR-483-3p	hsa-miR-1291
hsa-miR-564	hsa-miR-302d#	hsa-miR-708#	hsa-miR-1275
hsa-miR-566	hsa-miR-367#	hsa-miR-92b#	hsa-miR-1183
hsa-miR-567	hsa-miR-374a#	hsa-miR-551b#	hsa-miR-1184
hsa-miR-569	hsa-miR-23b#	hsa-miR-202#	hsa-miR-1276
hsa-miR-586	hsa-miR-376a#	hsa-miR-193b#	hsa-miR-320B
hsa-miR-587	hsa-miR-377#	hsa-miR-497#	hsa-miR-1272
RNU44	ath-miR159a	hsa-miR-518e#	hsa-miR-1180
hsa-miR-588	hsa-miR-30b#	hsa-miR-543	hsa-miR-1256
hsa-miR-589	hsa-miR-122#	hsa-miR-125b-1#	hsa-miR-1278
hsa-miR-550	hsa-miR-130a#	hsa-miR-194#	hsa-miR-1262
hsa-miR-591	hsa-miR-132#	hsa-miR-106b#	hsa-miR-1243
hsa-miR-592	hsa-miR-148a#	hsa-miR-302a#	hsa-miR-663B
hsa-miR-593	hsa-miR-33a	hsa-miR-519b-3p	hsa-miR-1252
hsa-miR-596	hsa-miR-33a#	hsa-miR-518f#	hsa-miR-1298
hsa-miR-622	hsa-miR-92a-1#	hsa-miR-374b#	hsa-miR-1290
hsa-miR-599	hsa-miR-92a-2#	hsa-miR-520c-3p	hsa-miR-1249
hsa-miR-623	hsa-miR-93#	hsa-let-7b#	hsa-miR-1248
hsa-miR-600	hsa-miR-96#	hsa-let-7c#	hsa-miR-1289
hsa-miR-624	hsa-miR-99a#	hsa-let-7e#	hsa-miR-1204
hsa-miR-601	hsa-miR-100#	hsa-miR-550	hsa-miR-1826
hsa-miR-626	hsa-miR-101#	hsa-miR-593	hsa-miR-1304
hsa-miR-629	hsa-miR-138-2#	hsa-let-7f-1#	hsa-miR-1203
hsa-miR-630	hsa-miR-141#	hsa-let-7f-2#	hsa-miR-1206
hsa-miR-631	hsa-miR-143#	hsa-miR-15a#	hsa-miR-548G
hsa-miR-603	hsa-miR-144#	hsa-miR-16-1#	hsa-miR-1208
hsa-miR-604	hsa-miR-145#	hsa-miR-17#	hsa-miR-548E
hsa-miR-605	hsa-miR-920	hsa-miR-18a#	hsa-miR-1274A
hsa-miR-606	hsa-miR-921	hsa-miR-19a#	hsa-miR-1274B
hsa-miR-607	hsa-miR-922	hsa-miR-19b-1#	hsa-miR-1267
hsa-miR-608	hsa-miR-924	hsa-miR-625#	hsa-miR-1250
hsa-miR-609	hsa-miR-337-3p	hsa-miR-628-3p	hsa-miR-548N
hsa-miR-633	hsa-miR-125b-2#	hsa-miR-20a#	hsa-miR-1283
hsa-miR-634	hsa-miR-135b#	hsa-miR-21#	hsa-miR-1247
hsa-miR-635	hsa-miR-148b#	hsa-miR-23a#	hsa-miR-1253
hsa-miR-637	hsa-miR-146a#	hsa-miR-24-1#	hsa-miR-720
hsa-miR-638	hsa-miR-149#	hsa-miR-24-2#	hsa-miR-1260
hsa-miR-639	hsa-miR-29b-1#	hsa-miR-25#	hsa-miR-664
hsa-miR-640	hsa-miR-29b-2#	hsa-miR-26a-1#	hsa-miR-1302
hsa-miR-641	hsa-miR-105#	hsa-miR-26b#	hsa-miR-1300
hsa-miR-613	hsa-miR-106a#	hsa-miR-27a#	hsa-miR-1284
hsa-miR-614	hsa-miR-16-2#	hsa-miR-29a#	hsa-miR-548L
hsa-miR-616	hsa-let-7i#	hsa-miR-151-5P	hsa-miR-1293
hsa-miR-617	hsa-miR-15b#	hsa-miR-765	hsa-miR-1825
hsa-miR-643	hsa-miR-27b#	hsa-miR-338-5P	hsa-miR-1296

Table A8 Proseek® inflammation panel (Olink, Sweden) protein biomarker list

Uniprot ID	Symbol	Description
Q13541	4E-BP1	Eukaryotic translation initiation factor 4E-binding protein 1
P00813	ADA	Adenosine Deaminase
Q5T4W7	ARTN	Artemin
O15169	AXIN1	Axin-1
P23560	BDNF	Brain-derived neurotrophic factor
P01138	Beta-NGF	Beta-nerve growth factor
Q14790	CASP-8	Caspase-8
P51671	CCL11	Eotaxin-1
Q99731	CCL19	C-C motif chemokine 19
P78556	CCL20	C-C motif chemokine 20
P55773	CCL23	C-C motif chemokine 23
O15444	CCL25	C-C motif chemokine 25
Q9NRJ3	CCL28	C-C motif chemokine 28
P10147	CCL3	C-C motif chemokine 3
P13236	CCL4	C-C motif chemokine 4
Q9BZW8	CD244	Natural killer cell receptor 2B4
P25942	CD40	CD40L receptor
P06127	CD5	T-cell surface glycoprotein CD5
Q8WWJ7	CD6	T cell surface glycoprotein CD6 isoform
Q9H5V8	CDCP1	CUB domain-containing protein 1
P09603	CSF-1	Macrophage colony-stimulating factor 1
P28325	CST5	Cystatin D
P78423	CX3CL1	Fractalkine
P09341	CXCL1	C-X-C motif chemokine 1
P02778	CXCL10	C-X-C motif chemokine 10
O14625	CXCL11	C-X-C motif chemokine 11
P42830	CXCL5	C-X-C motif chemokine 5
P80162	CXCL6	C-X-C motif chemokine 6
Q07325	CXCL9	C-X-C motif chemokine 9
Q8NFT8	DNER	Delta and Notch-like epidermal growth factor-related receptor
P80511	EN-RAGE	Protein S100-A12
O95750	FGF-19	Fibroblast growth factor 19
Q9NSA1	FGF-21	Fibroblast growth factor 21
Q9GZV9	FGF-23	Fibroblast growth factor 23
Q8NF90	FGF-5	Fibroblast growth factor 5
P49771	Flt3L	Fms-related tyrosine kinase 3 ligand
P39905	GDNF	Glial cell line-derived neurotrophic factor
P14210	HGF	Hepatocyte growth factor
P01579	IFN-gamma	Interferon gamma
P01583	IL-1 alpha	Interleukin-1 alpha
P22301	IL10	Interleukin-10
Q13651	IL-10RA	Interleukin-10 receptor subunit alpha
Q08334	IL-10RB	Interleukin-10 receptor subunit beta
P29460	IL-12B	Interleukin-12 subunit beta
P35225	IL13	Interleukin-13
Q13261	IL-15RA	Interleukin-15 receptor subunit alpha
Q16552	IL-17A	Interleukin-17A
Q9P0M4	IL-17C	Interleukin-17C
Q14116	IL18	Interleukin-18
Q13478	IL-18R1	Interleukin-18 receptor 1
P60568	IL2	Interleukin-2
Q9NYY1	IL-20	Interleukin-20
Q9UHF4	IL-20RA	Interleukin-20 receptor subunit alpha
Q8N6P7	IL-22 RA1	Interleukin-22 receptor subunit alpha-1
Q13007	IL-24	Interleukin-24
P14784	IL-2RB	Interleukin-2 receptor subunit beta
O95760	IL33	Interleukin-33
P05112	IL4	Interleukin-4
P05113	IL5	Interleukin-5
P05231	IL6	Interleukin-6
P13232	IL7	Interleukin-7
P10145	IL8	Interleukin-8
P01137	LAP TGF-beta-1	Latency-associated peptide transforming growth factor beta-1
P15018	LIF	Leukemia inhibitory factor
P42702	LIF-R	Leukemia inhibitory factor receptor
P13500	MCP-1	Monocyte chemotactic protein 1

P80075	MCP-2	Monocyte chemotactic protein 2
P80098	MCP-3	Monocyte chemotactic protein 3
Q99616	MCP-4	Monocyte chemotactic protein 4
P03956	MMP-1	Matrix metalloproteinase-1
P09238	MMP-10	Matrix metalloproteinase-10
Q99748	NRTN	Neurturin
P20783	NT-3	Neurotrophin-3
O00300	OPG	Osteoprotegerin
P13725	OSM	Oncostatin-M
Q9NZQ7	PD-L1	Programmed cell death 1 ligand 1
P21583	SCF	Stem cell factor
Q8IXJ6	SIRT2	SIR2-like protein 2
Q13291	SLAMF1	Signaling lymphocytic activation molecule
P50225	ST1A1	Sulfotransferase 1A1
O95630	STAMPB	STAM-binding protein
P01135	TGF-alpha	Transforming growth factor alpha
P01375	TNF	Tumor necrosis factor
P01374	TNFB	TNF-beta
Q07011	TNFRSF9	Tumor necrosis factor receptor superfamily member 9
O43557	TNFSF14	Tumor necrosis factor ligand superfamily member 14
P50591	TRAIL	TNF-related apoptosis-inducing ligand
O14788	TRANCE	TNF-related activation-induced cytokine
Q969D9	TSLP	Thymic stromal lymphopoietin
O43508	TWEAK	Tumor necrosis factor (Ligand) superfamily, member 12
P00749	uPA	Urokinase-type plasminogen activator
P15692	VEGFA	Vascular endothelial growth factor A

Appendix B

Table B1 ANCOVA statistical analyses for each parameter in the OMC+BA supplement human intervention (Chapter Six). One-way ANCOVA analyses were applied to all normally-distributed data to ascertain the significance of the difference between pre and post values. Partial η^2 provides an interpretable value on the magnitude of the effect of the supplement intervention. Note that additional proteins were examined, but did not demonstrate statistically significant differences.

Parameter	Estimated marginal means		P-value	F-test	P-value	Partial Eta^2 ($\eta 2$)
	Placebo	Treatment				
Platelet adhesion	76.45	71.30	0.001	141337	0.001	0.56
Platelet aggregation	130.79	94.46	0.05	1731.29	0.001	0.47
8-OHdG	213.38	201.06	0.71	8.44	0.10	0.01
TGF-α	13.79	9.94	0.03	13.73	0.003	0.53
Axin-1	3.47	7.03	0.05	4.98	0.84	0.29
STAMBP	9.08	14.96	0.04	5.21	0.81	0.30

Ethical approval Granted by DCU Research Ethics Committee

Ollscoil Chathair Bhaile Átha Cliath
Dublin City University

Dr Ronan Murphy
School of Health and Human Performance

27 February 2017

REC Reference: **DCUREC/2016/221**

Proposal Title: **To Investigate the Anti-Oxidative Effect of Functional Drink Supplement**

Applicant(s): **Dr Ronan Murphy**

Dear Ronan,

Further to expedited review, the DCU Research Ethics Committee approves this research proposal.

Materials used to recruit participants should note that ethical approval for this project has been obtained from the Dublin City University Research Ethics Committee.

Should substantial modifications to the research protocol be required at a later stage, a further amendment submission should be made to the REC.

Yours sincerely,

Donal O' Gorman

Dr Dónal O'Gorman
Chairperson
DCU Research Ethics Committee

DCU
Research & Innovation

Taighde & Nuálaíocht Tacaíocht
Ollscoil Chathair Bhaile Átha Cliath,
Baile Átha Cliath, Éire

Research & Innovation Support
Dublin City University,
Dublin 9, Ireland

T +353 1 700 8000
F +353 1 700 8002
E research@dcu.ie
www.dcu.ie

Application to Dublin City University Research Ethics Committee for human intervention

The information contained herein is, to the best of my knowledge and belief, accurate. I have read the University's current research ethics guidelines, and accept responsibility for the conduct of the procedures set out in the attached application in accordance with the form guidelines, the REC guidelines, the University's policy on Conflict of Interest, Code of Good Research Practice and any other condition laid down by the Dublin City University Research Ethics Committee.

I have attempted to identify all risks related to the research that may arise in conducting this research and acknowledge my obligations and the rights of the participants.

If there exists any affiliation or financial interest for researcher(s) in this research or its outcomes or any other circumstances, which might represent a perceived, potential or actual conflict of interest this should be declared in accordance with Dublin City University policy on Conflicts of Interest.

I and my co-investigators or supporting staff have the appropriate qualifications, experience and facilities to conduct the research set out in the attached application and to deal with any emergencies and contingencies related to the research that may arise.

By signing this agreement you are confirming you accept responsibility for the conduct of the procedures set out in the application.

Investigator name (print)	**Signature**	**Date**
Ronan Murphy		28th November, 2016
Robert Wallace		28th November, 2016

(Please insert further lines if necessary)

Important Notes:

· Please ensure you upload any additional relevant documentation to your application: E.G. copy of Survey/Questionnaire, copy of Interview/Focus Group schedule, copy of permission/approval from external sources (i.e. approval to access individuals in an organisation, school, community group)

· The application should be completed entirely through the online form. No supplementary information should be sent by email or hardcopy.

· All sections of the application form must be answered. The completed application must be proofread and spellchecked before submission to REC

· Student applicants must include their supervisor contact details in this form. This applies to all student applicants (masters and postgraduate). The submission confirmation form should be approved and signed by all research team members in advance of submission to REC. This form must be uploaded with the application.

· Applications which do not adhere to these requirements will not be accepted for review and will be returned directly to the applicant. The administrator to the Research Ethics Committee will assess, on receiving such notification, whether the information provided is adequate.

· Project supervisors have the primary responsibility to ensure that students do not take on research that could expose them and the participants to significant risk, such as might arise, for example, in interviewing members of vulnerable groups such as young children. In general, please refer to the REC Guidelines for further guidance on what research procedures or circumstances might make a higher level of ethical approval necessary. See https://www4.dcu.ie/researchsupport/research_ethics/guidelines.shtml

Figure B1 Human Trial Recruitment poster with tear-off contact details

Human intervention plain language statement

Dublin City University

Plain Language Statement

I. Introduction to the Research Study

This research study will assess the beneficial effects of two functional health supplements (1) Deep Ocean Minerals (principally ionic Magnesium) with Boswellia serrata extract, and (2) Deep Ocean Minerals alone. We will assess various biological parameters before and after the 4-week supplementation trial- Height and weight (BMI), Blood pressure, platelet function and oxidative stress in the blood. It will run as part of the health trial on a functional drink for Neal's Yard Remedies and Oriel Deep Ocean Minerals Supplements, at the School of Health & Human Performance, DCU. Various experiments in the fields of immunology/inflammation and physiology will take place. The platelet function test, BMI and blood pressure will fall under the physiological measurement. Biomarker studies will look at cardiovascular and inflammatory health.

The purpose of this project is to therefore, examine the anti-oxidative and anti-inflammatory effects of these two natural products (Deep Ocean Minerals and Boswellia serrata extract) as well as platelet activity in a cohort of 45-65 year old healthy females. Platelets are tiny fragments of larger cells, which circulate within the blood stream. Their main function is to aid in primary hemostasis - blood clotting. They complete this by sticking to an injured vessel wall and then sticking to each other to form a small clot. Platelet activity can vary amongst individuals of varying health status/fitness/age and is increasingly being noted as a marker of vascular health. The inflammatory markers to be measured are an indicator of sub-clinical health and are not a disease diagnostic or prognostic, but rather a measure of your cardiovascular competence and over all physiological health. On the extremely low chance that we discover an incidental finding that may have implications on your health, you will be informed in accordance with best practice, guidelines and protocol laid out by Susan M. Wolf et al., J Law Med Ethics. 2008; 36(2): 219-211 Managing Incidental Findings In Human Subjects Research: Analysis and Recommendations.

We would like to profile the platelet activity, blood pressure and biomarker signature of the study volunteers and correlate this measurement to Functional Food/Nutraceutical supplementation. This has never previously been investigated with these supplements and interesting and beneficial health information could arise.

Why is blood sampling required? Platelet reactivity and circulating biomarkers can only be measured in blood samples. An instrument called a cone and plate analyser will help to measure your platelet activity. Biomarkers will be assessed using the most advanced testing platform available- Proseek® technology on a Fluidigm platform.

Dr. Ronan Murphy, DCU, is the Principle Investigator of the study. Ms. Laura Twomey will be carrying out the platelet function study and Mr. Robert Wallace, in conjunction with OLINK Sweden will carry out the biomarker studies. Dr. Ronan Murphy will supervise all aspects of this project.

II. Details of what involvement in the Research Study will require

This experiment will require you to complete a general questionnaire and give two blood samples (4.5mls) both pre- and post- study at the laboratories in DCU (before supplementation and day 29 one day after trial finishes). This will be done using a small gauge needle and will take approximately five minutes. Blood pressure will also be measured both before and after the trial, and you will be required to attend the labs at two time points both before and after the study. This will allow a 24 hour blood pressure reading to be measured which is best practice and most accurate. The blood samples will be obtained at one of these time points before and after the trial. For the supplementation trial, you will be required to take either health supplement (or placebo) twice daily for 28 days. The dosage of Magnesium is well within the Recommended Daily Allowance (350mg and 400mg for females and males respectively). The daily dosage will be 70mg approximately for Magnesium. The concentration for the Boswellia serrata extract is well below levels commonly used in previous trials.

III. Potential risks to participants from involvement in the Research Study

There is a minor risk of experiencing discomfort during blood draw and a small bruise may appear on your arm. There is also a small risk of infection, but by using the appropriate techniques this risk is minimal.

IV. Benefits (direct or indirect) to participants from involvement in the Research Study

After completing the study you will be given a report of your results, which will include your body mass index, your blood pressure platelet function readout, and biomarker profile.

V. Advice as to arrangements to be made to protect confidentiality of data, including that confidentiality of information provided is subject to legal limitations

Your confidentiality will be protected, as each participant being assigned to an ID number, and their file will be password protected in Dublin City University. Data will also be stored in password-protected files on campus.

The results of the study will be used for a project report to be submitted to both Oriel Marine Minerals and Neal's Yard Remedies. Dependent on findings, they may be published in academic journals. You will not be identified, as your information will be presented as part of a group. Confidentiality of information provided can only be protected within the limitations of the law.

VI. Advice as to whether or not data is to be destroyed after a minimum period

Data will be destroyed by the Principle Investigator after a period of 5 years after the research study has been completed. Your blood samples will be destroyed with 12 months of the trial completion.

VII. Statement that involvement in the Research Study is voluntary

Participation in the Research Study is voluntary and you may withdraw from the research study at any point.

If participants have concerns about this study and wish to contact an independent person, please contact:

The Secretary, Dublin City University Research Ethics Committee, c/o Research and Innovation Support, Dublin City University, Dublin 9. Tel 01-7008000

Human intervention questionnaire

General Health Questionnaire

Name: .....

Age: ……

Occupation: .....

Address: .....

.....

.....

Telephone: (Home) ..... (Work) .....

Do you have, or have you ever suffered from:

Diabetes? Yes / No

Asthma? Yes / No

Epilepsy? Yes / No

Have you ever had pains in your chest or heart? Yes/ No

Do you ever feel faint or have spells of dizziness? Yes / No

Do you have or have you ever had high blood pressure? Yes / No

Do you have any current injuries or illnesses? Yes / No

In the past week, have you suffered from any illness,

which required you to be in bed or off work for one day or more? Yes / No

Do you smoke? Yes / No

If yes, how many per day?

Do you drink? Yes / No

If yes, how many units per week?

Is there a good physical or medical reason not mentioned here why you should not carry out laboratory testing? Yes / No

Please provide any further information concerning any condition/complaints that you suffer from and any medication that you may be taking by prescription or otherwise:

.....

Date:

Signature:

Authorizing Signature:

Informed consent form for human intervention

Informed Consent Form

Research Study Title: To assess the health benefits of two natural drink supplements on platelet function, age related oxidative stress and inflammation in the body and blood pressure.

School of Health and Human Performance, Dublin City University
Principal Investigator: Dr. Ronan Murphy.

II. Clarification of the purpose of the research

To investigate the health benefits of Deep Ocean Mineral (principally Magnesium) supplementation or Deep Ocean Minerals in conjunction with natural *Boswellia serrate* extract. Both been supplements have individually been demonstrated to have multiple health benefits. If the results of the trial are positive, then these supplements may be used to promote Healthy Ageing and provide a protective effect on the body against inflammation.

III. Confirmation of particular requirements as highlighted in the Plain Language Statement

Participant – please complete the following (Circle Yes or No for each question)

I have read the Plain Language Statement (or had it read to me)	Yes/No
I understand the information provided	Yes/No
I have had an opportunity to ask questions and discuss this study	Yes/No
I have received satisfactory answers to all my questions	Yes/No

IV. Confirmation that involvement in the Research Study is voluntary

You may withdraw from the Research Study at any point.

V. Advice as to arrangements to be made to protect confidentiality of data, including that confidentiality of information provided is subject to legal limitations

I understand that my confidentiality will be protected, insofar as this is permitted by Irish law, and that the research may be published in scientific journals and / or presented and discussed at scientific meetings, without revealing any of my personal details. Data will be shredded after 5 years by Dr. Murphy.

VI. Any other relevant information

If you are in a dependent relationship with any of the researchers, your involvement/non-involvement in the project will not affect your ongoing assessment/grades/management.

VII. Signature:

I have read and understood the information in this form. The researchers have answered my questions and concerns, and I have a copy of this consent form. I understand I will attend DCU on four occassions- twice on consecutive days before and after the 28-day trial for a period of approximately 30 minutes. I understand that I will take the supplements twice a day for the period of the trial (28 days). Therefore, I consent to take part in this research project

Participants Signature: _____

Name in Block Capitals: _____

Witness: _____ **Date:** _____

Participant Recruitment

- Participants will be healthy, medication naïve female subjects between the age of 45-65 years.

- 60 participants will be recruited through poster and email advertisement/internally within the School of Health and Human Performance in DCU. There will be 3 arms to the study with 20 volunteers per group 1) 20 on Neal's Yard Functional drink, 2) 20 on Oriel mineral supplementation alone, and 3) 20 control subjects.

- In conjunction with Neal's Yard and Oriel Sea Salt, participants will be required to orally take a health drink supplement (Either placebo, Neal's Yard Supplement or Neal's Yard + Oriel Supplement).

- The supplement will be consumed twice daily, 7 days a week for 4 weeks.

- Subjects will be required to attend DCU **twice** for testing, before and **twice** after the 4-week supplementation. At these testing's, the subjects blood pressure and BMI will be measured, in addition to two blood samples (pre- and post- study) - which will be used to test biomarkers of inflammation, oxidative stress and platelet function.

Safety data sheets

NYR Boswellia Sacra Glyceric Extract

Last update: 26/07/2016

1- Chemical product and company identification

Product name: NYR Boswellia Sacra Glyceric Extract

INCI name: GLYCERIN, BOSWELLIA CARTERII GUM EXTRACT, BOSWELLIA CARTERII RESIN EXTRACT, CITRIC ACID.

CTFA name: GLYCERIN, BOSWELLIA CARTERII GUM EXTRACT, BOSWELLIA CARTERII RESIN EXTRACT, CITRIC ACID.

Kind of product: vegetal extract

Uses: ingredient for cosmetic and food supplements

2- Hazards identification

No known health hazards.

3- Composition, information on ingredients

GLYCERIN Q,S. to 100% w/w (CAS 56-81-5 EINECS 200-289-5)

BOSWELLIA CARTERII

GUM EXTRACT, 18-25% w/w (CAS 89957-98-2 ; EINECS 289- 289-620-2)

BOSWELLIA CARTERII

RESIN EXTRACT

CITRIC ACID 3 % w/w (CAS 77-92-9 / 5949-29-1 EINECS 201-069-1)

4- First aid measures

Ingestion: considered not hazardous

Inhalation: considered not hazardous

Skin contact: considered not hazardous

Eye contact: considered not hazardous

5- Fire fighting measures

Extinguishing media: water spry, powders, carbon dioxide.

6- Accidental release measures

No special precautions necessary.

CLEANING TECHNIQUES

Collect with a mop and store in a bucket until disposal. Clean the contaminated zone with

water.

7- Handling and storage

HANDLING

No special precautions are necessary for safe handling.

STORAGE

Store under dry conditions at room temperature in tightly closed containers, in dark place

Keep out of direct sunlight.

8- Exposure controls, personal protection

No particular protections needed.

9- Physical and chemical property

Appearance Physical state: glycerol solution

Colour: characteristic

Odour: characteristic

Property Value Temperature or pressure

pH 2,6- 3,5

Boiling point > 110°C 760mmHg

Density ≈1.2 g/cm3

Solubility Water solubility: completely soluble

Other solvent: glycerin

10- Stability e reactivity

CHEMICAL STABILITY

Stabile.

Condition to avoid: exposure to oxidant agent and light.

HAZARDOUS DECOMPOSITION PRODUCTS

None known.

HAZARDOUS POLYMERIZATION

None known.

11- Toxicological information

The product is not expected to be hazardous to human beings.

TOXICOLOGICAL INFORMATION

No data available.

12- Ecological information

The product is not expected to be hazardous to environment.

ECOTOXICITY

No data available.

13- Disposal conditions

Product: dispose of considering local authority regulations.

Container: can be recycled

14- Transport information

RID/ADR

Non-hazardous for transport.

IMDG

Non-hazardous for sea transport.

IATA

Non-hazardous for air transport.

15- Regulatory information

Labelling According to Directives 67/548/EC and 1999/45/EC :

Symbol : N/A

R-phrase : N/A

S-phrase : N/A

This product is not considered a dangerous substance in accordance with the European Directives 88/379/ EC and 67/548 /EC and its amendment 97/69/EC.

16- Additional information

The information contained herein is based on the present state of our knowledge and does not

therefore guarantee certain properties. Since the conditions of handling and use are beyond our control, we make no guarantee of results, and assume no liability for damage incurred by use of this material. It is the responsibility of the user to comply with all applicable laws and regulations.

TECHNICAL DATA SHEET:
NYR Boswellia Sacra Glyceric Extract

Kind of product.....
water based extract *Boswellia carterii* (gum resin), solvent free (no organic extract used during any production step), preservative free for cosmetic and food supplement applications.

INCI: GLYCERIN, BOSWELLIA CARTERII GUM EXTRACT, BOSWELLIA CARTERII RESIN EXTRACT, CITRIC ACID.

CTFA : GLYCERIN, BOSWELLIA CARTERII GUM EXTRACT, BOSWELLIA CARTERII RESIN EXTRACT, CITRIC ACID.

Composition.....

GLYCERIN	Q.S. to 100% w/w	(CAS 56-81-5 EINECS 200-289-5)
BOSWELLIA CARTERII GUM EXTRACT, BOSWELLIA CARTERII RESIN EXTRACT	18-25% w/w	(CAS 89957-98-2 ; EINECS 289- 289-620-2)
CITRIC ACID	3 % w/w	(CAS 77-92-9 / 5949-29-1 EINECS 201-069-1)

Characteristics .....
- Aspect: glycerol solution
- Colour: characteristic
- Odour: characteristic
- pH: 2,6 – 3,5
- Boiling point: > 110°C (at 760mmHg)
- Density ≈ 1.2 g/cm^3
- Water solubility: soluble
- Other solvents: glycerine
- Total microbial load < 100 CFU/g
- Pathogens: none in 1 g
- The product has not been tested on animals

Recommendations .....
Dilute the product in the water phase, both in hot or cold condition, during cosmetic preparation.
During formulation consider that the product has an acidic pH.
Store in a cool dry place, avoid prolonged exposure to light and heat.
Due to the naturalness of the product a light precipitation might occur.

Last update: 26/07/2016

Phenbiox s.r.l.

PHENBIOX srl, via D'Azeglio 51, 40123 Bologna, Italy -C.F. / P.IVA 02696621206 - tel +39 051 726640- e-mail : export@phenbiox.it

Date: October 1st 2015

STATEMENT OF FACT

The following statements of fact are made by and on behalf of the Oriel Sea Salt Company in respect of the ingredients and raw materials contained in the named products:

Concentrated Deep Sea Minerals also known as Oriel Mineral Extract or Oriel Mineral Infusions.
And
Oriel Mineral Sea Salt in Natural or Kiln Dried form also known as Abra-Smooth Mineral Sea Salt.

1. **We hereby state that the raw materials used in in the above named products do not contain any Plant or Animal parts or extracts.**

2. **We hereby state that the raw materials used in the above named products have not been subjected to any form of animal testing (Ref EC No 1223/2009) at any time or by any other company or entity.**

3. **We hereby state that the raw materials used in in the above named products do not contain any NANO Particles.**

4. **We hereby state that the raw materials used in in the above named products do not contain any Synthetic materials or any materials not naturally present in pure clean deep sea water. No chemicals have been added or used in the extraction, harvesting or concentration process.**

5. **We hereby state that the raw materials used in in the above named products are not Genetically Modified and do not contain any Genetically Modified Organisms. No GMO products, ingredients or potential sources are used or present in our processing facility.**

6. **We hereby state that the raw materials and process equipment used in in the above named products have not been handled by, exposed to or have been treated with irradiation or sewage sludge.**

Signed on behalf of The Oriel Sea Salt Company Limited

.....
Brian Fitzpatrick
Managing Director

The Oriel Sea Salt Company Ltd, Port Oriel, Clogherhead, Drogheda, County Louth, Ireland
Office: +353 (0) 1 8329675 Plant: +353 (0) 41 9889624. Fax: +353 (0) 1 8329675. E: info@orielseasalt.com W: www.orielseasalt.com

Origin Green
IRELAND
an initiative by Bord Bia
This certificate recognises that
Oriel Sea Salt Company
is a verified member of the
Origin Green
Sustainability Programme
To check certificate validity, please click on the company logo at
http://www.origingreen.ie/companies/verified-members
Aidan Cotter,
Chief Executive, Bord Bia
SGS
Growing the success of Irish food & horticulture
Bord Bia
Irish Food Board

Certificate of Analysis

Prepared by:

The Questor Center, Queens University Belfast

QUESTOR ID	**16-Aug-10**
Oriel Batch No:	**M1009**

Mineral Name	Mineral Symbol	Analysis Type	Result	Unit of Measurement	Molarity
Magnesium	Mg	ICP-OES	76650	mg/l	3.15
Potassium	K	ICP-OES	23928	mg/l	0.61
Sodium	Na	ICP-OES	14144	mg/l	0.62
Boron	B	ICP-OES	245	mg/l	0.023
Calcium	Ca	ICP-OES	37.9	mg/l	0
Copper	Cu	ICP-OES	2.39	mg/l	0
Nickel	Ni	ICP-OES	1.09	mg/l	0
Silicon	Si	ICP-OES	0.96	mg/l	0
Zinc	Zn	ICP-OES	0.11	mg/l	0
Aluminium	Al	ICP-OES	<0.05	mg/l	0
Arsenic	As	ICP-OES	<0.05	mg/l	0
Barium	Ba	ICP-OES	<0.05	mg/l	0
Cadmium	Cd	ICP-OES	<0.05	mg/l	0
Cobalt	Co	ICP-OES	<0.05	mg/l	0
Chromium	Cr	ICP-OES	<0.05	mg/l	0
Iron	Fe	ICP-OES	<0.05	mg/l	0
Mercury	Hg	ICP-OES	<0.05	mg/l	0
Manganese	Mn	ICP-OES	<0.05	mg/l	0
Lead	Pb	ICP-OES	<0.05	mg/l	0
Antimony	Sb	ICP-OES	<0.05	mg/l	0
Selenium	Se	ICP-OES	<0.05	mg/l	0
Tin	Sn	ICP-OES	<0.05	mg/l	0
Strontium	Sr	ICP-OES	<0.05	mg/l	0
Titanium	Ti	ICP-OES	<0.05	mg/l	0
Vanadium	V	ICP-OES	<0.05	mg/l	0

ORGANIC TRUST LIMITED

CERTIFIED PRODUCTS SCHEME

ORGANIC TRUST CERTIFIED PRODUCT

This is to certify that the Organic Trust Symbol under the Certified Products Scheme has been awarded to

Extraction, Processing, Packaging & Distribution of Sea Salt and Sea Minerals

The OT Certified Products Scheme covers approved products acceptable for use in organic systems- such products lie outside the legislative scope of (EC) Regulations 834/2007 and 889/2008 as amended

Certification for above product has been granted to

Oriel Sea Salt Company Ltd

(John Delany & Brian Fitzpatrick)

at

Port Oriel, Clogherhead, Drogheda, Co. Louth

Symbol No. CP318

Valid From: 01/01/2016

Signed: _____

Valid Until: 31/12/2016

National Co-ordinator of the Organic Trust Ltd,
Vernon House, 2 Vernon Avenue, Clontarf, Dublin 3.
Telephone/Fax: 01 8530271. Email: organic@iol.ie
Web: www.organictrust.ie

The Organic Trust Limited is an EU Approved Organic Certification Body. Products and/or processes which are certified under the Organic Trust Certified Products Scheme are not ISO17065 accredited activities.

Feidhmeannacht na Seirbhíse Sláinte
Health Service Executive

Environmental Health Services
HSE Dublin North East
1st Floor, Old St. Mary's Hospital
Dublin Road
Drogheda, Co. Louth

Tel: +353 (0)41 980 1062
Fax: +353 (0)41 983 3641

25 July 2013

Mr. Brian Fitzpatrick,
Managing Director,
The Oriel Sea Salt Co. Ltd.
Port Oriel,
Clogherhead,
Co. Louth.

REGISTRATION OF FOOD BUSINESS ESTABLISHMENT
European Communities (Hygiene of Foodstuffs) Regulations 2006

Dear Mr. Fitzpatrick,

I wish to acknowledge receipt of your notification of the Food Business Establishment Form in accordance with regulation 6(2) of Council Regulation 852/2004.
The Food Business has been placed on our register with the following information:

Name of Food Business: The Oriel Sea Salt Co. Ltd.

Trading Address: Port Oriel,
Clogherhead,
Co. Louth.

The main activities carried out in the Food Business:
Extraction and harvesting of sea water to produce sea salt and sea minerals.

Yours sincerely,

Aoife Cathcart
Senior Environmental Health Officer

Please Note: - *If there is any significant change in activities, change of ownership or cessation of an existing establishment the HSE must be notified.*

UKAS Testing Laboratory No: 1187

LGC
Newmarket Road
Fordham
Cambridgeshire
CB7 5WW
UK

Tel: +44 (0)1638 720500
Fax: +44(0)1638 724200
Email: info@lgcgroup.com
www.lgcgroup.com

Dr Ronan Murphy
Dublin City University
School of Health & Human Performance
Glasnevin
Dublin 9
Ireland

Date Issued: 8 November, 2016

CERTIFICATE OF ANALYSIS: 116169

LGC Supplement Screen

Consignment Number:	post
Delivery Date:	24 October, 2016
Date Analysis Commenced:	24 October, 2016
Purchase Order Number:	N/A

Product:	Cardio Revive	**Pack Size:**	30ml
Flavour:		**Programme:**	Custom
Batch No:	M1006	**Sample Type:**	Routine
Batch Expiry:	10/2017	**LGC Reference:**	871927

The sample was analysed using documented LGC screening methods for the compounds specified within the Service Level Agreement: Nutritional Supplements V2.0.**

GCMS:
None were found.

LCMS:
None were found.

Signed

Suzanne Lister
Senior Scientist

Test results apply to the portion of product taken.
* or isomers of - as specified within the Service Level Agreement.

** In a change to the above Service Level Agreement, as of the 9th August 2016 the compound diethylpropion will not be included within standard screening protocols.

This certificate may not be reproduced, except with the prior written approval of the issuing laboratory.

R-2616

LGC Limited Registered office: Queens Road, Teddington, Middlesex TW11 0LY, UK Registered in England No 2991879 VAT No. 674 0567 21